

# **Optimisation of Automated Gas Metal Arc Fillet Welding**

PhD Thesis

Jonathan Cairns

Department of Mechanical and Aerospace Engineering

University of Strathclyde, Glasgow

April 22, 2021

This thesis is the result of the author's original research. It has been composed by the author and has not been previously submitted for examination which has led to the award of a degree. The copyright of this thesis belongs to the author under the terms of the United Kingdom Copyright Acts as qualified by University of Strathclyde Regulation 3.50. Due acknowledgement must always be made of the use of any material contained in, or derived from, this thesis.

Signed:

Date:

## Abstract

Gas Metal Arc Welding (GMAW) has been one of the most widely used industrial welding processes since around the middle of the 20<sup>th</sup> Century. However, the large number of input parameters and variables makes it extremely challenging to understand exactly what impact the variation of each of the inputs (and their interactions with each other) has on the resultant fillet weld. Although the GMAW welding process is a mature and generally well understood process, there is little to no evidence of research specifically focused on understanding what impact the torch orientation (travel angle and gun angle) and parameter interactions have on the resultant fillet weld geometry and structure. The purpose of this study is to provide an improved understanding of the main GMAW process parameters (current, voltage, travel speed, shielding gas flow rate, electrode, travel angle and gun angle), which can then be applied to a robotic welding set up in order to optimise the process by minimising heat input, distortion and cost whilst achieving satisfactory penetration and leg length. Artificial Neural Networks (ANNs) and Regression analysis were used to identify the key parameters and interactions that impact a fillet weld geometry. These results highlighted that the torch travel angle was significant in determining both the shape and also the level of asymmetry between the horizontal and vertical leg lengths of the fillet weld. Finite Element Analysis was then used to determine how the fillet weld geometry impacts the temperature distribution and distortion of the fillet welded assembly. The FEA model demonstrated that varying the fillet weld geometry impacts the temperature distribution and distortion of the fillet welded structure. Specifically the results suggest that welding the fillet with a larger horizontal leg length appears to generate less overall deflection on the baseplate. This reinforces that that in order to control the level of distortion of a welded structure it is important to tightly control the size and shape of the fillet weld. A Schlieren study was conducted to visualise the behaviour of the shielding gas around the fillet weld. This study highlighted that the shielding gas flow rate can be significantly reduced, for a fillet weld, without compromising the quality of the weld. This improved understanding, from the ANN, FEA and visualisation studies has the potential to generate significant benefits if applied to a robotic welding set up. Creating a more robust process that can be optimised to achieve a target geometry, minimise the heat input and distortion and minimise the overall cost of the weld.

## Acknowledgements

Firstly I would like to express my gratitude to Dr Norman McPherson and Professor Alexander Galloway for providing me with the opportunity to undertake this research and the support and encouragement to bring it to a conclusion.

I would also like to thank the technical staff at the University, specifically James Kelly for assistance and guidance in preparing and analysing samples in the metrology lab and also Steven Black for his support in setting up and operating the welding rig.

BAE Systems Naval Ships, for ultimately funding the research and William McAlister for providing the space and time for me to work on this project, in parallel with work duties, over the last couple of years. I'd also like to thank Dr Stuart Hambling, BAE Systems Submarines, for his support in the preparing and processing of the hardness maps.

Professor Andrew Moore and Ioannis Bitharis, Heriot Watt University, for their expertise and support in undertaking the fillet weld shielding gas visualisation study.

Special thanks to my family, without whose support I would never have been able to complete this work.



# Table of contents

Abstract.....	iii
Acknowledgements.....	iv
Table of contents .....	v
List of Tables.....	ix
List of Figures .....	x
List of Symbols .....	xv
Abbreviations .....	xvi
Chapter 1 Introduction.....	1
1.1    Background .....	1
1.1.1    Gas Metal Arc Welding.....	1
1.1.2    Fillet Welds.....	6
1.1.3    Industrial Background .....	11
1.1.4    Fillet Weld Design Standards .....	14
1.2    Outline of Research.....	23
1.3    Summary .....	27
1.4    References.....	28
Chapter 2 Literature Review .....	31
2.1 Introduction .....	31
2.2 Identification of Key GMAW Parameters – Methodologies .....	31
2.2.1 Artificial Neural Networks (ANN) .....	32
2.2.2 ANN + Mathematical Modelling Approach .....	33
2.2.3 Finite Element Modelling .....	34
2.3 GMAW Process Inputs.....	35
2.3.1 Welding Torch Angle (gun angle and travel angle).....	36
2.3.2 Shielding Gas Behaviour for Fillet Welds .....	37
2.3.3 Process Efficiency .....	38
2.3.4 Weld Procedures.....	39
2.4 GMAW Process Outputs.....	39
2.4.1 Geometry .....	39
2.4.2 Thermal and mechanical impact of GMAW Process.....	40
2.4.3 Metallurgical/Mechanical Properties of GMAW welded joint.....	41
2.5 Process Cost Analysis .....	43

2.6 Summary .....	43
2.7 References.....	44
Chapter 3 Methodology.....	50
3.1 Introduction .....	50
3.2 ANN Model Development.....	50
3.3 Regression Analysis .....	54
3.4 FEA Model Development .....	56
3.5 Shielding Gas Visualisation.....	66
3.6 GMAW Fillet Welding Experiments.....	71
3.6.1 Equipment.....	71
3.6.2 Hardness Testing.....	77
3.6.3 Macrographs /Microstructure .....	82
3.6.4 Fillet Weld Geometry Measurement System.....	85
3.7 References.....	87
Chapter 4 GMAW Fillet Welding Process Capability Analysis.....	89
4.1 Semi-Automatic vs Robotic Welding - Results .....	89
4.2 Process Capability Analysis - Discussion .....	93
4.3 References.....	94
Chapter 5 Using Statistical Modelling to identify key parameters affecting fillet weld geometry.....	95
5.1 Results .....	95
5.1.1 ANN - Identification of key parameters using ANN/Sensitivity Analysis .....	95
5.1.2 ANOVA - Fillet Weld - Key Parameter Interactions Analysis of Variables.....	96
5.1.3 Regression Analysis - Identifying key fillet weld parameters.....	102
5.1.4 Relationship between fillet weld parameters and heat affected zone (HAZ).....	113
5.1.5 Summary .....	115
5.2 Welding Torch - Travel angle .....	116
5.2.1 Travel angle impact on fillet weld geometry .....	116
5.2.2 Torch travel angle impact on fillet weld microstructure .....	120
5.2.3 Travel angle impact on fillet weld hardness .....	122
5.2.4 Torch travel angle impact on current/voltage .....	123
5.3 Discussion – Key Fillet Weld Geometry.....	125
5.3.1 Penetration .....	125
5.3.2 Leg Length .....	128
5.3.3 Weld Shape (Throat + Reinforcement) .....	129

5.3.4 Hardness.....	131
5.3.5 Microstructure .....	131
5.4 References.....	132
Chapter 6 Finite Element Modelling .....	134
6.1 Finite Element Modelling – GMAW Fillet Weld .....	134
6.1.1 Baseplate vs Stiffener Heat Flow – FEA Model Validation.....	134
6.1.2 Impact of individual input parameters on the heat flow through the fillet welded joint .....	136
6.1.3 Impact of Asymmetrical Leg Lengths on the heat flow through fillet welded joint. ....	137
6.2 Heat Input & Distortion Discussion.....	142
6.2.1 Process Parameters.....	142
6.2.2 Asymmetrical Leg Lengths.....	143
6.2.3 Heat Affected Zone / Distortion.....	144
6.3 References.....	146
Chapter 7 Shielding Gas Visualisation.....	147
7.1 Overview of Schlieren Results.....	147
7.2 Shielding Gas Flow Reduction – Impact on fillet weld geometry .....	150
7.3 Electrode Impact on reducing shielding Gas Flow .....	151
7.3.1 Solid Wire .....	152
7.3.2 Flux Cored Wire.....	153
7.4 Travel angle impact on shielding gas flow .....	155
7.5 Shielding Gas - Discussion .....	158
7.5.1 General Gas Flow Observations .....	158
7.5.2 Influence of travel angle on gas flow .....	159
7.5.3 Influence of gas flow rate on weld quality.....	160
7.3 References.....	163
Chapter 8 GMAW Filler wire study .....	164
8.1 Electrode Experiment Results .....	164
8.1.1 Results – Impact of Electrode on Hardness .....	166
8.1.2 Results – Impact of Electrode on Metallurgical Structure .....	167
8.2 Electrode .....	170
8.2.1 Heat Affected Zone .....	170
8.2.2 Weld Area.....	171
8.3 References.....	171

Chapter 9 GMAW Fillet Weld Process Cost Analysis.....	172
9.1 Fillet Weld Cost Model.....	172
9.1.1 Cost Model Development .....	172
9.1.2 Cost Impact of each welding parameter .....	174
9.1.3 Estimating fillet weld cost by leg length .....	175
9.2 Fillet Weld Cost Modelling - Discussion .....	176
9.3 References.....	178
Chapter 10 Conclusions.....	179
Chapter 11 Future Work .....	181
11.1 References.....	182
Appendices.....	183
Appendix 1 Publications.....	183
Appendix 2 Weld Procedure Examples .....	184
Appendix 3 Finite Element Analysis – Temperature Dependent Material Properties.....	187
Density .....	187
Thermal Conductivity .....	188
Enthalpy .....	188
Elastic Modulus .....	189
Poisson Ratio .....	189
Coefficient of Thermal Expansion .....	190
Appendix 4 Length of Fillet Welding / Ship.....	191
Appendix 5 Using FEA to support Weld Procedure Development.....	192
Appendix 6 Tables of Experimental Results.....	193

## List of Tables

Table 1-1	Definitions of key fillet weld geometric features.....	8
Table 1-2	Welder Survey - Variation in parameter settings for manual welding .....	12
Table 1-3	Welder Survey – Travel and Gun Angle guidance for different electrodes .....	13
Table 1-4	Process inputs and outputs used to develop ANN.....	23
Table 2-1	Comparison of Torch Travel Angle Guidance.....	36
Table 3-1	GMAW Input-Output Parameters.....	55
Table 3-2	Gas Visualisation Welding Parameters (Constant) .....	69
Table 3-3	Gas Visualisation Welding Parameters (Variables) .....	70
Table 3-4	Gas Visualisation Experimental Schedule .....	70
Table 3-5	Chemical Composition for S355 J2+N Steel Plate .....	73
Table 3-6	Chemical Composition for Metal Core, Flux Core and Solid electrodes .....	74
Table 3-7	GMAW Fillet Weld Experimental Parameter Settings .....	75
Table 4-1	Summary of Semi-Automatic vs Automated process capability analysis .....	93
Table 5-1	Top 3 significant parameters impacting fillet weld geometry .....	102
Table 5-2	Inputs and Outputs used in Regression Model .....	103
Table 5-3	Comparison summary of results from ANN/ANOVA and Regression Analysis	116
Table 5-4	Travel Angle Experiment Parameters .....	117
Table 5-5	Travel Angle Experiment Results.....	118
Table 5-6	Travel Angle - % variation of arc current and voltage.....	124
Table 5-7	Calculating ‘effective’ wire feed speed for pushing and pulling travel angles.	127
Table 6-1	Comparison of Actual vs Predicted HAZ size with varying leg lengths .....	138
Table 6-2	Inputs and Outputs from Unequal Leg Length FEA Structural Model. ....	142
Table 7-1	Geometry of fillet weld samples from gas flow experiments .....	151
Table 8-1	Parameters kept constant during experiments .....	165
Table 8-2	Experimental input settings used for each electrodes .....	165
Table 9-1	Comparison of GMAW Welding Cost breakdown %.....	172
Table 9-2	Fillet weld shielding gas flow reduction – estimated savings .....	177

## List of Figures

Figure 1-1	Gas Metal Arc Welding (GMAW) set up [1.1] .....	1
Figure 1-2	Typical GMAW Torch.....	3
Figure 1-3	Examples of Manual, Semi-Automatic ‘Weldy Car’ and Robotic welding.....	4
Figure 1-4	Pictures of a fillet welded structure and cross sectioned macrograph of a fillet weld .....	6
Figure 1-5	GMAW Fillet Weld Process Diagram.....	7
Figure 1-6	Fillet Weld Penetration .....	8
Figure 1-7	Diagram highlighting some of the key fillet weld geometrical features (Leg Length, Throat and Reinforcement) .....	9
Figure 1-8	Fillet weld heat affected zones (HAZ) .....	9
Figure 1-9	Image showing fillet weld ‘penetrating’ the horizontal (baseplate) and vertical (stiffener) axes .....	10
Figure 1-10	Example of a welded panel assembly used in ship construction.....	11
Figure 1-11	CAD Image of welded panel assembly .....	11
Figure 1-12	Key features required to calculate the maximum lack of allowable penetration in a fillet weld .....	15
Figure 1-13	Key features required to calculate the acceptable leg length of a fillet weld	16
Figure 1-14	Key features required to calculate the acceptable level of leg length asymmetry for a fillet weld.....	17
Figure 1-15	Key features required to calculate the acceptable throat thickness of a fillet weld .....	18
Figure 1-16	Key features of a fillet weld required to calculate throat stress.....	20
Figure 1-17	Key features required to calculate the acceptable convexity for a fillet weld .....	21
Figure 1-18	Acceptable undercut for a fillet weld.....	21
Figure 1-19	Diagram showing fillet weld area and throat thickness.....	22
Figure 1-20	Research methodology mapped against fillet weld parameters .....	23
Figure 1-21	Visual definition of gun angle.....	24
Figure 1-22	Visual definition of travel angle .....	24
Figure 2-1	Macrograph showing location of weld (1), heat affected zone (2) and unaffected parent material (3). .....	42

Figure 3-1	Typical Example of ANN Architecture .....	51
Figure 3-2	Visual Representation of selected ANN architecture .....	53
Figure 3-3	Example of Minitab Regression Analysis outputs .....	56
Figure 3-4	FEA Fillet Weld Mesh .....	57
Figure 3-5	FEA Model Development Process .....	58
Figure 3-6	Schematic showing characteristics of volumetric heat source.....	59
Figure 3-7	FEA Mechanical Boundary Conditions .....	61
Figure 3-8	Schematic showing how fillet assembly was supported on the rig during welding .....	61
Figure 3-9	Comparison of Fillet Weld Macrograph and FEA thermal nodal solution .....	63
Figure 3-10	Example of a Surface Map using output from laser measurement system...	63
Figure 3-11	Schematic and photographs showing laser system used for measuring distortion of steel plates.....	64
Figure 3-12	FEA Model – Example of thermal plots.....	65
Figure 3-13	FEA Model – Example of Mechanical plot.....	66
Figure 3-14	Schematic diagram of Schlieren rig set up [3.11] .....	67
Figure 3-15	Annotated photograph of Schlieren rig set up [3.11] .....	68
Figure 3-16	Shielding Gas visualisation - through high speed camera [3.11] .....	69
Figure 3-17	Automated Welding Rig at the University of Strathclyde .....	71
Figure 3-18	Diagram showing welded test piece dimensions, location of thermocouples and tack welds .....	73
Figure 3-19	Range of possible welding torch gun angles.....	76
Figure 3-20	Range of possible welding torch travel angles.....	77
Figure 3-21	Example of mounted and polished sample.....	78
Figure 3-22	IACS W28 Fillet Weld [3.10] .....	79
Figure 3-23	Hardness results from parent plate .....	80
Figure 3-24	Example of automated hardness map of fillet weld sample.....	81
Figure 3-25	Example polished test piece used to generate hardness map .....	82
Figure 3-26	Fillet Weld Sample after etching.....	83
Figure 3-27	Microstructure of unaffected baseplate .....	84
Figure 3-28	Results from Gage Reproducibility and Repeatability Study .....	86
Figure 4-1	Semi-Automatic Set up – Vertical Leg Length Process Capability Graph .....	90
Figure 4-2	Robotic Set up – Vertical Leg Length Process Capability Graph.....	90

Figure 4-3	Semi-Automatic Set up – Horizontal Leg Length Process Capability Graph ..	91
Figure 4-4	Robotic Set up – Horizontal Leg Length Process Capability Graph .....	91
Figure 4-5	Semi-Automatic Set up – Penetration Process Capability Graph .....	92
Figure 4-6	Robotic Set up – Penetration Process Capability Graph .....	92
Figure 5-1	ANN Model Results (Actual vs Predicted) .....	95
Figure 5-2	Results of ANN Sensitivity Analysis .....	96
Figure 5-3	Sensitivity and Interaction Results for Penetration .....	97
Figure 5-4	Sensitivity and Interaction Results for Vertical Leg Length.....	98
Figure 5-5	Sensitivity and Interaction Results for Horizontal Leg Length .....	99
Figure 5-6	Sensitivity and Interaction Results for Throat.....	100
Figure 5-7	Sensitivity and Interaction Results for Reinforcement .....	101
Figure 5-8	Regression Model validation results for Throat and Penetration.....	104
Figure 5-9	Regression Model validation results for Vertical and Horizontal Leg Length .....	105
Figure 5-10	Penetration significant parameters .....	106
Figure 5-11	Vertical Leg Length - significant parameters.....	108
Figure 5-12	Vertical Leg Length - significant interactions .....	108
Figure 5-13	Horizontal Leg Length - significant parameters .....	110
Figure 5-14	Horizontal Leg Length - significant interactions.....	110
Figure 5-15	Asymmetric Leg Length - significant parameters.....	111
Figure 5-16	Range of leg length asymmetry by torch travel angle .....	112
Figure 5-17	Heat Affected zones of a fillet weld .....	113
Figure 5-18	Strength of relationship between the process inputs and outputs .....	114
Figure 5-19	Significance of input parameters in determining size of HAZ.....	115
Figure 5-20	Travel Angle Weld Macros .....	117
Figure 5-21	Macrographs showing HAZ areas for varying leg lengths.....	119
Figure 5-22	Locations of weld and heat affected zone regions microstructure images	120
Figure 5-23	Microstructure of Weld Area (push/pull/neutral) .....	121
Figure 5-24	Microstructure of Heat Affected Zone (push/pull/neutral).....	121
Figure 5-25	Hardness profiles for push, pull and neutral travel angles .....	123
Figure 5-26	Graph showing current (A) readings from PAMs unit during welding.....	124
Figure 5-27	Graph showing voltage (V) readings from PAMs unit during welding.....	125



Figure 5-28	Distance from torch nozzle to stiffener for pushing, pulling and neutral travel angles.....	126
Figure 5-29	Calculation of wire feed speed for pushing and pulling travel angles .....	128
Figure 5-30	Macrograph images showing pull and push fillet welds. ....	130
Figure 6-1	Actual vs Predicted temperature readings plotted over time .....	135
Figure 6-2	Schematic showing direction of heat flow through the welded fillet joint. ....	136
Figure 6-3	Comparison of predicted temperature flow through stiffener by varying input parameters by 10%.....	137
Figure 6-4	Comparison of predicted temperature variation through stiffener and baseplate by varying the unequal leg length.....	139
Figure 6-5	Comparison of HAZ between macrograph and FEA Model .....	140
Figure 6-6	FEA Structural Model showing the deflection in each axis by varying leg length.....	141
Figure 7-1	Schlieren visualisation at 15l/min gas flow rate .....	147
Figure 7-2	Schlieren visualisations at 15, 12, 9 and 6 l/min gas flow rates.....	148
Figure 7-3	Convective heat flux and temperature along the edge of the baseplate and stiffener [7.1]. ....	149
Figure 7-4	Hardness Scans of solid wire welds at 12l/min & 6l/min gas flow rates .....	152
Figure 7-5	Macro of acceptable solid wire fillet weld at 12l/min and unacceptable fillet weld at 6l/min gas flow rate.....	153
Figure 7-6	Microstructure Image of solid wire welds at 12l/min & 6l/min gas flow rates .....	153
Figure 7-7	Hardness Scans of flux core wire welds at 12l/min & 3l/min gas flow rates.....	154
Figure 7-8	Macro image of flux cored wire welds at 12l/min & 3l/min gas flow rates. ....	154
Figure 7-9	Microstructure Image of flux cored wire welds at 12l/min & 3l/min gas flow rates .....	155
Figure 7-10	Visualisation of shielding gas flow for pushing and pulling travel angles [7.1] .....	155
Figure 7-11	Temperature profile on workpiece for pushing and pulling travel angles [7.1] .....	157
Figure 7-12	Push vs Pull Solid Wire Hardness maps - shielding gas flow rate 6l/min.....	161
Figure 8-1	Hardness Maps for Solid, Flux Cored and Metal Cored Wire welds .....	166
Figure 8-2	Microstructure of Weld Area using different electrodes.....	167

Figure 8-3	Microstructure of Heat Affected Zone using different electrodes .....	168
Figure 8-4	Locations of microstructure images.....	169
Figure 9-1	Percentage (%) breakdown of Fillet Weld Costs [BAE Systems Naval Ships]173	
Figure 9-2	% cost impact by varying each parameter individually by 10% .....	174
Figure 9-3	Graph showing GMAW fillet weld leg length against process costs .....	175
Figure 10-1	Diagrammatic representation of fillet welding project .....	179
Figure A-1	FEA Weld Procedure parameters comparison .....	192

## List of Symbols

$h_p$	Maximum allowable lack of penetration
$h_L$	Difference between horizontal and vertical leg lengths
$h_T$	Acceptable throat thickness
$P$	Applied load
$t$	Weld throat
$l$	Length of weld
$C$	Convexity
$S_k$	Sensitivity
$\sigma_k^2$	Variance of the input (sensitivity analysis)
$\beta$	Regression coefficient
$q_{vol}$	Volumetric heat input
$\mu$	Process efficiency coefficient
$V$	Voltage
$I$	Current
$l_w$	length of triangular fusion zone
$b_w$	width/depth of triangular fusion zone
$h_w$	height of triangular fusion zone
$q_{c+rad}$	heat flow by convection and radiation (combined)
$h_c$	film coefficient due to convection
$h_r$	film coefficient due to radiation
$T_s$	temperature of heated surface
$T_a$	Ambient temperature
$HV$	Hardness Value
$F$	Applied load (kN)
$\delta$	thermal efficiency factor
$TS$	Travel speed

## Abbreviations

ANN	Artificial Neural Network
MLP	Multi-Layer Perceptron
GFF	Generalised Feedforward
PNN	Probabilistic Neural Network
GMAW	Gas Metal Arc Welding
FEA	Finite Element Analysis
CFD	Computational Fluid Dynamics
PAMS	Portable Arc Measuring System
MC-1	Metal Cored Wire
Gage R&R	Gage Repeatability and Reproducibility
MSA	Measurement System Analysis
CTWD	Contact Tip to work distance
Image J	Image analysis software
Ansys	Finite Element Modelling software

# Chapter 1 Introduction

## 1.1 Background

### 1.1.1 Gas Metal Arc Welding

Gas Metal Arc Welding (GMAW) has been one of the most widely used industrial welding processes since around the middle of the 20<sup>th</sup> Century. This popularity is due to its flexibility, higher travel speeds and relatively low costs, generated by higher productivity. GMAW is a commonly used process in the shipbuilding and construction industries, specifically in the fabrication and joining of steel structures and assemblies. Figure 1-1, below, shows the basic GMAW process set up. The heat required for the GMAW [1.1] process is generated through an electric arc created between a continuously fed anode (welding torch) and a cathode (welded metal). The arc and molten weld pool is typically protected from environmental contaminants by means of an inert shielding gas.

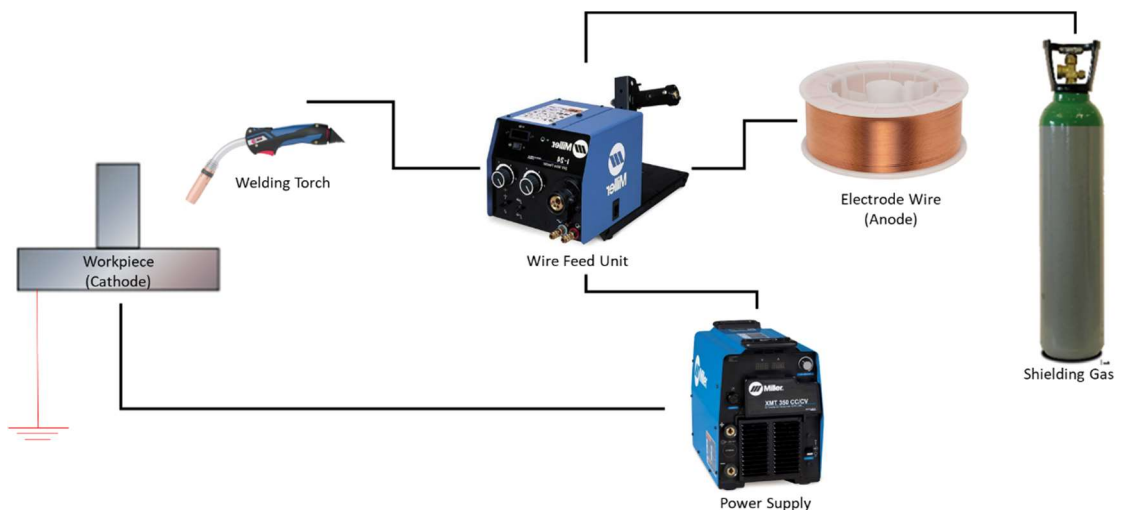


Figure 1-1 Gas Metal Arc Welding (GMAW) set up [1.1]

The GMAW process has four different modes of transferring the metal from the wire fed electrode into the welded workpiece. The method of transfer used is heavily influenced by the orientation and material of the joint and the parameters used.

- Short circuit mode occurs when the electrode physically touches the workpiece and creates a short circuit. It is a low energy (100-200A, 17-22V) method of transferring the metal from the electrode onto the workpiece and is generally used on thin plate structures. In short circuit mode a constant CTWD (contact tip to work distance) needs to be maintained in order to generate a smooth weld.
- Globular transfer mode transmits larger droplets of metal, greater than the diameter of the electrode, across the arc onto the workpiece. Globular transfer requires higher voltage and current than short circuit mode (>200A, >22V) and is preferably used in the downhand/flat welding positions due to difficulties in controlling the larger/heavier droplets in the vertical and overhead welding positions.
- Spray transfer mode is a high energy method of transferring the metal to the workpiece. This method results in small molten droplets being transferred across the arc, produces very little spatter and is generally used for the welding of thick (>6.4mm) metals in the downhand position.
- Pulse spray mode is a variation of spray transfer mode, whereby a pulsing current is used to melt the electrode, one droplet per pulse. This mode requires less heat and a special power source and can be used for vertical and overhead welding of thicker metals.

The purpose of the shielding gas is to prevent the molten weld pool from being exposed to oxygen, nitrogen and hydrogen in the atmosphere. Exposure of the weld pool to these elements increases the likelihood of porosity in the weld (compromising the quality of the weld) and reduces the stability of the arc (increased levels of spatter). Argon, helium, carbon dioxide and oxygen are the most common shielding gases used in GMAW welding. The type and mixture of shielding gases used has an impact on the cost, penetration, appearance, material properties and productivity of the welding process so it is important that the correct gas is chosen for the selected application [1.2], [1.3]. A mixture of argon (80%) and carbon dioxide (20%) is used for the GMAW process within the BAE Systems Naval Ships production facilities and so will predominantly be the gas mixture used throughout the experiments detailed within this project.

The welding torch is an important component of the GMAW process. The torch is responsible for initiating the arc, feeding the electrode into the weld and delivering the shielding gas around the arc. A 'goose' necked torch is typically used for manual GMAW process [Figure 1-2] as it provides better ergonomics; however a straight necked torch was used for the experimental work, detailed in Chapter 3, as it is difficult to measure and control the angle and position of the torch, relative to the workpiece, with the "goose' necked torch.

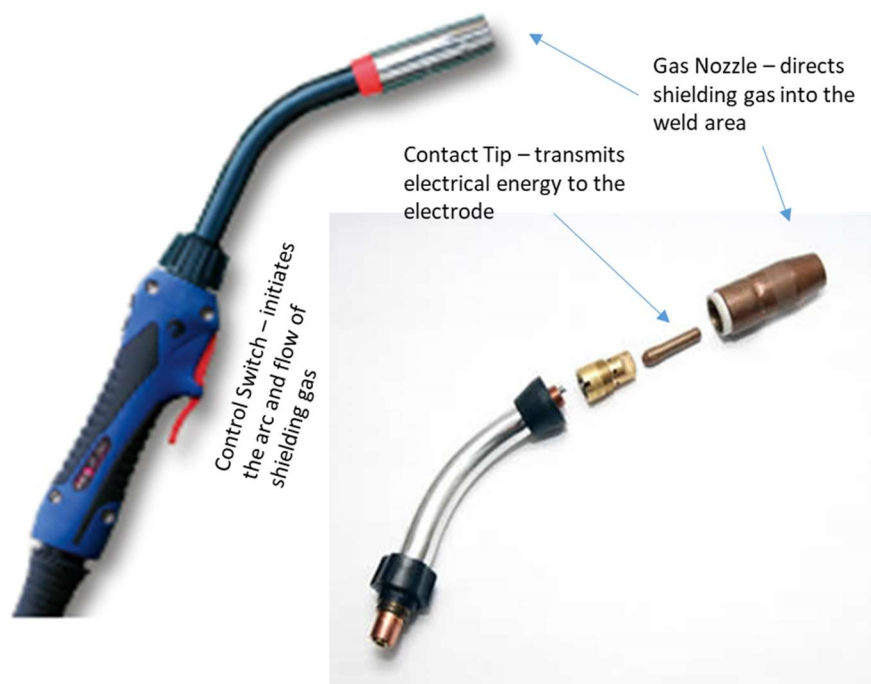


Figure 1-2 Typical GMAW Torch

The type of electrode used for the GMAW process has a significant impact on the resultant mechanical/metallurgical properties of the weld. The choice of electrode will ultimately be dictated by the weld requirements specified by the design. The three types of wire that will be included within this research are solid, flux cored and metal cored wires. Solid Wire electrodes tend to provide a higher deposition rate and thus provide a high level of efficiency (>95%). Solid wires produce a smooth, clean weld; however, they tend to not work well in exposed, draughty production areas. Flux Cored electrodes provide a form of shielding round the weld. This causes the weld to solidify faster which is useful when

welding overhead or on the vertical (minimises the impact of gravity). Anecdotal feedback [Table 1-3] from welders advise that the orientation of the torch is critical for flux cored welding as a 'pushing' travel angle increases the likelihood of porosity, caused by gas from the flux becoming trapped in the weld before it solidifies. Metal cored electrodes are more expensive than the equivalent solid and flux cored wires; however, they do provide a higher deposition rate and better penetration due to the higher current density [1.4] and so are favourable to support high volume automated welding. There are typically three methods of deploying the GMAW process within the shipyard environment, shown in Figure 1-3 below. Manual welding is 100% reliant on competence of welder. It can be difficult to maintain a constant gun angle and CTWD over long distances for a prolonged period of time. However, the flexibility of the welder can allow easy access to complex joints in difficult to access areas. The close proximity of the welder also allows for a quick feedback loop to alter position or parameters based on the quality of the arc.



Figure 1-3 Examples of Manual, Semi-Automatic 'Weldy Car' and Robotic welding

The semi-automatic process requires to be manually set up and configured by the welder and is generally used for long straight, uninterrupted welds. The semi-automatic process



requires close monitoring so that any adjustments can be made to compensate for any variation in the material flatness along the length of the weld. One of the main benefits of the semi-automatic process is that it maintains a constant travel speed, travel angle and gun angle, once set up. In fully automated (robotic) welding the welders' skills lies in the set up, programming and sequencing of the robot. This usually requires fairly significant capital investment; however, once set up the process can be monitored remotely and provides a more consistent/repeatable method of controlling the process parameters.

There are generally two different types of welding power sources, constant current (CC) or constant voltage (CV). Due to the nature of the welding arc the current and voltage are constantly fluctuating. In order to maintain a stable arc the power source is constantly monitoring the arc and compensating for these fluctuations. A CC power source will keep the current stable irrespective of large variations in voltage and a CV power source will maintain a constant voltage regardless of any fluctuations in current. For GMAW processes CV is preferred [1.5], and was used for the experimentation work detailed in Chapter 3. Generally the voltage setting controls the arc length (distance from end of electrode to the workpiece) and the width/volume of the resultant weld bead whereas the current setting directly impacts the consumption rate of the electrode. The higher the current, the faster the electrode melts. Consequently the current and wire feed speed (WFS) are directly related. On a GMAW CV power supply the current is altered by changing the wire feed speed. For the experiments detailed in Chapter 3 the voltage was set directly from the power supply and the current setting was controlled by altering the wire feed speed and measured using the portable arc measuring system (PAMS).

The three main factors that determine the heat input for a GMAW fillet weld are shown in Eqn 1-1 below:

$$Q = \frac{V \times I}{1000 \times TS} \times \delta \quad \text{Eqn. 1-1}$$

Where: Q is the heat input (kJ/mm)

V is the arc voltage (V)

I is the arc current (A)

$\delta$  is the thermal efficiency factor

$TS$  is the travel speed (mm/sec)

### 1.1.2 Fillet Welds

A fillet weld is a weld with a triangular shaped cross section that is used to join two pieces of metal, usually at right angles [Figure 1-4]. Fillet welded joints are one of the most widely used welded joint configurations, especially in the construction and shipbuilding industries.

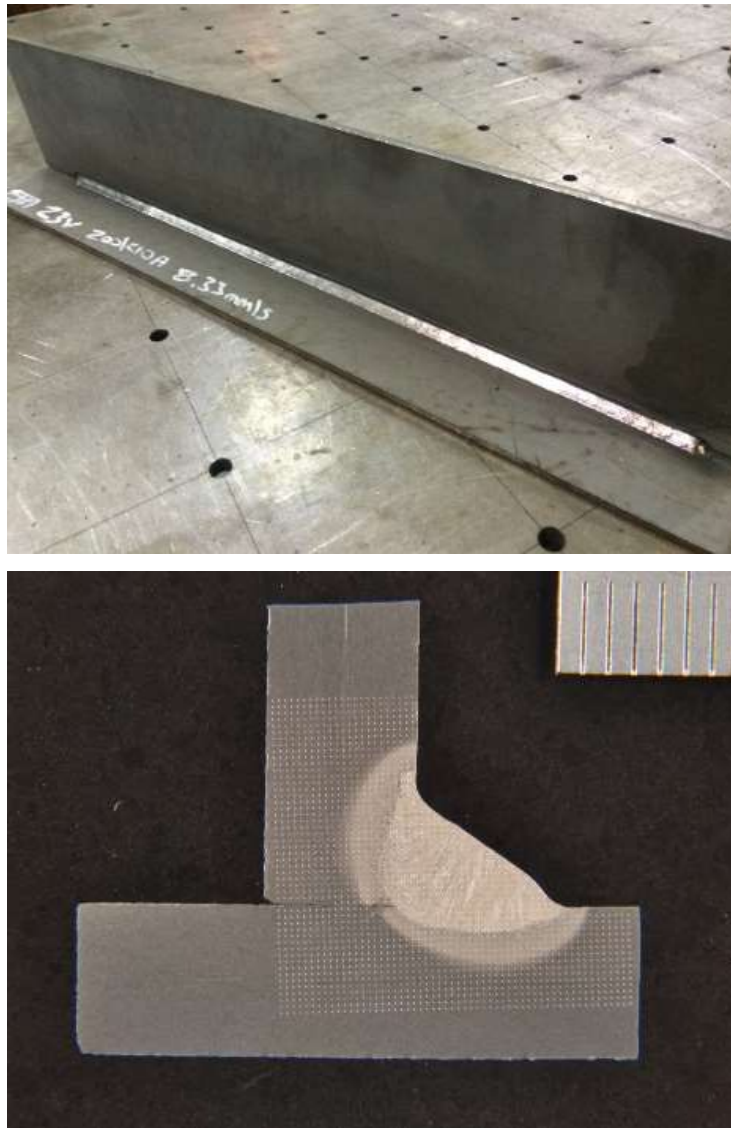


Figure 1-4 Pictures of a fillet welded structure and cross sectioned macrograph of a fillet weld

Figure 1-5, below, shows the key GMAW fillet welding process inputs and outputs and highlights the larger number of parameters/variables which need to be understood in order to manage this process closely.

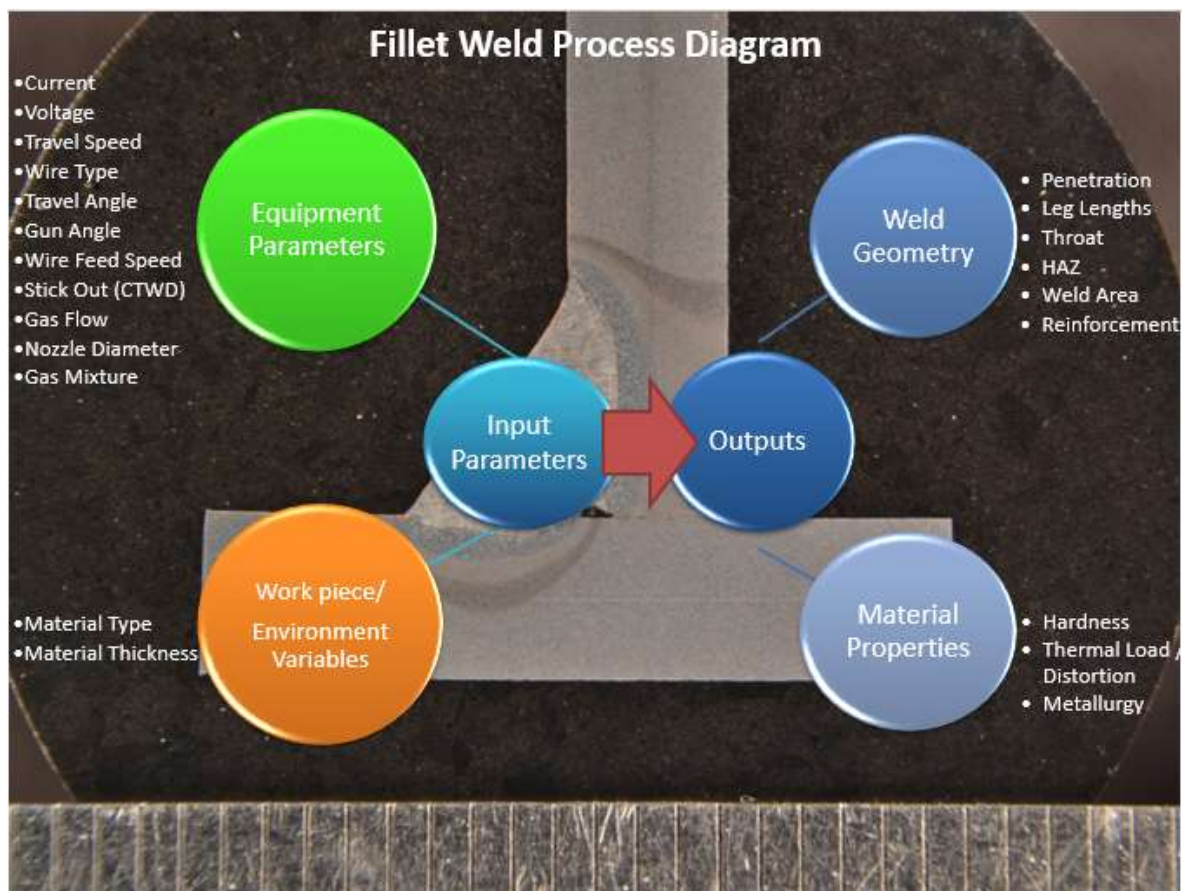


Figure 1-5 GMAW Fillet Weld Process Diagram

The resultant weld geometry is one of the key outputs of the GMAW fillet weld process. Figures 1-6, 1-7, 1-8 and Table 1-1 define the key areas of fillet weld geometry that will be investigated in further detail over the forthcoming chapters. Presently there is no economic technology available to accurately measure the actual internal geometry of a fillet weld without destructively testing the work piece. The external geometry of a fillet weld can be measured easily using specifically designed gauges, but the internal characteristics, such as penetration, cannot be measured as easily. The penetration of a fillet weld [Table 1-1, Figure 1-6] is critical in determining the structural integrity of the weld

Table 1-1 Definitions of key fillet weld geometric features

Geometry	Definition
<b>Bottom (Horizontal) Leg Length</b>	Horizontal distance from the intersection of the baseplate and stiffener to the edge of the fillet weld
<b>Top (Vertical) Leg Length</b>	Vertical distance from the intersection of the baseplate and stiffener to the edge of the fillet weld
<b>Throat</b>	Distance between the root and the centre of the face of the weld
<b>Reinforcement</b>	Size of the convex 'cap' on the top of the fillet weld
<b>Baseplate Penetration</b>	Amount of weld material that has 'penetrated' into the baseplate parent material
<b>Stiffener Penetration</b>	Amount of weld material that has 'penetrated' into the stiffener parent material
<b>Intersect Penetration</b>	Amount of weld material that has 'penetrated' across the intersection of the fillet joint.
<b>Heat Affected Zone (HAZ)</b>	Area of the parent material that has not been melted but has had its microstructure/properties changed by the heat from the weld.

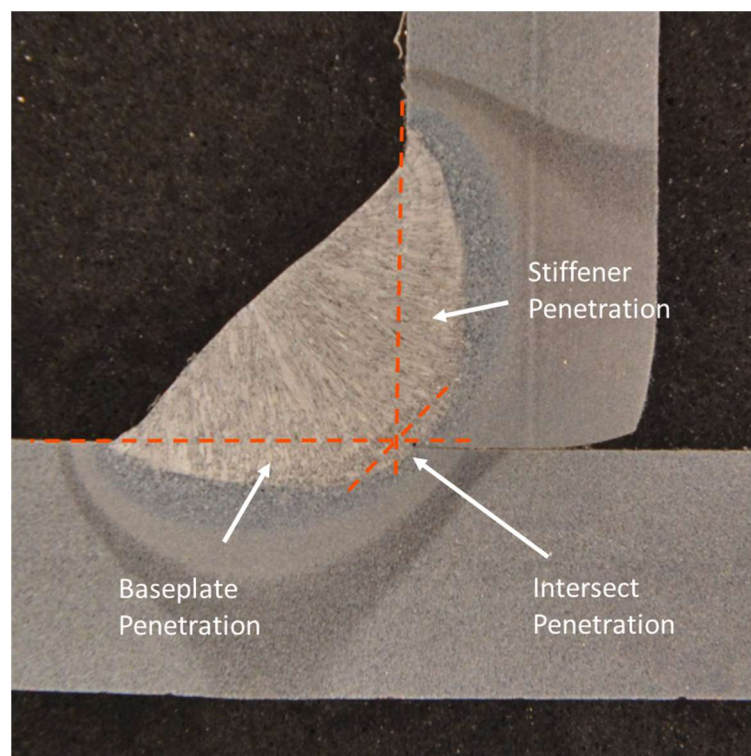


Figure 1-6 Fillet Weld Penetration



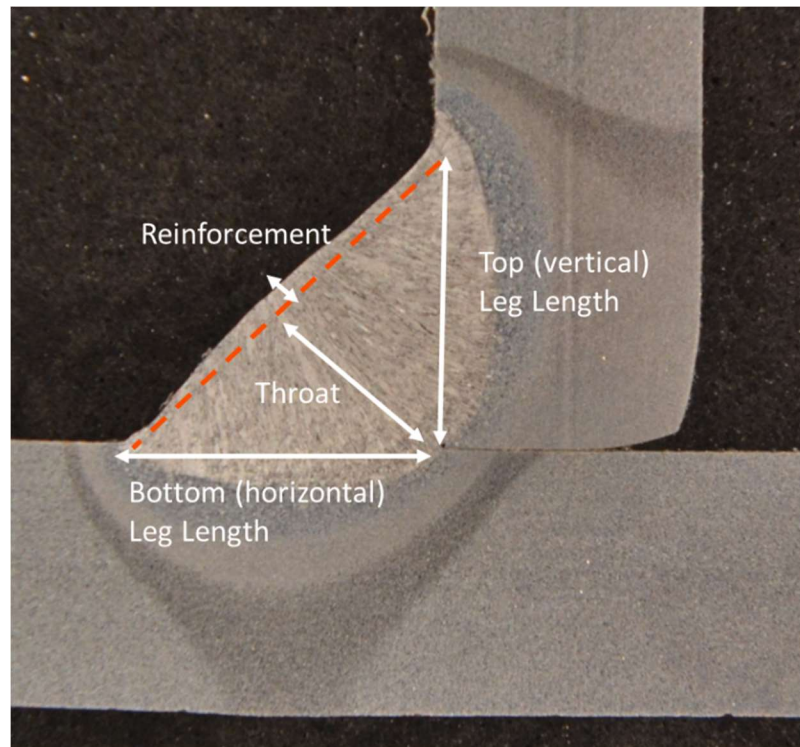


Figure 1-7 Diagram highlighting some of the key fillet weld geometrical features (Leg Length, Throat and Reinforcement)

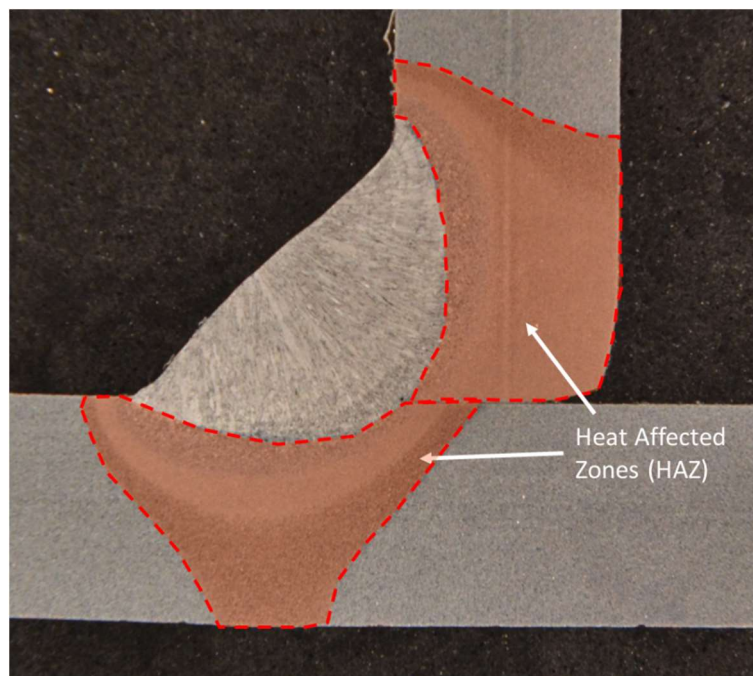


Figure 1-8 Fillet weld heat affected zones (HAZ)

It is important to ensure that the weld penetrates through the intersection of the X and Y axis of the fillet joint as shown in Figure 1-9 [1.6]. Since the actual penetration cannot be easily measured, the only way to be able to ensure satisfactory penetration is through the control of the process parameters.

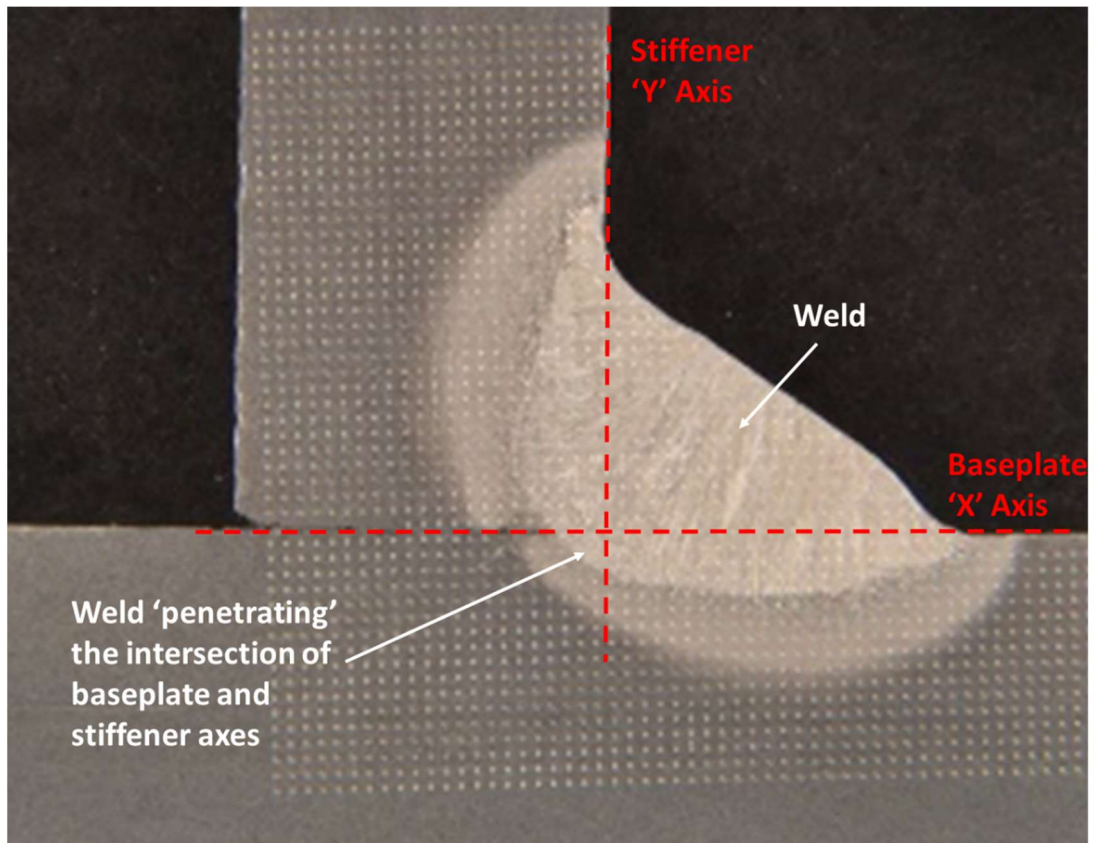


Figure 1-9 Image showing fillet weld 'penetrating' the horizontal (baseplate) and vertical (stiffener) axes

As a result of the difficulty in measuring penetration, structural fillet welds tend to be 'over welded' in order to guarantee that satisfactory penetration is achieved. This results in excessive heat being applied to the structure, increasing distortion and residual stress [1.6]. The welder is faced with a balancing act to try and minimise the heat applied to the joint whilst achieving satisfactory penetration [1.7]. A good understanding of the input parameters and their interactions is therefore critical to achieving a high level of control.

### 1.1.3 Industrial Background

In an increasingly competitive market place there is a great demand for reducing costs and improving productivity. One of the key challenges in naval ship design and manufacture is trying to find the balance between reducing ship weight (reducing plate thickness) and minimising production costs. As plate thickness reduces below 6mm, the amount of distortion increases exponentially as does the associated production costs due to increased levels of rework and alignment activities required to flatten the plates [1.8].



Figure 1-10 Example of a welded panel assembly used in ship construction

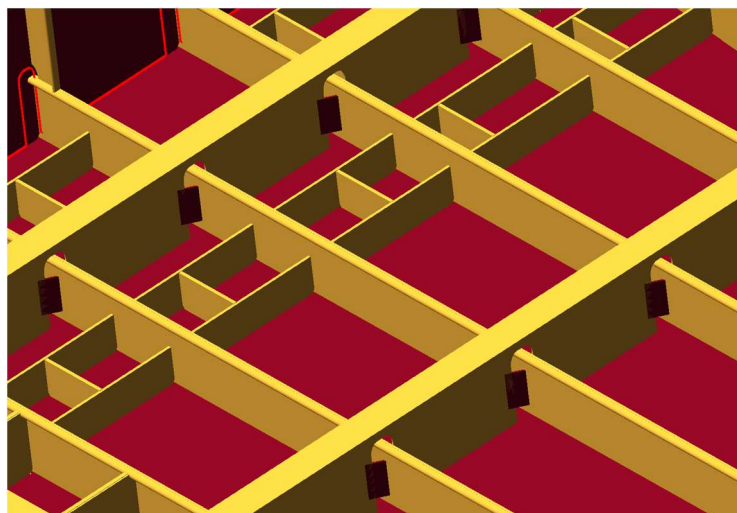


Figure 1-11 CAD Image of welded panel assembly

Fillet welding accounts for more than 80% of the structural welding of a naval vessel and so represents a significant opportunity for improving productivity and reducing levels of distortion and rework. Due to its flexibility, robustness and relatively low costs GMAW fillet welding can be relatively easily automated. Automation provides the opportunity to standardise the quality of welding. Figures 1.10 and 1.11 provide examples of typical flat panel assemblies used in shipbuilding that would benefit from an automated fillet welding process due to the volume of fillet welding. Both figures highlight the large amount of welding that is required in order to connect the stiffeners (bars) onto the flat steel panels. This high concentration of welding (heat) is one of the main causes of distortion in the panel assembly. In order to minimise the heat input to the panel, both the sequence of welding and the control of the welding process parameters need to be considered. Tables 1-2 and 1-3 below shows the results of a short study of a number of welders indicating the parameters they used to complete a series of downhand fillet welds. The variation seen in this study highlights the fact that even within a group of experienced welders there is a high level of variation of the input parameter settings for a relatively simple fillet weld arrangement. There is also significant variation on what is considered the 'optimal' travel angle and highlighting the knowledge gap that exists.

Table 1-2 Welder Survey - Variation in parameter settings for manual welding

<i>Welder</i>	<i>Current (A)</i>	<i>Volts (V)</i>	<i>Heat Input (kJ/mm)</i>
<b>1</b>	204	20.8	0.636
<b>2</b>	224	22.1	0.743
<b>3</b>	238	19.8	0.707
<b>4</b>	236	22	0.779
<b>5</b>	212	21.5	0.684
<b>6</b>	234	22.9	0.804
<b>7</b>	240	24.8	0.893
<b>8</b>	229	24.4	0.838
<b>9</b>	224	22.8	0.766
<b>10</b>	215	24.6	0.793
<b>Average</b>	225.6	22.57	0.764
<b>Min</b>	204	19.8	0.636
<b>Max</b>	240	24.8	0.893
<b>Variation (%)</b>	15.0%	20.2%	28.7%



Welding procedures are used to demonstrate welding process control and provide the welder with the allowable range of parameters that can be used in each specific welding application. Generally welding procedures for GMAW provide information on current, arc voltage, travel speed, wire diameters and electrode extension. Examples of typical welding procedures can be found in Appendix 2.

Table 1-3 Welder Survey – Travel and Gun Angle guidance for different electrodes

<b>Welder</b>	<b>Solid Wire</b>	<b>Flux Core</b>	<b>Metal Core</b>
<b>A</b>	slight push	Pull - prevents slag from running in front of weld pool (pull with slag)	slight push
<b>B</b>		pulling - more turbulence/spatter, more penetration pushing - smoother arc/less spatter, less penetration	
<b>C</b>	pull ~45°	push ~45°	push ~45°
<b>D</b>	push 30°	pull 30-45°	push 30°
<b>E</b>	-	pull - prevents slag from contaminating the weld pool	push
<b>F</b>	45° from baseplate 80° push	45° from baseplate 60/70° pull	45° from baseplate, 60/70° push
<b>H</b>		pushing more unstable, higher volume of spatter	

Weld procedures can allow between 10-15% variation of input parameters which can generate a maximum of 25% variation of heat input being applied to the joint. This provides the welder with a large amount of flexibility, but consequently enables a significant amount of variation in the resultant weld geometry and heat being applied to the joint. One of the main areas of focus of this project is to conduct an analysis of the practical and economic benefits of being able to employ a controlled fillet welding process. In order to exploit fully the benefit of automation, a greater understanding and level of control of the input parameters and their interactions are required. This would provide greater control over the size of the fillet weld, level of penetration and level of heat applied into the assembly.

As previously mentioned, one of the biggest challenges in the design and manufacture of welded structures is around the prediction, mitigation and rectification of distortion. Anecdotal evidence from the shipbuilding industry suggests that the majority of the focus and expenditure tends to be on improving distortion rectification processes (the most expensive solution) rather than focusing on minimising the level of distortion in the first

instance. Weld procedures, as detailed above, provide guidance on the range of acceptable input parameters that ultimately dictates the amount of heat applied to the weld. Improving understanding of what impact the input parameters and interactions have on the quality, geometry and heat input to the weld is key to minimising the amount of distortion.

#### 1.1.4 Fillet Weld Design Standards

Naval Ships in the UK are designed and built to Lloyds Standards (Rules and Regulations for the classification of Naval Ships, Jan 2011) [1.9]. British Standard, BS EN ISO 5817:2003 [1.10], also documents the acceptable quality standards for a fillet weld, including acceptable convexity, asymmetry, throat thickness and penetration.

##### 1.1.4.1 Penetration

British Standard, BS EN ISO 5817:2003, [1.10] provides the following equation for calculating the maximum lack of allowable penetration. This standard was used to assess the quality of the fillet welds during the experimentation and results phase of this project.

$$h_p \leq 0.2 \times a \quad (\text{max } 2 \text{ mm}) \quad \text{Eqn 1.2}$$

Where:  $a$  is the theoretical throat thickness  
 $h_p$  = maximum lack of penetration

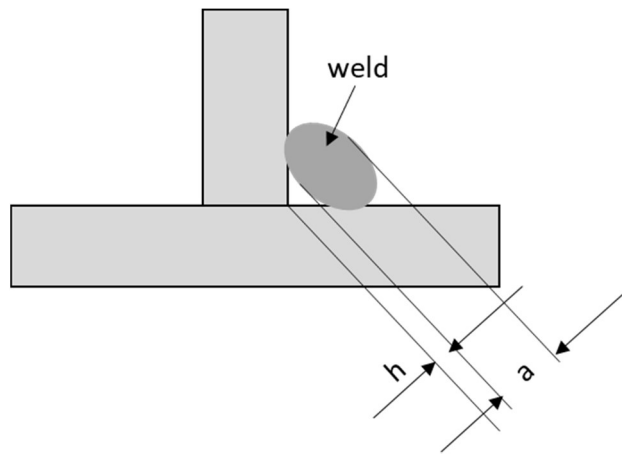


Figure 1-12 Key features required to calculate the maximum lack of allowable penetration in a fillet weld

#### 1.1.4.2 Leg Length

The size of an equal leg fillet weld is the leg length of the largest inscribed right-angled isosceles triangle. Generally, the Leg Length of the weld is to not be less than  $\sqrt{2}$  times the specified throat thickness [1.9]

$$L \geq \sqrt{2} \times T \quad \text{Eqn 1.3}$$

Where: L is the leg length of the fillet weld  
T is the throat thickness

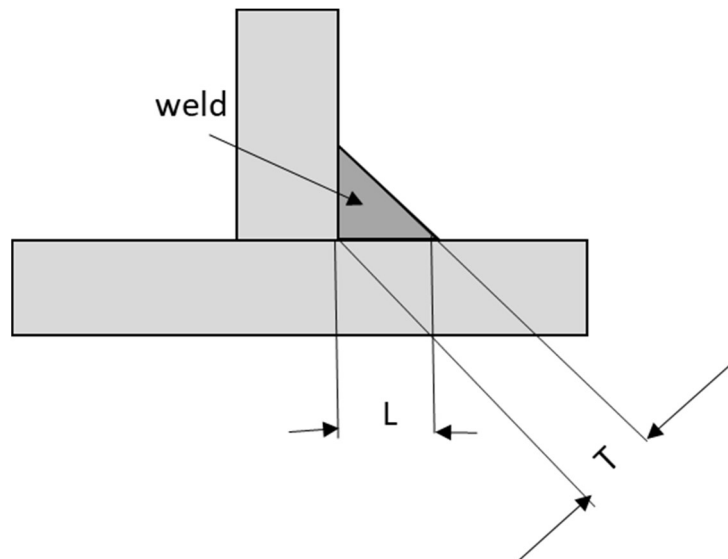


Figure 1-13 Key features required to calculate the acceptable leg length of a fillet weld

The maximum acceptable level of asymmetry (difference between horizontal and vertical leg lengths) of a fillet weld can be calculated using the following equation.

$$h_l \leq 2\text{mm} + 0.2a \quad \text{Eqn 1.4}$$

Where:

- $h_l$  is the difference between horizontal and vertical leg length
- $a$  is the theoretical throat thickness
- $Z_2$  is the vertical leg length
- $Z_1$  is the horizontal leg length

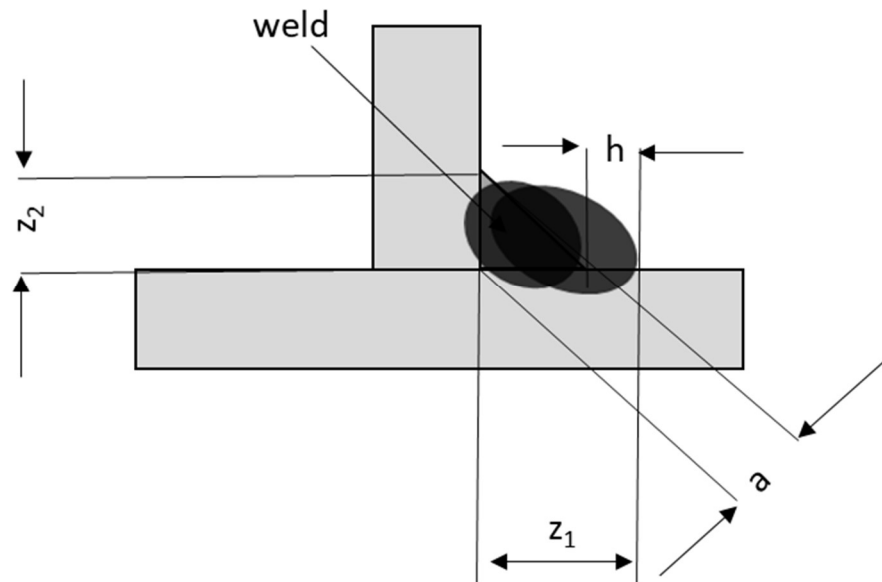


Figure 1-14 Key features required to calculate the acceptable level of leg length asymmetry for a fillet weld

### 1.1.4.3 Throat

The load bearing capacity of a fillet welded joint is based on its throat thickness. For Naval ships built using Lloyds rules [1.9] the acceptable throat thickness can be generally calculated using the following equation.

$$\text{weld throat thickness} = \text{leg length} / 1.41 = 0.71 \times \text{leg length} \quad \text{Eqn 1.5}$$

British Standard, BS EN ISO 5817:2003, [1.10] provides the following equation for calculating the acceptable throat thickness.

$$h \leq 0.3 + 0.1a \quad (\text{max } 2\text{mm}) \quad \text{Eqn 1.6}$$

Where:  $h$  is the difference between the actual and theoretical throat thickness  
 $a$  is the theoretical throat thickness

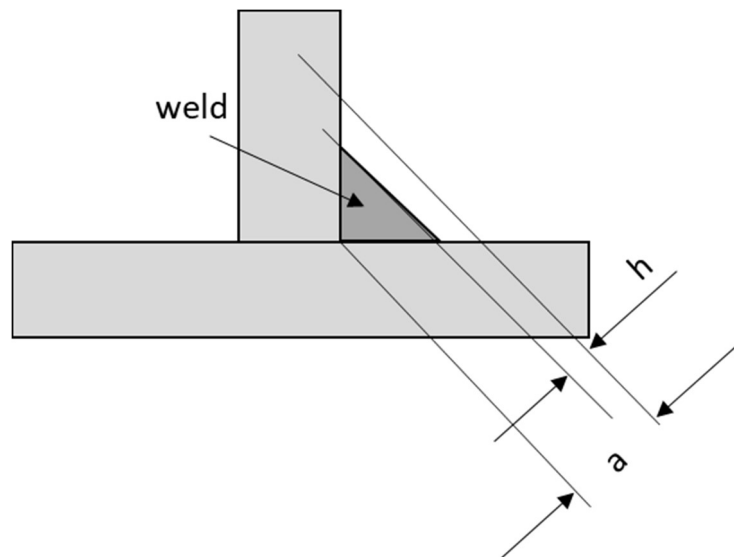


Figure 1-15 Key features required to calculate the acceptable throat thickness of a fillet weld

The load bearing capacity of a fillet weld joint is expressed in terms of stress across the weld throat area [1.11]. Hence the resultant geometry of the fillet weld is critical in determining the load bearing capacity of the joint. Complex calculations have been developed for calculating the theoretical fillet weld design; however, due to the nature of the fillet weld it is almost impossible to measure certain characteristics of the weld, such as penetration, without destructively testing the joint. This makes it impossible to verify the design against the actual weld. Nevertheless the results of the complex and simple fillet weld design calculations are very similar. The simple calculations [Eqn 1.7] define the fillet weld requirement in terms of characteristics which are practicably measurable (throat and length) and so make assumptions on characteristics such as penetration. The weld throat stress can be calculated using the following formula [1.11]

$$\text{Throat Stress} = P / t \times L \quad \text{Eqn 1.7}$$

Where:  $P$  is the applied load  
 $t$  is the weld throat size  
 $L$  is the weld length

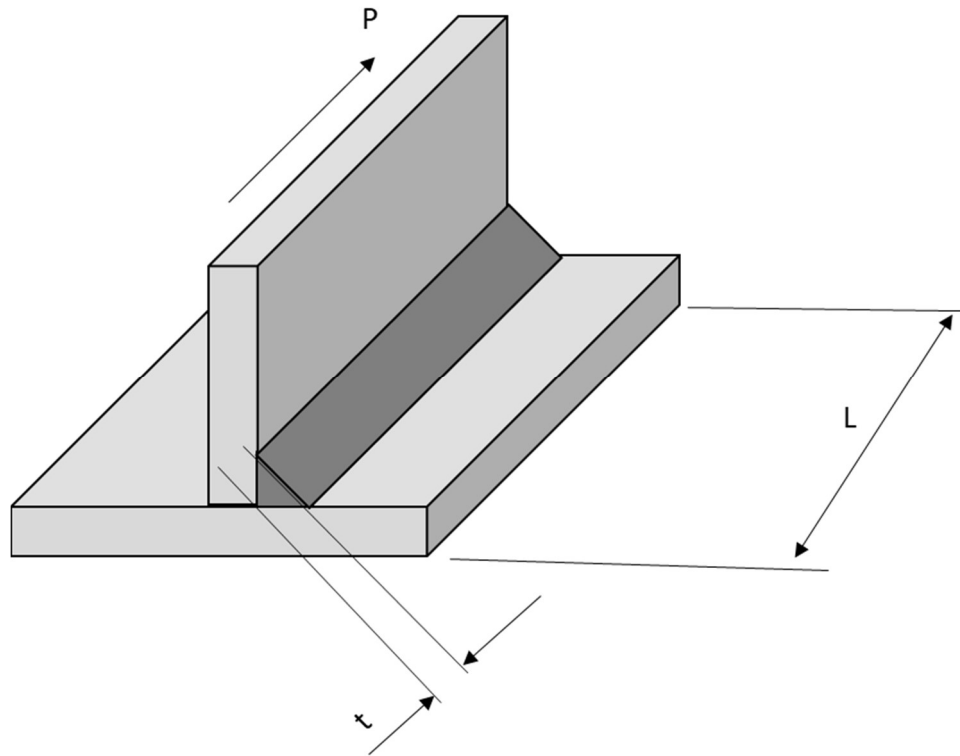


Figure 1-16 Key features of a fillet weld required to calculate throat stress

#### 1.1.4.4 Convexity

The maximum allowable level of convexity of a fillet weld can be calculated using the following equation. The maximum allowable convexity is 5mm.

$$h \leq 1\text{mm} + 0.25b_w \quad \text{Eqn 1.8}$$

Where:  $h$  is the convexity of the weld  
 $b$  is the width of the weld bead



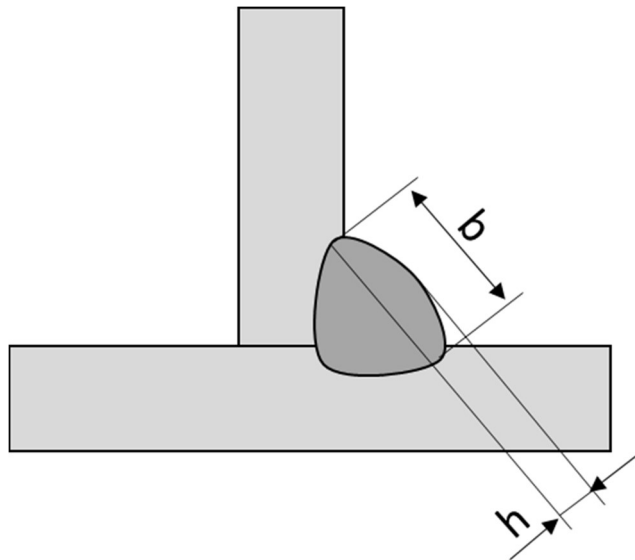


Figure 1-17 Key features required to calculate the acceptable convexity for a fillet weld

#### 1.1.4.5 Undercut

Undercut is a flaw that occurs near the toe of the weld [Figure 1-18], reducing the thickness of the baseplate. Undercut is generally caused by excessive heat input. British Standard, BS EN ISO 5817:2003, [1.10] provides the following equation for calculating the acceptable level of undercut.

$$h \leq 0.2t \text{ (max 1mm)}$$

Eqn 1.9

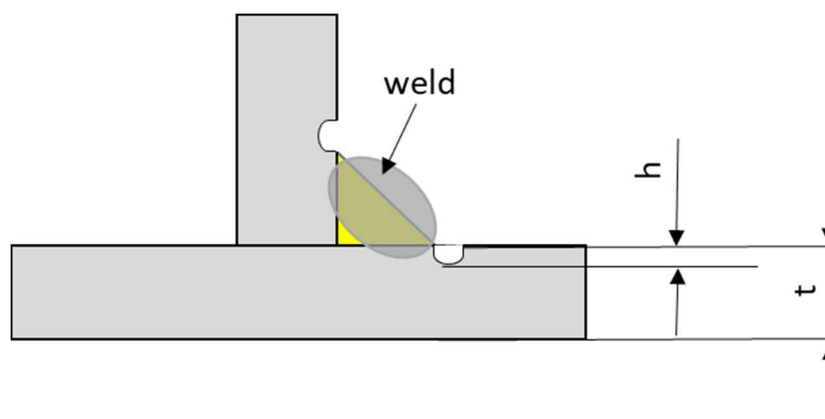


Figure 1-18 Acceptable undercut for a fillet weld

#### 1.1.4.6 Area of a fillet weld

The area of a fillet weld is directly related to the travel speed of the welding torch and the wire feed speed. The relationship is shown below in Eqn 1.10 and Figure 1-19.

$$TS \times A_f = WFS \times T_f \quad \text{Eqn 1.10}$$

Where:  $TS$  is the travel speed  
 $A_f$  = fillet weld area  
 $WFS$  is the wire feed speed  
 $T_f$  = fillet weld throat thickness

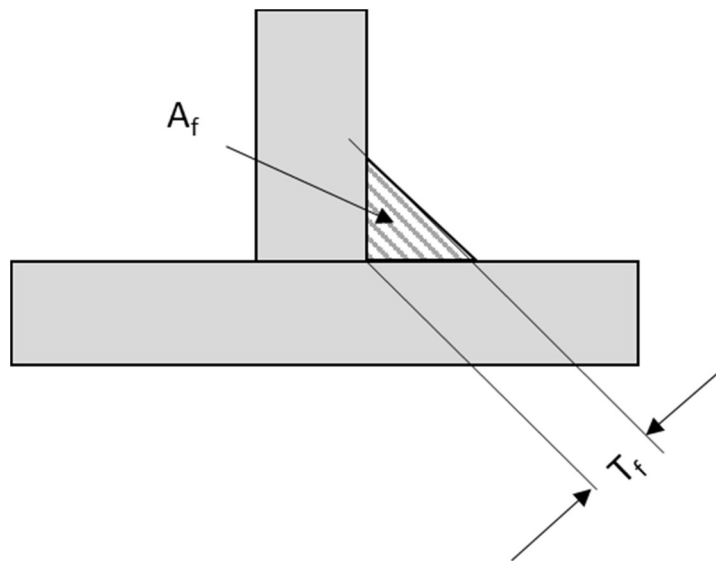


Figure 1-19 Diagram showing fillet weld area and throat thickness

## 1.2 Outline of Research

The research for this study was spilt up into a number of packages. Figure 1-20 below provides an overview of the various methodologies employed and the corresponding parameters investigated.

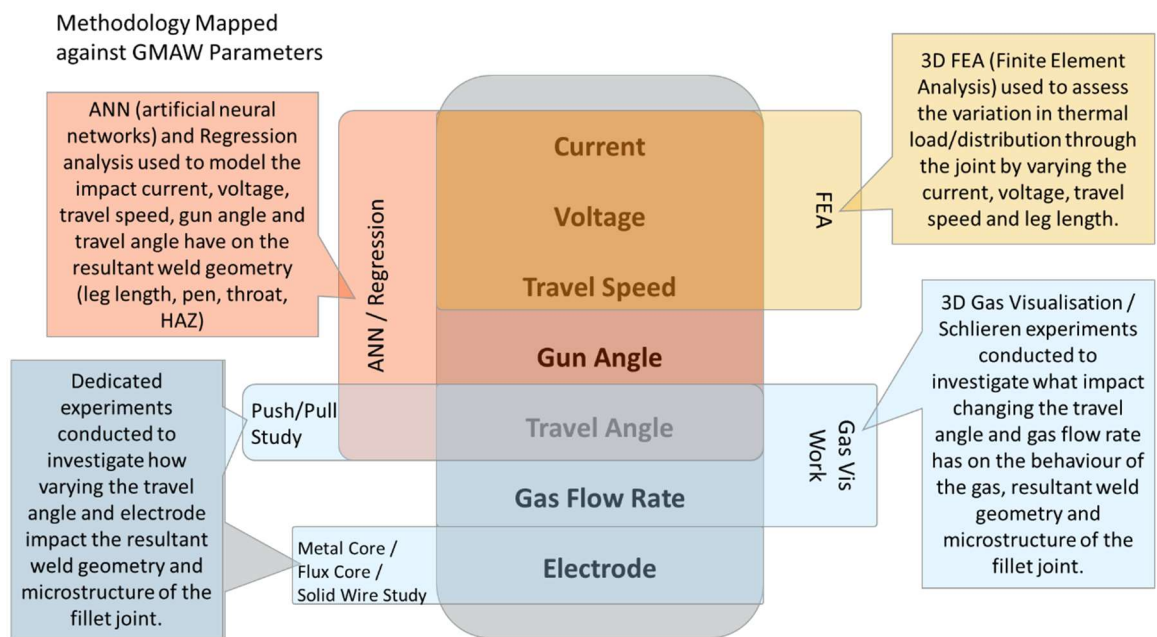


Figure 1-20 Research methodology mapped against fillet weld parameters

The first package of work used Artificial Neural Networks (ANN) [1.12] and Regression Analysis to model the relationship between the following inputs and outputs for the downhand GMAW fillet welding process (Table 1-4)

Table 1-4 Process inputs and outputs used to develop ANN

Inputs	Outputs
Current (A)	Penetration
Voltage(V)	Leg Length (top and bottom)
Travel Speed (m/s)	Throat
Gun Angle (°)	Reinforcement
Travel angle (°) – push/pull	

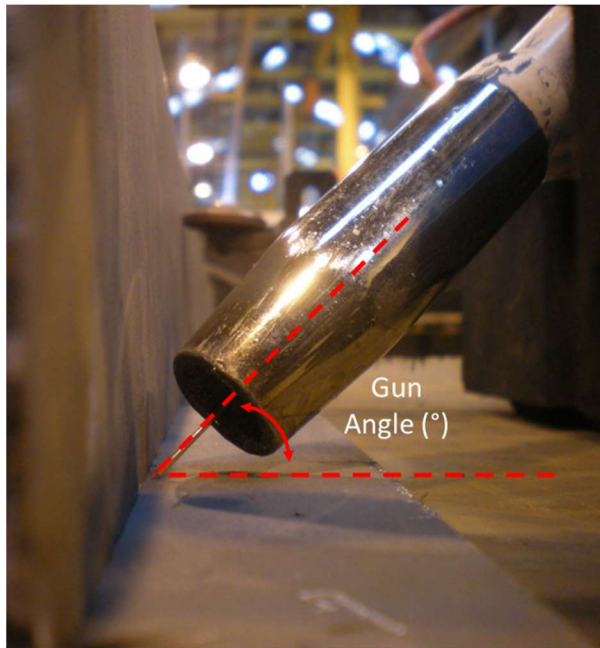


Figure 1-21 Visual definition of gun angle

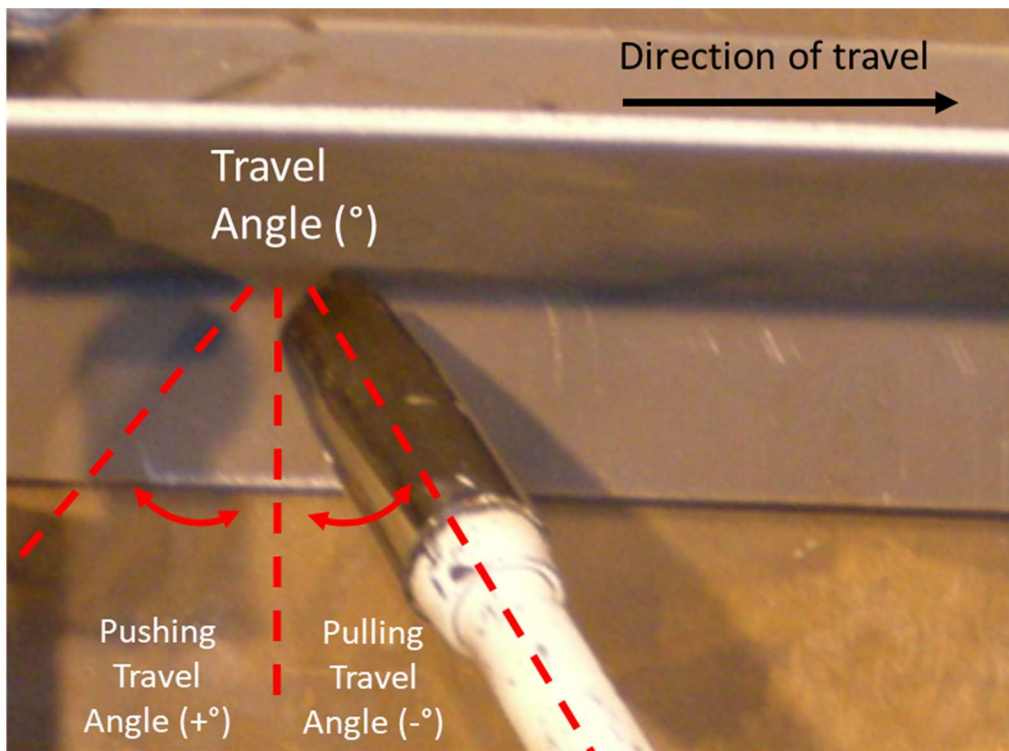


Figure 1-22 Visual definition of travel angle

As will be discussed in the following chapter, there are numerous studies that have successfully used ANN to model the GMAW process. A recent ANN study in 2012 [1.13], specifically focused on fillet welding, proved inconclusive when attempting to model the downhand GMAW fillet welding process. This suggested that there were input parameters that were not being satisfactorily controlled in the dataset used to generate the ANN. This research looks to investigate these 'uncontrolled' parameters in order to generate a stable model and better understand the relationship between the process inputs and outputs. The ANN model was developed using Neurosolutions for Excel and the results from a series of fillet weld experiments. The geometry of the fillet welds was measured using image analysis software, ImageJ, and these results were used to create a model which would be able to predict the geometry of the fillet weld given a series of input parameters. The model was also used to identify how significant each of the input parameters is in determining the various geometrical characteristics of the fillet weld. One of the limitations of ANN [1.14], is that it does not explain patterns and does not always find the optimal solution. In order to validate the results of the ANN a statistical regression analysis was also used to model the relationship between the same GMAW process parameters identified in Table 1-4. Regression Analysis has been used in this instance to verify that the results of the ANN are aligned to the statistical relationships between the inputs and outputs and to help explain the interactions between the parameters.

The gun angle and travel angle are two parameters that are generally left up to the experience and preference of the welder. As will be identified later on, the guidance available on the ideal torch set up angle differs depending on who you speak to and can be confusing depending on what process, material, electrode and shielding gas is being used. Within this package of work all parameters were kept constant apart from the gun and travel angle. The aim was to understand what impact the torch orientation had on the resultant geometry and metallurgical structure of the fillet weld. The heat input, shielding gas, electrode and material thickness were all kept constant. Also included within the phase of the project was a GMAW process capability analysis which compared the capability of both the semi-automatic and robotic GMAW fillet welding processes.

The purpose of the second section of the project was to develop an FEA model which can predict the impact of varying the vertical and horizontal leg lengths has on the thermal load/distortion of a fillet welded joint. As previously mentioned, one of the biggest

challenges faced in the fabrication of steel structures is controlling the level of distortion. It is widely understood, through numerous studies [1.17], that the level of distortion in a steel structure or panel is directly related to the amount of heat applied. However, from a practical perspective it is not always immediately obvious exactly what impact altering each of the input parameters individually has on the thermal load that is applied to the structure. Finite element modelling is commonly used to model the thermal and mechanical effects of the GMAW process [1.8]. The FEA model would also be used to assess what the individual impact each of the input parameters (current, travel speed, voltage) has on the resultant thermal load on the fillet welded joint.

The third package of work was focused on understanding what impact the consumable electrode has on the geometry and metallurgical structure of the fillet weld. As mentioned in Chapter 1.1.1, the consumable electrode wire is a key feature of the GMAW process. There is a variety of electrode wire types that can be used in the GMAW process. Generally, the three main types of electrode that are utilised within shipyards are solid wire, flux cored wire and metal cored. The chemical composition for each type of electrode can be found in Chapter 3.6. Each wire has its own characteristics and the choice of wire is dependent on the welded application. This study will be investigating what impact changing the type of electrode has on the resultant geometry and structure of the fillet weld (controlled for energy/heat input).

The fourth section of the research was focused on improving an understanding of how the shielding gas behaves in a fillet weld configuration. The shielding gas is a key component of the GMAW process as described in Chapter 1.1.1 and for a shipbuilder welding shielding gas costs represent an important and significant expenditure. (A 50% reduction in the shielding gas flow rate will generate in the region of £100k saving per annum). Generally, the recommended gas flow rate settings are not application specific (e.g. the shielding gas flow rate is the same for butt welds and fillet welds). Fillet welds by their nature provide a level of self-shielding due to the presence of the vertical stiffener. This study will investigate the behaviour of the shielding gas around the fillet welded joint with a view to understanding if the gas flow rate can be reduced without compromising the quality of the joint or the robustness of the process. The study assesses what impact the gun angle, travel angle and gas flow rate have on the behaviour of the shielding gas during the fillet weld process. It also looks to determine what impact, if any, the presence of the vertical plate/stiffener in

the fillet configuration has on the behaviour and coverage of the shielding gas. Bitharis et al [1.15] and Beyer et al [1.16], demonstrated that the shielding gas flow rate could be reduced to 12l/min for GMAW butt welds without compromising the quality of the weld. Bitharis et al [1.15] also used Schlieren imaging to successfully validate the results from MHD (magneto hydrodynamic) FE model for GMAW butt welds. The analysis detailed herein aims to understand the behaviour of the shielding gas for fillet welds (an area where there appears to be little previous work) by using the same Schlieren visualisation and MHD modelling technique. This was a particularly challenging experimental set up and has not been reported on previously.

### 1.3 Summary

There have been numerous publications and also studies undertaken on the subject of controlling GMAW weld parameters and resultant geometry. However, as Figure 1-5 shows, the large number of input parameters and variables makes it extremely challenging to understand exactly what impact the variation each of the inputs (and their interactions with each other) has on the resultant fillet weld. What is clear is that in order to maintain consistent quality fillet welds it is critical to understand the extent to which each of these input parameters, and their interactions, affects the resultant outputs. Furthermore, if a robust process control model can be developed which can demonstrate tight control of the parameters and interactions which affect the joint geometry, then confidence can be increased that sufficient penetration is being achieved whilst heat input and distortion is minimised. Although the GMAW welding process is a mature and generally well understood process, there is little/no evidence of research specifically focused on understanding what impact the travel angle, gun angle and parameter interactions have on the resultant fillet weld geometry and structure. The research detailed within this thesis is focused on:

- Identifying the critical input parameters and interactions for GMAW downhand fillet welding
- What relationship the welding torch position/angle, relative to the workpiece has on the resultant fillet weld
- What impact the variation in weld leg length has on the thermal load and distortion of the welded joint

- Developing a robust model that can be used to support the development and optimisation of fillet weld procedures
- Understanding and optimising the overall GMAW fillet weld process costs

## 1.4 References

- 1.1. Naidu, D. S., Ozcelik, S., & Moore, K. L. (2003). Modeling, Sensing and Control of Gas Metal Arc Welding. In *Modeling, Sensing and Control of Gas Metal Arc Welding*. <https://doi.org/10.1016/B978-0-08-044066-8.X5000-9>
- 1.2. Moravec, J., Rohan, P. (2011). Influence of different gas-shielded types on weld pool's geometry for MIG welding method. METAL 2011, Brno, Czech Republic.
- 1.3. Campbell, S. W., Galloway, A. M., & McPherson, N. A. (2012). Artificial neural network prediction of weld geometry performed using GMAW with alternating shielding gases. *Welding Journal*, vol.91, no.6. June 2012. Supplement: Welding Research. pp.174s-181s, ISSN: 0043-2296
- 1.4. American Welding Society. (2004). Welding handbook volume 2: welding processes, part 1. In *American Welding Society - AWS*.
- 1.5. Lincoln Electric. *Constant Current vs. Constant Voltage Output*. [online] available at <https://www.lincolnelectric.com/en-gb/support/process-and-theory/Pages/constant-current-vs-constant-voltage-output.aspx>
- 1.6. BSI. (2007). BS EN ISO 5817:2007 Welding — Fusion-welded joints in steel , nickel , titanium and their alloys ( beam welding excluded ) — Quality levels for imperfections. *BSI Standards Publication*.



- 1.7. Rosenthal, J. W. (2001). Ten steps to reducing your welding costs. *Welding Journal (Miami, Fla)*.
- 1.8. Gray, T., Camilleri, D., & McPherson, N. (2014). Control of Welding Distortion in Thin-Plate Fabrication: Design Support Exploiting Computational Simulation. In *Control of Welding Distortion in Thin-Plate Fabrication: Design Support Exploiting Computational Simulation*. <https://doi.org/10.1533/9780857099327>
- 1.9. Lloyds' Register, Rules and Regulations for the classification of Naval Ships, Jan 2011, Volume 1, Part 6, Chapter 6, Section 4, pp11-17.
- 1.10. BS EN ISO 5817:2003 Welding — Fusion-welded joints in steel, nickel, titanium and their alloys (beam welding excluded) — Quality levels for imperfections
- 1.11. Hicks, J. (2001). *Welded Design: Theory and Practice*, Woodhead Publishing, ISBN 9780815514749
- 1.12. Bhadeshia, H. K. D. H. (1999). Neural networks in materials science. *ISIJ International*. <https://doi.org/10.2355/isijinternational.39.966>
- 1.13. Beckett, S., MacPherson, M. J., McPherson, N. A. (2011). Improved welding control of automated fillet welding for ship structures using Artificial Neural Networks (ANN). JOM 16 Conference, Denmark.
- 1.14. Navarro, H., Bennum, L. (2014). Descriptive examples of the limitations of Artificial Neural Networks applied to the analysis of independent stochastic data. *International Journal of Computer Engineering and Technology*.
- 1.15. Bitharis, I., McPherson, N. A., McGhie, W., Roy, D., & Moore, A. J. (2018). Visualisation and optimisation of shielding gas coverage during gas metal arc welding. *Journal of Materials Processing Technology*. <https://doi.org/10.1016/j.jmatprotec.2017.11.048>
- 1.16. Beyer, V., Campbell, S. W., Ramsey, G. M., Galloway, A. M., Moore, A. J., & McPherson, N. A. (2013). Systematic study of effect of cross-drafts and nozzle

diameter on shield gas coverage in MIG welding. *Science and Technology of Welding and Joining*. <https://doi.org/10.1179/1362171813Y.0000000143>

- 1.17. McPherson, N.A., Galloway, A.M., & McGhie, W. (2013). Thin plate buckling mitigation and reduction challenges for naval ships. *Journal of Marine Engineering and Technology*. <https://doi.org/10.1080/20464177.2013.11020282>

## Chapter 2 Literature Review

### 2.1 Introduction

This chapter reviews the various studies and developments that have been undertaken over the years in order to improve the understanding of the key parameters of gas metal arc fillet welding (GMAW). The first section of the review will include an analysis of a variety of methodologies that have been employed to analyse the GMAW process. This section will be specifically interested in the design and architecture of the models used, the range of process inputs and outputs considered and what relationships were identified. The second section will focus on reviewing studies into some of the GMAW process inputs. This includes the guidance relating to the setting of the torch travel and gun angles, studies looking at the impact of the shielding gas flow rate and examples of the input parameter guidance provided on weld procedures. The third section will focus on studies into the main process outputs of the GMAW process; geometry, mechanical properties and temperature distribution/distortion. The fourth section is focused on assessing the breakdown of costs for the GMAW process. This section will be comparing different approaches employed for breaking down the process into its constituent cost elements and also provide a benchmark against which to compare the results detailed within the later chapters.

### 2.2 Identification of Key GMAW Parameters – Methodologies

As highlighted in Chapter 1, gas metal arc welding (GMAW) is a widely used welding process and is consequently an extensively researched process. Benyounis et al [2.1] conducted a review of the different approaches employed to analyse and optimise the welding process. The approaches reviewed included Artificial Neural Networks, Genetic Algorithms (GA's), Response surface methodology (RSM), Taguchi and factorial design. The study concluded that combining two optimisation techniques is beneficial and would provide good results for identifying optimal welding conditions.

### 2.2.1 Artificial Neural Networks (ANN)

There are numerous examples of studies whereby an ANN approach has been used to analyse the GMAW process. Campbell et al [2.2] developed an ANN Model to simulate the impact that alternating shielding gases has on the geometry of a fillet weld. The welding process variables considered were current, voltage, travel speed and shielding gas frequency and the measured output geometry was the leg length, penetration and throat thickness. The welding torch orientation was not considered as one of the key input parameters and there did not appear to be any consideration made as to the effect of interacting input parameters. Dadgar [2.3] used Matlab to successfully develop an ANN to predict the penetration of a weld bead using 5 input variables (current, travel speed, voltage, nozzle to plate distance and torch angle). This study is limited to bead on plate experiments and does not clearly articulate whether it is the travel angle or gun angle that is being controlled and so it is difficult to extrapolate the results for a fillet weld configuration. Nagesh and Datta [2.4] used ANN to model the link between GMAW input parameters (wire feed speed, arc power, voltage, current, arc length and travel speed) and weld geometry (bead height, bead width, depth of pen and area of pen). Only 18 experiments were used to test and train the model. This would appear to be quite a small dataset considering the number of input/output variables being analysed. The study also does not take into account the torch or travel angle. Beckett et al [2.5] demonstrated that it was possible to develop a robust ANN model with a low volume of test data for vertical fillet welding. The research also suggested that downhand fillet welding was more sensitive to torch position than vertical (which used an oscillator) and that further work would be required to understand the criticality of the travel angle. Chan, Pacey and Bibby [2.6] also demonstrated that weld bead geometry can be accurately modelled by using an ANN approach for GMAW. Their investigation also suggests that the technology can be extended to other welding processes. However, the study was based on the results of bead on plate experiments so do not fully represent many of the practical challenges faced in a production environment. Also, the travel angle and parameter interactions did not appear to be taken into consideration.

## 2.2.2 ANN + Mathematical Modelling Approach

Moon and Na [2.7] considered the effects of using a mathematical model and ANN to identify the optimal welding process variables for GMAW. The main emphasis was on current, voltage, speed, offset distance and gas flow. However, the analysis did not consider either the torch geometry or the combination effect of process variables on control of the fillet weld. The analysis also only considered shielding gas flow rates of 14l/min and 18l/min, so can only provide guidance on the impact of the shielding gas flow rate over this narrow range. Nagesh and Datta [2.8] also described an approach of using design of experiments (DOE), Artificial Neural Network (ANN) and a Genetic Algorithm (GA) to model the parameters of the GMAW fillet weld process. The key characteristics of the fillet weld which were investigated were leg length, penetration, throat thickness and reinforcement height. The welding process variables analysed were welding speed, current, arc voltage, shielding gas flow rate and offset distance. It was also observed that the predicted results are in good agreement with the experimental values if both main and interaction effects are considered rather than just the main effects. However, the relatively small data set generated would provide limited opportunity to fully understand the impact of any interactions. Kumar and Debroy [2.9] established a model, using a genetic algorithm and ANN, which can calculate the welding conditions needed to obtain a target weld geometry, for GMAW fillets. The inputs to the model were current, voltage, welding speed and wire feed speed. The outputs (weld geometry) of the model were penetration, throat and leg length. Kim et al [2.10] demonstrated that it is possible to model the GMAW process using regression analysis and neural networks. However, the travel angle, gun angle, wire type and gas flow have not been considered and the experimental data was produced using bead on plate experiments and so they do not fully consider the practical challenges of welding in a production environment. Nagesh and Datta [2.11] used a combination of regression analysis and ANN to predict weld geometry from experimental input parameters. One of the outcomes of this study suggested that interactions (of process input variables) are critical as results were more accurate when impact of interactions were included. However, the results of only 16 experiments were used to develop the model based on a relatively small number of experiments to fully assess the interactions of all the input parameters.

### 2.2.3 Finite Element Modelling

Finite element analysis (FEA) is a common approach employed to model the GMAW welding process. Although the principles of FEA software are standard, there are some specific considerations when modelling a GMAW fillet weld. When developing a thermo-mechanical FEA model, there is a decision to be made regarding whether to employ either an uncoupled or coupled simulation. An uncoupled approach first calculates and saves the temperature profile of the structure as the arc (heat source) travels along the length of the joint. Once all of the temperatures have been calculated, the simulation is re-run as a mechanical model where all of the pre-saved temperatures are applied step by step to the model so that mechanical loads (as a result of the heat) can be calculated. The alternative is to run a coupled approach. This involves calculating both the thermal profile and then mechanical loads for each step of the process before moving onto the next step. The coupled approach more closely reflects the real life process; however, it tends to be more complex and time consuming to solve. The Uncoupled method is simpler and faster. Mollicone et al [2.12] created an FEA model to predict the residual stress of GMAW Butt and Fillet Welds. Investigation was focused on 6mm thick steel plates and utilised an uncoupled approach whereby the thermal loads were first calculated and then input into an elastic plastic mechanical simulation. Frazer Nash [2.13] also utilised an uncoupled approach as part of their study to simulate the impact of the reduction of the size of a fillet from 4.5mm to 3.5mm has on the resultant distortion of a fillet welded T-Joint.

There are also three common approaches, discussed by Gray et al [2.14], for modelling the heat input for the welding process. These approaches are:

- Applying the heat flux to a specific surface area within the model
- Inserting elements into the model at a specific temperature
- Applying heat generation to defined elements within of the weld volume

Gray et al [2.14] highlight that the difference in outcomes for each of these approaches is not very significant and at distances, even close to the weld, there is a little difference between the minimum and maximum temperatures. The authors conducted the majority of simulations using a volumetric heat source because firstly it is relatively easy to implement

as the element sizes and heat input can be easily matched to known sizes and parameters and secondly the heat input can be easily calibrated by adjusting the efficiency factor.

One of the main challenges faced when modelling a welding process is how to simulate the addition of material (weld metal) into the model as the joint is welded. The simulation of the addition of the weld metal is important to ensure that both the thermal and mechanical responses from the model are as close to real life as possible. In order to achieve this an element birth and death functionality can be utilised. Camilleri, Gray and Nash. [2.15] and Mollicone et al [2.12] both demonstrated the successful use of element birth and death to simulate weld disposition with an FEA model.

The geometry of a fillet joint provides some additional modelling complications. Due to the natural geometry of the joint and lack of symmetry, there is no opportunity to simplify the model by splitting it in half. Compared to a butt welded joint, a fillet welded joint has more conduction paths and so will usually require a 3D analysis in order to accurately model the process. The interface between the stiffener and baseplate also needs to be considered. Gray et al [2.14] advise that if the interface is not intimately bonded then the modelling assumption should be to assume no heat transfer across the interface. Camilleri et al [2.15] also successfully simulated the thermal gap by unmerging nodes at the boundary between the baseplate and stiffener.

### 2.3 GMAW Process Inputs

There are many sources of guidance on input parameter selection for GMAW, in both academic and industrial publications. However, on closer inspection, the wealth of guidance on offer can be confusing and at times contradictory.

### 2.3.1 Welding Torch Angle (gun angle and travel angle)

The following examples, taken from a mixture of supplier’s websites, technical documentation and academic publications, highlight the level of variation and the complexities involved in trying to identify exactly what the optimum gun and travel angles are for GMAW fillet welding. Miller Electric [2.16] advise that a pushing travel angle of between 5°-15° produces less penetration, flatter bead and a more stable process. BOC [2.17] also advise that for metal cored GMAW a pushing travel angle should be used; but, the angle should be between 20°-30°. Esab’s online handbook [2.18] confirms that a forehand (pushing) technique reduces the penetration and bead width of the resultant weld however recommends a backhand (pulling) technique in order to reduce spatter and produce a more stable arc. Lincoln Electric [2.19] also advise using a ‘pulling’ angle of between 20°-30°. Harwig [2.20] advises that higher deposition rates can be achieved with a 15° ‘pushing’ travel angle, however Bhattacharya [2.21] advises that in general ‘pushing’ reduces deposition efficiency.

Table 2-1 Comparison of Torch Travel Angle Guidance

SOURCE [REF]	LINCOLN ELECTRIC [2.19]	ESAB [2.18]	MILLER ELECTRIC [2.16]	BOC [2.17]	HARWIG [2.20]	BHATTACHARYA [2.21]
TRAVEL ANGLE GUIDANCE	<b>Pulling 20°-30°</b>	<b>Pulling recommended to reduce spatter</b>	<b>Pushing 5°-15° (&gt;25° creates more spatter)</b>	<b>Pushing 20°-30°</b>	<b>Pushing 15° - higher deposition rates</b>	<b>Pushing reduces deposition efficiency</b>
SHIELDING GAS COMPOSITION	<b>Did not specify</b>			<b>100% CO<sub>2</sub> or ArCO<sub>2</sub></b>	<b>Ar/CO<sub>2</sub> (90/10)</b>	<b>Argon</b>

The range of gun angles also varies depending on what publication is being referred to. Lincoln Electric [2.19] recommends using a gun angle of less than 45° and BOC [2.17] a gun angle range of 30°-40°. Tham et al [2.22] also conducted investigations using a fixed gun angle of 45°. As mentioned earlier, Bhattacharya [2.21] investigated what impact the torch travel angle had on the weld deposition efficiency and resultant plate distortion for pulsed GMAW Butt Welds. 3 travel angles were investigated (25°push, perpendicular and



25° pulling) at 3 different voltages (21.5V, 24.5V and 27.5V) all other parameters were being kept constant. The study provided evidence of a definite interaction between travel angle, peak voltage, distortion efficiency, transverse shrinkage and angle distortion. However, further investigation is required to analyse the interactions and to assess if results are applicable to fillets as well as butt welds. Allen et al [2.23] used polynomial regression analysis to develop a method for identifying process settings for robotic GMAW sheet metal. The work highlighted that the gun angle and root opening had an impact on the achievable travel speed and suggested that shielding gas composition, travel and gun angle should be included in any related future work.

### 2.3.2 Shielding Gas Behaviour for Fillet Welds

As discussed in Chapter 1, the shielding gas is a critical element of the GMAW process. Campbell et al [2.2] investigated the impact of alternating the shielding gas, between Argoshield and Helium, during welding. The study determined that increasing the frequency at which the shielding gases were alternated increased penetration and throat thickness of the weld. Beyer et al [2.24] also demonstrated that it is possible to reduce the shielding gas flow rate down to around 9l/min for butt welds without compromising the final weld quality. These studies were focused on downhand butt welds and so further investigation would be required to assess if the gas flow rate could be reduced further for fillet welds due to the inherent shielding provided by the 'upright' (stiffener). Bitharis et al (2.25) conducted a visualisation analysis, using a Schlieren set up, to assess the gas flow around a GMAW Butt Weld. Both 80% Ar/20% CO<sub>2</sub> shielding gas, and 86% Ar/12% CO<sub>2</sub>/2% O<sub>2</sub> shielding gas were used during these experiments. The study indicated that the torch standoff had no significant impact on the oxygen concentration around the weld as long as there was sufficient gas flow to cover the weld. The study indicated that the flux cored electrode produced better shielding coverage than the solid wire electrode. It was concluded that the presence of the flux provides additional shielding around the weld at lower gas flow rates. This study was again focused on butt welds so further analysis would be required to assess the behaviour of the shielding gas around a fillet weld and if the gas flow rate could be reduced even further for fillet welds. There have been studies focused on identifying how low the gas flow rate can be reduced without compromising the shielding around the weld.

Results have shown that the gas flow rate can be reduced significantly. However there has been limited work carried out on the gas visualisation of a fillet weld and what impact the gas flow rate has on the resultant weld shape.

### 2.3.3 Process Efficiency

As described in Chapter 1.1.1, the heat required for the GMAW process is generated by an electric arc. Consequently, the thermal efficiency of the arc produced during the GMAW process is critical in determining the amount of heat that is applied to the welded joint. In comparison with other welding process GMAW is reasonably efficient. There has been a number of studies focused at understanding what the arc efficiency is for GMAW. Du Pont [2.26] conducted an investigation on the melting efficiency of different welding processes. The study concluded that the arc efficiency for the GMAW process was  $0.84 \pm 0.04$ . The results also highlighted that the efficiency of the arc did not vary significantly over the range of currents investigated (230A-375A). Singh [2.27] states that the GMAW process efficiency is within the range of 75%-93% (mean – 85%). This range allows for a variety of external and environmental factors (ambient temp, presence of cross drafts, condition of consumables, length of cable, etc.) which will determine the actual resultant efficiency. Haelsig [2.28] conducted a study to assess the effective efficiency of various gas shielded arc welding processes. This work challenged that for GMAW previous assumptions for effective efficiencies were not ‘meaningful’ and could provide misleading results. The results produced a range of efficiencies for the GMAW process, depending of the method of transfer: Dip – 0.85, pulsed – 0.77, spray – 0.69. The study also investigated what impact the shielding gas had on the effective efficiency. Of all the shielding gases investigated only Helium had a positive influence on the efficiency. The % of CO<sub>2</sub> in the Argon shielding gas had no significant impact on the effective process efficiency for GMAW. The research contained herein does not purport to challenge or further investigate the thermal efficiency of the GMAW process.

### 2.3.4 Weld Procedures

Welding procedures are commonly used to identify the range of parameters that are to be used in order to achieve an acceptable weld for various weld processes and configurations. BS EN ISO 15614 [2.29] defines the specification for developing a welding procedure.

Typically weld procedures specify the following:

Material specification, thickness, Welding Process, position, no of runs, Electrode material and thickness, shielding Gas type and flow rate, current, voltage, preheat temperature, travel speed.

Appendix 2 provides some examples of the type and range of parameters captured within welding procedures. It can be noted that gun angle, travel angle and parameters interactions are not identified/referenced on any of these procedures. The procedures also do not identify which parameters the welders should prioritise on controlling.

## 2.4 GMAW Process Outputs

### 2.4.1 Geometry

There are numerous studies focused at understanding how the GMAW input parameters influence the resultant geometry. Miller [2.30] documented some thoughts on penetration achieved during fillet welding. The author considers that if a weld has penetration beyond the root, then the leg length can be reduced and the same weld strength can be achieved. He also claims but does not prove that the quantity of filler wire can be reduced but gives no figures to reinforce the statement. It is considered that designers could use the increase in throat thickness to reduce leg length requirements. However, this assumes that a consistent weld can be obtained. In effect he is stating that all variables will be under control. This highlights the potential benefits that can be achieved by having good understanding and control of weld parameters and the resultant geometry. Kaewsakul [2.31] conducted a study focused on identifying the impact that current, voltage and travel speed have on the resultant penetration for 2.5mm thick steel plate. The study concluded that the depth of penetration increases as both the current and voltage increases, but that the current has a more significant impact (x2.5). However, the limitations with these results

are that the travel angle, gas flow rate, wire feed speed and electrode were all kept constant so only a subset of the key input parameters were investigated and so any potential critical interactions were not taken into consideration. Nagesh and Datta [2.8] confirmed the importance of parameter interactions as the results were more accurate when the impact of interactions were included. Travel and Gun angles were also not considered as part of this study; thus further experimentation would be required in order to fully understand the impact of the interactions and also the significance of the torch orientation. Campbell et al [2.2] reported that the travel speed is the most influential parameter when predicting geometry. Nagesh and Datta [2.4] created an ANN mode that showed that the welding current was significant in controlling both the bead width and penetration. Moon and Na [2.7] reported that the speed current and voltage determined the weld shape and Nagesh and Datta [2.8] found that the welding speed, current and arc voltage were the dominant variables in determining fillet weld joint shape. Yadav et al [2.32] reported that an increase in voltage resulted in increased penetration.

#### 2.4.2 Thermal and mechanical impact of GMAW Process

The following section provides a review of studies into the thermal and mechanical outputs of the GMAW process. Pal et al [2.33] established that the arc power was higher for both pushing and pulling when compared to a perpendicular travel angle. The pushing travel angle also had a reduced deposition rate, mainly due to increased levels of spatter and as a consequence had an increased rate of shrinkage/distortion. The study also concluded that a pulling travel angle reduces distortion and improves deposition efficiency; however, further investigation is required to analyse the interactions and to assess if results are applicable to fillets as well as butt welds. Frazer Nash [2.13] confirmed that larger distortions were measured for the 4.5mm leg length compared to the 3.5mm leg length. The difference was measured as approximately  $0.05^\circ$  between the two plates. However, the impact of the travel angle and gap between the plate and stiffener was not considered and only a limited range of input parameters was considered. Assumption was also made that the fillet weld had equal leg lengths. Asifa et al [2.34] documented development of FEA Model using Ansys to simulate the thermal profile in a GMAW fillet weld. Results showed that the heat energy, welding speed, gun angle and plate thickness have a significant effect on temperature distribution of the fillet joint with this affecting the shape of the melt pool zone (MPZ) and

heat affected zone (HAZ). The results from the model showed that as the electrode (gun) angle increases, relative to the horizontal baseplate, the amount of heat applied to the stiffener (vertical plate) also increases and at a gun angle of 45° the heat appears to be evenly distributed between the baseplate and stiffener. However, the analysis only focused on the thermal profile and so further analysis would be required to assess what impact this variation would have on the resultant distortion of the joint. The model also appears to assume that there is 100% conduction between the baseplate and stiffener, contradicting guidance from Gray et al [2.14], who reported that, for a fillet weld set up, the interface between the stiffener and plate should be 'unmerged' in order to simulate the thermal gap that exists between the two surfaces and improve the accuracy of the model.

#### 2.4.3 Metallurgical/Mechanical Properties of GMAW welded joint

As described in Chapter 1.1.1, the GMAW process requires a moving heat source in order to melt the wire fed electrode and the welded workpiece. This heating and subsequent cooling have an impact of the metallurgical structure of welded joint. Metallurgically the welded joint can be split up into 3 distinct areas as shown in Figure 2-1:

1. Weld
2. Heat Affected Zone(s) (Table 1-1)
3. Unaffected parent material

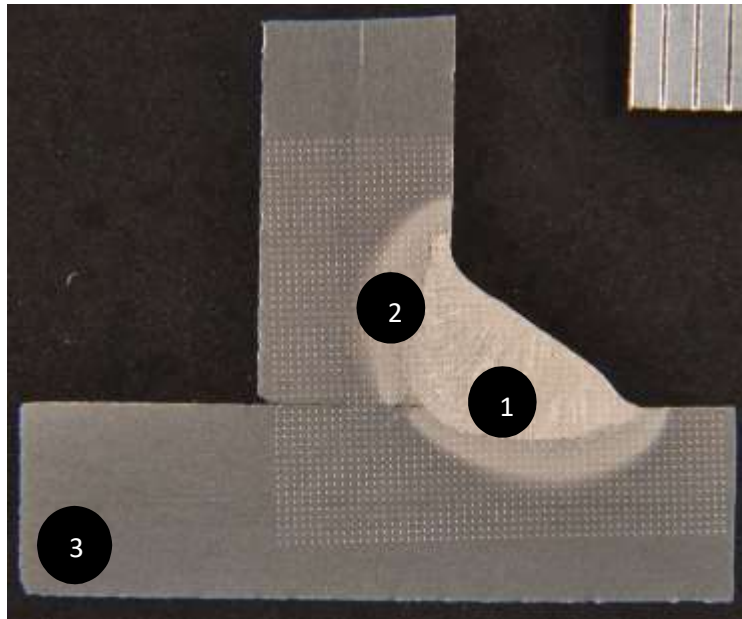


Figure 2-1 Macrograph showing location of weld (1), heat affected zone (2) and unaffected parent material (3).

Changes to the metallurgical structure of the weld result in impacting the hardness, toughness and strength of the weld and so it is important that they are considered as part of optimising the GMAW process. Khamari [2.35] reported a difference in microstructure between the weld and HAZ. A coarse structure formed in the weld area was compared to a much finer structure in the HAZ. The study also highlighted that the hardness of the HAZ was higher compared to the weld area and the base material. Boumerzoug [2.36] also observed that the microstructure of the centre of the weld is completely different from the heat affected zone. Equbal [2.37] reported that the cooling rate had a significant effect on the microstructure and mechanical properties of the steel once the structure has been cooled to room temperature. Ali Rizvi [2.38] conducted a study to investigate what effect different heat inputs had on the microstructure of the parent metal, coarse heat affected zone, fine grain heat affected zone and the fusion zone of a welded joint. The results confirmed that both the microstructure and hardness of the joint are significantly affected by the heat input. At high heat input the microstructure of the weldment starts to become coarse and the strength and hardness are reduced.

Sloderback [2.39] conducted an analysis to determine the range of the heat affected zone in a welded structure. This study identified the heat affected zone furthest from the weld to be the 'Subcritical' HAZ which was heated to a temperature range of between 600°C-700°C.

This range was used to help compare the heat affected zones identified on the weld macrographs and the output of the FEA model in Chapter 5.

## 2.5 Process Cost Analysis

In order to fully optimise a process an understanding of the constituent costs is required. One such study has been undertaken by Boiko et al [2.40] to understand what influence the composition of the shielding gas has on the cost of a fillet welded joint. Experiments were conducted on 5mm thick steel plates and a comparison was done between using pure carbon dioxide and Argoshield (Ar/CO<sub>2</sub>) as the shielding gas. For the pure carbon dioxide the cost breakdown was approximately; labour 58%, wire costs, 36% and gas costs 6%. However, when using Ar/ CO<sub>2</sub> (Argoshield mixture) the gas % increases to around 24% (labour 55%, wire 21%). The results provide a good cost comparison for the two shielding gases, but the figures are significantly different to the values calculated as part of this study which will be discussed further in Chapters 4 and 5. Stapon et al [2.41] suggest that the shielding gas typically accounts for less than 5% of the overall welding cost. OTC Daihen [2.42] estimate that the cost breakdown for a GMAW semi-Automatic process is as follows; labour costs (93%), electrode (5%) and shielding gas (2%). Esab [2.41] estimate that the cost breakdown for MIG (GMAW) welding is; Labour and Overhead (68%), electrode (22%), gas (10%). Chapter 7 provides analysis of the cost breakdown of the BAE Naval Ships GMAW process and some discussion around the significant variation in cost breakdown figures presented across all these studies.

## 2.6 Summary

GMAW is a relatively mature and commonly used industrial welding process. Over the years there have been significant developments and improvements made to the equipment, process and consumables. Many of the studies conducted over the years have been done on butt welds or have utilised 'bead on plate' experiments. This could be partly down to the added complexities of welding a fillet (preparing the joints, positional alignment of the torch relative to both plates). The results of experiments conducted on butt welds/bead on plate welds are not always directly transferable to a fillet weld set up which makes it

difficult to extrapolate the results from studies. There is a general consensus that current, wire feed speed, travel speed, voltage are the most significant and hence most researched parameters in GMAW welding. However, there is limited research on what impact torch travel angle and gun angle and also the interactions between the individual parameters may have on the resultant fillet weld geometry. Artificial Neural Networks and Mathematical Modelling have been proven to be robust and reliable methods of analysing the GMAW process. There are also many examples of FEA being used to successfully model the thermal and mechanical impacts of the GMAW process; however, there is little evidence of any previous research undertaken into what impact an asymmetrical fillet weld (unequal leg length) has on the heat flow and resultant distortion of a fillet welded joint. Previous studies have also highlighted that there is a significant difference between the microstructure of the heat affected zone (HAZ) and the weld. There is no available research on what impact, if any, the welding torch travel angle (push vs pull) has on the metallurgical properties of the weld and HAZ. There is a significant amount of research being undertaken to assess what impact varying the composition and flow rate of the shielding gas has on the resultant weld bead, but the majority of this work has been focused on downhand butt welds. There appears to be no evidence of prior research into understanding the behaviour and coverage of the shielding gas flow around a fillet weld.

## 2.7 References

- 2.1 Benyounis, K. Y., & Olabi, A. G. (2008). Optimization of different welding processes using statistical and numerical approaches - A reference guide. *Advances in Engineering Software*. <https://doi.org/10.1016/j.advengsoft.2007.03.012>
- 2.2 Campbell, S.W., Galloway, A.M., McPherson, N.A. 2012. Artificial Neural Network Prediction of Weld Geometry performed using GMAW with Alternating Shielding Gases. *Welding Journal*, vol.91, no.6. June 2012. Supplement: Welding Research. Pp.174s-181s, ISSN: 0043-2296
- 2.3 Dadgar, A.Y., Mostafa, N.B., Panahizadeh, V., Seyedkashi, S.M.H. 2011. Prediction of Weld Penetration in FCAW of HSLA Steel using Artificial Neural Networks. *AIP Conf.Proc.1315,884* . DOI: 10.1063/1.3552564.



- 2.4 Nagesh, D.S., Datta, G.L.2002. Prediction of Weld Bead Geometry and Penetration in shielded metal-arc welding using artificial neural networks. *Journal of Materials Processing Technology*, vol.123, no.2.pp303-312, April 2002 [DOI:10.1016/S0924-0136\(02\)00101-2](https://doi.org/10.1016/S0924-0136(02)00101-2)
- 2.5 Beckett, S., MacPherson, M. J., McPherson, N. A. (2011). Improved welding control of automated fillet welding for ship structures using Artificial Neural Networks (ANN). JOM 16 Conference, Denmark.
- 2.6 Chan, B., Pacey, J., Bibby, M. 1998. Modelling Gas Metal Arc Weld Geometry Using Artificial Neural Network Technology. *Canadian Metallurgical Quarterly*, vol.38, no.1. January 1999. Pp43-51. [DOI:10.1016/S0008-4433\(98\)00037-8](https://doi.org/10.1016/S0008-4433(98)00037-8)
- 2.7 Moon, H., Na, S. 1997. Optimum Design Based on Mathematical Model and Neural Network to Predict Weld Parameters for Fillet Joints. *Journal of Manufacturing Systems*. 01/1997; 16(1):13-23. DOI: 10.1016/S0278-6125(97)88402-6
- 2.8 Nagesh, D.S., Datta, G.L.2008. Modeling of fillet welded joint of GMAW process: integrated approach using DOE, ANN and GA. *International Journal for Interactive Design and Manufacturing (IJIDeM)* 07/2008; 2(3):127-136. DOI: 10.1007/s12008-008-0042-8
- 2.9 Kumar, A., Debroy, T. 2007. Tailoring Fillet Weld Geometry Using a Genetic Algorithm and a Neural Network Trained with Convective Heat Flow Calculations. *Welding Journal*, vol.86, no.1. January 2007, pp.26-33
- 2.10 Kim, I. S., Son, J. S., Park, C. E., Kim, I. J., & Kim, H. H. (2005). An investigation into an intelligent system for predicting bead geometry in GMA welding process. *Journal of Materials Processing Technology*, 159, 113–118. <https://doi.org/10.1016/j.jmatprotec.2004.04.415>
- 2.11 Nagesh, D.S., Datta, G.I. (2007) Genetic Algorithm and Artificial Neural Networks Application for modeling of fillet welded joint of GMAW Process. *3<sup>rd</sup> JOIN Conference, Lappeenranta, Finland, August 2007*

- 2.12 Mollicone, P., Gray, T. G. and Camilleri, D. (2012) 'Experimental investigation and finite element analysis of welding induced residual stresses', *The Journal of Strain Analysis for Engineering Design*, 47(3), pp. 140–152. doi: 10.1177/0309324712438653.
- 2.13 Frazer Nash Consultancy (2007), 'Assessment of the distortion benefits due to a reduction in weld volume, FNC 33026/31815R.
- 2.14 Gray, T., Camilleri, D., & McPherson, N. (2014). Control of Welding Distortion in Thin-Plate Fabrication: Design Support Exploiting Computational Simulation. In Control of Welding Distortion in Thin-Plate Fabrication: Design Support Exploiting Computational Simulation. <https://doi.org/10.1533/9780857099327>
- 2.15 Camilleri, D., Gray, T.G.F., Nash, D.H. (2008) Mitigation of welding distortion and residual stresses via cryogenic CO2 cooling - a numerical investigation. 17th International Conference on Computer Technology in Welding and Manufacturing: Proceedings of Conference Held at Cranfield University in June 2008. TWI Ltd. ISBN 9781903761076
- 2.16 Miller Electric Mfg. LLC. (2012). *Guidelines for Gas Metal Arc Welding (GMAW)*. [online] available at [https://www.millerwelds.com/-/media/miller-electric/files/pdf/resources/mig\\_handbook.pdf](https://www.millerwelds.com/-/media/miller-electric/files/pdf/resources/mig_handbook.pdf)
- 2.17 **BOC**, Fundamentals of flux and Metal Cored Arc Welding, Section 8: Consumables (2007), pp322-325.
- 2.18 ESAB. *MIG Welding Handbook*. [online] available at [http://www.esabna.com/euweb/mig\\_handbook/592mig7\\_1.htm](http://www.esabna.com/euweb/mig_handbook/592mig7_1.htm).
- 2.19 Lincoln Electric, Innershield Welding Guide, Publication C3.2400, Issue Date 02/11, pp21-31
- 2.20 Harwig, D. 2000. Arc Wise – Optimisation, Productivity and Quality in Arc Welding, Materials Joining Technology Newsletter, vol.13, no 2.

- 2.21 Pal, K., Bhattacharya, S., Pal, S.K. 2010, Multisensor-based monitoring of weld deposition and plate distortion for various torch angles in pulsed MIG welding, *Int J Adv Manuf Technol* (2010) 50:543-556
- 2.22 Tham, G., Yaakub, M.Y., Abas, S.K., Manurung, Y., Jalil, B.A., 2012. Predicting the GMAW 3F T-Fillet Geometry and its Welding Parameter. *Procedia Engineering*, International Symposium on Robotics and Intelligent Sensors, vol.41, 2012, pp1794-1799. [DOI:10.1016/j.proeng.2012.07.385](https://doi.org/10.1016/j.proeng.2012.07.385)
- 2.23 Allen, T. T., Richardson, R. W., Tagliabue, D. P., & Maul, G. P. (2002). Statistical process design for robotic GMA welding of sheet metal. *Welding Journal (Miami, Fla)*.
- 2.24 Beyer, V., Campbell, S. W., Ramsey, G. M., Galloway, A. M., Moore, A. J., & McPherson, N. A. (2013). Systematic study of effect of cross-drafts and nozzle diameter on shield gas coverage in MIG welding. *Science and Technology of Welding and Joining*. <https://doi.org/10.1179/1362171813Y.0000000143>
- 2.25 Bitharis, I., McPherson, N. A., McGhie, W., Roy, D., & Moore, A. J. (2018). Visualisation and optimisation of shielding gas coverage during gas metal arc welding. *Journal of Materials Processing Technology*. <https://doi.org/10.1016/j.jmatprotec.2017.11.048>
- 2.26 DuPont, J.N., Marder, A.R. (1995). Thermal Efficiency of Arc Welding Processes. *Welding Journal*, 1995, s406-s416
- 2.27 Singh, R. (2016). *Applied Welding Engineering Processes, Codes and Standards*, 2<sup>nd</sup> Edition, Butterworth-Heinemann, pp131-162. <https://doi.org/10.1016/C2015-0-00784-5>
- 2.28 Haelsig, A., Kusch, M., Mayr, P. (2012). New findings on the efficiency of gas shielded arc welding. *Welding in the World, Vol 56, 2012, pp98-104*.
- 2.29 ISO 15614-7:2016 Specification and qualification of welding procedures for metallic materials
- 2.30 Miller, D. K. (1998). Consider Penetration when determining fillet weld size. *Welding Innovation Volume XV, No 1, 1998*.

- 2.31 Kaewsakul, N., Putrontaraj, R., Kimapong, K. (2015). The Effects of GMAW Parameters on Penetration, Hardness and Microstructure of AS3678-A350 High Strength Steel. *International Journal of Advanced Culture Technology*, Vol.3, No.1, pp. 169-178. doi: 10.17703/IJACT.2015.3.1.169
- 2.32 Yadav, P.K, Abbas, M., Pate, S. (2014). Analysis of heat affected zone of mild steel specimen developed due to MIG Welding. *International Journal of Mechanical Engineering and Robotics Research*, Vol. 3, No. 3, pp. 399-404, July 2014.3(3).
- 2.33 Pal, K., Bhattacharya, S. and Pal, S. K. (2010) 'Multisensor-based monitoring of weld deposition and plate distortion for various torch angles in pulsed MIG welding', *The International Journal of Advanced Manufacturing Technology*, 50(5-8), pp. 543–556. doi: 10.1007/s00170-010-2523-8.
- 2.34 Asifa, K., Li, H., Li, L. and Khurram, S. (2011) 'Parametric Study of Welding Temperature Distribution in T-Joint Fillet Weld Using FEM', *Advanced Materials Research*, 328-330, pp. 492–496.
- 2.35 Khamari, B. K., Kumar Sahu, P., & Biswal, B. B. (2018). Microstructure Analysis of Arc Welded Mild Steel Plates. *IOP Conference Series: Materials Science and Engineering*. <https://doi.org/10.1088/1757-899X/377/1/012049>
- 2.36 Boumerzoug, Z. (2010). Effect of Welding on Microstructure and Mechanical Properties of an Industrial Low Carbon Steel. *Engineering*. <https://doi.org/10.4236/engineering.2010.27066>
- 2.37 Equbal, M.I., Alam, P., Ohdar, R., Anand, K.A., Alam, M.S. (2016). Effect of cooling rate on the microstructure and mechanical properties of medium carbon steel. *International Journal of Metallurgical Engineering*, Vol.5, No.2, pp21-24. doi:10.5923/j.ijmee.20160502.01
- 2.38 Ali Rizvi, S., Ahamad, M. (2018). Effect of heat input on the microstructure and mechanical properties of a Welded joint-A Review. *International Journal of Applied Engineering Research*, ISSN 0973-4562, Vol. 13, pp184-188, ISSN 0973-4562

- 2.39 Sloderbach, Z., Pajak, J. (2015). 'Determination of ranges of components of heat affected zone including changes of structure', *Archives of Metallurgy and Materials*, Vol.60, Issue 4, DOI: 10.1515/amm-2015-0421
- 2.40 Boiko, I., Avisans, D. (2013). 'Study of shielding gases for MAG welding', *Materials Physics and Mechanics*, Vol.16, March 2013, pp126-134
- 2.41 Stapon, W., Lyttle, K. (2007). *7 Effects of Shielding Gas*. [online] available at <https://www.thefabricator.com/thewelder/article/arcwelding/7-effects-of-shielding-gas>.
- 2.42 Daihen-USA. *Welding Cost Analysis*. [online] available at <https://www.daihen-usa.com/resources/welding-cost-analysis/>. [Accessed April 2019]

## Chapter 3 Methodology

### 3.1 Introduction

As described in Chapter 1, the research has been split up into 4 distinct packages of work. This section provides a detailed explanation of the various methodologies employed to assess the GMAW fillet welding process, why they were used and what contribution each made to the overall study. Figure 1-20 provides an overview and high level summary of the key areas of the investigation.

### 3.2 ANN Model Development

Artificial Neural Networks (ANNs) are computing systems consisting of a collection of interconnected processing elements/nodes which are able to represent complex interactions between process inputs and outputs, such as that shown for fillet welding [Figure 1-5]. The way in which the nodes are interconnected defines the network architecture. There is a variety of different ANN architectures that can be used depending on the situation/process being analysed. The diagram below [Figure 3-1] details the basic architecture of a typical ANN.

- Input Layer – raw data that is fed into the system (e.g. current, voltage, travel speed, gun angle, travel angle)
- One or More Hidden Layers – array of interconnected processing elements with different weights between each connection.
- Output Layer – The signal (output) of the process is dependent on the outcomes and weights of the processing elements in the hidden layers.

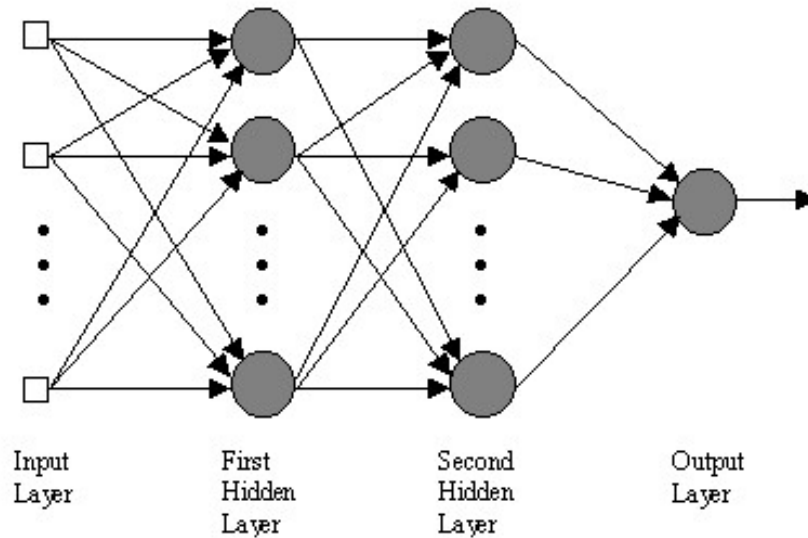


Figure 3-1 Typical Example of ANN Architecture

Mathematically, the output from an ANN model can be represented as shown in Eqn.3-1:

$$O = \sum_{i=0}^n (I_i \times W_i) \quad \text{Eqn. 3-1}$$

Where:

- $O$  is the output
- $I_i$  = the  $i^{th}$  input sample
- $W_i$  = the weight of the  $i^{th}$  sample
- $n$  = number of samples
- $i$  = variable

The main benefits of ANNs are:

- They do not require any predefined relationship between the variables to be understood
- They allow patterns, trends and interactions to be identified that otherwise would be impossible/very difficult to detect
- They allow process which cannot be physically modelled to be investigated
- They work well when there is a large number of diverse variables to analyse
- They can be used and applied to a variety of problems in different fields
- They can be used to analyse both quantitative and qualitative data

There are however some important limitations in using ANN models that need to be understood.

- They do not explain why patterns and/or interactions exist, so it requires analyses and interpretation of the results
- They may not always find the optimal solution
- The model development requires an element of trial and error (trying different network topologies, iterations, number of layers...etc.) in order to try and create the most accurate model.

Bhadeshia [3.1] suggests that ANNs are ideal for determining welding process parameters such as penetration. ANNs which could accurately predict the penetration and internal geometry of a fillet joint would provide a great benefit by greatly reducing the cost (material and labour) by trialling and testing new welding procedures and processes. Prior downhand fillet weld analysis conducted by Beckett [3.2] had proven inconclusive, suggesting that some input parameters were not being satisfactorily controlled in the dataset used to generate the ANN.

ANN's have been used in this study to model the relationship between the GMAW fillet weld process inputs (current, voltage, travel speed, gun angle, travel angle) and the resultant fillet weld geometry (leg length, throat, reinforcement and penetration). They will also be used to analyse if the interactions between these input parameters are significant in influencing the resultant weld geometry. 'Neurosolutions for Excel' was used to develop the Artificial Neural Network (ANN). A total of 97 test pieces were analysed in order to develop the model. 72 samples were used to train the model and 25 for testing the model. The input variables to the model were current, voltage, travel speed, travel angle and gun angle. The desired 'output' variables to the model were penetration, vertical leg length and horizontal leg length. One of the key tasks in developing an ANN model is choosing the optimal network Architecture. During the model development (Neurosolutions) a number of different network topologies were assessed including Multi-Layer perceptron (MLP), Generalised feedforward forward (GFF) and probabilistic neural networks (PNN). The analysis concluded that a Multi-Layer Perceptron Model with 5 inputs (current, voltage, travel speed, gun angle and travel angle), 2 hidden layers and 3 output layers (horizontal leg length, vertical leg length and penetration) produced the lowest error between predicted vs



actual results and so was chosen. Figure 3-2 shows a representation of the ANN model architecture.

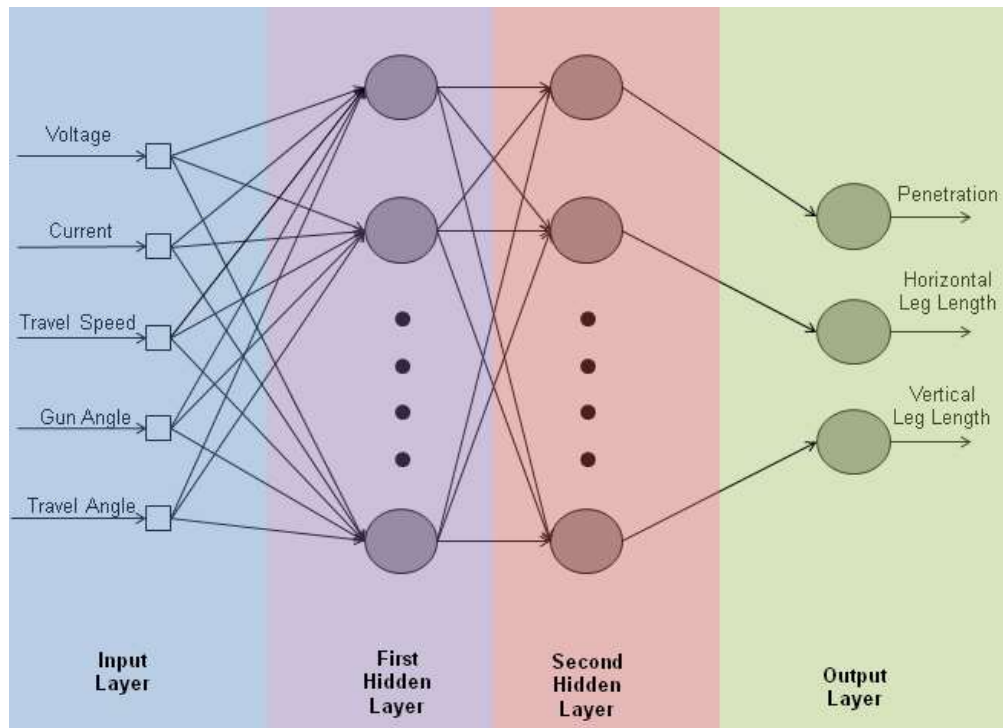


Figure 3-2 Visual Representation of selected ANN architecture

Once the model had been trained and tested, its ability to predict fillet weld leg length and penetration given input values for current, voltage, travel speed, gun angle and travel angle was further validated with some additional experimental data, as will be detailed in Chapter 5. Gas flow rate and electrode were excluded as variables in this analysis. A separate analysis was conducted specifically looking at the impact of the shielding gas and the selection of electrode and will be detailed within Chapters 5 and 6. This was deemed to be the most practical solution as adding both shielding gas and electrode type as variables would have increased the number of experiments required to generate a suitable dataset from which a successful model could be developed and trained. Also changing the electrode impacts the selection of current, voltage, travel speed in order to generate a stable weld whilst maintaining a constant heat input. This would have complicated the dataset and made it more difficult to compare the results.

## Sensitivity Analysis

A sensitivity analysis is a tool that can be used to identify how much impact each of the inputs have on determining the outputs of a process. Neurosolutions has a functionality that allows a sensitivity analysis to be conducted once the neural network has been trained. Each of the inputs is then varied individually whilst all other variables are kept constant so that the change in the output can be measured. The equation for the sensitivity analysis is shown in Eqn 3-2: [3.3]

$$S_k = \frac{\sum_{n=1}^p \sum_{i=1}^o (y_{ip} - \tilde{y}_{ip})^2}{\sigma_k^2} \quad \text{Eqn. 3-2}$$

Where:

- $S_k$  is the sensitivity for input k
- $y_{ip}$  is the  $i^{th}$  output obtained with the weights fixed for the  $n^{th}$  pattern
- $o$  is the number of outputs from ANN model
- $p$  is the number of patterns
- $\sigma_k^2$  is the variance of the input

## 3.3 Regression Analysis

Multiple linear regression analysis is a statistical process used to estimate relationships between two or more variables. Regression analysis can be used to model the relationship between a wide variety of processes where a large amount of historical data has been captured and has been used regularly to model the relationship between GMAW parameters. [3.4, 3.5]

Mathematically the multiple linear regression model can be simplified and expressed as:

$$y = \beta_0 + \beta_1x_1 + \beta_2x_2 + \cdots \beta_kx_k + \varepsilon \quad \text{Eqn. 3-3}$$

Where:  $y$  is the output  
 $k$  = number of variables  
 $\beta$  = regression coefficients  
 $\varepsilon$  = model deviations

The actual equations for the regression models that were developed to understand the relationship between the inputs and outputs in Table 3-1 below are detailed in Chapter 5.1.3.

Table 3-1 GMAW Input-Output Parameters

Input Parameters	Output (Weld Geometry)
Current (A)	Leg Length (Horizontal/Vertical)
Voltage (V)	Penetration
Travel Speed (mm/min)	Throat
Travel angle (Push v Pull)	
Gun angle	

As described previously one of the limitations of ANN is that it does not explain patterns and does not always find the optimal solution. Regression Analysis has been used in this instance to verify that the results of the ANN are aligned to the statistical relationships between the inputs and outputs and to help explain the interactions between the parameters. The regression model was developed using Minitab. Minitab is a widely used statistical analysis software package that can be used to analyse, interpret and graphically present complex and multi-variable datasets. The inputs and outputs identified in Table 3-1 were provided from 82 experimental fillet welds whose geometry was measured using ImageJ digital analysis software, as will be described in Section 3.6. The software was then used to run 5 individual regression analyses for each of the output (response variables), using the input data for the 5 input parameters. Minitab automatically assessed whether or not the sample size was sufficient to confirm the relationship between the inputs and outputs. The software was then used to calculate the strength of the relationship between

the variables, the equation of the regression model and what impact each of the inputs and the interactions have on the chosen output. Figure 3-3 provides an example of the regression analysis output from Minitab.

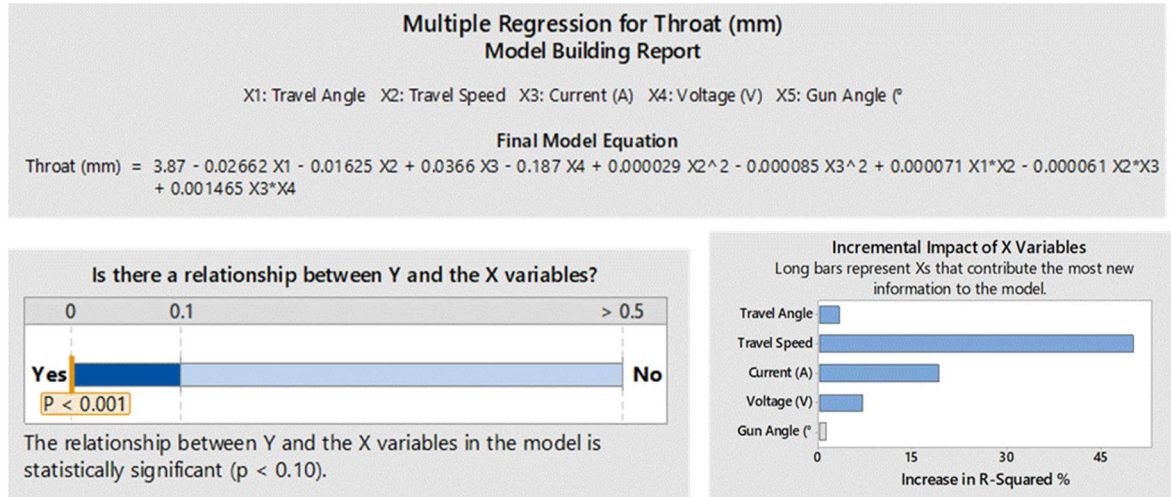


Figure 3-3 Example of Minitab Regression Analysis outputs

### 3.4 FEA Model Development

Finite Element Analysis (FEA) is used widely to predict the behaviour of welding processes and the relationship between variables. FEA works by modelling the structure using a mesh of elements interconnected by nodes. Material properties are applied to the elements and then loading conditions can be simulated on the nodes and elements to predict real life situations. In this study ANSYS was used to develop a FEA Model to predict the changes to the thermal loads and hence resultant distortion caused by varying the following characteristics of a DH36 carbon steel fillet welded joint.

- Weld Geometry (leg length, throat)
- Unequal Leg Lengths
- Heat Input
- Plate Thickness
- Current, Voltage and Travel Speed

## Model Development

The model was created by initially creating a 2D outline of the fillet joint and then utilising the extrusion function to generate a 3D representation of the fillet welded assembly. A mesh was then applied to the assembly. Since the main area of interest in the model is around the fillet weld (heat source), a tighter mesh was applied in that area so as to produce a greater level of accuracy in this area of the model [Figure 3-4].

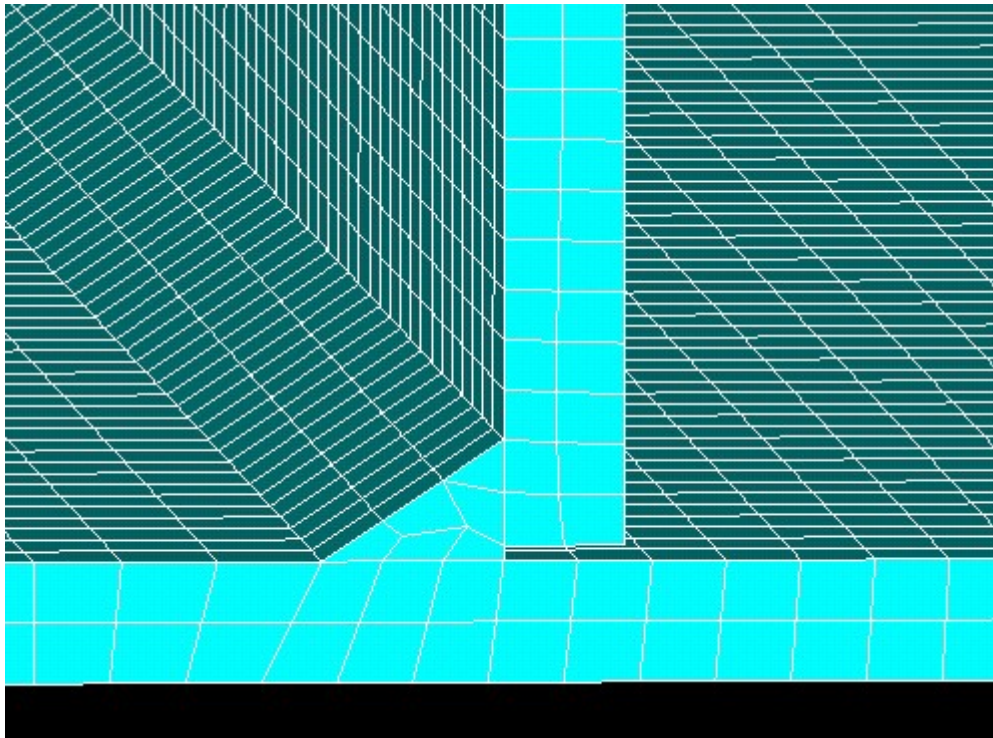


Figure 3-4 FEA Fillet Weld Mesh

Figure 3-5 provides an overview of the model development process. An uncoupled thermal-mechanical approach was used. This involves initially calculating the heat generation rate for each step of the welding process. Once completed the model is then converted to a structural simulation and the previously calculated element temperatures are then applied step by step to the model in order to simulate the overall mechanical loads being applied to the welded joint. Temperature dependant material properties (density, thermal conductivity, enthalpy, elastic moduli, Poisson Ratio and coefficient of thermal expansion) for S355 (DH36) Mild Steel were applied to the elements of the model. The material

properties used were similar to those used by Camilleri et al [3.8] and are contained with Appendix 3.

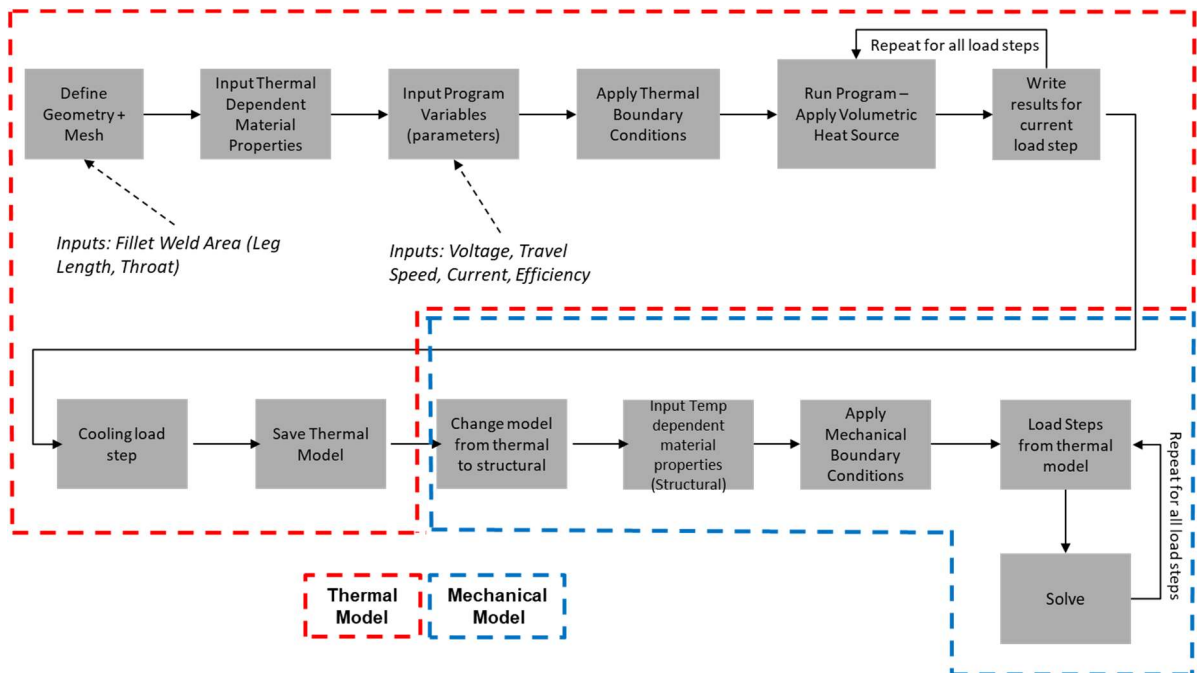


Figure 3-5 FEA Model Development Process

Element birth and death functionality of ANSYS was applied to the fillet weld volume to simulate the deposition of weld metal during the GMAW process. This technique involves de-activating all of the elements within a specific volume at the start of the process, the triangular fillet weld volume in this instance. The elements are then progressively re-activated along the length of the volume over time in order to simulate the deposition of weld metal as the torch moves along the workpiece. The element birth and death function is applied to both the thermal and structural steps of the model. During the thermal stage of the model the element deactivation is achieved by applying a significant reduction factor to the conduction matrix for the relevant elements. During the structural stage of the model the deactivation is achieved by applying a similar reduction factor to the stiffness (Young's Modulus) of the identified volume. The de-activated elements are then progressively reactivated at the same time as the heat source is applied so as to simulate

the deposition of weld metal. The re-activation is achieved by removing the reduction factor that had been applied during the element de-activation stage, for the specific group of elements to which the heat is being applied. This process is then repeated for each step of the process until the heat source has finished moving along the structure and all the elements of the fillet weld volume have been re-activated. A volumetric heat source [3.6] was used in this model to represent the heat applied by the moving torch head during the GMAW process. Mathematically this can be expressed by:

$$q_{vol} = \frac{(2\mu VI)}{(l_w b_w h_w)} \quad \text{Eqn. 3-4 [3.6]}$$

Where:  $q_{vol}$  is the volumetric heat input  
 $\mu$  = process efficiency coefficient  
 $V$  = voltage  
 $I$  = current  
 $l_w$  = length of triangular fusion zone  
 $b_w$  = width/depth of triangular fusion zone (horizontal leg length)  
 $h_w$  = height of triangular fusion zone (vertical leg length)

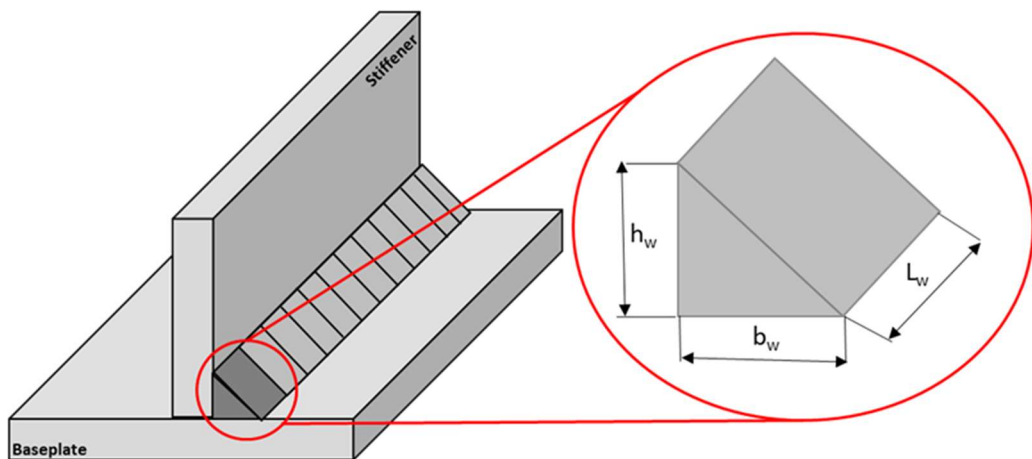


Figure 3-6 Schematic showing characteristics of volumetric heat source

The overall impact of convection and radiation on the heat flow through the workpiece is minor in comparison to the impact of conduction [3.6]; however, it is significant enough to be considered when developing the finite element model. For modelling purposes the heat losses due to convection and radiation are combined into a single film coefficient value which is then applied individually to the exposed surfaces of the modelled structure. Mathematically the heat losses due to convection and radiation can be expressed by the following formula:

$$q_{c+rad} = (h_c + h_r)(T_s - T_a) \quad \text{Eqn. 3-5 [3.6]}$$

Where:  $q_{c+ra}$  is the heat flow by convection and radiation (combined)  
 $h_c$  = film coefficient due to convection  
 $h_r$  = film coefficient due to radiation  
 $T_s$  = temperature of heated surface  
 $T_a$  = ambient temperature

The film coefficient used in the model was calibrated against the actual rate of cooling which was measured during experimentation. The film coefficient used in the model was then adjusted until the modelled rate of cooling was comparable with the measured rate of cooling.

The structural boundary conditions are critical in order to obtain a reliable solution. A variety of boundary constraints were investigated but the most realistic solution was generated by restraining all four corners of the baseplate in the vertical direction (y-axis) and restraining 2 corners in the horizontal direction (x & z axis). This is visualised in Figure 3-7 and Figure 3-8 provides an schematic illustration of how the welded assembly was supported during welding.



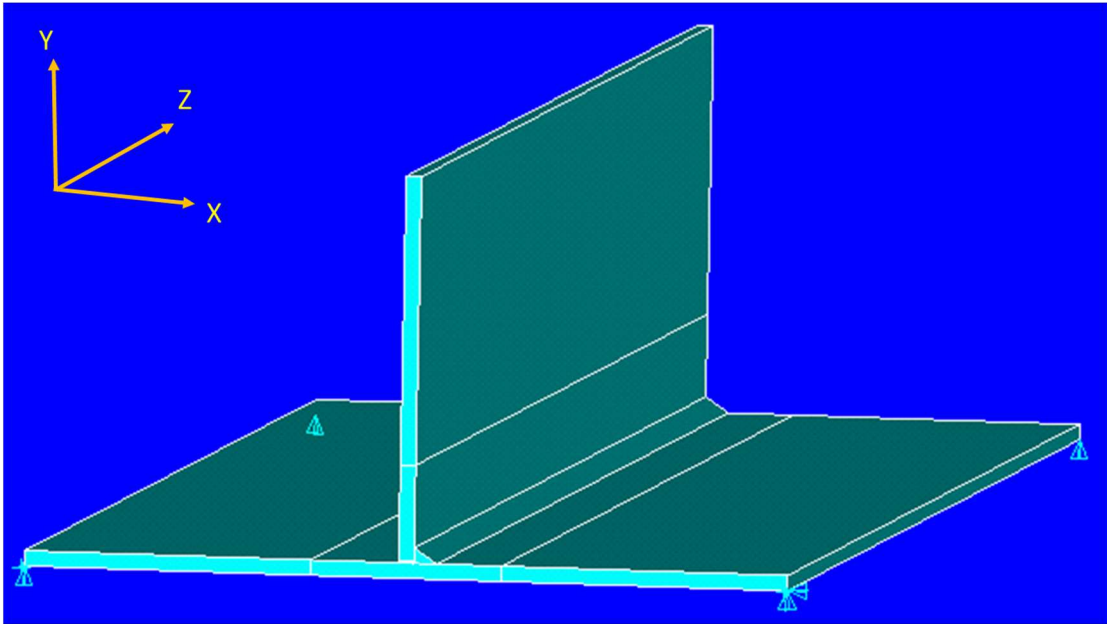


Figure 3-7 FEA Mechanical Boundary Conditions

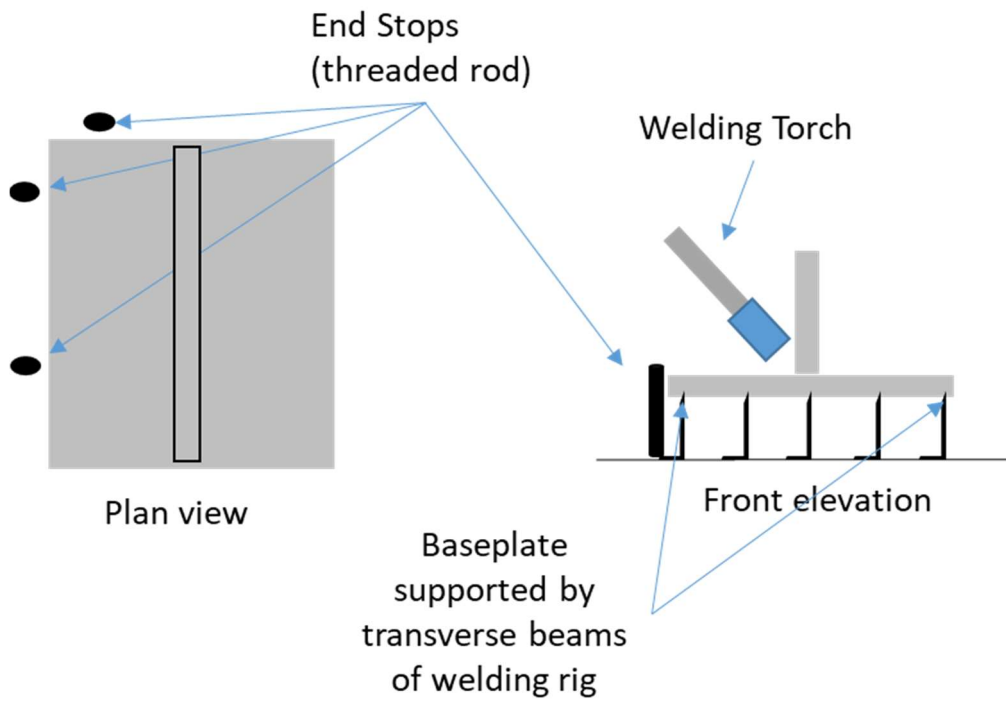


Figure 3-8 Schematic showing how fillet assembly was supported on the rig during welding

In practice, during experimentation, the baseplate was supported by the transverse beams of the welding rig [Figure 3-8], the stiffener was tacked to the baseplate prior to welding at the locations shown in Figure 3-18 and the position of the welding torch was controlled using the jig shown in Figure 3-16. The position of the baseplate on the welding rig was maintained using threaded rod end stops. These allowed the plate to be positioned in a repeatable position on the welding rig table whilst not restricting any deformation of the structure during welding.

A number of assumptions were made during the development of this model. Firstly, both the baseplate and stiffener are assumed to be straight and flat before any heat is applied. Thermal conduction between the baseplate and stiffener, prior to welding, is assumed to be negligible due to the air gap along the interface between the two plates. The impact of the local fume extraction system is assumed to be negligible and the ambient room temperature is constantly set at 20 °C. Thermal validation of the FEA model was conducted by attaching thermocouples to a welded fillet joint on the welding rig. The same welding parameters used in the experiment were then input into the model so that the predicted vs actual thermal profiles could be compared. The process efficiency factor was used to calibrate the model against the actual measured results. Similar to the film coefficient, the process efficiency factor was used as a fine adjustment until the modelled results were comparable with the measured temperatures. The weld macrographs were also used as a means of validating the output from the FEA model. The heat profiles from the FEA model were compared against the actual heat affected zones identified on the macrograph [Figure 3-9]. This provided confirmation that the model was distributing the heat correctly between the baseplate and stiffener.

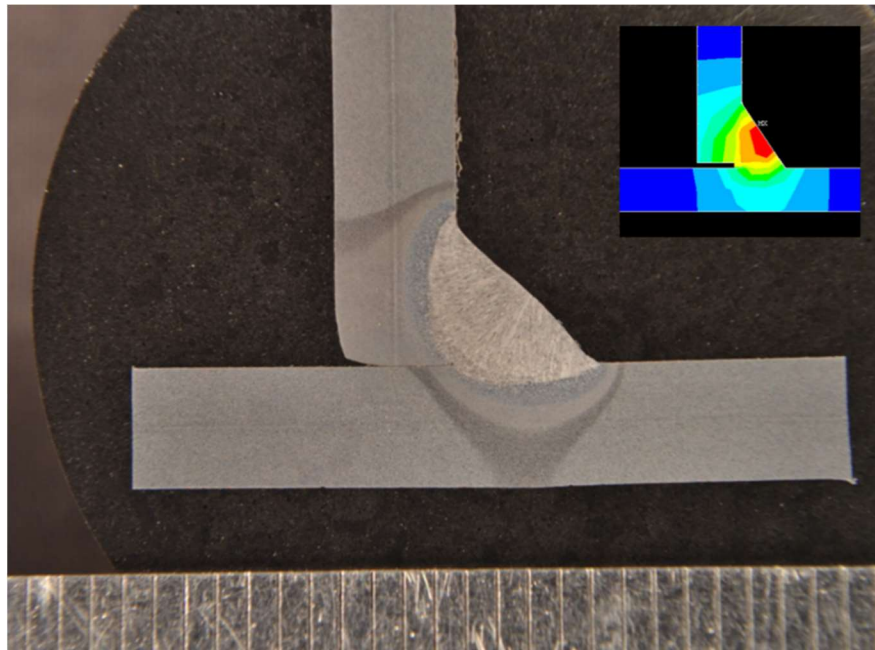


Figure 3-9 Comparison of Fillet Weld Macrograph and FEA thermal nodal solution

Mechanical validation of distortion was measured using laser measurement system on welding rig [Figure 3-11]. The laser was programmed to traverse back and forwards across the plate, as indicated in Figure 3-11, taking height readings every second. Threaded rod end stops were used to ensure that the plate was in the same location before and after welding. The results were then captured directly into an excel spreadsheet which allowed a surface map to be created, similar to Figure 3-10.

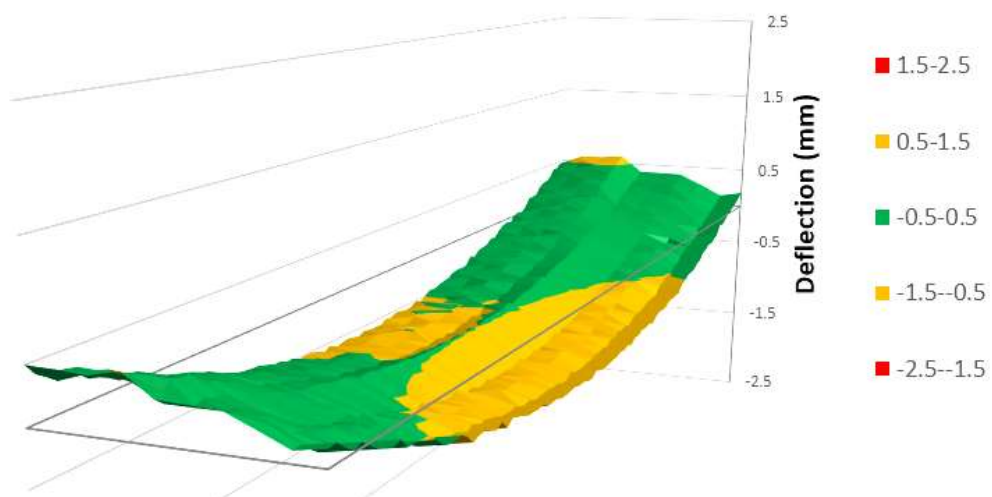


Figure 3-10 Example of a Surface Map using output from laser measurement system

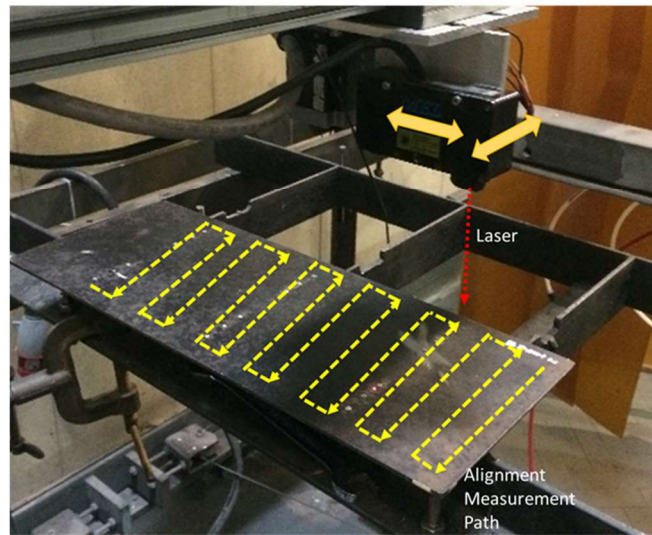
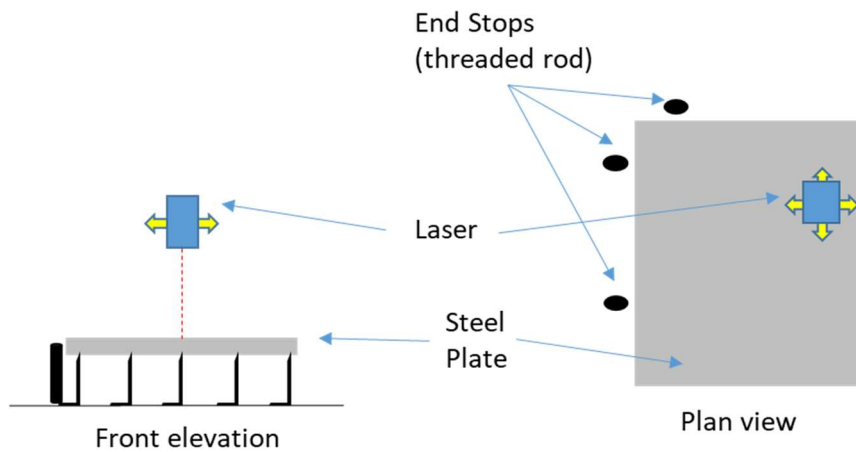


Figure 3-11 Schematic and photographs showing laser system used for measuring distortion of steel plates.

The measurement system shown in Figure 3-11 was only able to measure vertical displacement ( $y$ -axis) of the baseplate so was unable to determine any distortion of the vertical stiffener. In order to generate an accurate 3D representation of the baseplate distortion, the measured points close to the stiffener were removed and smoothed, using data points either side of the stiffener. The model demonstrated reasonable performance between actual vs predicted as will be described in Chapter 6. The model can be easily configured to predict changes in the temperature and distortion through the fillet welded joint caused by varying the input parameters and weld geometry.

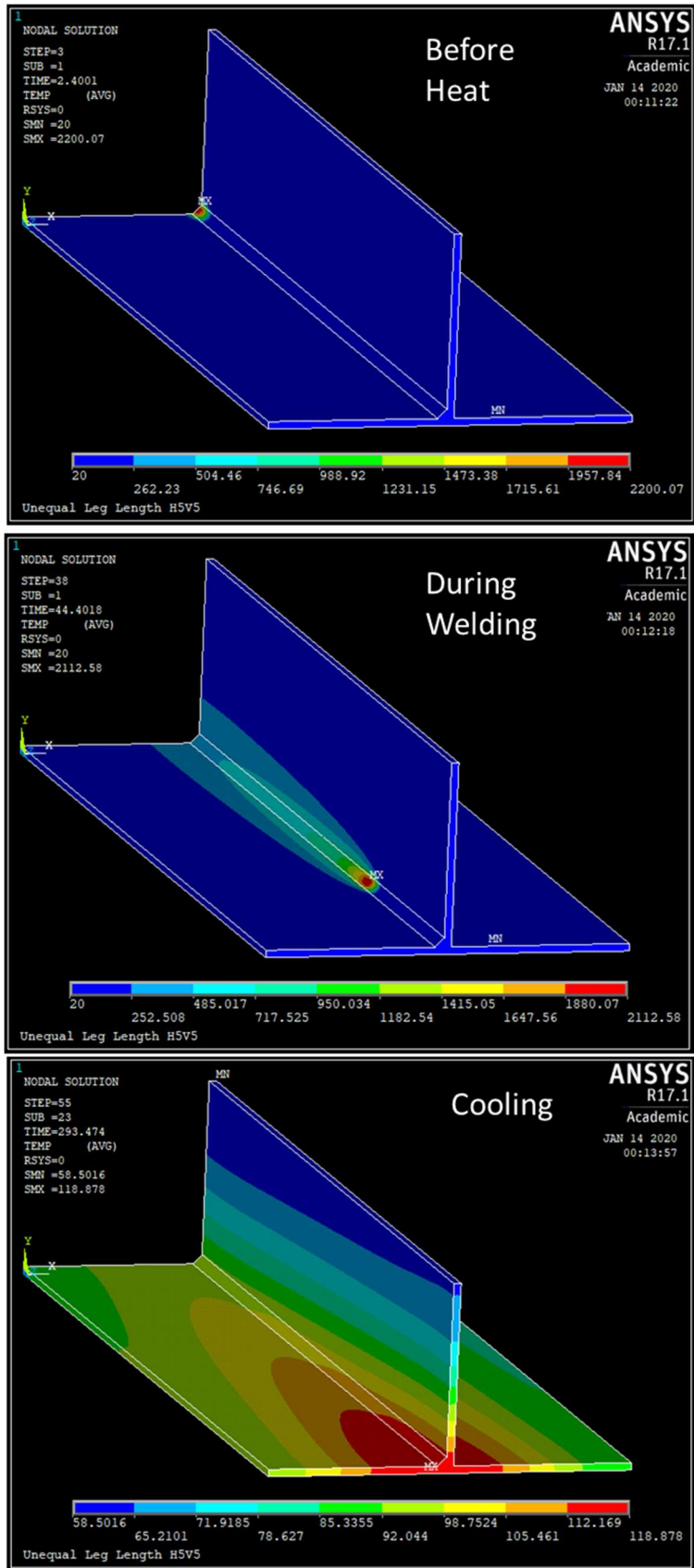


Figure 3-12 FEA Model – Example of thermal plots

Some examples of the FEA Model outputs are shown next. Figure 3-12 provides an example of the 3D Thermal model which shows how the temperature is distributed across the steel plates as they are welded. Figure 3-13 provides an example of the 3D mechanical model plot which shows how the plates are displaced (distorted) as a consequence of the temperature profiles from welding. Both models can be animated to show how the thermal and mechanical loads vary over time.

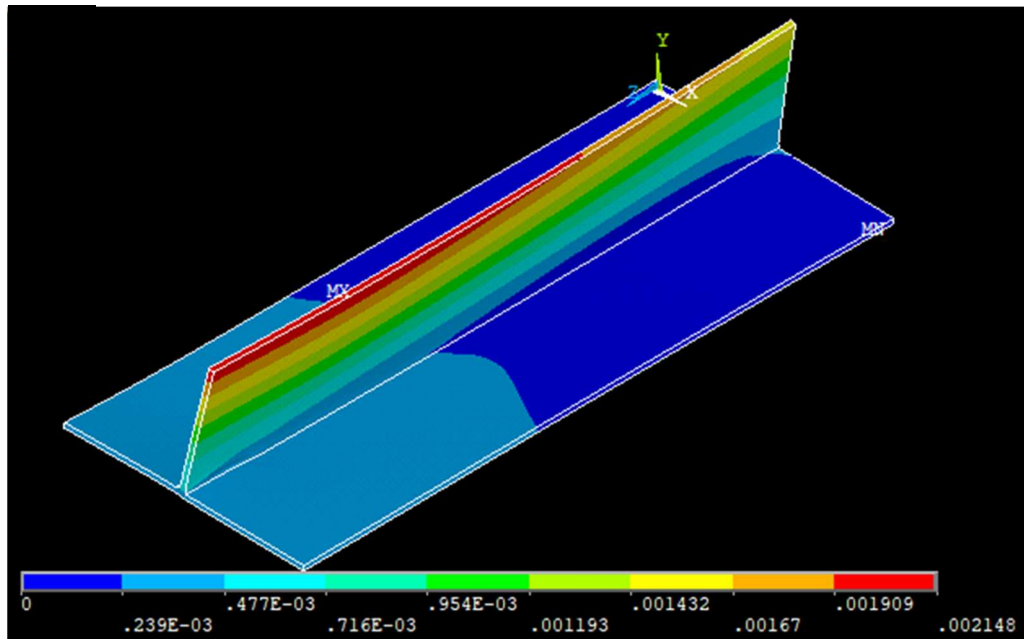


Figure 3-13 FEA Model – Example of Mechanical plot

### 3.5 Shielding Gas Visualisation

The shielding gas is one of the key input parameters to the GMAW process. The shielding gas is typically delivered to the joint through the torch (see Chapter 1); as a consequence the angle that the torch is positioned relative to the joint may have a significant influence on the behaviour of the shielding gas during the welding process. The analysis detailed within this thesis was a follow on to a study undertaken by Bitharis [3.9] to visualise the behaviour of the shielding gas at different flow rates for GMAW butt welds. The study demonstrated that it was possible to reduce the shielding gas flow rate to as low as 9l/min for a GMAW butt weld without compromising the quality of the resultant weld. This raised the question as to whether the gas flow rate could be lowered further for a fillet weld, due

to the natural shielding provided by the vertical 'stiffener' in a fillet weld set up, without significantly impacting the geometry and quality of the weld.

### Experimental Set Up

The study used a Schlieren rig, at Heriot Watt University, School of Engineering and Physical Sciences, to record and visualise the shielding gas during the welding process. The observed shielding gas flows were then validated against both 2D and 3D CFD (COMSOL) simulations, developed by Bitharis [3.11], which modelled the flow of the gas and the coverage of the shielding gas around the weld. The Schlieren set up consisted of a high intensity light source, an arrangement of parabolic mirrors, a range of filters and a high-speed camera as shown in Figures 3-14 and 3-15.

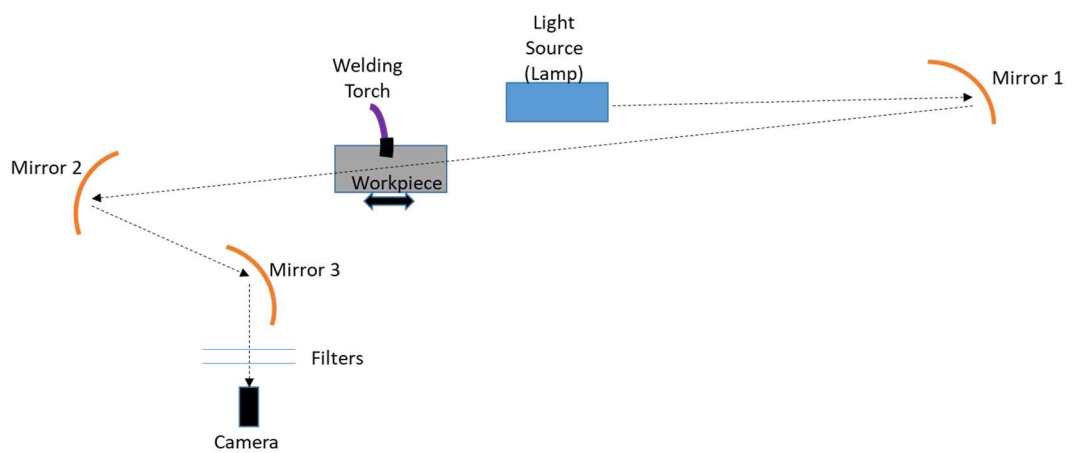


Figure 3-14 Schematic diagram of Schlieren rig set up [3.11]



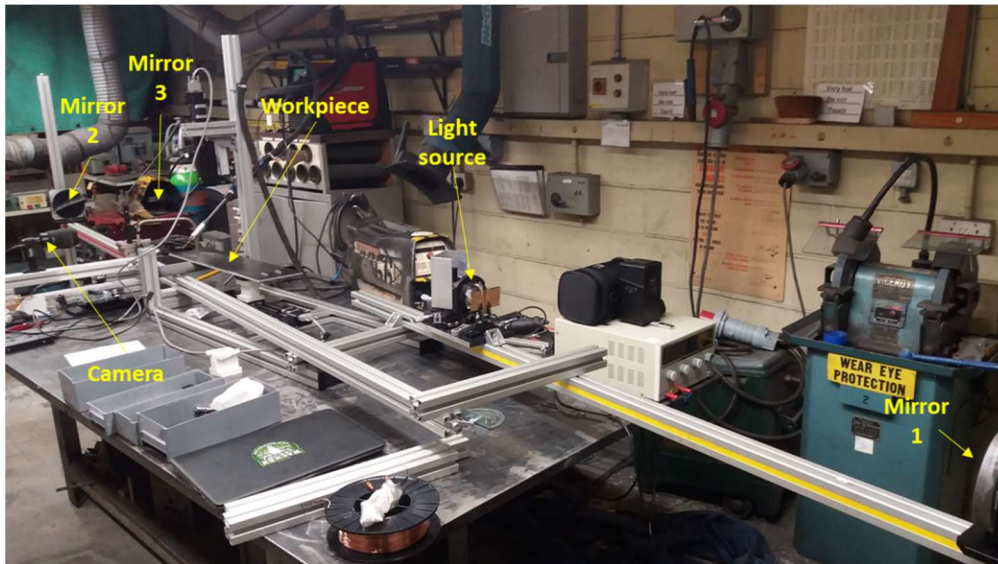


Figure 3-15 Annotated photograph of Schlieren rig set up [3.11]

This set up allows the shielding gas to be visualised through the high speed camera so that the behaviour of the gas can be monitored during the welding process [Figure 3-16]. The welding process was conducted using a stationary welding torch located between the two parabolic mirrors. The gas flow was measured before each experiment using a calibrated gas flow meter. The following Tables 3-2 and 3-3 show the parameters that were kept constant and varied during the experiments. Figure 3-16 provides an example of the shielding gas visualisation/image that is achieved through the above Schlieren set up. The Schlieren set up works as a consequence of light rays being deflected when they pass through fluids of varying densities. It also allows the interaction of the shielding gas to the surrounding air to be visualised (due to the different densities of these gases). Also because of the high temperatures generated during the welding process, the Schlieren process also provides a visualisation of any large temperature gradients (which result in a change in the density of the surrounding gas)



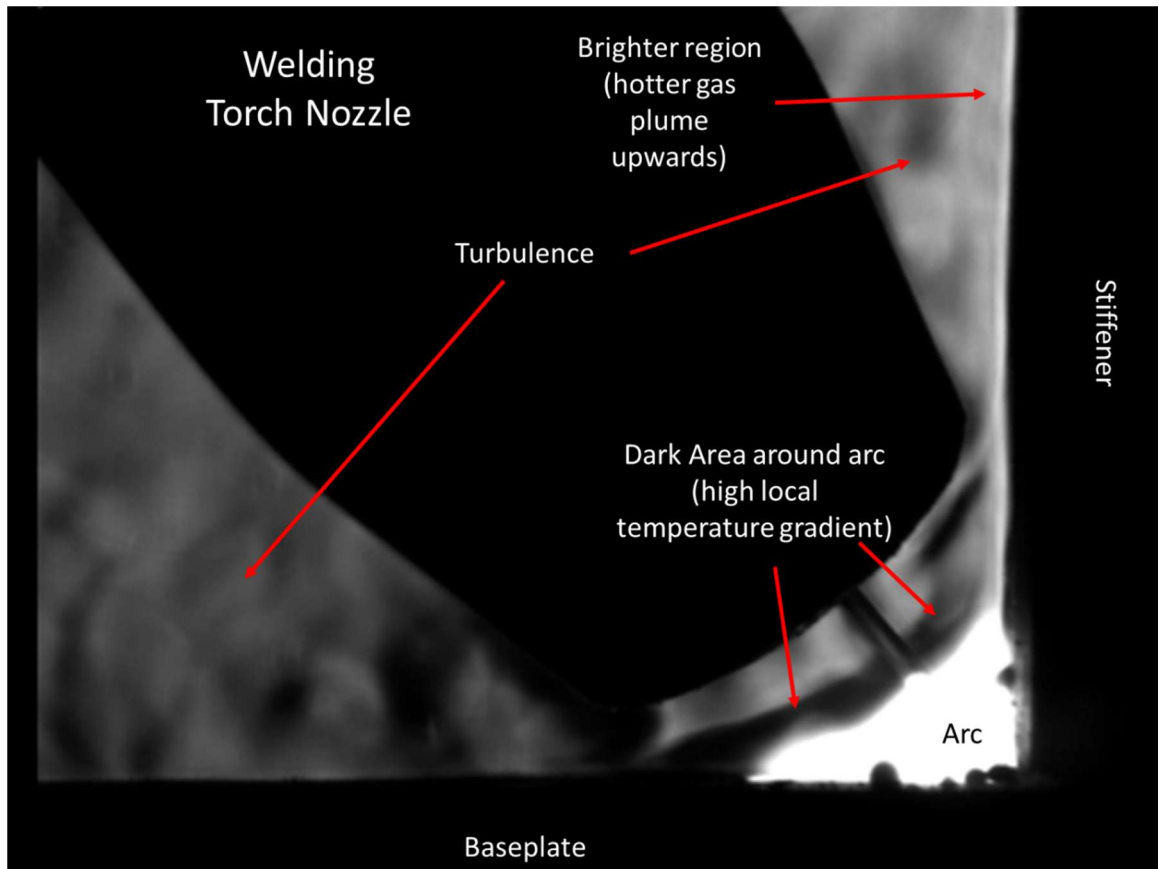


Figure 3-16 Shielding Gas visualisation - through high speed camera [3.11]

Table 3-2 Gas Visualisation Welding Parameters (Constant)

Gun angle	Travel angle	Wire Feed Speed (m/min)	Nozzle Diameter (mm)	Arc Energy (kJ/mm)	Wire Stick Out (mm)	Material
45°	30°	~10	16	0.75	15	DH36 6mm carbon steel

Table 3-3 Gas Visualisation Welding Parameters (Variables)

Welding Process	Electrode	Shielding Gas	Current (A)	Voltage (V)	Travel Speed (mm/s)	Shielding Gas Flow Rate (l/min)	Travel angle
GMAW	Solid Carbofil 1	Argon	180	27	6.5	6, 9, 12, 15	Push/Pull
FCAW	SF 1A	Argoshield (20% CO <sub>2</sub> )	235	28.5	9	0,3,6,9,12,15	Push/Pull

Both flux core and solid core welding processes were tested during this experiment. The solid wire was used to validate against a 3D fluid flow model (COMSOL) [3.11] and the flux cored process was used to reflect current welding processes used within BAE Naval Ships. Although the results from the two sets of experiments are not directly comparable, they provide a reasonable method of comparing welding processes against a validated 3D model. The experimental schedule is detailed in the Table 3-4 below.

Table 3-4 Gas Visualisation Experimental Schedule

GMAW – Solid Wire			FCAW – Flux Cored Wire		
Expt #	Gas Flow (l/min)	Torch Orientation	Expt #	Gas Flow (l/min)	Torch Orientation
1	20	Push	F2	15	Push
3	20	Pull	F3	15	Pull
6	15	Push	F4	12	Push
7	15	Pull	F5	12	Pull
4	12	Push	F6	9	Push
5	12	Pull	F7	9	Pull
8	9	Push	F8	6	Push
11	9	Pull	F9	6	Pull
9	6	Push	F10	3	Push
10	6	Pull	F11	3	Pull
			F12	0	Push
			F13	0	Pull

## 3.6 GMAW Fillet Welding Experiments

### 3.6.1 Equipment

Initial experiments were carried out in BAE Systems Naval Ships, Govan Training Centre using actual calibrated production equipment in a controlled /training centre environment. These experiments provided a good representation of the challenges faced by welders when trying to maintain a consistent fillet weld during 'real' production conditions. There were, however, significant limitations with this set up. Due to the configuration of the equipment it was difficult to control the travel and gun angles accurately which hence made it impossible to run repeatable experiments. All subsequent experiments were conducted on a custom-made welding rig within the University of Strathclyde, Mechanical Engineering and Aerospace Dept Laboratory [Figure 3-17]. This rig provided an increased level of control over the speed and position of the welding torch.

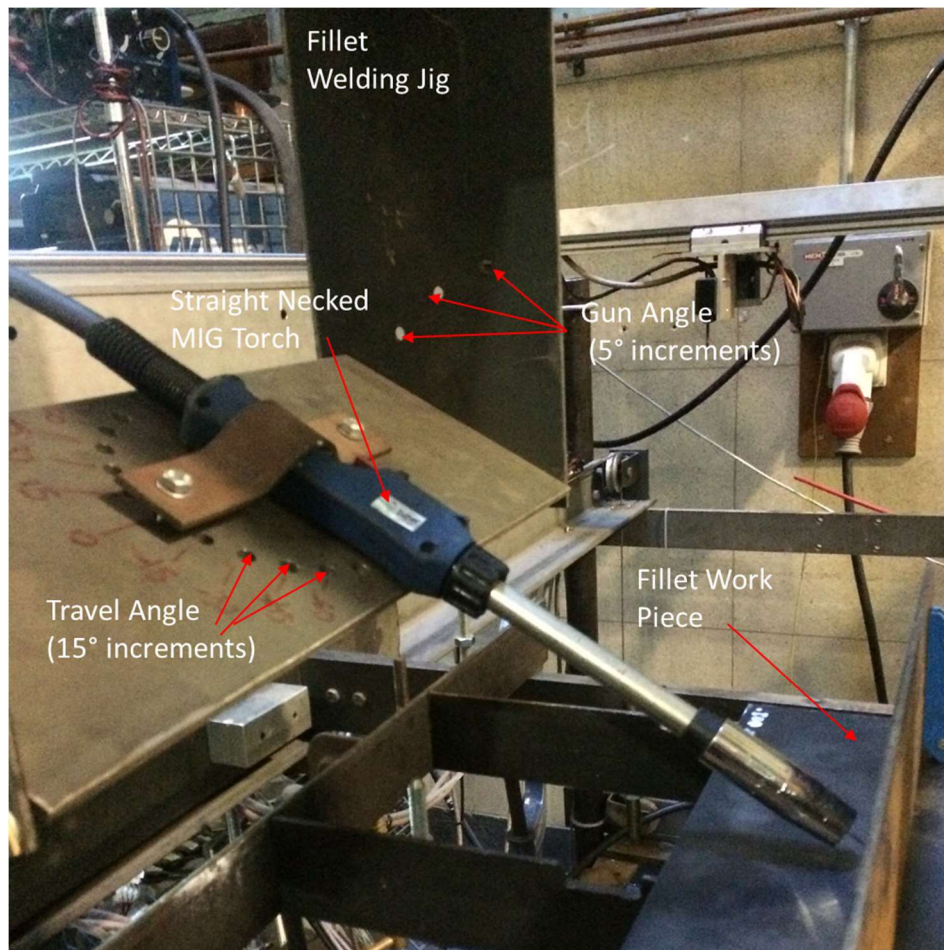
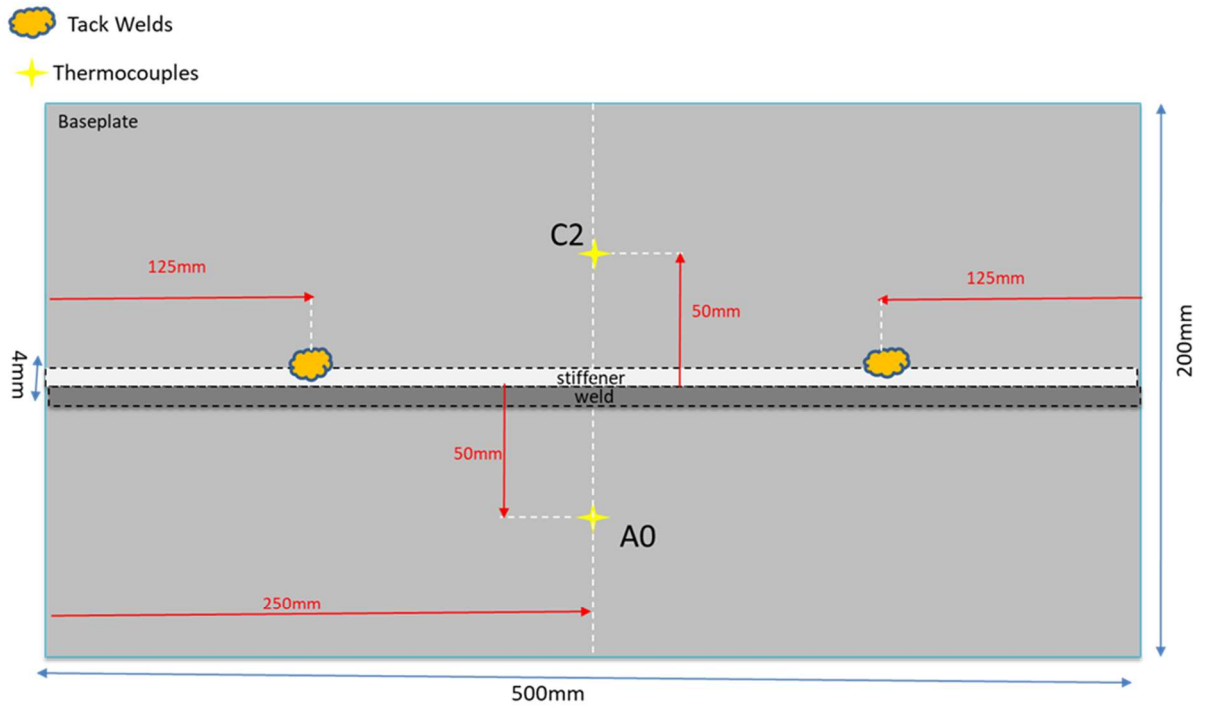


Figure 3-17 Automated Welding Rig at the University of Strathclyde

The speed of the rig is controlled by two programmable stepper motors. Prior to each batch of experiments the rig speed was calibrated using a measuring tape and a stopwatch to ensure consistency across all the experiments. The variation between the set and actual speed varied between 3.5%-4.9% across all experiments. A customised jig was developed to set the gun and travel angle. The jig was designed to allow the gun angle to be set at 5° increments from 35° - 50° relative to the horizontal base plate. The jig also allowed the torch travel angle to be set 15° increments from -30° to +30° relative to the direction of travel. The gun angle was manually confirmed with an inclinometer in order to ensure repeatability across all experiments. A pre-calibrated Portable Arc Monitoring System (PAMS) was connected to the equipment during the experiments to obtain accurate readings for the arc voltage and current. The PAMS produced a printed reading of the current and voltage readings at 1 second intervals for each experimental weld. Prior to each experimental run the set voltage and current were compared with the output readings on the PAMS units. Across the full range of experiments the variation between the pre-set and the actual voltage and current readings ranged from between 4-7%. This provided confidence that there were minimal losses between the welding power source and the arc at the end of the torch. The GMAW process was completed using the following equipment:

- Miller AMT 304 Series Power Supply
- Miller 20 Series 24V wire feeder
- Oerlikon straight necked torch

S355 J2+N was the carbon steel material used in this research project. This is equivalent to DH36. The chemical composition is shown below in Table 3-5. The fillet weld joints were fabricated from 4mm thick base plates (500mm x 200mm x 4mm) with a 4mm thick stiffener. The stiffener was positioned in the centre of the baseplate and was held in place with two tack welds positioned approximately equidistant along the length of the welded specimen. Both the baseplate and stiffener were coated in a weldable primer (Interplate 855 grey) in order to best simulate actual production conditions of material condition of supply. For the purpose of these experiments the impact of the weldable primer on the overall welding process is assumed to be negligible.



(Thermocouple on reverse side of welded fillet joint)

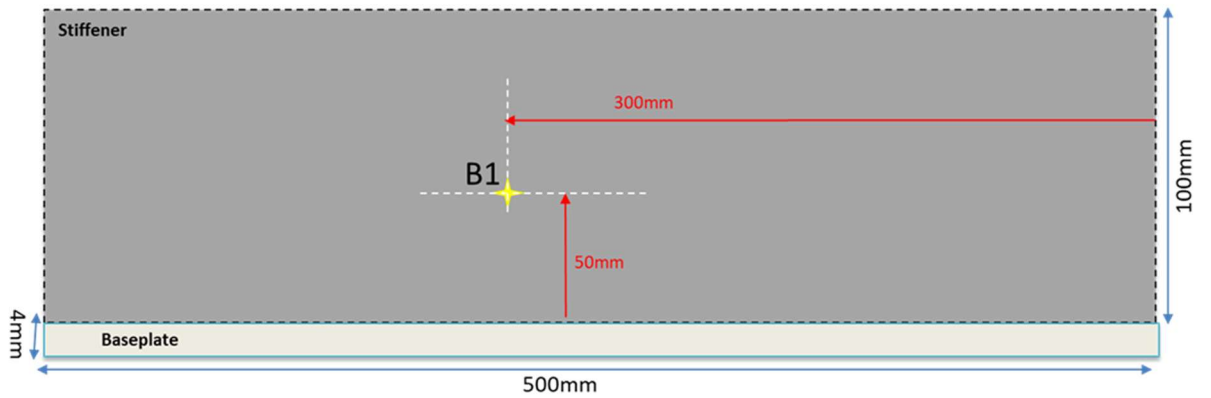


Figure 3-18 Diagram showing welded test piece dimensions, location of thermocouples and tack welds

Table 3-5 Chemical Composition for S355 J2+N Steel Plate

Element	Mn	P	S	C	Si	Al	Cu
Content (%)	1.097	0.012	0.003	0.136	0.168	0.036	0.013
Element	Nb	Ni	Cr	V	Mo	Ti	N
Content (%)	0.012	0.009	0.012	0.001	0.001	0.001	0.003

Metal Core Electrodes (MC-1) were used for the majority of the experiments. The chemical composition for this filler wire is shown below in Table 3-6. Metal cored electrodes were the preferred option as they provide a higher deposition rate and better penetration due to the higher current density and so are favourable to support high volume automated welding. However, a comparison of the geometrical and metallurgical impact of changing between metal cored, solid and flux cored wire electrodes is included within Chapter 8. The shielding gas used during the experiments was a mixture of Argon (80%) and Carbon Dioxide (20%) which was supplied from a gas cylinder located adjacent to the rig. The bottle was connected to a digital gas flow meter so that the gas flow from the cylinder could be monitored and controlled during experiments.

Table 3-6 Chemical Composition for Metal Core, Flux Core and Solid electrodes

Element		C	Si	Mn	P	S	Cu
Content (%)	Metal Core (MC-1)[3.12]	0.06	0.50	1.50	<0.015	<0.015	-
	Flux Cored (SF-1A)[3.12]	0.05	0.41	1.36	0.010	0.008	0.26
	Solid[3.13]	0.08	0.9	1.50	<0.025	<0.025	-

### 3.6.1.1 Experimental Parameters

Table 3-7 details which parameters were varied and which were kept constant during the experiments.

Table 3-7 GMAW Fillet Weld Experimental Parameter Settings

	Parameter	Setting	Description
<b>Variables</b>	Gun angle (°)	40,45,50	Controlled using pre-set jig, checked and measured using magnetic inclinometer
	Travel angle(°)	-30, -15, 0, 15, 30	Controlled using pre-set jig (-ve travel angle = pull, +ve travel angle = push)
	Travel Speed (mm/min)	300,400, 500	Set using Matlab software connected to Welding Rig. Calibrated prior to each test run
	Voltage (V)	21,24,26	Controlled using Miller Power Source and measured on calibrated PAMS unit
	Current (A)	170, 220, 270	
	Contact Tip to work distance (CTWD) (mm)	15	Measured with steel ruler prior to each experiment
	Gap (mm)	0	Gap between the stiffener and baseplate
<b>Constants</b>	Wire Type	MC-1 (metal cored)	-
	Material	S355 Mild Steel Primed Plate – Interplate 855 Grey	-
	Gas Flow (l/min)	18 l/min	Measured using calibrated gas flow meter
	Shielding Gas	BOC Specshield 20% CO <sub>2</sub> / 80% Argon	-
	Nozzle Diameter (mm)	16mm	-
	Plate Thickness (mm)	4mm	-

### 3.6.1.2 Practical Challenges

There was a number of unique challenges specifically around the welding of a fillet joint. Maintaining control of both the gun angle and travel angle during set up took longer than expected as between experiments. The gun and travel angles had to be re-checked to ensure that the torch position had not moved relative to the test piece. 1-2mm changes in vertical and horizontal position of the torch had a major impact on torch set up. A significant amount of time was also required to ensure that the torch maintained a

consistent distance from the base of the stiffener. The experimental set up made it difficult to alter the torch position once the arc had been struck and so in order to maintain a consistent standoff along the length of the weld a 'dry run' was conducted before every weld so that the standoff distance could be measured along the length of the test piece to ensure that any slight deflections/imperfections in the plates would not impact the location of the torch relative to the baseplate and stiffener. The size of the nozzle has a practical impact on the range of available gun angles. A 16mm nozzle was used for all experimental work detailed within this study. Figures 3-19 and 3-20 illustrate the range of available gun angles and CTWDs available for a 16mm nozzle in a downhand (2F) configuration.

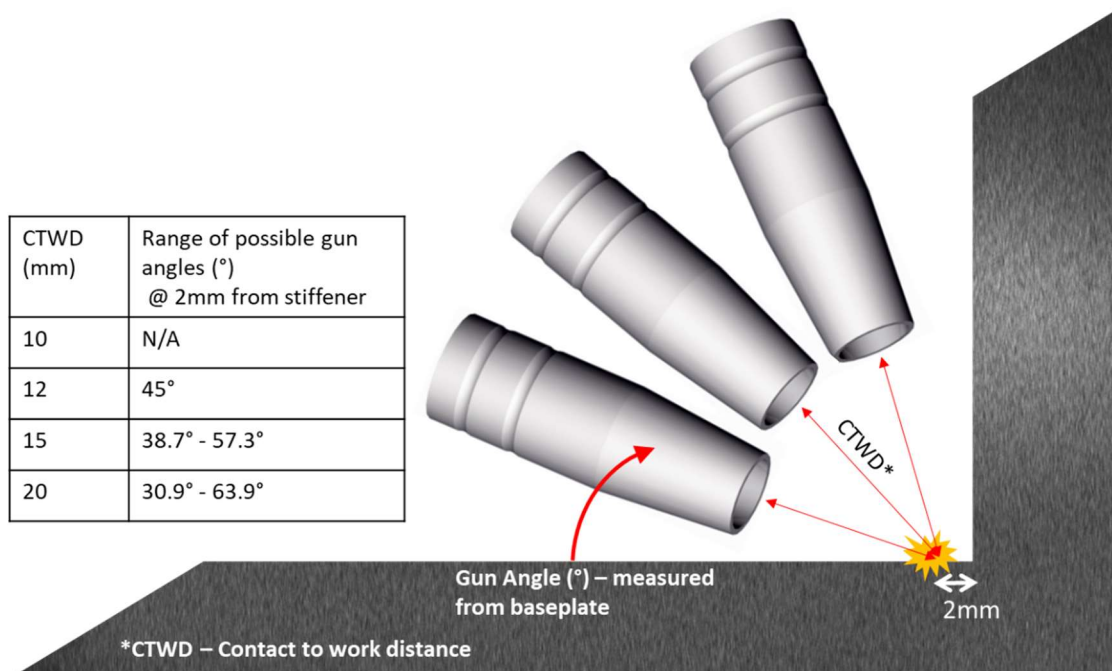


Figure 3-19 Range of possible welding torch gun angles



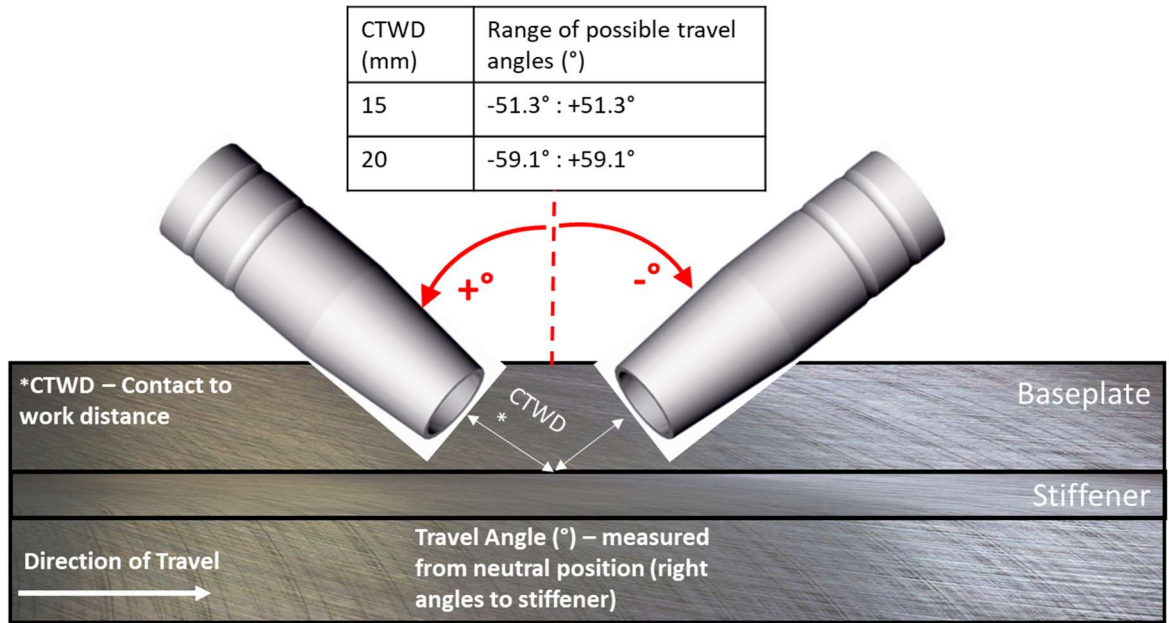


Figure 3-20 Range of possible welding torch travel angles

### 3.6.2 Hardness Testing

After welding, the test pieces were cut down to 30 mm x 30 mm x 20mm sized samples using a Struers Discotom cutting machine. Once the samples had been cut to size, they were hot mounted in a Bakelite compound using a hot press and finally polished using a series of grinding discs and polishing stones. Figure 3-21 shows an example of a mounted and polished fillet weld sample.



Figure 3-21 Example of mounted and polished sample

The manual hardness results were carried using a Mitutoyo MVK-G1 hardness testing machine. This machine calculates the hardness by using a diamond tipped indenter to apply a load into the test metal. The size of the indent is then measured and the hardness of the material calculated using the following equation.

$$HV = C \times \frac{F}{D^2} \quad \text{Eqn. 3-6}$$

Where:  $HV$  is the Hardness Value  
 $C$  = constant for the indenter  
 $F$  = applied load (kN)  
 $D$  = average diagonal of the indentation (mm)

The settings used were Lens x55, Timer 15secs and HV-200g Vickers. This process was then repeated using the IACS, International Association of Classification Societies, [3.10] W28 welding qualification hardness test procedure [Figure 3-22] for positional guidance.

According to IACS the results from the hardness test are not to exceed:

- 350HV/10 for steels with a minimum yield strength ( $R_{eH}$ )  $\leq$  420 MPa
- 420HV/10 for steels with a minimum yield strength ( $R_{eH}$ ) between 420 MPa-690MPa

The minimum yield strength of the DH36 Steel plate used within the experiments was 390MPa.

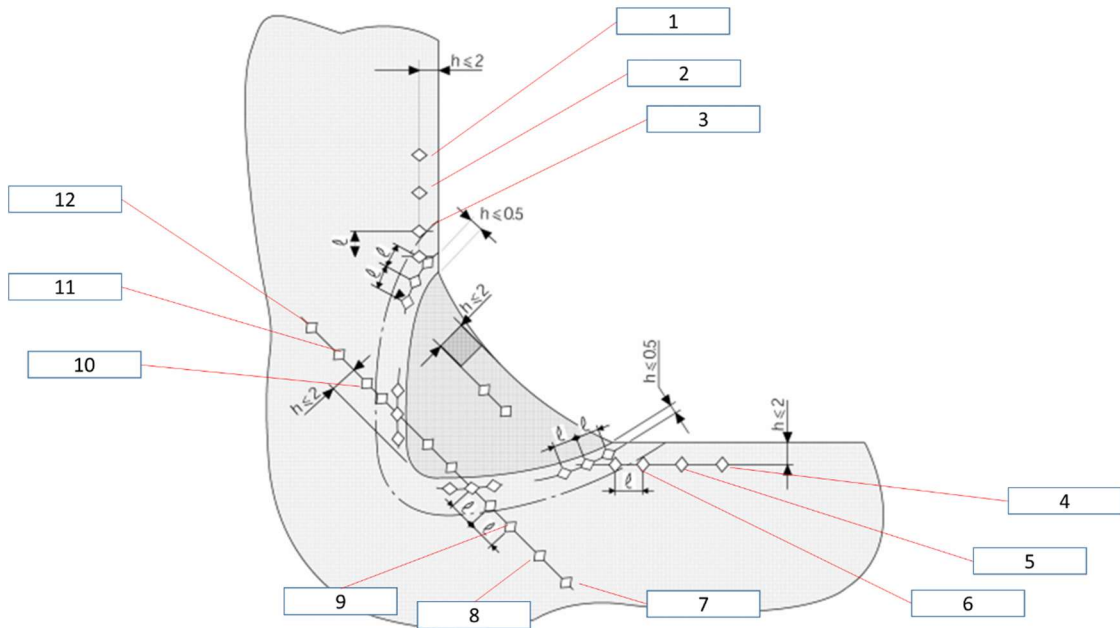


Figure 3-22 IACS W28 Fillet Weld [3.10]

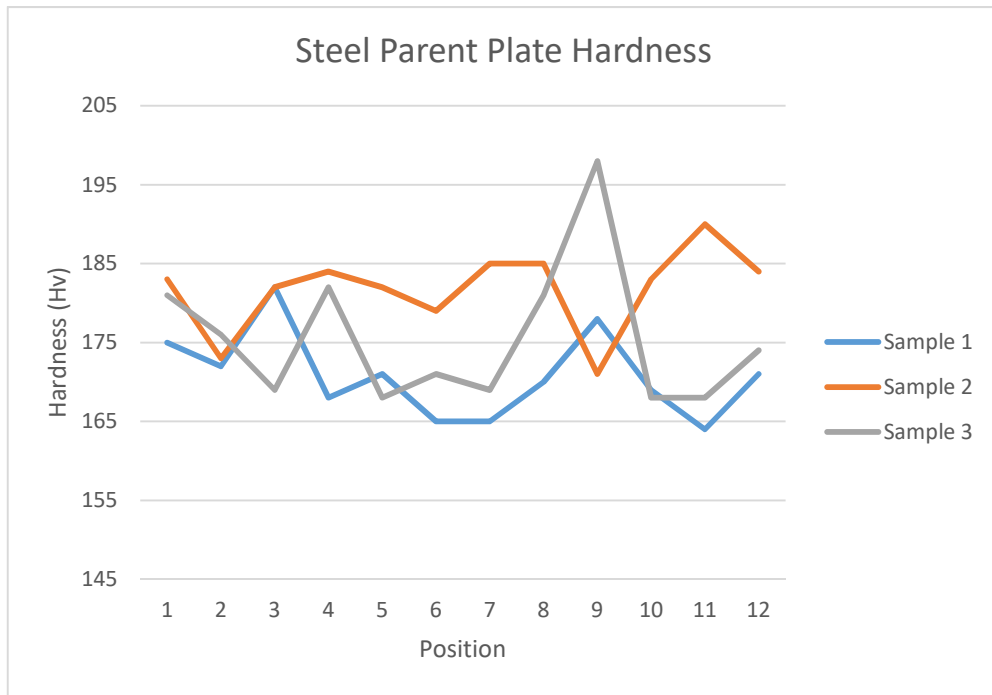


Figure 3-23 Hardness results from parent plate

The location of the results in Figure 3-23, along the x-axis, are highlighted in Figure 3-22. The results highlighted a range of between 2%-15% variation between the readings on similar points across the 3 samples. This suggested that this method of comparing the samples would be satisfactory for drawing indicative conclusions; however, due to the variation it would not be a reliable method for drawing concrete conclusions. The cause of this variation is due to the fact that a small point sample is used to represent the hardness of a much larger area. Consequently, an alternative method of measuring the hardness profile of weld samples was investigated. BAE Systems Barrow have an automated hardness profiling machine which maps the hardness using a large number of point results over the measured area. The samples were prepared and polished in a similar way, but instead were inserted into a pre-programmed hardness machine which took a large number of hardness measurements over a predefined area (square grid visible around weld area on macro below). The output of this analysis is an excel file with the hardness results which can then be used to create a hardness map [Figure 3-24]. Due to the larger dataset produced, this method of hardness profiling produces a much more accurate understanding of the overall hardness of the weld.

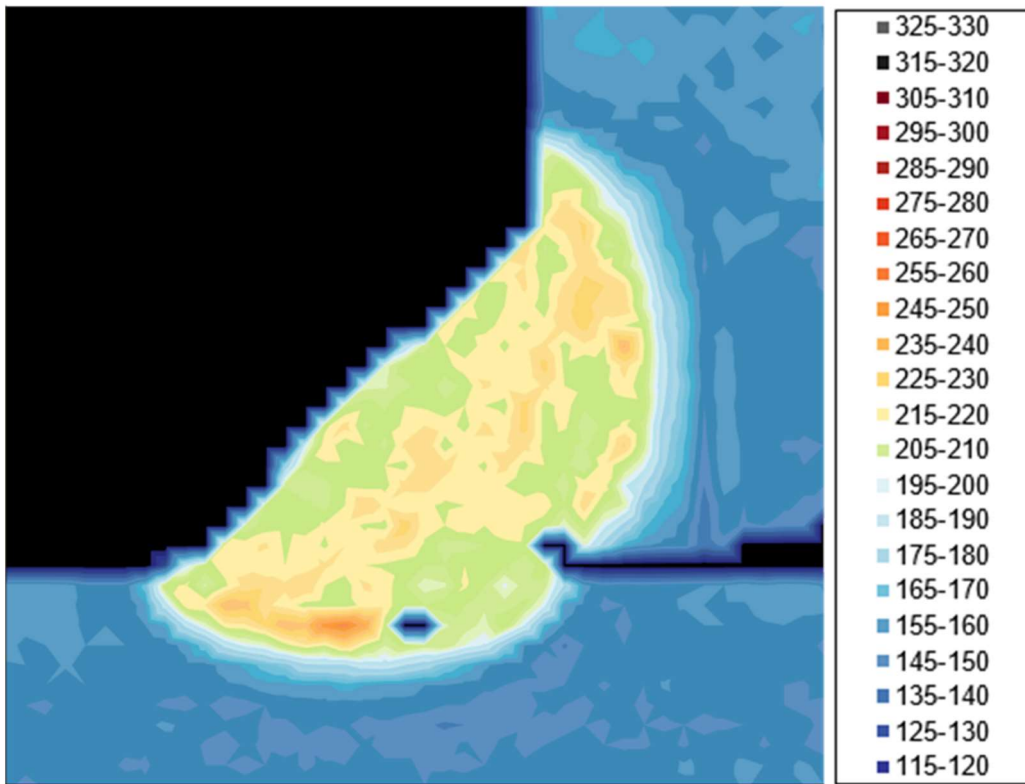


Figure 3-24 Example of automated hardness map of fillet weld sample



Figure 3-25 Example polished test piece used to generate hardness map

### 3.6.3 Macrographs /Microstructure

Macrographs of the samples were then created by firstly applying some etchant with a cotton bud onto the polished surface. The etchant brightens the weld area and heat affected zones and makes the macro grain structure visible, [Figure 3-26]. Once the grain structure is visible the etchant was then washed off the sample and it was then photographed with a steel ruler in shot. This photograph was then used to measure the internal geometry of the weld using ImageJ (picture analysing software) using the steel ruler to calibrate the quantity of pixels/mm for each image.

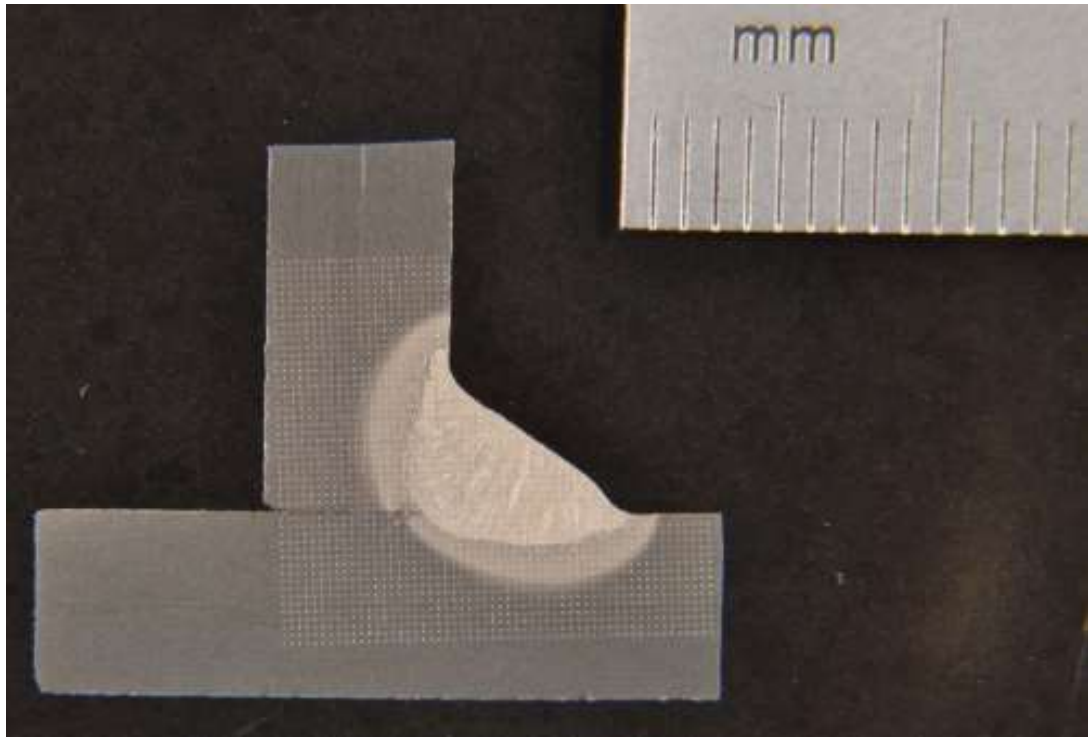


Figure 3-26 Fillet Weld Sample after etching

After the samples had been etched, they were then photographed under a microscope which was able to produce a 500x magnification of weld and surrounding areas, which allowed the microstructure of the test samples to be visualised and compared. Figure 3-27 is an image of the microstructure of the original steel plate material that has not been affected by the heat from the welding process. The steel plate has a typical banded ferrite pearlite microstructure. The light areas are the ferrite grains and the darker regions are pearlite. Pearlite has a harder microstructure compared to ferrite. When this structure is affected by the heat from the weld, it changes and the resultant structure is a function of how close the HAZ region was to the weld.



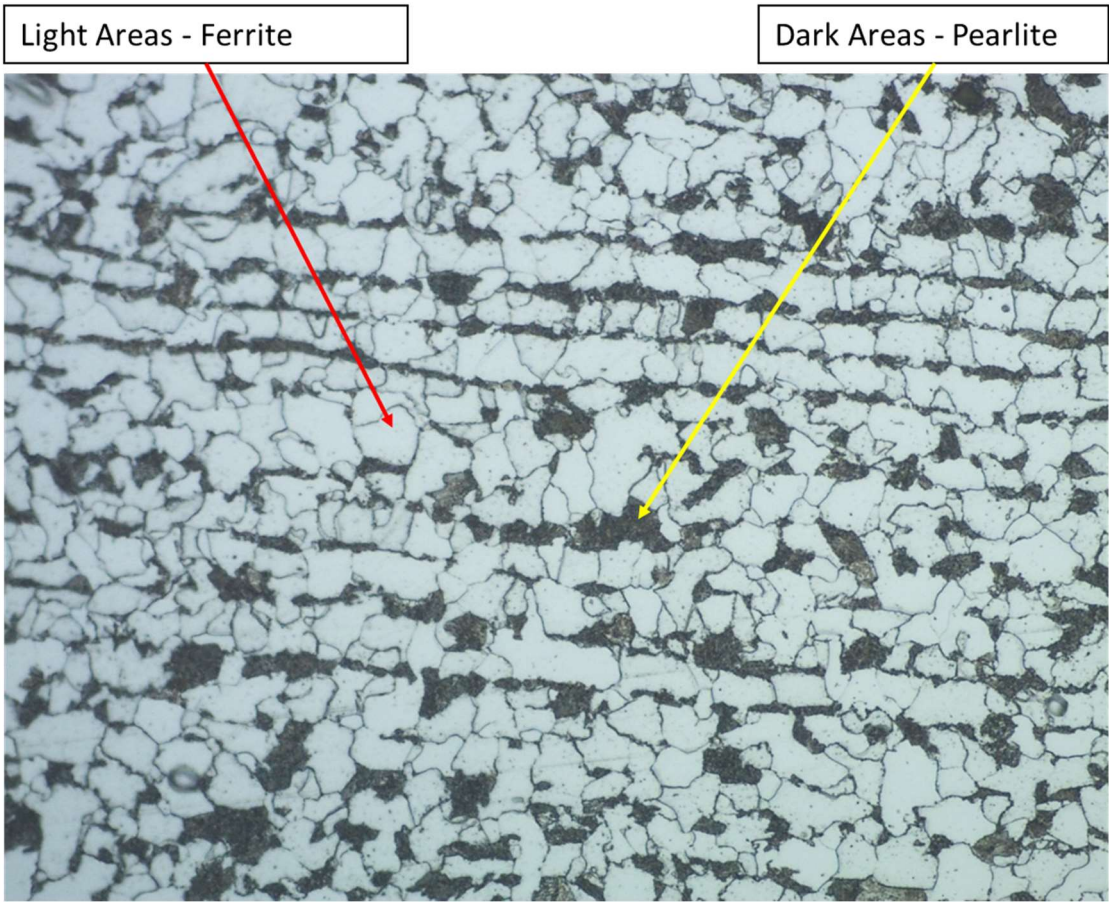
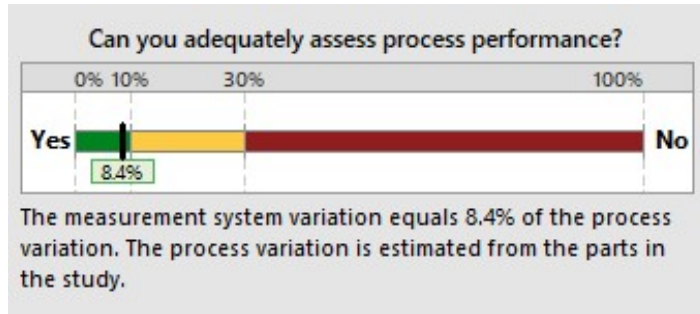


Figure 3-27 Microstructure of unaffected baseplate



### 3.6.4 Fillet Weld Geometry Measurement System

ImageJ (image analysis software) was used to measure the internal geometry of the fillet welds from the respective macrograph images. The individual macro images were loaded into ImageJ and a line was then drawn between the 5mm and 10mm markers on the ruler in the top right hand side of the picture. This line was used to calibrate the number of pixels over a known distance (5mm). Once calibrated the internal geometry of the weld could be measured using the 'line' and 'measure' functionality within the toolset. In order to ensure that this measurement system is capable of accurately measuring the internal geometry of a fillet weld, a simple Gage R&R (repeatability and reproducibility) study was conducted. Four 'operators' were trained how to use the measuring system and asked to make 10 measurements on 2 fillet weld macros. This was repeated 3 times so that both the repeatability (variation in measurement taken by a single operator) and reproducibility (variation in average measurements of different operators) could be assessed. The measured results were then input into Minitab and a MSA (measurement system analysis) was initiated. The results of the analysis are shown below in Figure 3-28.



<10% - World Class  
 10-30% - Acceptable  
 >30% - Unacceptable

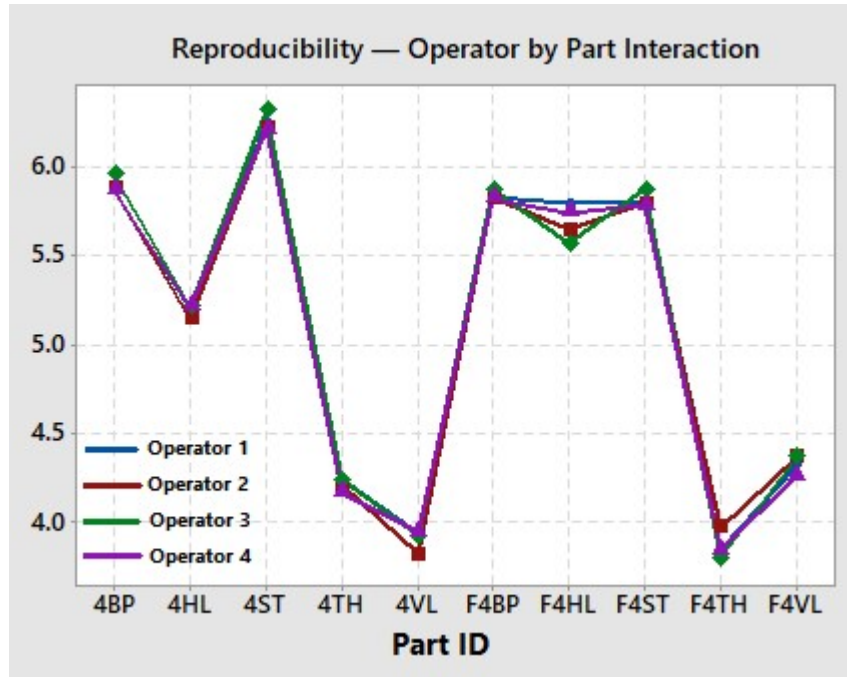


Figure 3-28 Results from Gage Reproducibility and Repeatability Study

The analysis highlighted that the measuring system variation was 8.4% of the process variation (estimated from the parts in the study). Variation of less than 10% is deemed to be World Class, 10-30% acceptable and if it is >30% then it is unacceptable measurement system. Thus it can be concluded from this analysis that the Image J measurement system, used to measure the fillet weld geometry, is an acceptable, repeatable method of measuring on average to within 0.05mm.

### 3.7 References

- 3.1. Bhadeshia, H. K. D. H. (1999). Neural networks in materials science. ISIJ International. <https://doi.org/10.2355/isijinternational.39.966>
- 3.2. Beckett, S., MacPherson, M. J., McPherson, N. A. (2011). Improved welding control of automated fillet welding for ship structures using Artificial Neural Networks (ANN). JOM 16 Conference, Denmark.
- 3.3. Campbell, S. W., Galloway, A. M., & McPherson, N. A. (2012). Artificial neural network prediction of weld geometry performed using GMAW with alternating shielding gases. *Welding Journal*.
- 3.4. Kim, I. S., Son, J. S., Park, C. E., Kim, I. J., & Kim, H. H. (2005). An investigation into an intelligent system for predicting bead geometry in GMA welding process. *Journal of Materials Processing Technology*, 159, 113–118. <https://doi.org/10.1016/j.jmatprotec.2004.04.415>
- 3.5. Carrino, L., Natale, U., Nele, L., Sabatini, M.L., Sorrentino, L. (2007). A neuro-fuzzy approach for increasing productivity in gas metal arc welding processes. *International Journal of Advanced Manufacturing Technology*, 32, 459-467. <https://doi.org/10.1007/s00170-005-0360-y>
- 3.6. Gray, T., Camilleri, D., & McPherson, N. (2014). Control of Welding Distortion in Thin-Plate Fabrication: Design Support Exploiting Computational Simulation. In *Control of Welding Distortion in Thin-Plate Fabrication: Design Support Exploiting Computational Simulation*. <https://doi.org/10.1533/9780857099327>
- 3.7. Kumar, A., Debroy, T. (2006). Neural network model of heat and fluid flow in gas metal arc fillet welding based on genetic algorithm and conjugate gradient optimisation. *Science and Technology of Welding and Joining*, <https://doi.org/10.1179/174329306X84319>

- 3.8. Camilleri D, Comlekci T, Lee C K, Tan H and Gray T G F: 'Investigation of temperature transients during flux-cored Ar/CO<sub>2</sub> butt welding of CMn steel plates,' Proc. Int. Conf. Metal Fabrication and Welding Technology (METFAB – 2003) Nottingham, UK 2003 107-16.
- 3.9. Bitharis, I., McPherson, N. A., McGhie, W., Roy, D., & Moore, A. J. (2018). Visualisation and optimisation of shielding gas coverage during gas metal arc welding. *Journal of Materials Processing Technology*.  
<https://doi.org/10.1016/j.jmatprotec.2017.11.048>
- 3.10. International Association of Classification Societies. Requirements concerning Materials and Welding, W28 Welding Procedure qualification tests of steels for hull construction and marine structures. IACS Req. 2005/Rev.2 2012, p.20
- 3.11. Bitharis, I. (2018) 'Visualisation of shielding gas flows during high value manufacture', Engineering Doctorate Thesis, Heriot Watt University, Edinburgh
- 3.12. NST. *Product Catalogue*. [online] available at  
<http://nst.no/dokumenter/diverse/NST%20Catalogue%2014032014.pdf>
- 3.13. Oerlikon. *Carbofil 1 Datasheet* [online] available at  
[http://www.afrox-welding.co.za/en/images/Carbofil1\\_tcm282-30192.pdf](http://www.afrox-welding.co.za/en/images/Carbofil1_tcm282-30192.pdf)

## Chapter 4 GMAW Fillet Welding Process Capability Analysis

### 4.1 Semi-Automatic vs Robotic Welding - Results

Process capability analysis [4.1] is a statistical tool regularly used within Six Sigma and process improvement projects to assess how 'capable' a process is at achieving the predefined customer requirement. It can be used to assess any process that has been broken down to measure inputs and outputs numerically. Process capability analysis has been used here to quantify the process benefits of moving from a semi-automatic welding process to a robotic welding process. For the analysis the target fillet weld leg length was  $5\text{mm} \pm 1\text{mm}$  and the target penetration was  $0.5\text{mm} \pm 0.4\text{mm}$ . The semi-automatic process was set up to replicate production conditions as closely as possible and the welding rig set up was designed to simulate a more automated/repeatable process. The key differences between the two process set ups were:

- Improved control of travel angle and gun angle on welding rig
- Gas flow monitored and controlled using gas flow meter
- Current/Voltage monitored and controlled through inline portable arc monitoring system PAMS unit
- Speed controlled using calibrated stepper motor vs weldy-car

The results of both the semi-automatic process and welding rig process can be seen below in Figures 4-1 to 4-6.

Vertical (top) Leg Length

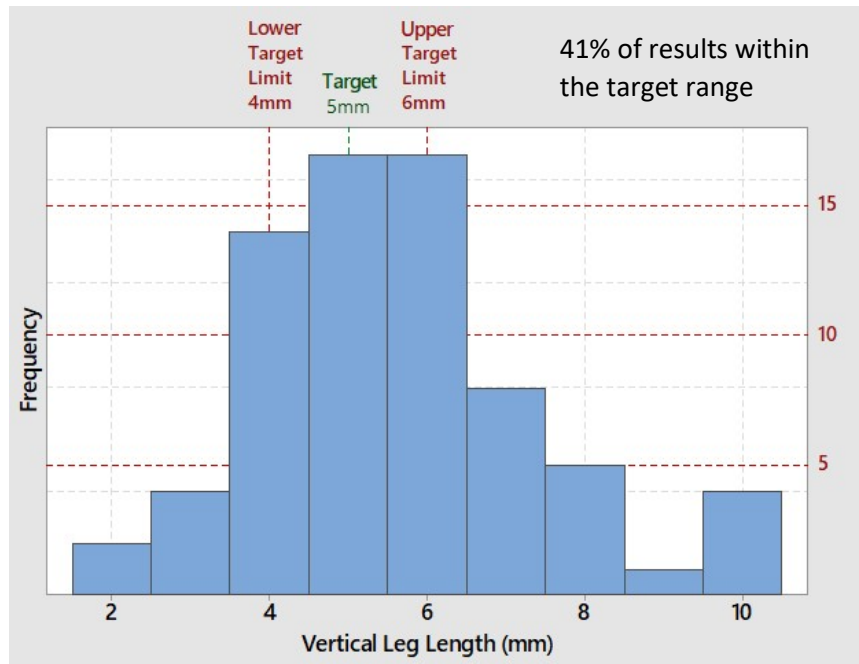


Figure 4-1 Semi-Automatic Set up – Vertical Leg Length Process Capability Graph

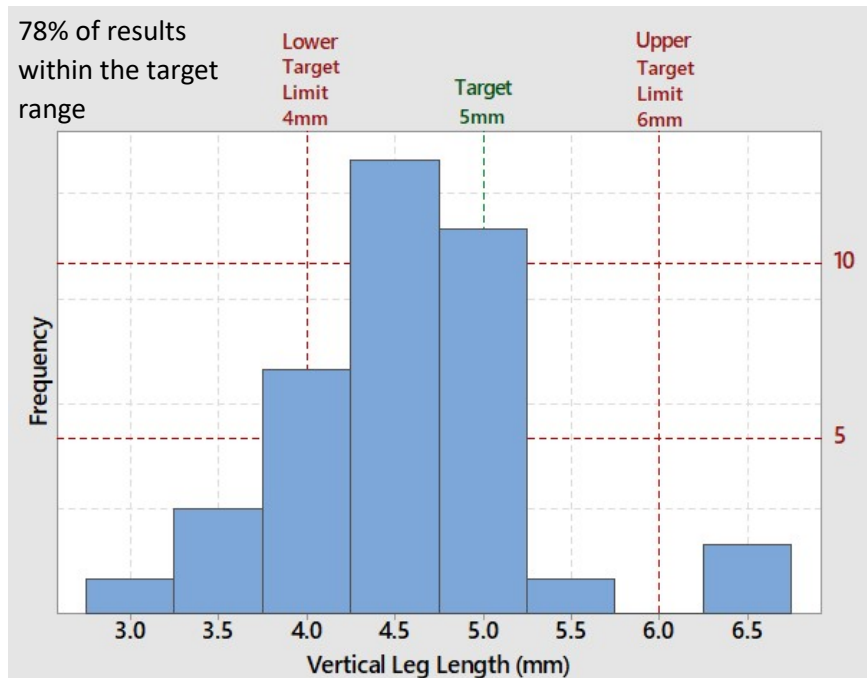


Figure 4-2 Robotic Set up – Vertical Leg Length Process Capability Graph

Horizontal (bottom) Leg Length

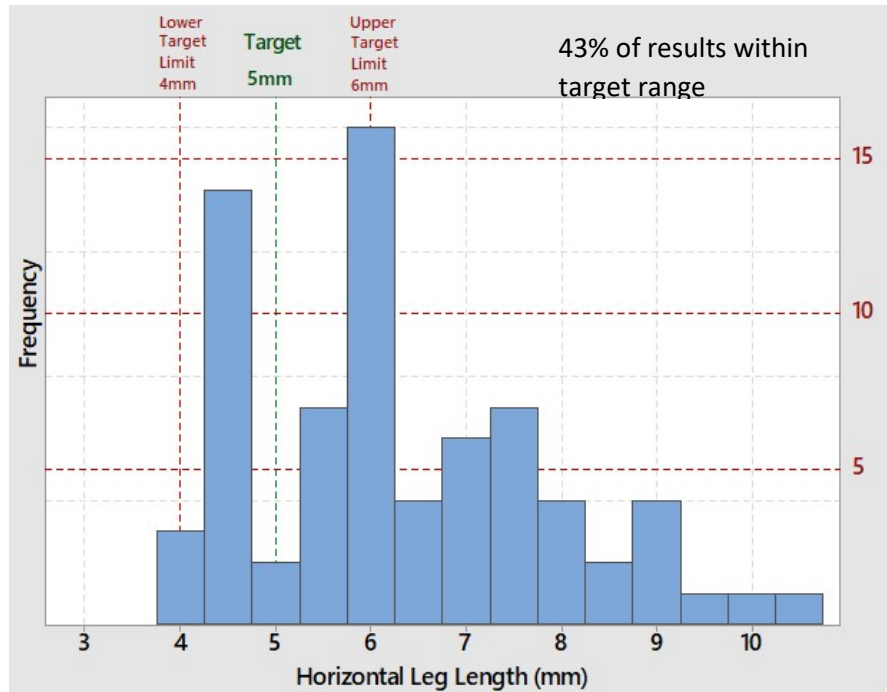


Figure 4-3 Semi-Automatic Set up – Horizontal Leg Length Process Capability Graph

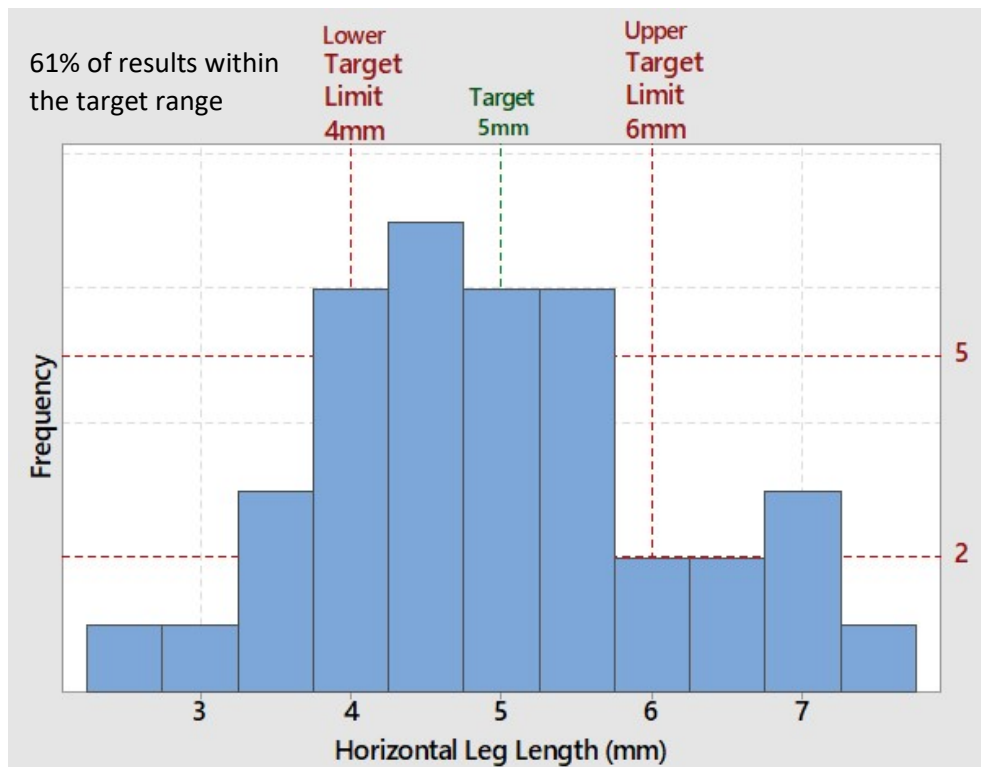


Figure 4-4 Robotic Set up – Horizontal Leg Length Process Capability Graph

Penetration

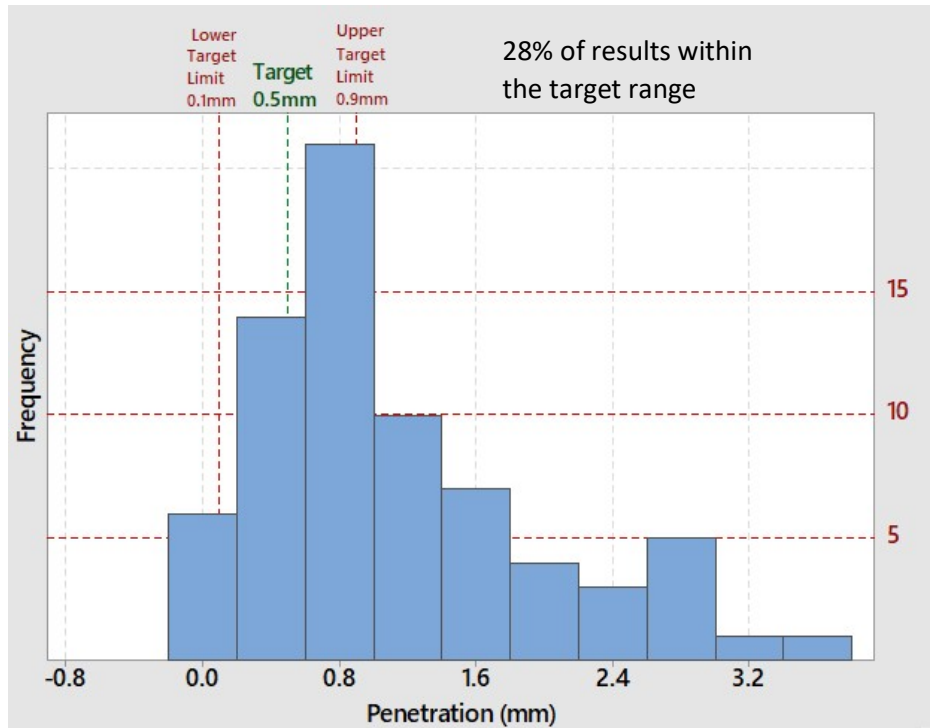


Figure 4-5 Semi-Automatic Set up – Penetration Process Capability Graph

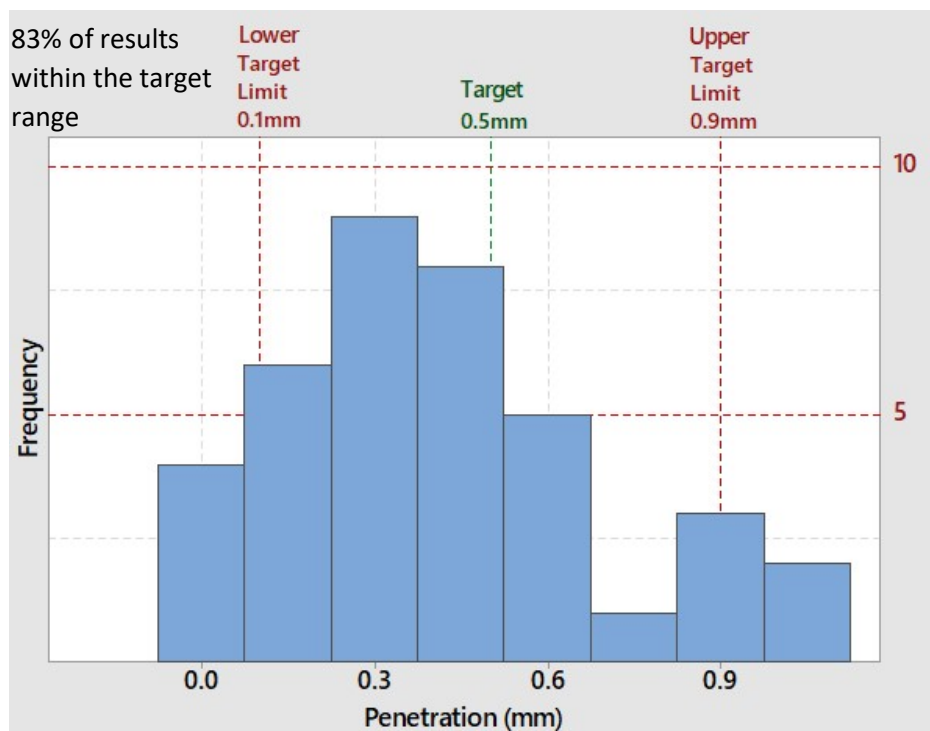


Figure 4-6 Robotic Set up – Penetration Process Capability Graph



The results from Figures 4-1 to 4-6 have been summarised in Table 4-1, provide a comparison of the process capability between a semi-automatic GMAW set up and a more tightly controlled process which would be comparable with an automated process.

Table 4-1 Summary of Semi-Automatic vs Automated process capability analysis

Geometrical Characteristic	Target Geometry (mm)	% of results within target	
		Semi-Automatic Process	Automated Process
Vertical Leg Length	5mm ± 1mm	41%	78%
Horizontal leg length	5mm± 1mm	43%	61%
Penetration	0.5mm ± 0.4mm	28%	83%

#### 4.2 Process Capability Analysis - Discussion

The results show a significant improvement in control of the resultant weld geometry through the automated process. Although based on a relatively small sample size and conducted in laboratory conditions, these results do provide a good indication of the process benefits that can be achieved through improving control and repeatability of the welding process parameters. Figure 4-5 highlights that a significant number of the semi-automatic welded test pieces were 'over penetrated'. This will result in additional heat being applied to the joint and in order to maintain a consistent throat with greater penetration a higher rate of wire deposition would be required. Figure 4-6 shows the number of over penetrated welds was reduced considerably using the automated process, reducing the weight and heat applied to the welded joint. This reinforces the potential savings that can be generated as a result of moving towards a fully automated robotic process.

Table 4-1 shows the capability of each process to achieve a target geometry of 5mm±1mm. The results, unsurprisingly, show that the automated/more tightly controlled process set up demonstrated a lower level of process variation, hence improved capability. By improving control of the welding torch orientation, the ability to control the process outputs is also

improved. This is evidenced by the significant increase in % of results within target for the automated set up, for both leg length and penetration in Table 4-1. The results of the sensitivity and interaction analyses, in Chapter 5, show that both the travel angle and gun angle are significant in determining the vertical and horizontal leg lengths of a fillet weld. This highlights that good control of the torch position, relative to the steel plates, is critical to ensuring a consistent leg length. The ability to control the weld geometry has significant benefits. Reducing the variation of leg length and penetration will improve the overall efficiency of the process by minimising the amount of over welding. This will result in less heat being applied (reducing distortion) to the structure, a reduced use of wire and shielding gas and also a reduction in weight of the welded structure.

### 4.3 References

- 4.1 Juran, J.M. (1998). 'Juran's Quality Control Handbook', 5th edition. (New York: McGraw-Hill)

## Chapter 5 Using Statistical Modelling to identify key parameters affecting fillet weld geometry

### 5.1 Results

#### 5.1.1 ANN - Identification of key parameters using ANN/Sensitivity Analysis

As described in Chapter 3 an ANN model was developed to predict the relationship between the GMAW fillet weld process inputs (current, voltage, travel speed, gun angle, travel angle) and the resultant fillet weld geometry (leg length, throat, reinforcement and penetration). Figure 5-1 graphs the output of the ANN model against the actual fillet weld geometry. The results show good overall agreement between the predicted and the actual outputs for both the vertical and horizontal leg length and the resultant penetration. The model was run 3 times in order to ensure acceptable levels of repeatability.

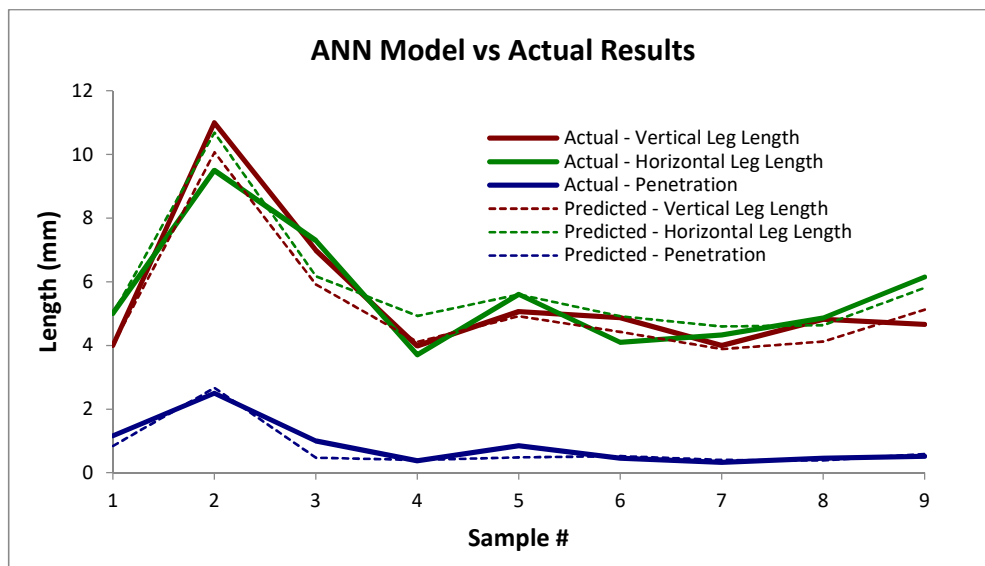


Figure 5-1 ANN Model Results (Actual vs Predicted)

Once the ANN model had been trained and tested, a sensitivity analysis was conducted using Neurosolutions for Excel. The results of the sensitivity analysis are shown in Figure 5-2. The analysis indicates that current was the most influential parameter in determining the penetration of the fillet weld and that the travel speed was the most influential parameter in determining the vertical and horizontal leg lengths, followed closely by the current.

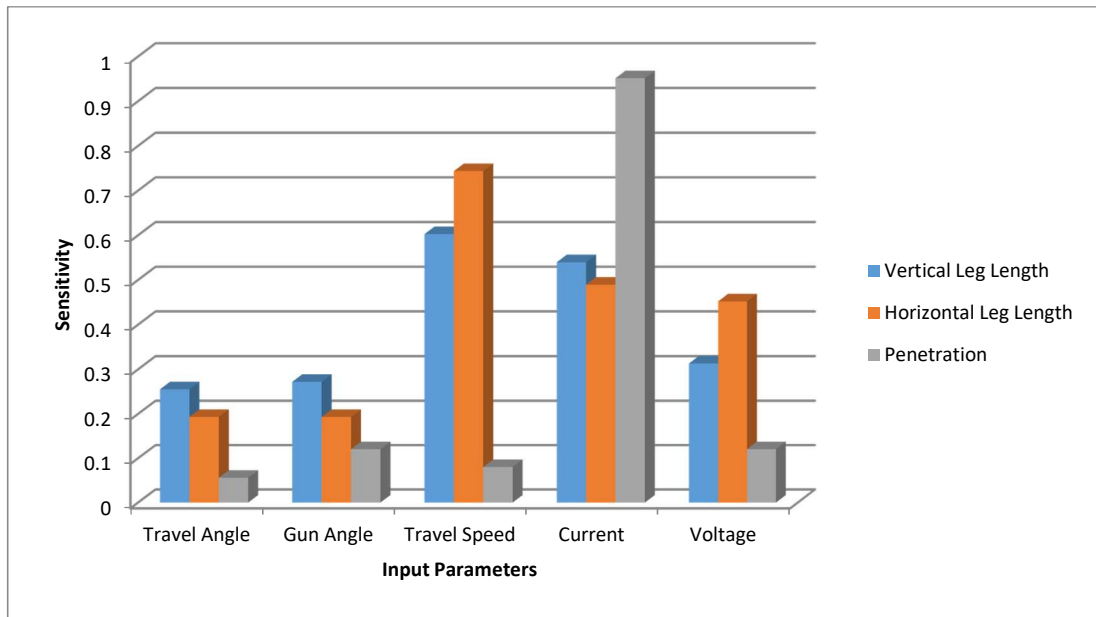
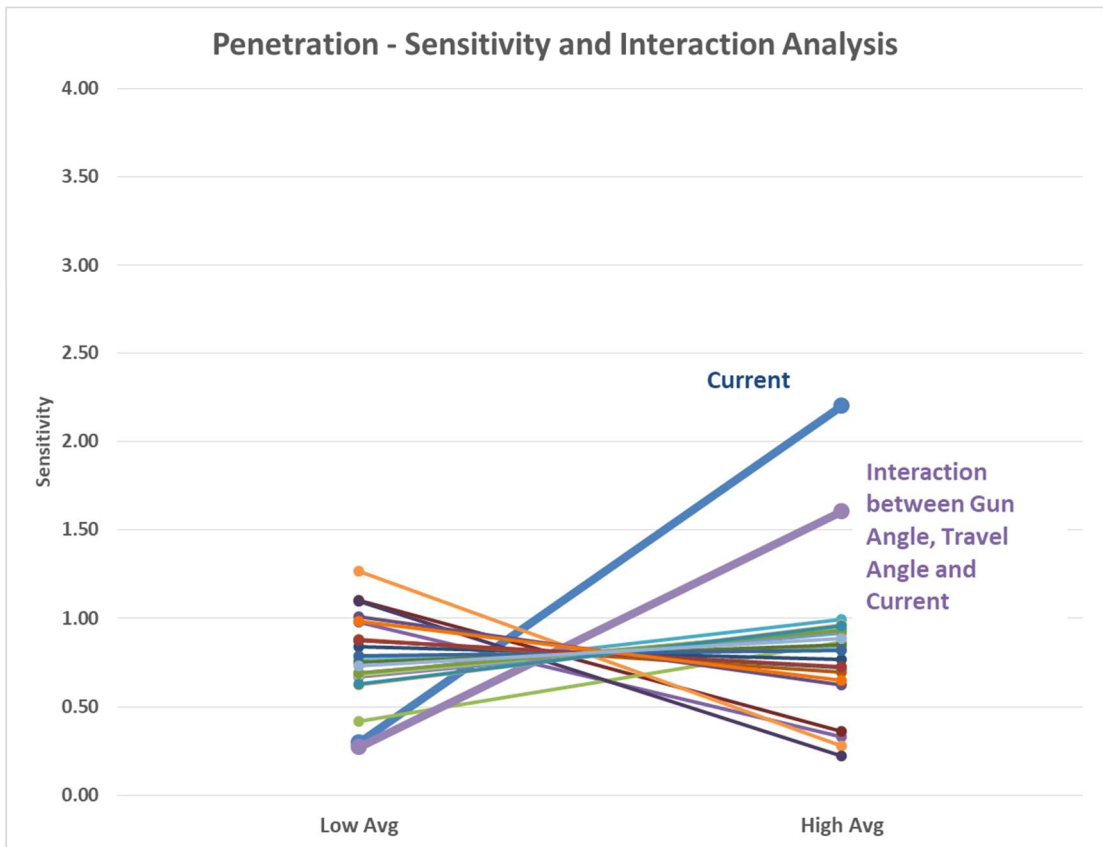


Figure 5-2 Results of ANN Sensitivity Analysis

This would be expected as both current and travel speed are directly linked to the heat input through equation 1-1 as described in Chapter 1. The analysis also shows that the travel angle and the gun angle are not insignificant in determining the vertical and horizontal leg lengths as single variables. This confirms the results of the regression analysis of the variables and their interactions and will be discussed in more detail later on in this chapter.

#### 5.1.2 ANOVA - Fillet Weld - Key Parameter Interactions Analysis of Variables

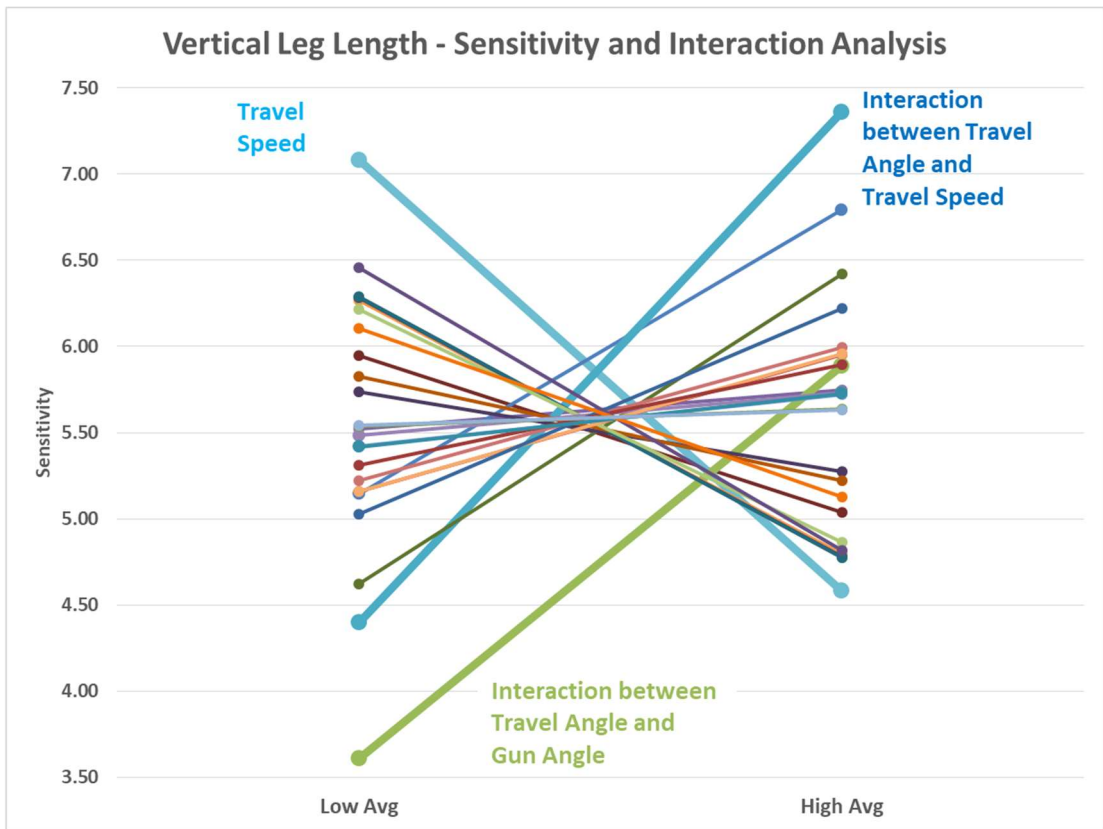
Following the results of the ANN model, an Analysis of Variance (ANOVA) [5.1] study was carried out in order to determine if any of the interactions between the input variables is significant in predicting the key geometrical features of the resultant fillet weld. The results are shown on Figures 5-3 to 5-7. The most significant parameters/interactions in identifying each of the key fillet weld features are highlighted on the respective graphs. The steeper the gradient of the lines on the graph the more significant the parameters in determining the output.



**Key Parameters and Interactions:**

- |  |  |  |
|--|--|--|
| <ul style="list-style-type: none"> <li>— A - Travel Angle (°)</li> <li>— D - Current (A)</li> <li>— AxC</li> <li>— BxC</li> <li>— CxD</li> <li>— AxBxC</li> <li>— BxCxD</li> <li>— AxBxCxD</li> <li>— AxBxCxDxE</li> </ul> | <ul style="list-style-type: none"> <li>— B - Gun Angle (°)</li> <li>— E - Voltage (V)</li> <li>— AxD</li> <li>— BxD</li> <li>— CxE</li> <li>— AxBxD</li> <li>— BxCxE</li> <li>— AxBxCxE</li> </ul> | <ul style="list-style-type: none"> <li>— C - Travel Speed (mm/min)</li> <li>— AxB</li> <li>— AxE</li> <li>— BxE</li> <li>— DxE</li> <li>— AxBxE</li> <li>— CxDxE</li> <li>— BxCxDxE</li> </ul> |
|--|--|--|

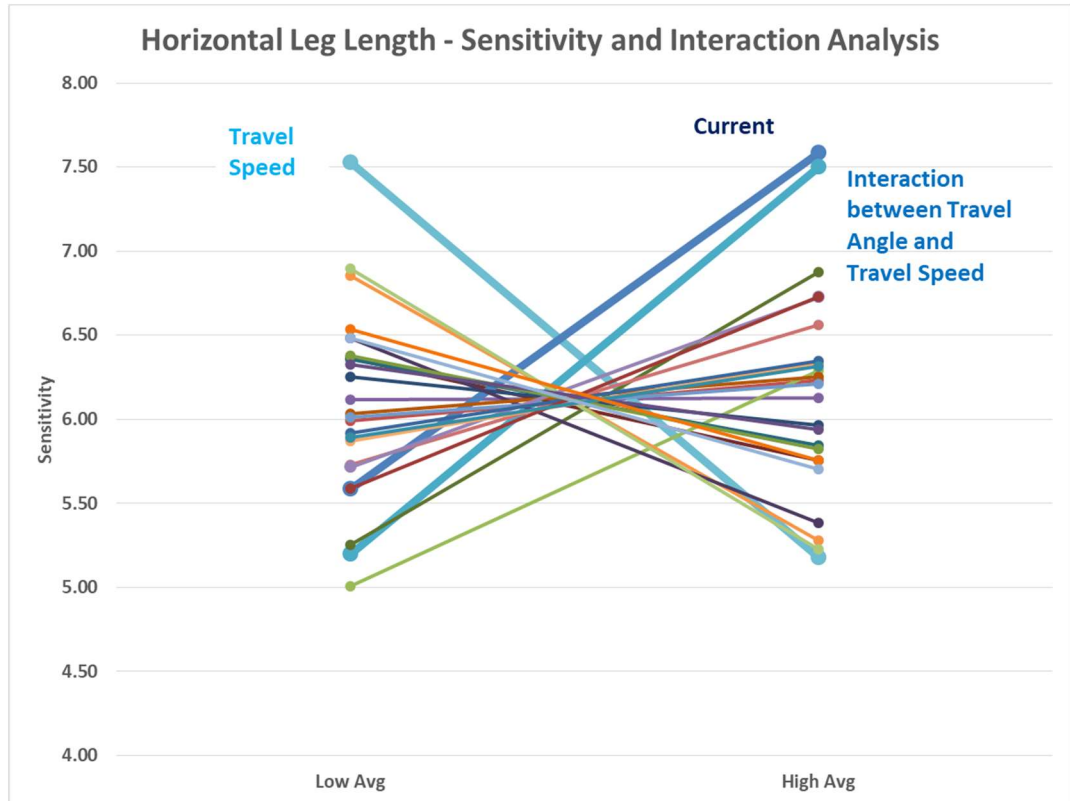
Figure 5-3 Sensitivity and Interaction Results for Penetration



**Key Parameters and Interactions:**

- |  |   |  |
|--|---|--|
| <ul style="list-style-type: none"> <li>—●— A - Travel Angle (°)</li> <li>—●— D - Current (A)</li> <li>—●— AxC</li> <li>—●— BxC</li> <li>—●— CxD</li> <li>—●— AxBxC</li> <li>—●— BxCxD</li> <li>—●— AxBxCxD</li> <li>—●— AxBxCxDxE</li> </ul> | <ul style="list-style-type: none"> <li>—●— B - Gun Angle (°)</li> <li>—●— E - Voltage (V)</li> <li>—●— AxD</li> <li>—●— BxD</li> <li>—●— CxE</li> <li>—●— AxBxD</li> <li>—●— AxBxCxE</li> </ul> | <ul style="list-style-type: none"> <li>—●— C - Travel Speed (mm/min)</li> <li>—●— AxB</li> <li>—●— AxE</li> <li>—●— BxE</li> <li>—●— DxE</li> <li>—●— AxBxE</li> <li>—●— CxDxE</li> <li>—●— BxCxDxE</li> </ul> |
|--|---|--|

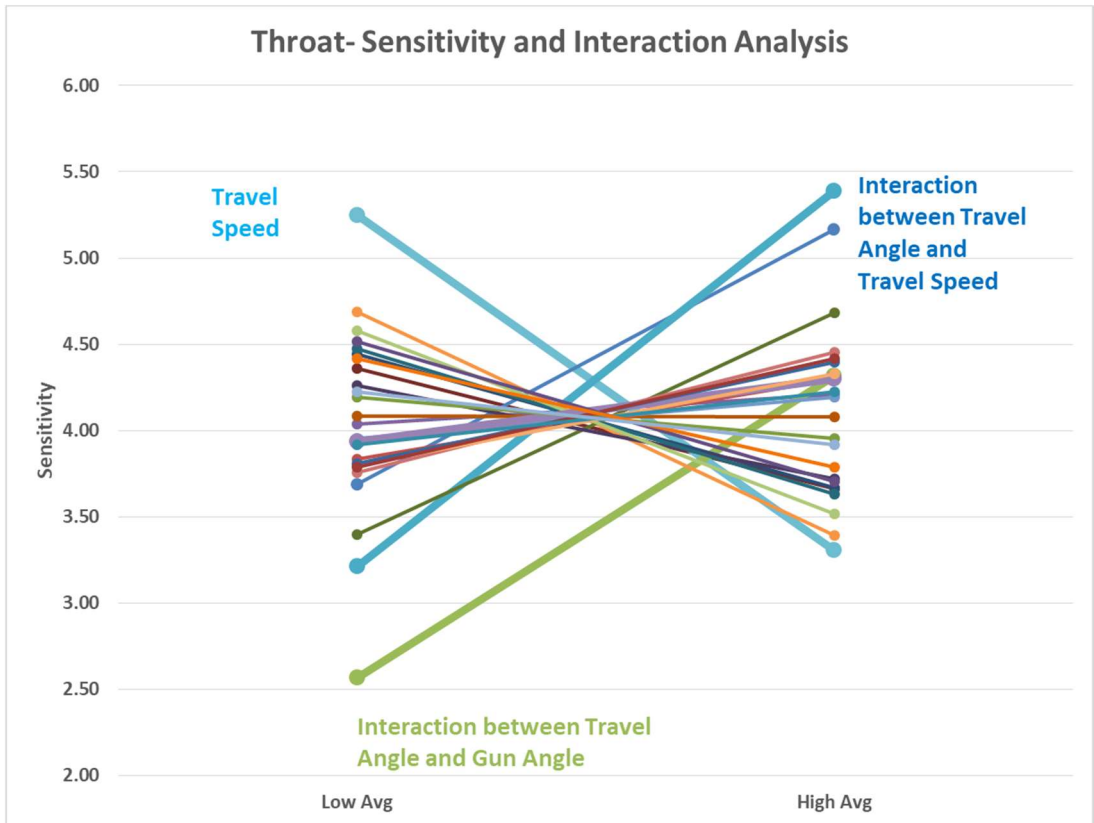
Figure 5-4 Sensitivity and Interaction Results for Vertical Leg Length



**Key Parameters and Interactions:**

- |  |  |  |
|--|--|--|
| <ul style="list-style-type: none"> <li>—●— A - Travel Angle (°)</li> <li>—●— D - Current (A)</li> <li>—●— AxC</li> <li>—●— BxC</li> <li>—●— CxD</li> <li>—●— AxBxC</li> <li>—●— BxCxD</li> <li>—●— AxBxCxD</li> <li>—●— AxBxCxDxE</li> </ul> | <ul style="list-style-type: none"> <li>—●— B - Gun Angle (°)</li> <li>—●— E - Voltage (V)</li> <li>—●— AxD</li> <li>—●— BxD</li> <li>—●— CxE</li> <li>—●— AxBxD</li> <li>—●— BxCxE</li> <li>—●— AxBxCxE</li> </ul> | <ul style="list-style-type: none"> <li>—●— C - Travel Speed (mm/min)</li> <li>—●— AxB</li> <li>—●— AxE</li> <li>—●— BxE</li> <li>—●— DxE</li> <li>—●— AxBxE</li> <li>—●— CxDxE</li> <li>—●— BxCxDxE</li> </ul> |
|--|--|--|

Figure 5-5 Sensitivity and Interaction Results for Horizontal Leg Length

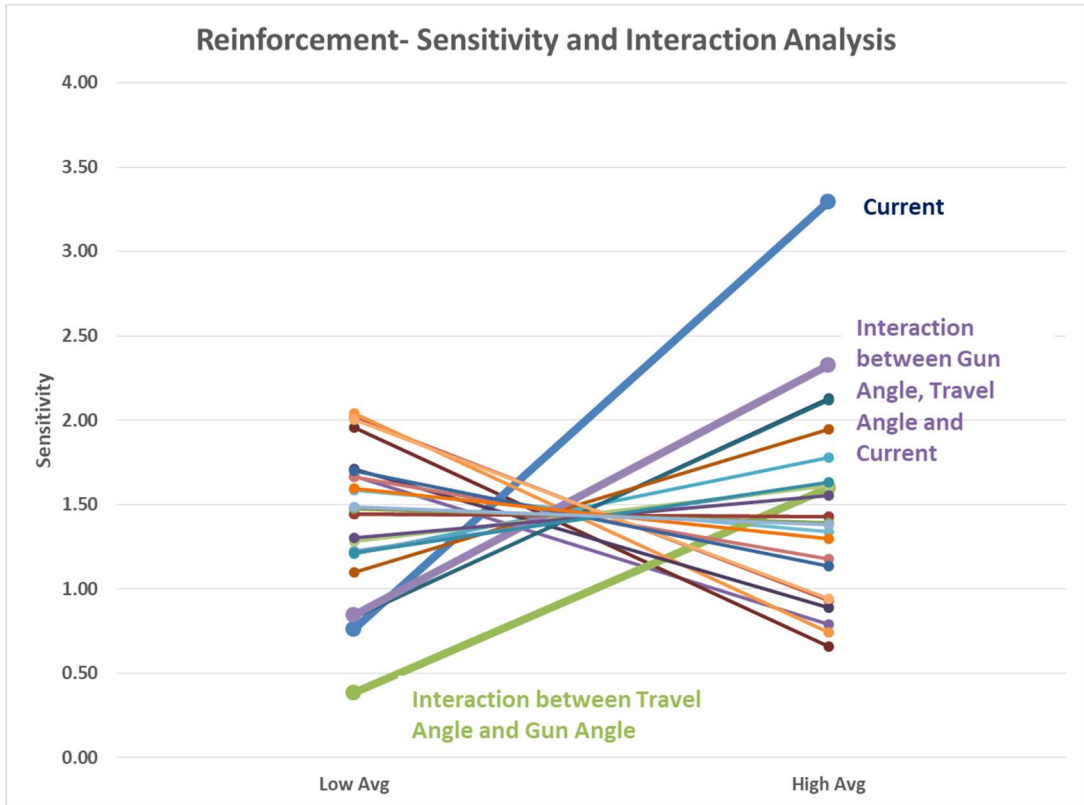


**Key Parameters and Interactions:**

- |  |  |  |
|--|--|--|
| <ul style="list-style-type: none"> <li>—●— A - Travel Angle (°)</li> <li>—●— D - Current (A)</li> <li>—●— AxC</li> <li>—●— BxC</li> <li>—●— CxD</li> <li>—●— AxBxC</li> <li>—●— BxCxD</li> <li>—●— AxBxCxD</li> <li>—●— AxBxCxDxE</li> </ul> | <ul style="list-style-type: none"> <li>—●— B - Gun Angle (°)</li> <li>—●— E - Voltage (V)</li> <li>—●— AxD</li> <li>—●— BxD</li> <li>—●— CxE</li> <li>—●— AxBxD</li> <li>—●— BxCxE</li> <li>—●— AxBxCxE</li> </ul> | <ul style="list-style-type: none"> <li>—●— C - Travel Speed (mm/min)</li> <li>—●— AxB</li> <li>—●— AxE</li> <li>—●— BxE</li> <li>—●— DxE</li> <li>—●— AxBxE</li> <li>—●— CxDxE</li> <li>—●— BxCxDxE</li> </ul> |
|--|--|--|

Figure 5-6 Sensitivity and Interaction Results for Throat





Key Parameters and Interactions:

- |                          |                       |                               |
|--------------------------|-----------------------|-------------------------------|
| —●— A - Travel Angle (°) | —●— B - Gun Angle (°) | —●— C - Travel Speed (mm/min) |
| —●— D - Current (A)      | —●— E - Voltage (V)   | —●— AxB                       |
| —●— AxC                  | —●— AxD               | —●— AxE                       |
| —●— BxC                  | —●— BxD               | —●— BxE                       |
| —●— CxD                  | —●— CxE               | —●— DxE                       |
| —●— AxBxC                | —●— AxBxD             | —●— AxBxE                     |
| —●— BxCxD                | —●— BxCxE             | —●— CxDxE                     |
| —●— AxBxCxD              | —●— AxBxCxE           | —●— BxCxDxE                   |
| —●— AxBxCxDxE            |                       |                               |

Figure 5-7 Sensitivity and Interaction Results for Reinforcement

The results showed that current and travel speed were the predominant discrete parameters in determining the fillet weld geometry. However, several interactions between the gun angle, travel angle, travel speed and current were also identified as being significant in determining the resultant geometry. Current, gun angle, travel angle, and travel speed are all key factors in determining the rate and the angle at which the fillet material is deposited into the weld and so logically it make sense that they are the key parameters involved into determining the shape of the weld. However the results appear to show the voltage as not being significant in determining the fillet weld geometry. This does

not align with the general understanding that the voltage controls the arc length and the width/volume of the resultant weld bead. The results of the top 3 significant parameters/interactions are summarised in Table 5-1 below.

Table 5-1 Top 3 significant parameters impacting fillet weld geometry

Fillet Weld Geometrical Feature	Top 3 Significant Parameters/Interactions		
	1	2	3
Penetration	Current	Gun angle x Travel angle x Current	--
Vertical Leg Length	Travel Speed	Travel angle x Travel Speed	Travel angle x Gun angle
Horizontal Leg Length	Travel Speed	Travel angle x Travel Speed	Current
Throat	Travel Speed	Travel angle x Travel Speed	Travel angle x Gun angle
Reinforcement	Current	Travel angle x Gun angle	Gun angle x Travel angle x Current

### 5.1.3 Regression Analysis - Identifying key fillet weld parameters

In this research a procedure was proposed to model and optimize weld bead geometry in GMAW process. Since the relationships between bead geometry characteristics and welding output variables are complicated, a regression-based method was employed to model the process. The experimental data for model development were gathered using the actual tests carried out by the authors. Along this line, using DOE approach and regression analysis, different mathematical models were developed to establish the relationships between welding input parameters and weld bead geometry outputs. The ANOVA results performed on different regression functions denote that the set of curvilinear models is the best representative for the actual GMAW process. The associated P-value for this model is lower than 0.05; i.e.  $\alpha = 0.05$  or 95% confidence level.

For each of the 82 experimental fillet welds the resultant key geometrical features were measured using ImageJ digital analysis software (as described in Chapter 3) and a succession of regression analyses was completed in order to:

1. identify the relationships between the input parameters and output geometry
2. Identify which of the parameters were statistically significant in determining /influencing the various output geometries.

Minitab was used to conduct the regression analysis and the following input and output parameters [Table 5-2] were used to analyse the GMAW fillet welding process.

Table 5-2 Inputs and Outputs used in Regression Model

<b>Input Parameters</b>	<b>Output (Weld Geometry)</b>
Current (A)	Vertical Leg Length
Voltage (V)	Horizontal Leg Length
Travel Speed (mm/min)	Penetration
Travel Angle (°)	Throat
Gun angle	

Once the regression model had been built, a validation was conducted using a sample of experimental results that's had been excluded from the dataset used to build the model. The results of the validation are shown in Figures 5-8 and 5-9

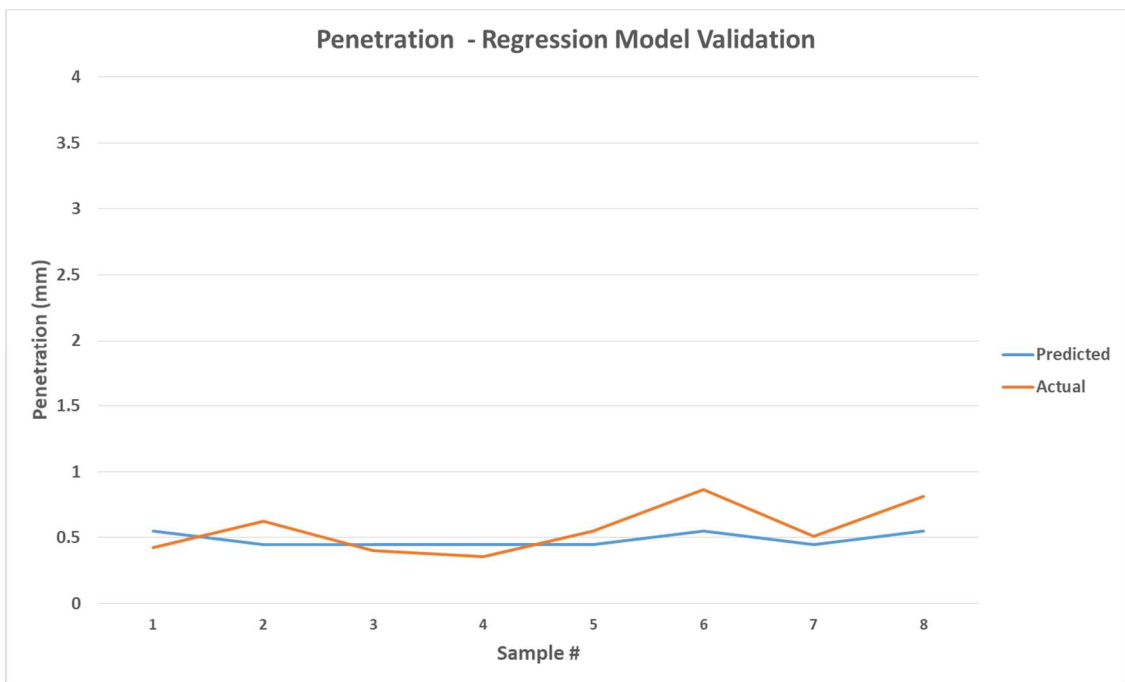
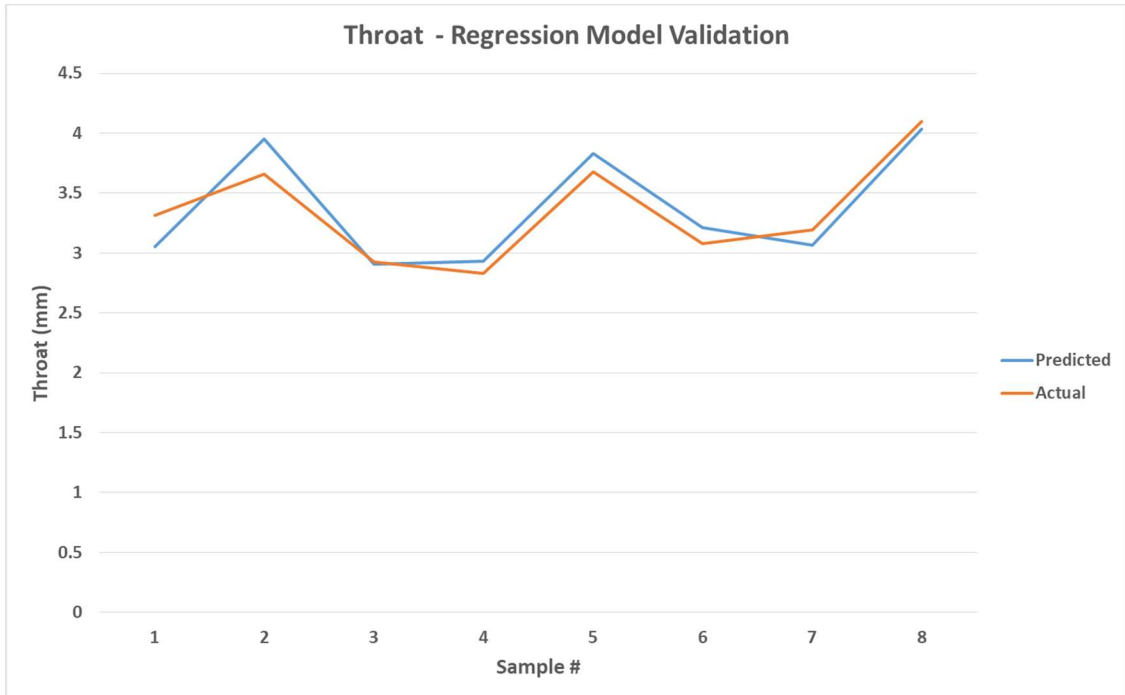


Figure 5-8 Regression Model validation results for Throat and Penetration

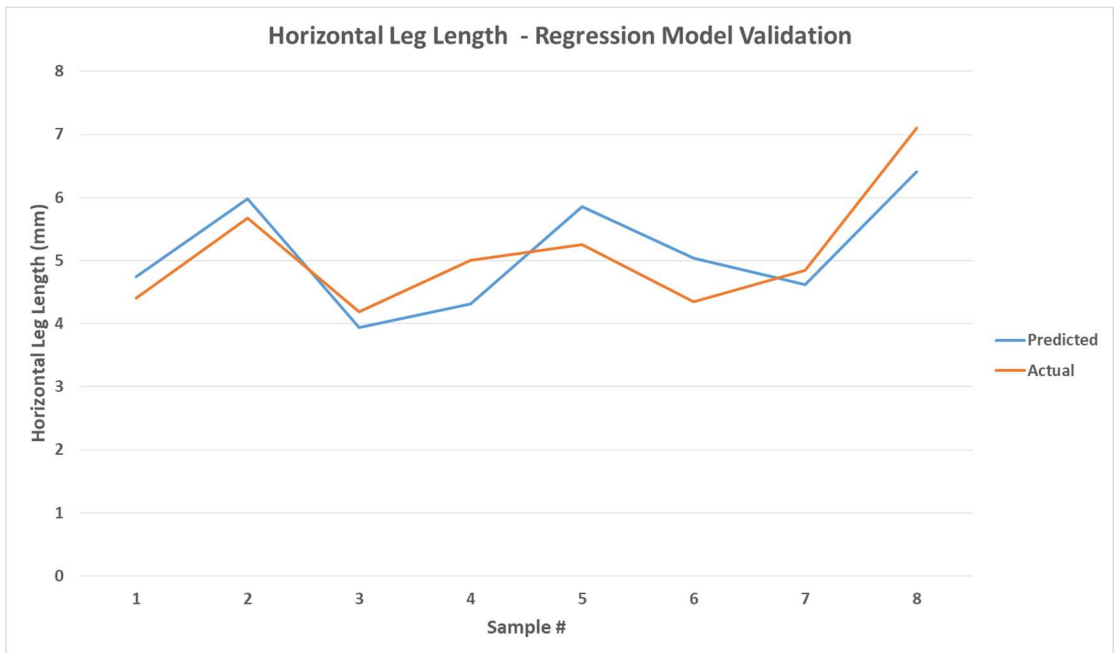
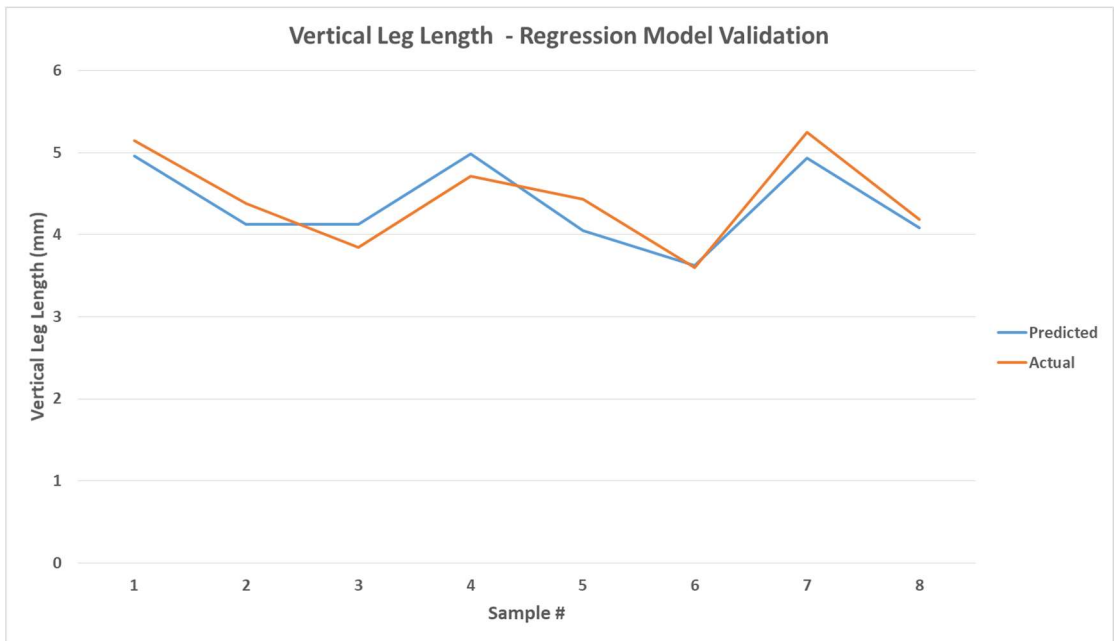


Figure 5-9 Regression Model validation results for Vertical and Horizontal Leg Length

### 5.1.3.1 Penetration

The regression analysis confirmed that there was a statistically significant relationship ( $p < 0.05$ ) [5.2] between the input parameters and the resultant penetration of the fillet weld. The relationship is shown below in Eqn 5-1. The analysis also highlighted that current was the only main effect when determining the penetration [Figure 5-10]. This result was validated by the ANOVA [Figure 5-3], which confirmed that the current was the most significant factor.

$$y_p = 4.15 + 0.00892x_2 - 0.0759x_3 + 0.0613x_4 - 0.000012x_2^2 + 0.000216x_3^2 \quad \text{Eqn. 5-1}$$

Where:

- $y_p$  = penetration
- $x_2$  = travel speed
- $x_3$  = current
- $x_4$  = voltage

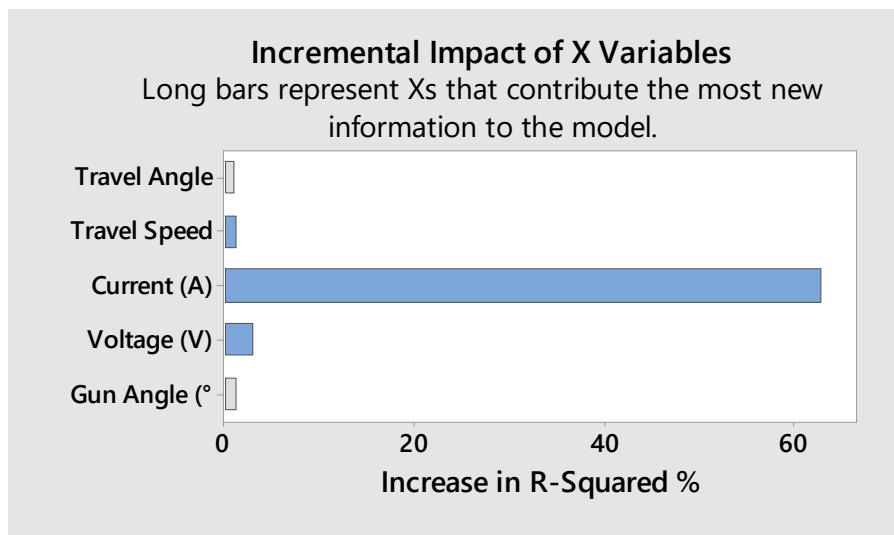


Figure 5-10 Penetration significant parameters

### 5.1.3.2 Vertical Leg Length

The regression analysis confirmed that there was a statistically significant relationship between the input parameters and the resultant vertical leg length of the fillet weld. This relationship is shown below in Eqn 5-2. The analysis also highlighted that the travel speed and current were the main effects [Figure 5-11] when determining the vertical leg length. The travel angle and voltage have a lesser impact. The interaction plot [Figure 5-12] also highlighted that there was a significant interaction between the following parameters:

- Travel Speed and Current – the impact of the travel speed is increasingly significant at higher current
- Travel Angle and Travel Speed – the travel angle becomes increasingly significant at higher travel speeds
- Current and Voltage – current is increasingly significant at higher voltage

$$y_v = 15.61 - 0.0381x_1 - 0.0138x_2 - 0.0220x_3 - 0.618x_4 + 0.00004x_2^2 + 0.000119x_1x_2 - 0.000124x_2x_3 + 0.003629x_3x_4 \quad \text{Eqn. 5-2}$$

Where:

- $y_v$  = vertical leg length
- $x_1$  = travel angle
- $x_2$  = travel speed
- $x_3$  = current
- $x_4$  = voltage

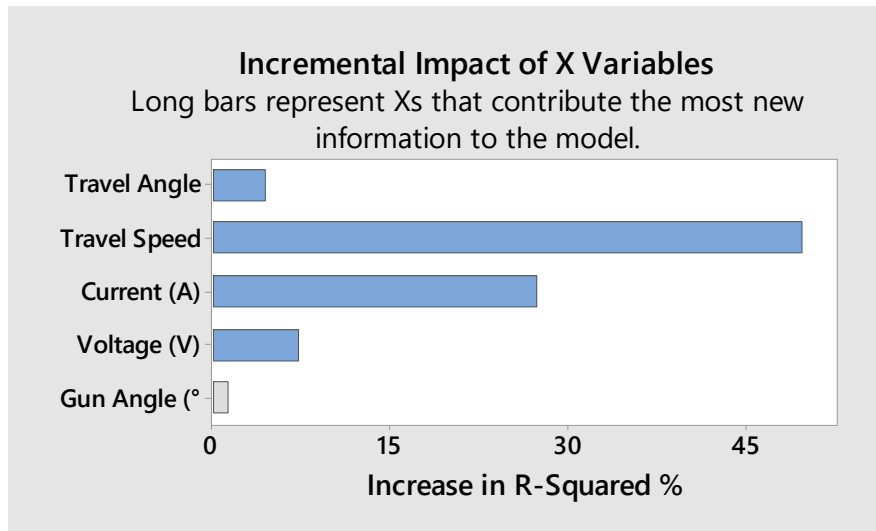


Figure 5-11 Vertical Leg Length - significant parameters

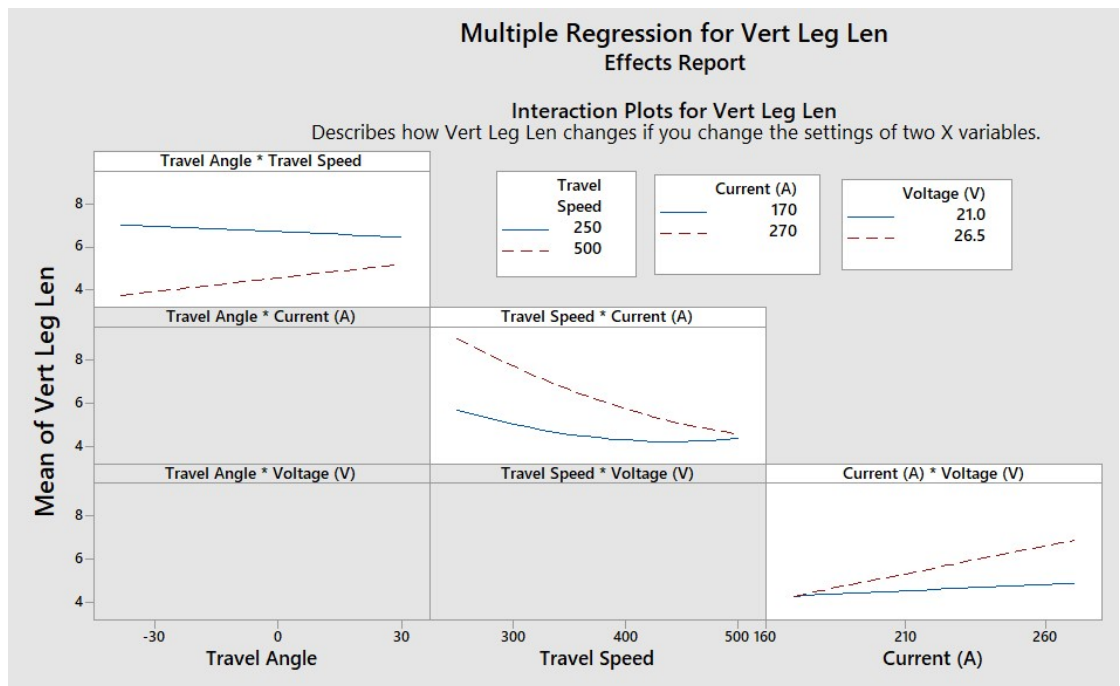


Figure 5-12 Vertical Leg Length - significant interactions



### 5.1.3.3 Horizontal Leg Length

The regression analysis confirmed that there was a statistically significant relationship between the input parameters and the resultant horizontal leg length of the fillet weld. The analysis also highlighted [Figure 5-13] that the travel speed was the most significant factor when determining the horizontal leg length. This result was further validated by the results from the ANOVA [Figure 5-5]. The interaction plot [Figure 5-14] also highlighted that there was a significant interaction between the current and travel speed. At higher current travel speed has a more significant impact on the horizontal leg length and at lower travel speeds the changes in current are more significant.

$$y_h = 4.34 - 0.0334x_2 + 0.0347x_3 + 0.1805x_4 + 0.000045x_2^2 - 0.000054x_2x_3 \quad \text{Eqn. 5-3}$$

Where:  $y_h$  = horizontal leg length  
 $x_2$  = travel speed  
 $x_3$  = current  
 $x_4$  = voltage

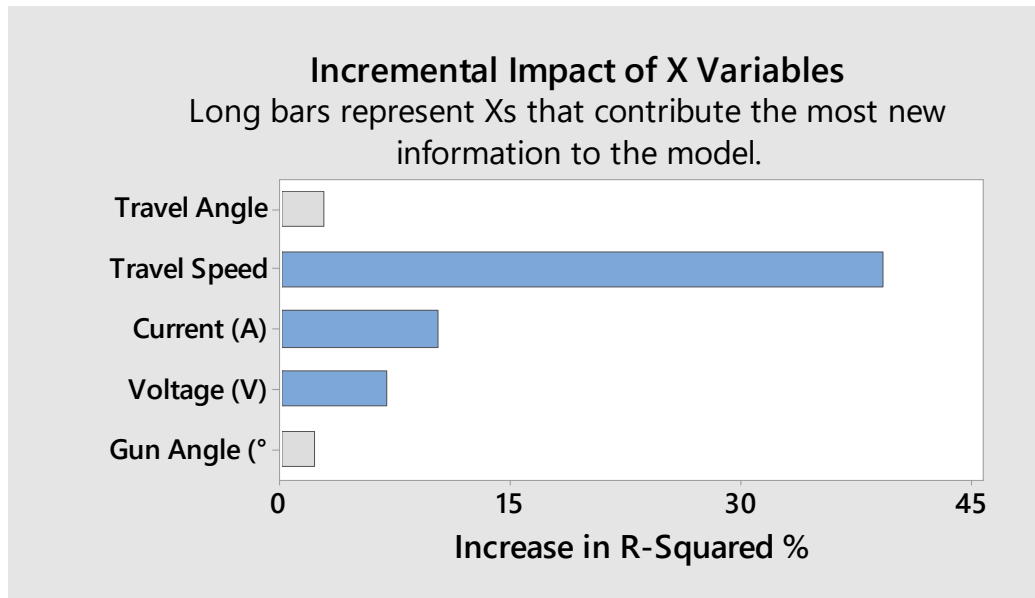


Figure 5-13 Horizontal Leg Length - significant parameters

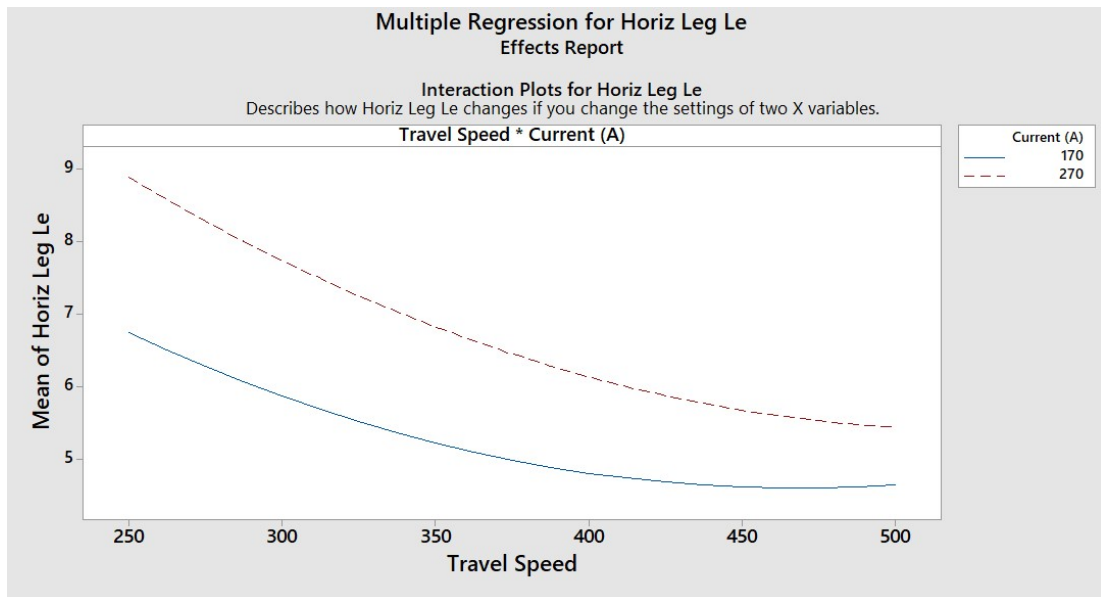


Figure 5-14 Horizontal Leg Length - significant interactions

### 5.1.3.4 Asymmetrical Leg Length

Figures 5-15 and 5-16 show the output of the regression analysis aimed at understanding which input parameters have the most significant impact on the asymmetry of the vertical and horizontal leg lengths. Figure 5-15 clearly shows that the travel angle has the highest gradient line between high and low settings, indicating that moving between these two settings has the most significant impact on the leg length variation. On the graph the negative travel angle represents a pulling torch configuration. The results indicate that a pulling travel angle results in greater variation in leg length and so a pushing travel angle would be the preferred configuration in order to reduce the variation in leg lengths. Figure 5-16 contains the boxplot graph highlighting the range of leg length variation identified for the 3 different travel angles (pushing, pulling, neutral). This clarifies the results shown in Figure 5-15 that a pushing travel angle reduces the variation between the vertical and horizontal leg lengths. The gun angle was not identified as being mathematically significant to influencing the variation in leg lengths, which is why it is not featured in Figure 5-15.

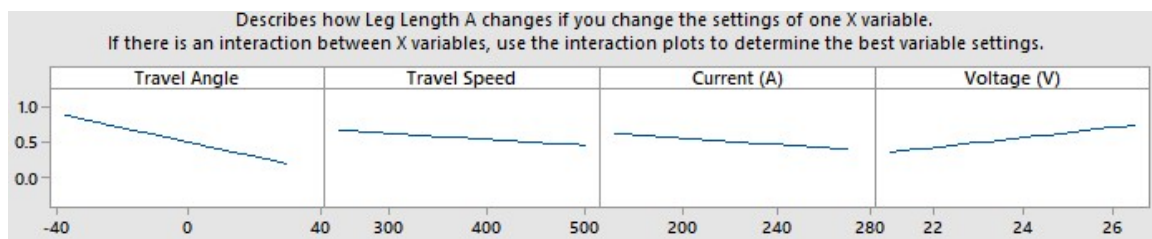


Figure 5-15 Asymmetric Leg Length - significant parameters

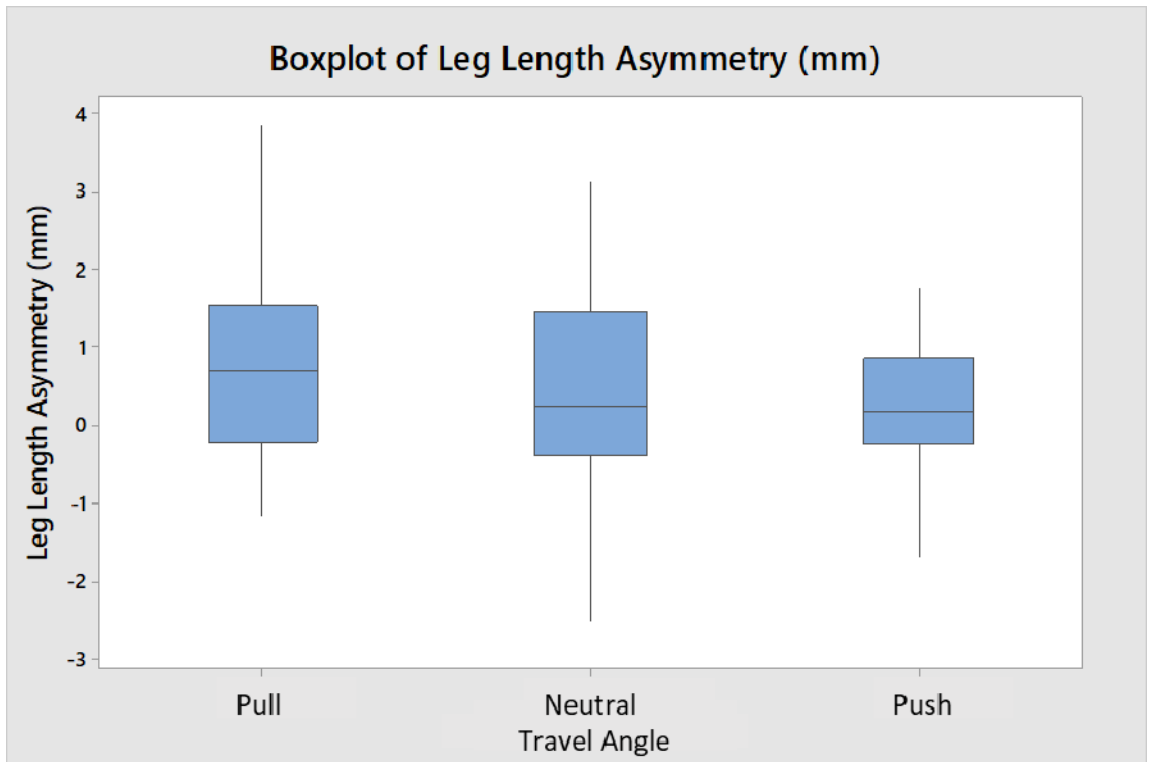


Figure 5-16 Range of leg length asymmetry by torch travel angle

#### 5.1.4 Relationship between fillet weld parameters and heat affected zone (HAZ)

As part of the fillet weld process, heat is applied to the joint. Generally, as more heat is applied to the joint, the larger the weld and heat affected zone around the weld. The resultant weld area + heat affected zone (HAZ) of a fillet welded joint is shown below in Figure 5-17.

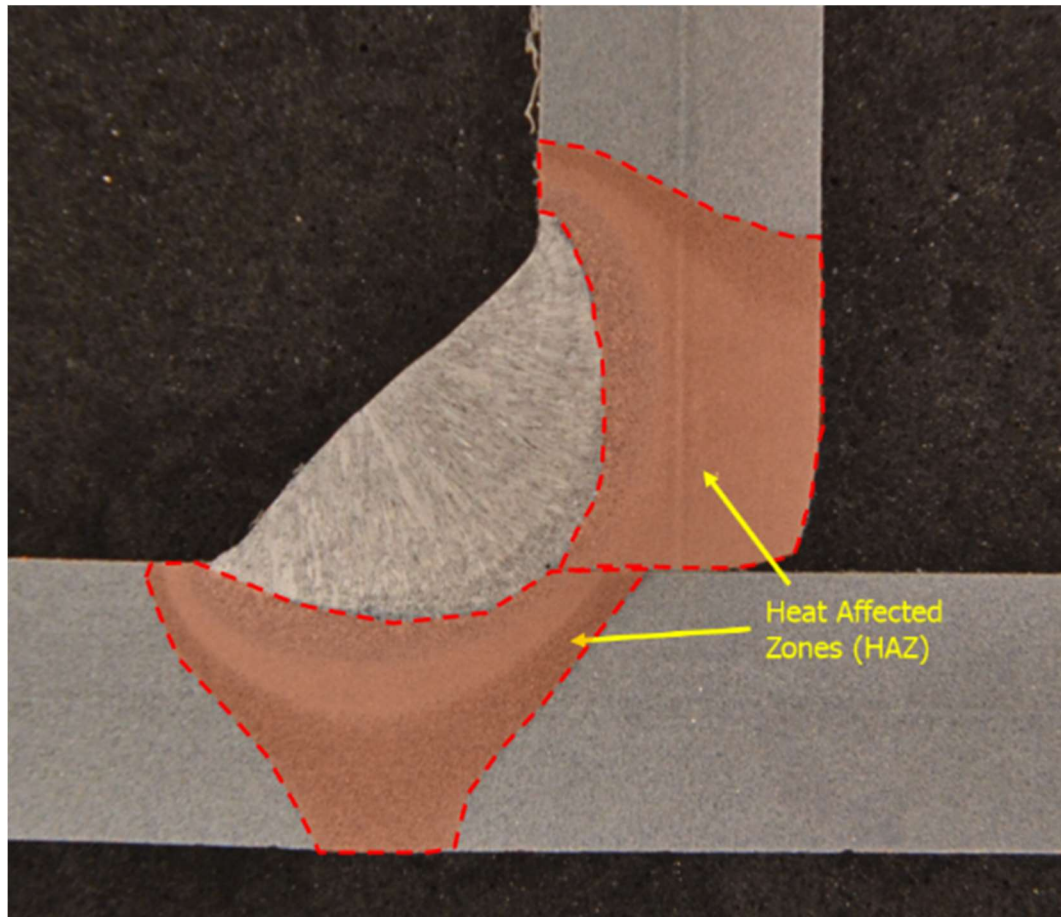


Figure 5-17 Heat Affected zones of a fillet weld

Minitab was used to assess the relationship between the input parameters (current, voltage, travel speed, travel angle and gun angle) and the resultant size of the weld and heat affected zone area. Image J (software) was used to measure the size of the heat affected zones in  $\text{mm}^2$ . This was achieved by tracing the outline of the heat affected zone [Figure 5-17] from the weld macro and the software calculated the area within the traced

shaped. Figure 5-18 highlights the strength of the relationship between the process inputs and outputs.

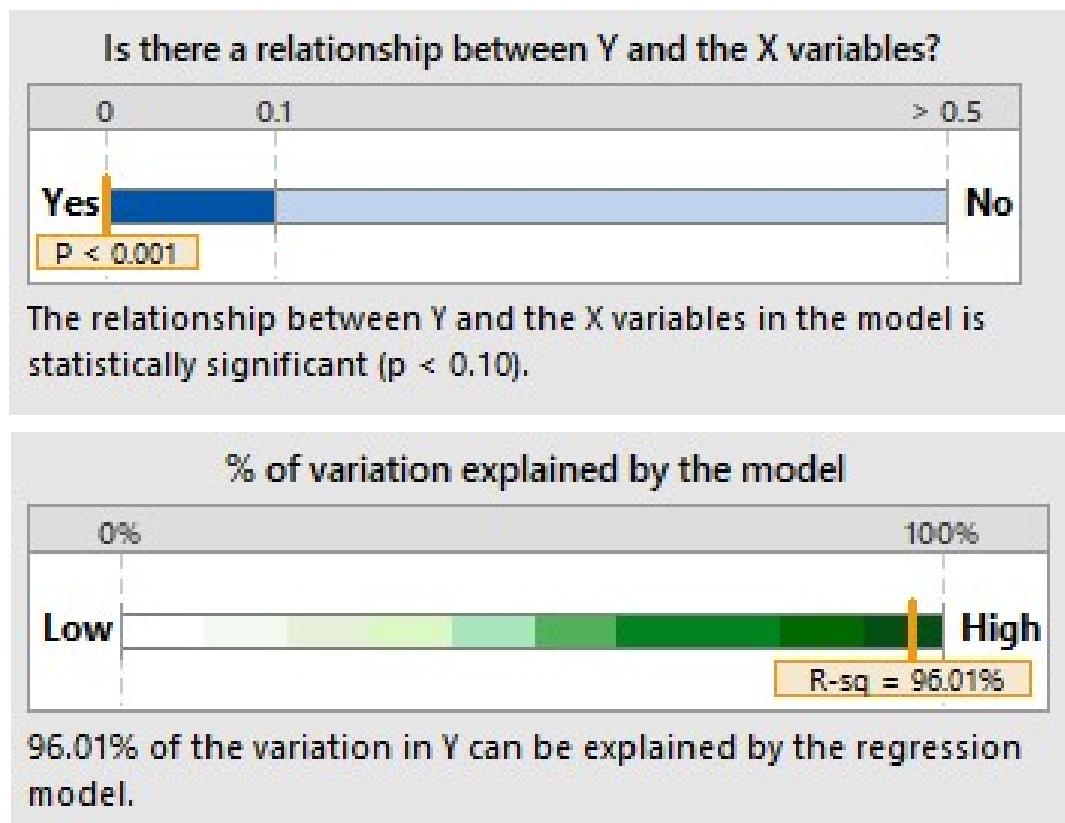


Figure 5-18 Strength of relationship between the process inputs and outputs

The current and travel speed were identified as the most significant parameters [Figure 5-19] in determining the resultant weld and heat affected zone area. This is in line with expectations as both parameters are significant in determining the heat input [Eqn 1-1] and the heat input is directly related to the size of the weld+ HAZ area.

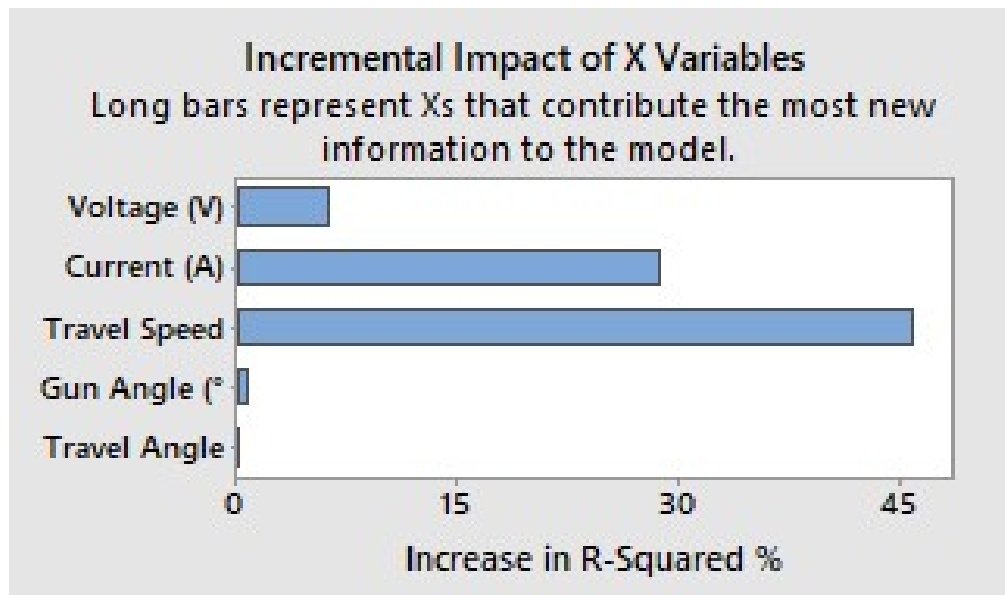


Figure 5-19 Significance of input parameters in determining size of HAZ

#### 5.1.5 Summary

Table 5-3 below provides a summary of the key results from the ANN/ANOVA and Regression Analyses. The results reinforce that both the travel speed and current are critical (independently and interactively) in determining the leg length of the fillet weld and that current is the main parameter in determining penetration. The results also indicate that the interaction between the travel angle and travel speed is significant in determining the resultant leg length.

Table 5-3 Comparison summary of results from ANN/ANOVA and Regression Analysis

Fillet Weld Geometry	Regression		ANN/ANOVA	
	Main Effects	Interactions	Main Effects	Interactions
Vertical Leg Length	Travel Speed	Travel Speed x Current	Travel Speed	Travel angle x Travel Speed
	Current	Travel angle x Travel Speed	Current	
		Current x Voltage		
Horizontal Leg Length	Travel Speed	Travel Speed x Current	Travel Speed	Travel angle x Travel Speed
	Current		Current	
	Voltage			
Penetration	Current	-	Current	Gun angle x travel angle x current

## 5.2 Welding Torch - Travel angle

### 5.2.1 Travel angle impact on fillet weld geometry

Chapter 5.1 identified the travel angle as significant in influencing the geometry of the fillet weld. Table 5-1 also identified the travel angle as the only parameter to significantly impact each of the key fillet weld geometrical features. There is also a certain amount of disagreement as to what the ideal travel angle should as previously referenced in Tables 1-3 and 2-1. The following section will further explore the impact of the travel-angle. A series of experiments were conducted to assess what impact changing the travel angle direction (pulling, pushing and neutral) has on the resultant geometry and structure of the welded joint, Table 5-4 shows the parameters selected. These parameters were selected based on the results from previous experiments. They would ensure a stable weld that would allow for the travel angle to be varied and assessed without compromising the overall quality of the weld.



Table 5-4 Travel Angle Experiment Parameters

EXPT No	Travel angle (°)	Travel Speed (mm/min)	Current (A)	Voltage (V)	Electrode	Gas Flow (l/min)
D1-0	-30 (Pull)	500	200	23.3	Metal Core	18
D2-3	-30 (Pull)					
O1-1	0					
O2-2	0					
P1-4	30 (Push)					
P2-5	30 (Push)					

Table 5-5 provides a summary of the experimental results and Figure 5-20 shows the macrographs for each travel angle configuration. Within Table 5-5 the neutral travel angle has been used as a reference to measure the percentage change of each of the geometrical characteristics for the push and pull results. The results highlight that the resulting fillet weld geometry is impacted by the travel angle of the welding torch.

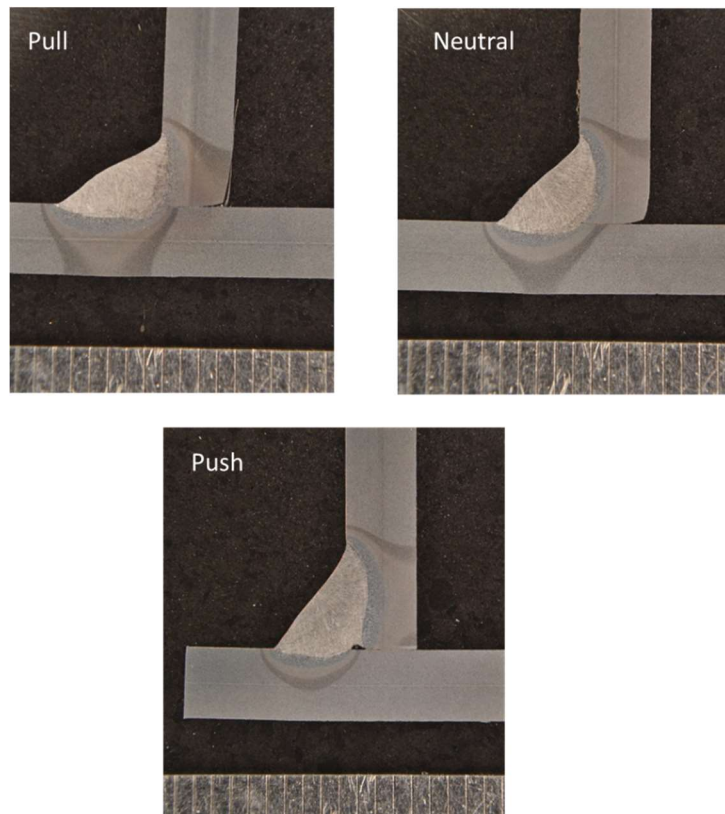


Figure 5-20 Travel Angle Weld Macros

Table 5-5 Travel Angle Experiment Results

Expt No	Throat (mm)		Vertical Leg Length (mm)		Horizontal Leg Length (mm)		Reinforcement (mm)		Penetration (mm)		HAZ Area (mm <sup>2</sup> )	
	Value	% Change	Value	% Change	Value	% Change	Value	% Change	Value	% Change	Value	% Change
Pull (D0)	3.10	2.8%	3.67	-16%	5.36	26%	0.25	55%	0.08	-77%	1.34	-30%
Pull (D3)												
Neutral (N1)	3.01	0.0%	4.37	0%	4.27	0%	0.16	0%	0.34	0%	1.92	0%
Neutral (N2)												
Push (P4)	3.07	1.7%	5.19	19%	3.78	-11%	0.15	-8%	0.20	-42%	0.74	-61%
Push (P5)												

The vertical leg length is larger when the travel angle is pushing and conversely the horizontal leg length is larger when the travel angle is pulling. The reinforcement of the fillet weld is larger (more rounded) when the travel angle is pulling. The penetration is higher when the torch is sitting at right angles to the fillet joint (neutral) and decreases as the travel angle increases in both the pulling and pushing direction. Consequently, the intersect penetration heat affected zone is larger when the travel angle is in the neutral position indicating that more of the heat is being directed straight into the joint. Figure 5-21 also shows that the size of the horizontal and vertical leg lengths directly correlate with the size of the HAZ area observed within the respective horizontal/vertical sections of the welded joint.

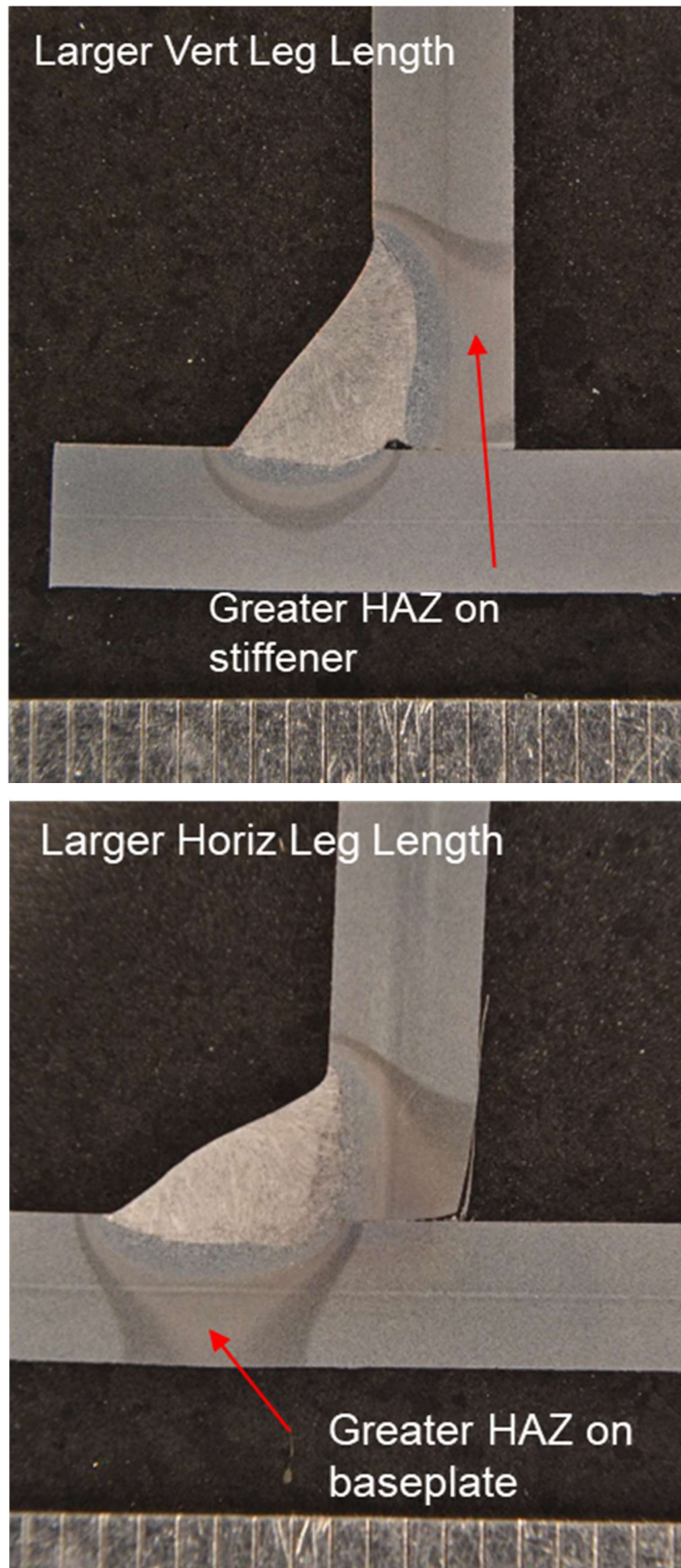


Figure 5-21 Macrographs showing HAZ areas for varying leg lengths.

## 5.2.2 Torch travel angle impact on fillet weld microstructure

### Microstructure

Figure 5-22 shows the locations where the microscope images were focused to capture images of the microstructure for the weld and heat affected zones. Figures 5-23 and 5-24 below show the variation in microstructure of the weld area and heat affected zone for the 3 different orientations of travel angle (push, pull and neutral).

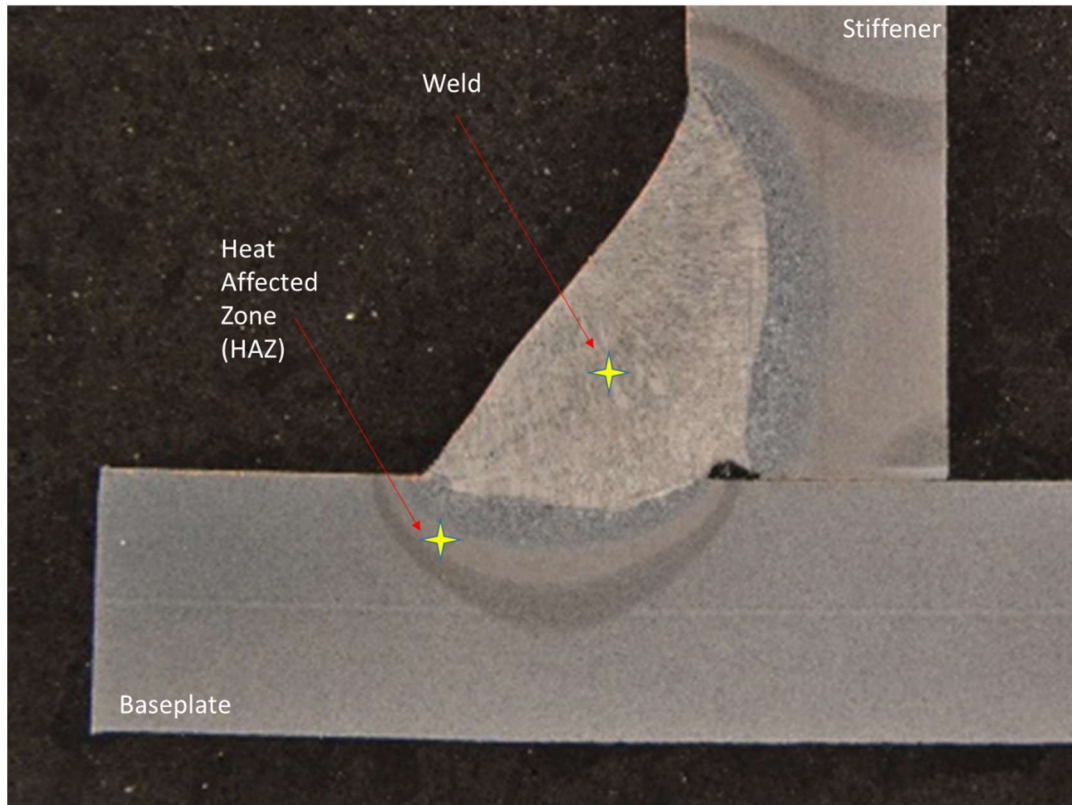


Figure 5-22 Locations of weld and heat affected zone regions microstructure images



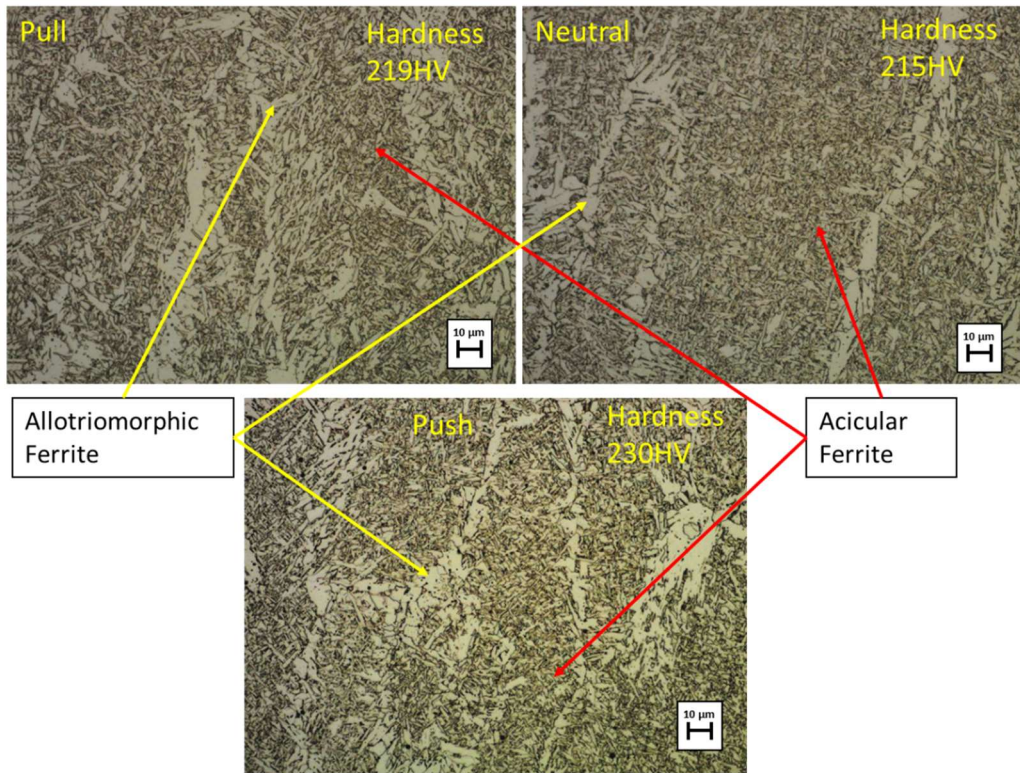


Figure 5-23 Microstructure of Weld Area (push/pull/neutral)

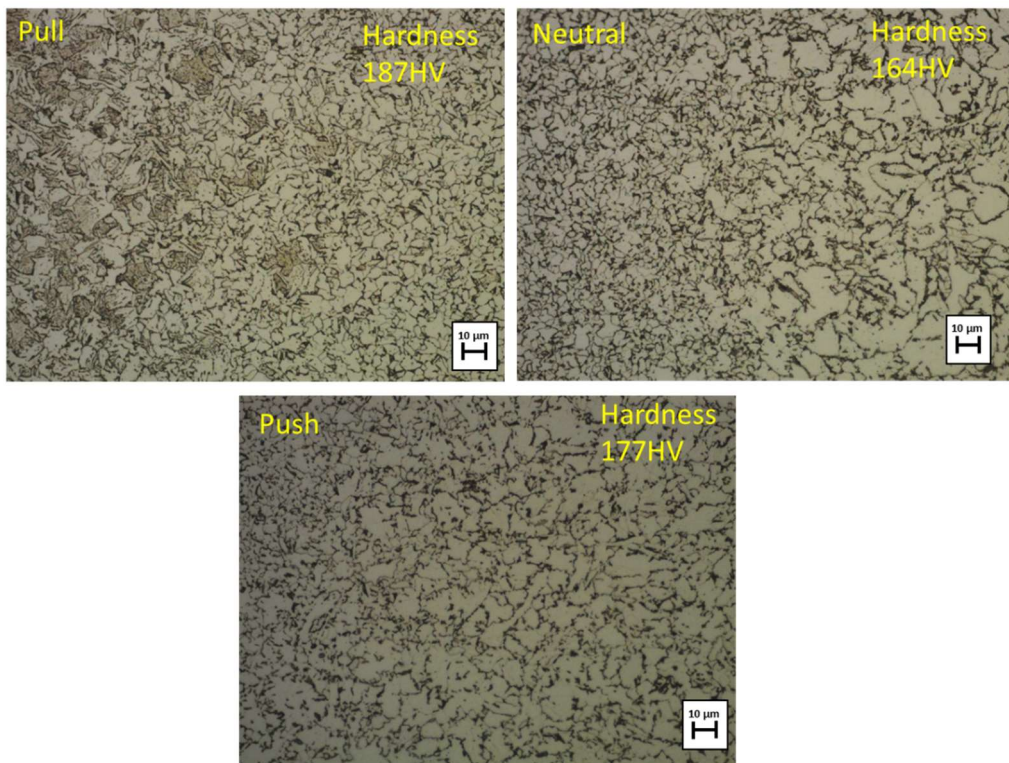


Figure 5-24 Microstructure of Heat Affected Zone (push/pull/neutral)

Moving away from the weld metal Figure 5-24 shows a more irregular ferrite structure with small areas of fine bainite. The results appear to highlight that there is no significant variation in grain size and microstructure as a result of altering between the 3 different 'pushing', 'pulling' and 'neutral' travel angles.

### 5.2.3 Travel angle impact on fillet weld hardness

Figure 5-25 below shows the hardness results using an automated hardness profiler. These results show that when the travel angle is pushing, the resultant weld is approximately 5-6% harder. However, in context the results are well within the acceptable limits for the material [5.3][5.4]; so from a practical perspective, unless operating at the limits of the material properties, the travel angle does not appear to have a significant impact on the structural properties of the weld for metal cored GMAW.

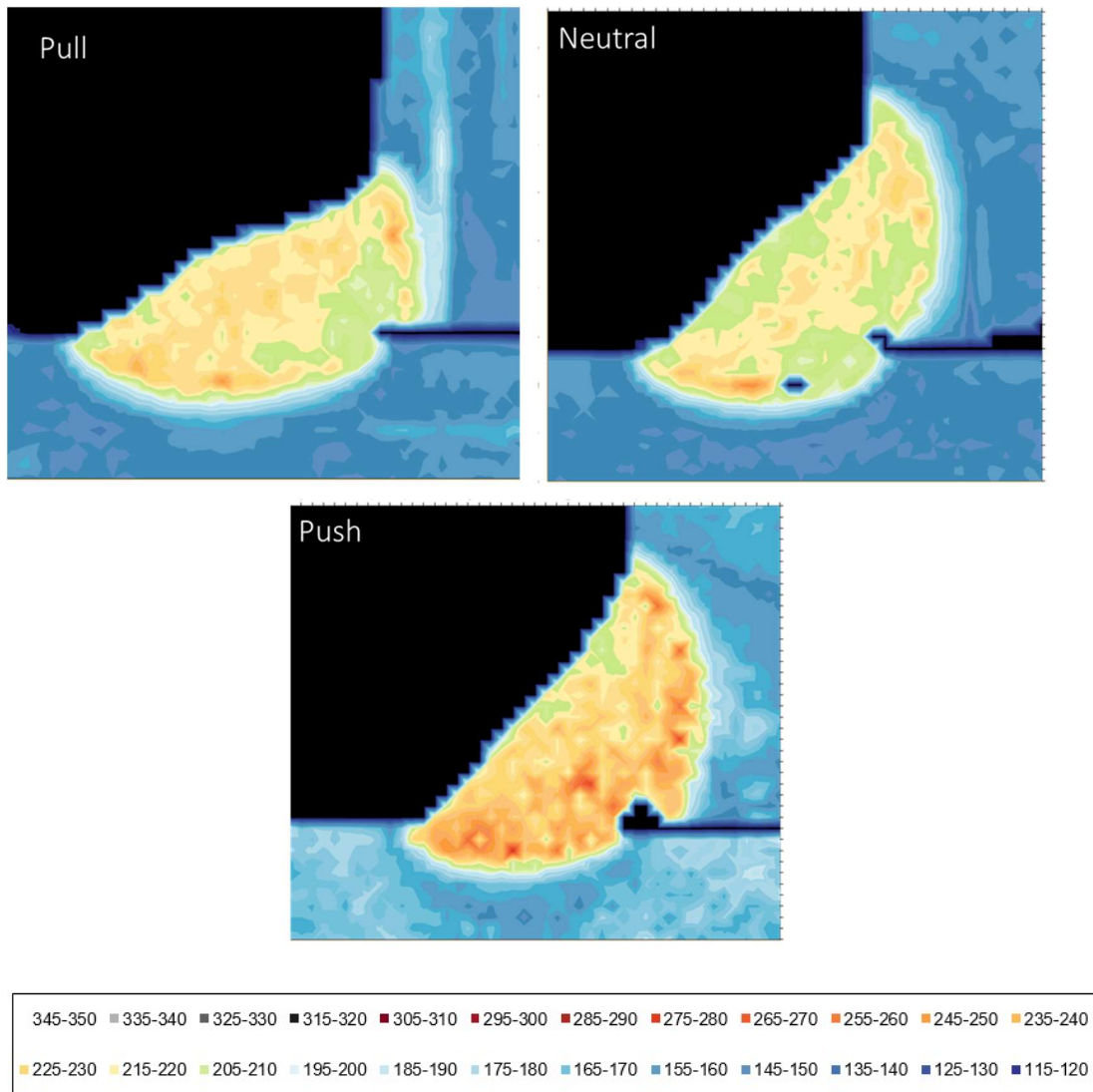


Figure 5-25 Hardness profiles for push, pull and neutral travel angles

#### 5.2.4 Torch travel angle impact on current/voltage

During experiments a PAMS (portable arc monitoring system) unit was connected to the welding equipment. This system allowed the actual arc voltage and current values to be monitored and recorded along the length of the weld. Table 5-6 and Figures 5-26, 5-27 below provide a sample summary of the % variation in current and voltage readings observed for the various travel angle configurations during welding. The results confirmed

that both the current and voltage settings were consistent throughout the experiments and that there was no significant impact on the arc current or voltage by altering the travel angle.

Table 5-6 Travel Angle - % variation of arc current and voltage

Travel Angle	% variation in voltage	% variation in current
Push	1.19%	3.25%
Neutral	0.50%	2.09%
Pull	1.15%	2.82%

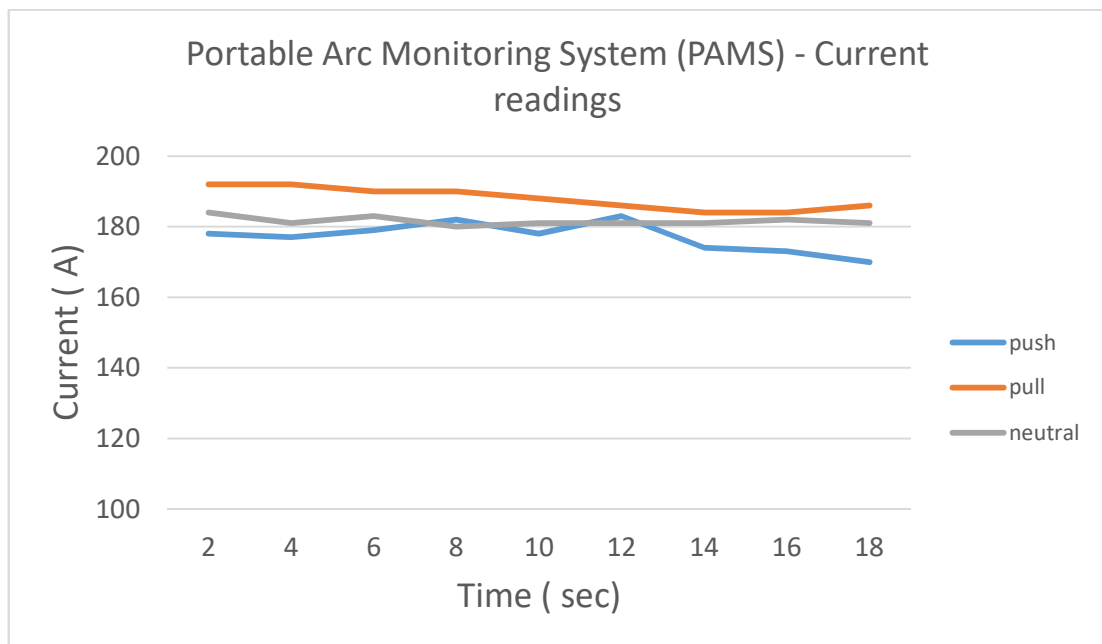


Figure 5-26 Graph showing current (A) readings from PAMs unit during welding



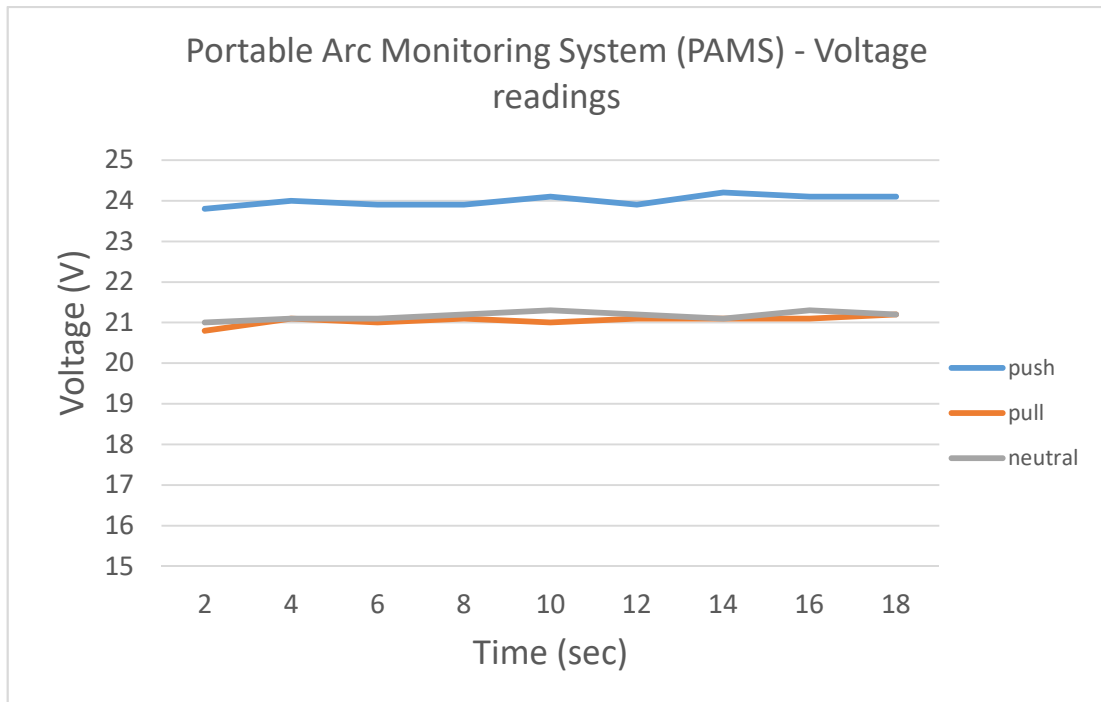


Figure 5-27 Graph showing voltage (V) readings from PAMs unit during welding

### 5.3 Discussion – Key Fillet Weld Geometry

As discussed in Chapter 1, the resultant weld geometry is one of the key outputs of the GMAW process. This section of the chapter will focus primarily on the penetration, leg length and throat thickness as these are the characteristics that will ultimately determine the loading bearing capacity of the weld [5.5]. Consideration will also be given to the asymmetry of the resultant leg length, as will discussed in chapter 6, this feature of the weld impacts the heat flow through the vertical and horizontal sections of the welded joint.

#### 5.3.1 Penetration

The ANN model and regression analysis both confirmed that arc current was the most influential parameter in determining the penetration of the fillet weld [Figures 5-2, 5-10]. The ANOVA analysis [Figure 5-3] also confirmed that current was the most influential parameter in determining penetration but also identified that there is a significant interaction between the travel angle, gun angle and current which impacts on the

penetration. As described in Chapter 1 [Table 1-1], the penetration was measured as the distance the weld 'penetrates' through the intersection of the horizontal and vertical axis at the root of the fillet joint. During experimentation, the welding torch was positioned with a 2mm stand off from the intersection of the fillet joint [Figure 5-28]. This results in any changes to the gun and travel angle of the torch varying the straight linear distance from the end of the torch to the root of the weld which will consequently have a combined impact on the depth of penetration. Figure 5-28 shows that for a stand-off of 2mm and a gun angle of 30deg the distance from the end of the electrode to the intersection of the fillet joint is 2.35mm, 17.5% further than if the torch was in the neutral position. This also helps to explain the penetration results from Table 5-5 where the neutral travel angle (neither pushing nor pulling) generated the highest penetration. As the travel angle moves further from the neutral position (using the end of the torch as the pivot point), the linear distance from the end of the torch to the point of intersection of the fillet joint will also increase, resulting in less penetration. These results are significant as they suggest that some sort of compensation, to either the electrode stick out or current, would need to be built into the robotic control system in order to maintain a constant penetration when varying the travel angle.

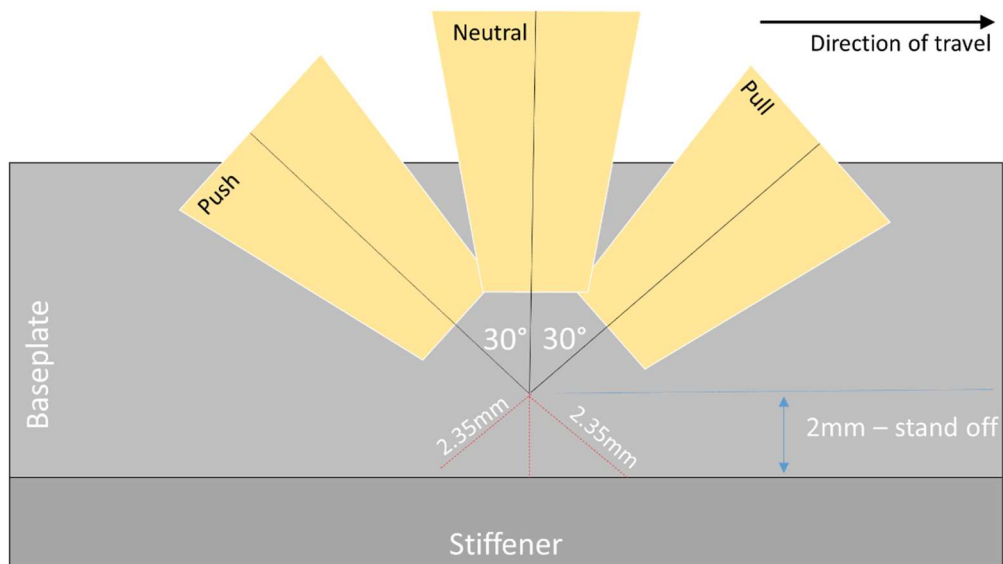


Figure 5-28 Distance from torch nozzle to stiffener for pushing, pulling and neutral travel angles

This can be explained because when the torch is being pushed, the electrode is being fed in the same direction as the torch is moving, increasing the 'effective' speed at which the electrode is being fed into the weld and increasing the penetration. Conversely when the torch is being pulled the electrode is being fed in the opposite direction as the torch is moving. Table 5-7 and Figure 5-29 show the calculated 'effective' wire feed speed for a pushing and pulling configuration using parameters taken from a sample weld procedure [Appendix 2]. The result shows that when the torch is in a pushing configuration the 'effective' speed at which the electrode is being fed into the weld area is around 7% higher than when the torch is pulling. These results were observed using a metal cored consumable electrode. This variation in 'effective' wire speed combined with the variation in torch position further highlights that the torch travel angle can have a significant impact on the resultant penetration and as such must be given appropriate consideration in the development of an automated welding system.

Table 5-7 Calculating 'effective' wire feed speed for pushing and pulling travel angles

	<i>Push</i>	<i>Pull</i>
<i>travel speed (mm/min)</i>	240	240
<i>wire feed speed (mm/min) @ 45° gun angle</i>	4572	4572
<i>'Effective' wire feed speed (mm/min)</i>	4748	4405

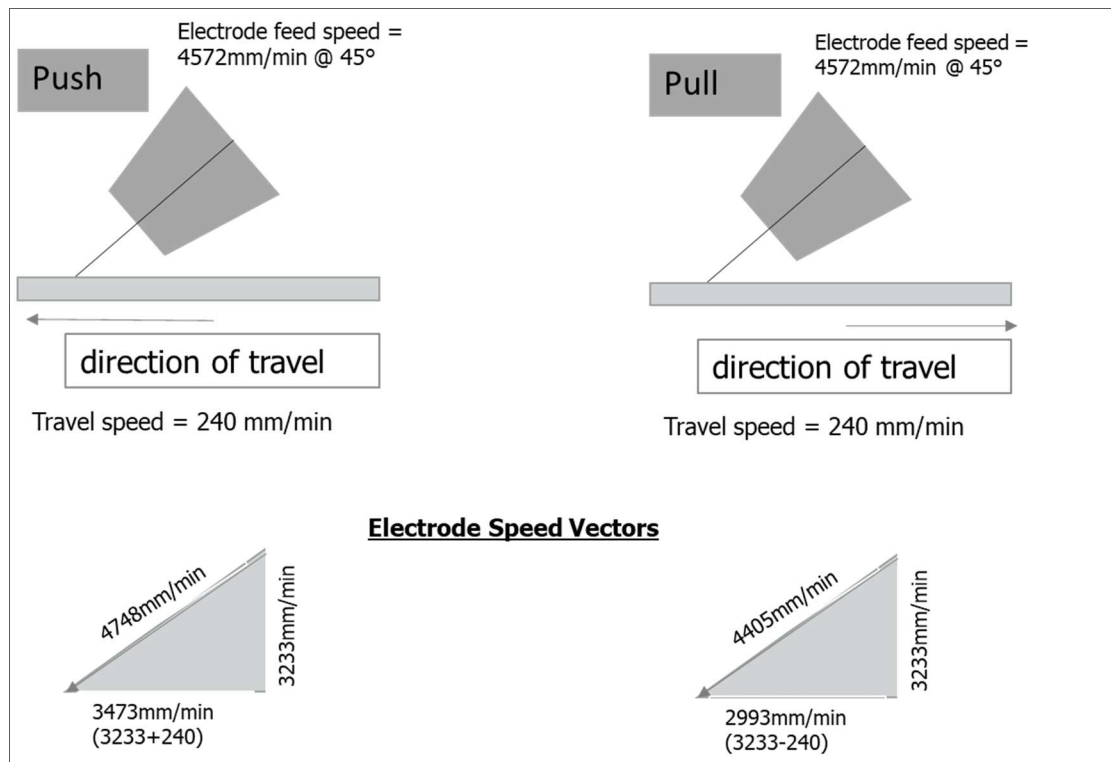


Figure 5-29 Calculation of wire feed speed for pushing and pulling travel angles

### 5.3.2 Leg Length

The ANN model and regression analysis both confirmed that travel speed was the most influential individual parameter in determining leg length, followed to a lesser extent by the current then voltage. [Figures 5-2, 5-11, 5-13]. The ANOVA analysis [Figures 5-4, 5-5] also confirmed that travel speed was the most influential parameter in determining leg length, but it also identified that there is a significant interaction between the torch travel angle and travel speed and also between the travel angle and the gun angle. If all other input parameters are being controlled, then the travel speed should be the critical input parameter for controlling the resultant leg length of the fillet weld. The significance of the travel speed in determining GMAW geometry reflects favourably with the data reported by Campbell et al [5.6] when developing an ANN model to predict GMAW weld geometry. As mentioned previously the voltage does not feature as significantly in the results as would have been expected. This can be partly explained by the use of a constant voltage power supply, where the voltage is kept constant irrespective of fluctuations in the current.

Looking closer at the interaction between the travel speed and travel angle, the travel speed is one of the key factors in determining the volume of filler material that is deposited at each position across the length of the weld. It is a valid conclusion that the angle of deposition (travel angle) and the volume of filler material deposited per unit length are the most influential factors in determining the leg length. This would explain why the interaction between these two parameters was identified as being a significant input parameter. One of the main challenges during experimentation was around controlling and maintaining a consistent torch position (gun angle and travel angle) relative to the baseplate and stiffener of the welded joint. It was observed that very slight changes to either the travel angle, gun angle or position of the test piece influenced the physical distance between the electrode tip to the workpiece (CTWD) and/or the stand-off position, both of which impact on the resultant weld quality and geometry. This level of sensitivity to changes in torch position may help to explain why the interaction between the gun angle and travel angle was identified as being a significant variable impacting the resultant leg length, throat and reinforcement.

The experimental results highlighted that the symmetry of the vertical and horizontal leg lengths was improved when the torch is in a pushing configuration. Figure 5-16 shows that when the torch was pulling, the range of asymmetry between the horizontal and vertical leg lengths was 5.02mm. For a neutral travel angle the range was 6.8mm but for a pushing travel angle the range was only 3.48mm. The results of the regression analysis [Figure 5-15] also confirm that the travel angle has the biggest impact on the asymmetry of the vertical and horizontal leg lengths of the GMAW fillet weld, with a pulling travel angle having a larger impact on the difference between the horizontal/vertical leg lengths than a pushing travel angle. These findings would suggest that a pushing travel angle is preferred in order to reduce the variation between the horizontal and vertical leg lengths.

### 5.3.3 Weld Shape (Throat + Reinforcement)

The ANOVA analysis [Figures 5-6, 5-7] identified that there is a significant interaction between the torch travel angle and travel gun angle which influences both the size of the throat and reinforcement of a fillet weld. Upon analysing the weld macros from the travel angle experiments [Table 5-5], it was observed that a pushing travel angle produces a

'flatter' weld bead and a pulling travel angle generates a more 'rounded' reinforcement [Figure 5-30]. The results also showed that the vertical leg length is larger when the travel angle is pushing and conversely, the horizontal leg length is larger when the torch is pulling. When the torch is pushing, the electrode is being fed in front of the torch and as the torch passes over the welded area the momentum of the electrode will naturally try to flatten the weld before it starts to solidify. Conversely, when the torch is being pulled the wire is being fed backwards (away from the direction of travel). Consequently, as the electrode is fed into the weld, a natural cap/peak will be formed which will not be flattened by the momentum of the electrode because it has already passed.

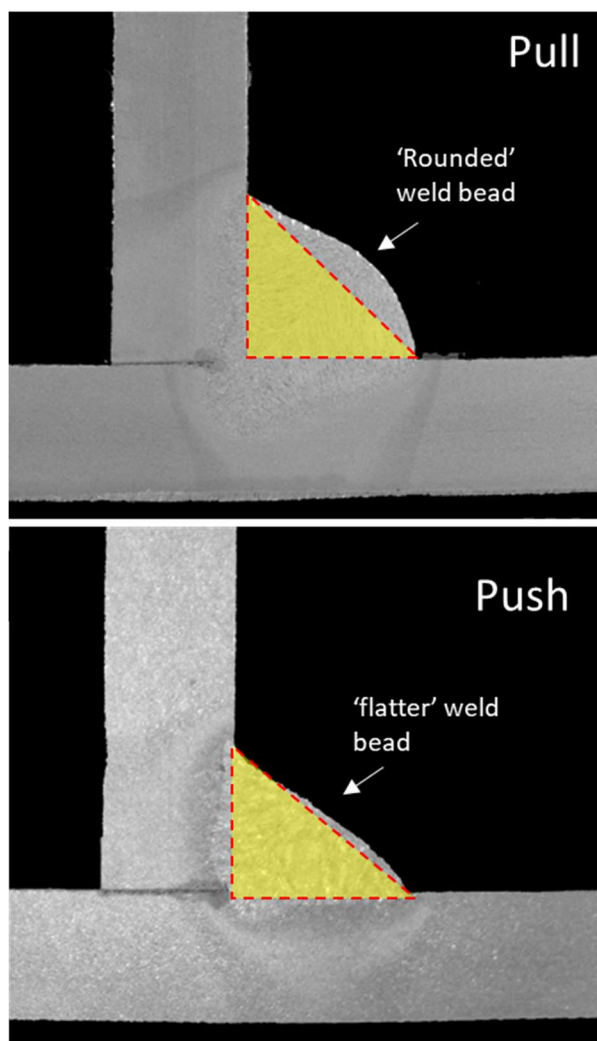


Figure 5-30 Macrograph images showing pull and push fillet welds.

The results discussed in this section provide an improved understanding of the GMAW process variables and their interactions. This improved understanding can be used to provide a greater level of process control and enable the benefits described in section 5.1. This level of control would also potentially allow the design size of weld to be determined by the penetration allowing the overall size of the weld to be reduced whilst maintaining the joint strength as proposed by Miller [5.7]

#### 5.3.4 Hardness

Figure 5-25 plots the hardness results from the baseplate, heat affected zone and weld area for samples welded in the pushing, pulling and neutral travel angle orientation. All samples were welded with a metal cored electrode. The results were all within the acceptable maximum limit of 350HV, as defined by IACS [5.8], and show that there is no significant impact to the hardness of the weld area or heat affected zone by varying the travel angle. The results also show that the weld area of the samples welded with a pushing travel angle were 5-6% harder, however there does not appear to be any corresponding impact to the resultant microstructure as previously discussed in Figures 5-23 and 5-24. The conclusion that can be drawn from reviewing these results is that the travel angle of the torch has no direct significant impact on the resultant hardness of the weld area or heat affected zone of the fillet weld. A sample of the natural fluctuations in voltage and current during the welding experiments was captured and summarised in table 5-6. Any slight variations in hardness could most likely be attributed to this natural fluctuation in the current and voltage readings during the welding process.

#### 5.3.5 Microstructure

Figures 5-23 shows the variation in microstructure of the weld area when the travel angle is pulling, pushing and neutral. The microstructure of all three samples appears to be very similar; predominantly made up of acicular ferrite with areas of allotriomorphic ferrite. Acicular ferrite is widely believed to be a desirable microstructure [5.9]. These results suggest that there is no significant impact to the microstructure of the weld area as a

consequence of changing the travel angle. Figure 5-24 shows the variation in the microstructure of the heat affected zone as it moves further away from the weld area. The results show that the torch travel angle appears to have no significant effect to the microstructure of each of the heat affected zones. Differences in the microstructure can usually be attributed to the differences in the cooling rate [5.10]. This will be discussed further in Chapter 6.

#### 5.4 References

- 5.1 Molugaram, K., Shanker Rao, G.(2017) 'Chapter 11 - ANOVA (Analysis of Variance)', *Statistical Techniques for Transportation Engineering*, 2017, pp 451-462
- 5.2 Rosenthal, J. W. (2001). Ten steps to reducing your welding costs. *Welding Journal (Miami, Fla)*.
- 5.3 BSI. (1998). BS EN ISO 9015-1:2001: Destructive tests on welds in metallic materials — Hardness testing. Part 1: Hardness test on arc welded joints. *BSI Standards Publication*
- 5.4 Welding Technology Institute of Australia (2006), TGN-PE-01, Hardness Testing of Welds
- 5.5 Hicks, J. (2000), *Welded Design: Theory and Practice*, Abington Publishing, Cambridge.
- 5.6 Campbell, S.W., Galloway, A.M., McPherson, N.A. 2012. Artificial Neural Network Prediction of Weld Geometry performed using GMAW with Alternating Shielding Gases. *Welding Journal*, vol.91, no.6. June 2012. Supplement: Welding Research. Pp.174s-181s, ISSN: 0043-2296
- 5.7 Miller, D. K. (1998). Consider Penetration when determining fillet weld size. *Welding Innovation Volume XV, No 1*, 1998.



- 5.8 International Association of Classification Societies. Requirements concerning Materials and Welding, W28 Welding Procedure qualification tests of steels for hull construction and marine structures. IACS Req. 2005/Rev.2 2012, p.20
- 5.9 Bhadeshia, H.K.D.H. (2008). Interpretation of Microstructure of Steels (University of Cambridge). [online] available at [https://www.phase-trans.msm.cam.ac.uk/2008/Steel\\_Microstructure/SM.html](https://www.phase-trans.msm.cam.ac.uk/2008/Steel_Microstructure/SM.html)
- 5.10 Winowlin, J.T., Alavudeen, A. (2006). A Textbook of Engineering Materials and Metallurgy, 1st Edition, USP/Laxmi Publications Ltd, ISBN 13: 9789380386980

## Chapter 6 Finite Element Modelling

### 6.1 Finite Element Modelling – GMAW Fillet Weld

A 3-Dimensional Finite Element Model was developed, as described in Chapter 3.4, to determine what impact varying the heat input and weld geometry has on the thermal distribution and resultant distortion of a fillet welded joint. The model has been used to:

- Assess what impact each of the individual input parameters has on the heat flow through the horizontal and vertical plates of the fillet welded joint.
- Understand what impact an unequal leg length has on the resultant heat flow through the welded joint. In practice it is not always possible to maintain a 100% consistent leg length and so it is important to understand what impact any variation in the leg length has on the corresponding heat flow through the weld and structure.

#### 6.1.1 Baseplate vs Stiffener Heat Flow – FEA Model Validation

As part of the model development process, a validation was undertaken to compare the predicted (modelled) results with actual measured readings. The temperature readings were taken using type K thermocouples attached to the steel plates. In order to attach the thermocouples to the plates, a series of 2mm diameter 1mm deep holes was drilled on the plates. These holes provided an interference fit for the thermocouples. The thermocouples were measuring the heat 1mm below the surface of the plate. This was taken into consideration when taking the readings from the FEA model. The locations of the temperature readings were chosen to show the thermal flow through the structure, as this would ultimately provide a greater indication of overall movement/distortion of the assembly. The readings were measured from 3 points equidistant (50mm) from the root of the fillet joint. Figure 3-18 shows the locations of the temperature readings relative to the fillet welded assembly. Figure 6-1 shows the actual vs predicted temperature readings at these 3 locations over time.

- Point A0 is located on the baseplate on the same side of the weld
- Point B1 is located on the stiffener
- Point C2 is located on the baseplate on the other side of the stiffener to the weld

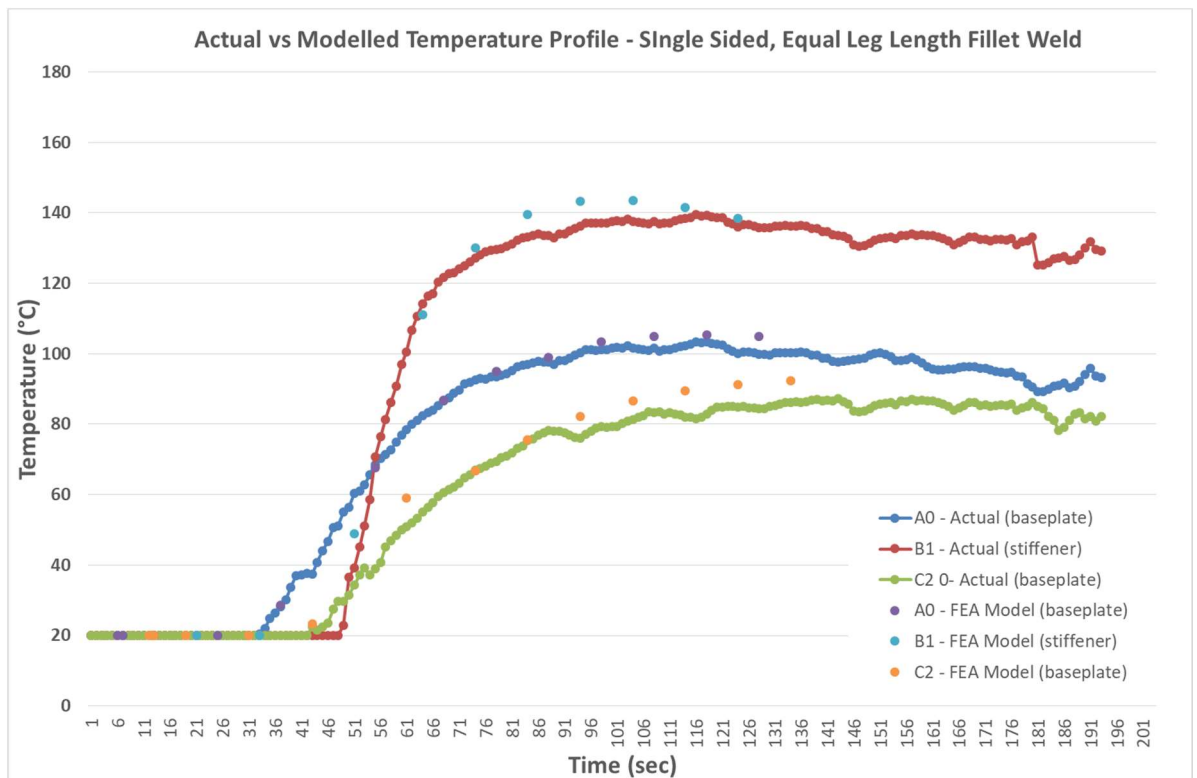


Figure 6-1 Actual vs Predicted temperature readings plotted over time

Overall the results are as expected. The stiffener heats up at a faster rate than the baseplate. The main method of heat transfer is conduction from the weld area to both the stiffener and baseplate. The baseplate would not be expected to heat up at the same rate as the stiffener due to the large area for the heat to dissipate. As shown in Figure 3-18 the baseplate is double the size of the stiffener. The heat source is applied at the centre of the baseplate and so the heat flows outwards, in both directions, towards the edge of the plate [Fig 6-2]. However the heat source is applied to the base of the stiffener and so the heat flows upwards towards the top of the stiffener. Although there is very little heat conduction across the interface between the baseplate and stiffener, as discussed in Chapter 2, the upwards flow of heat (due to convection and radiation) from the baseplate to the stiffener will also contribute to the stiffener heating up at a faster rate.

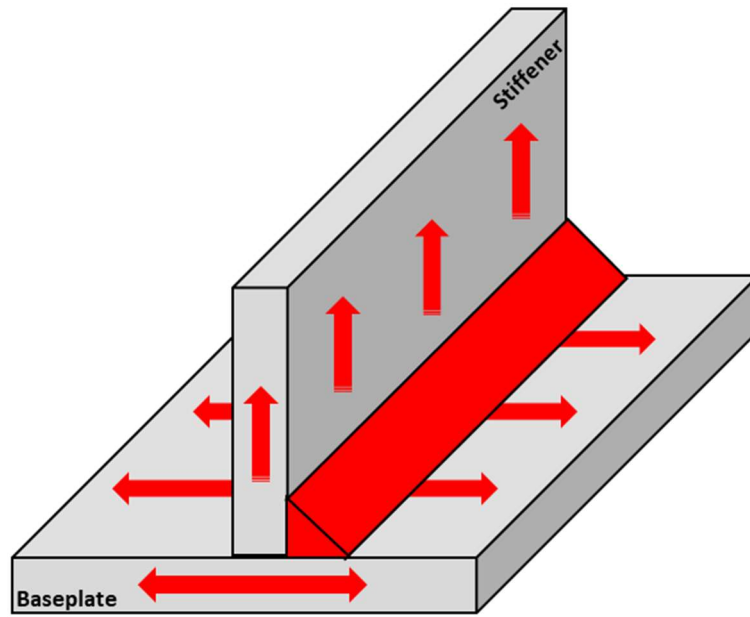


Figure 6-2 Schematic showing direction of heat flow through the welded fillet joint.

### 6.1.2 Impact of individual input parameters on the heat flow through the fillet welded joint

Figure 6-3 below shows the results, from the 3D FEA model, tracking the changes in temperature through the stiffener (vertical) plate by altering each of the key input parameters individually by 10%. The modelled geometry of the weld was updated, using experimental data, to reflect the actual changes in geometry that would result by altering the individual parameters. The graph shows that a 10% increase of either the current or voltage results in an 8% increase in the peak temperature flowing through the structure of the fillet joint. The graph also highlights that a 10% increase in the travel speed reduces the peak temperature flowing through the structure by 18%.

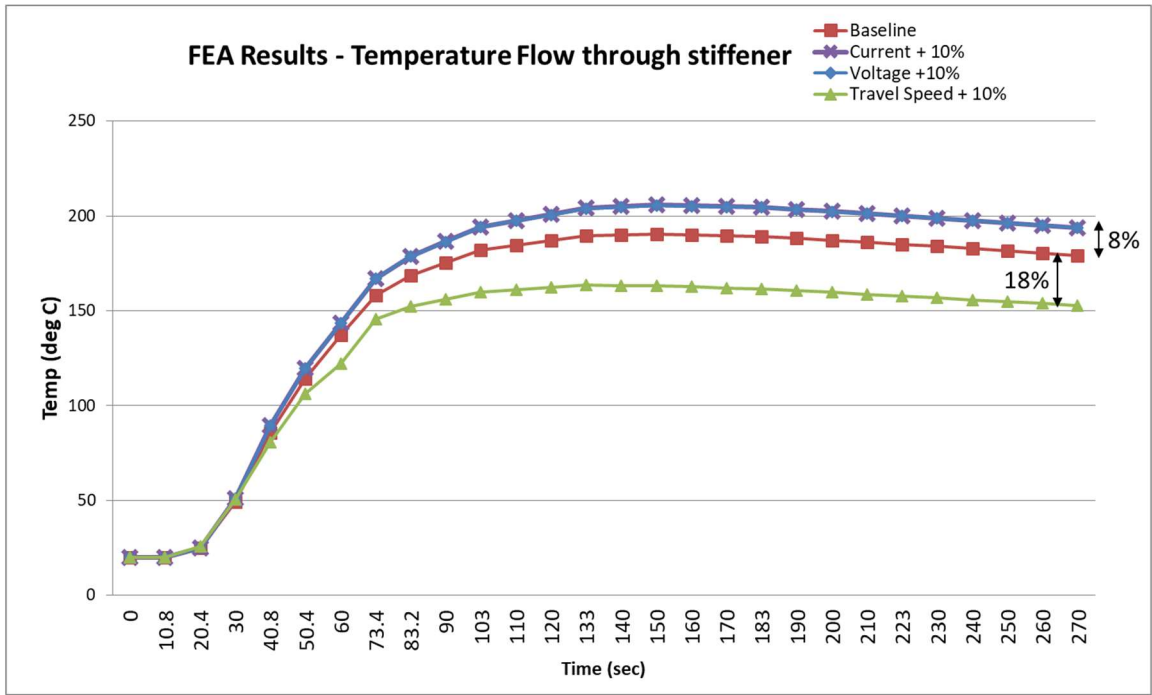


Figure 6-3 Comparison of predicted temperature flow through stiffener by varying input parameters by 10%.

### 6.1.3 Impact of Asymmetrical Leg Lengths on the heat flow through fillet welded joint.

In practical terms it is difficult to produce a fillet weld with identically sized vertical and horizontal leg lengths, when welding a continuous fillet weld. The 3D FEA model was used to investigate what impact varying the individual leg lengths of a fillet weld has on the resultant thermal load applied through the joint. For the experiment all parameters were kept constant (same heat input) and only the resultant shape of the fillet weld was altered to model unequal leg lengths. The experimental parameters along with the actual and predicted heat affected zones areas are contained in Table 6-1.

Table 6-1 Comparison of Actual vs Predicted HAZ size with varying leg lengths

	Current (A)	Voltage (V)	Travel Speed (m/sec)	Vertical Leg Length (mm)	Horizontal Leg Length (mm)	Stiffener HAZ (mm <sup>2</sup> )	Base plate HAZ (mm <sup>2</sup> )	HAZ Ratio (Stiffener: Baseplate)
<b>Expt 1 (Actual)</b>	200	23.3	0.0083	6.04	4.14	19.72	9.09	2.06
<b>Expt 1 (FEA)</b>	200	23.3	0.0083	6	4	15.4	7.47	2.17
<b>Expt 2 (Actual)</b>	200	23.3	0.0083	3.98	5.97	14.78	24.27	0.61
<b>Expt 2 (FEA)</b>	200	23.3	0.0083	4	6	14.1	21.069	0.66

Figure 6-4 shows that when comparing the temperature readings of expt1 and expt2, there is a peak variation of 15% as a consequence of varying the asymmetry of the fillet weld. However, as the assembly cools, this temperature variation drops to around 3-4%.

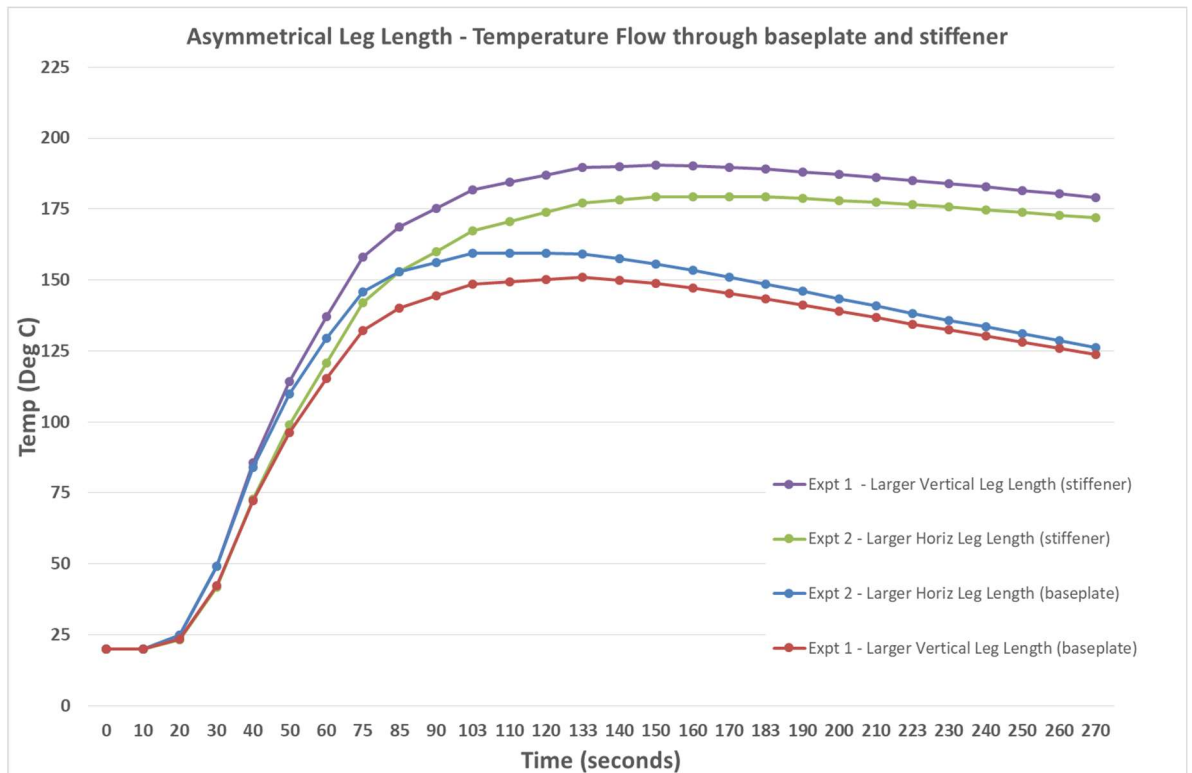


Figure 6-4 Comparison of predicted temperature variation through stiffener and baseplate by varying the unequal leg length

As the geometry would imply, an unequal fillet with greater vertical leg length applies a greater thermal load to the stiffener. Conversely, an unequal fillet with greater horizontal leg length applies a greater thermal load to the baseplate. This can be further confirmed by Figure 6-5 below which shows the macro and heat affected zone of the two unequal leg length samples and their corresponding modelled image. The first image shows a fillet weld with a larger vertical leg length and a larger heat affected zone on the stiffener. The second image shows a fillet weld with a larger horizontal leg length and a larger heat affected zone on the baseplate. The corresponding modelled images show similar results.

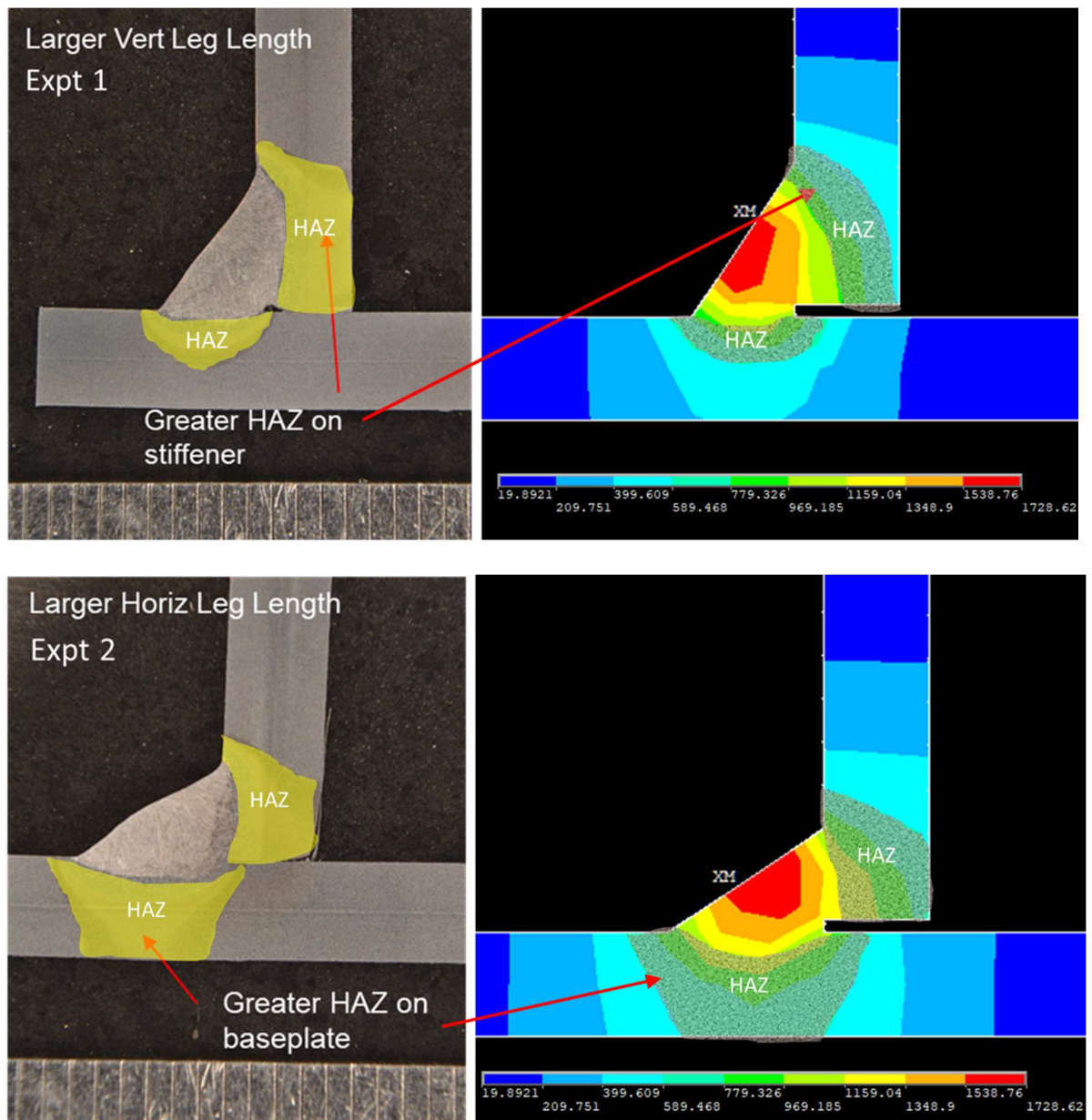


Figure 6-5 Comparison of HAZ between macrograph and FEA Model

The macrographs were used to calibrate and validate the results of the FEA model. Sloderback [6.1] conducted an analysis to determine the range of the heat affected zone in a welded structure. This study identified that the temperature at which the heat affected zone begins is around 600°C. This temperature was used to identify the size of the HAZ in the FEA image. Table 6-1 shows the comparison between the size of the actual HAZ and the predicted HAZ in the modelled image. The results show good agreement between the actual HAZ area and the modelled HAZ area for both configurations of leg length.



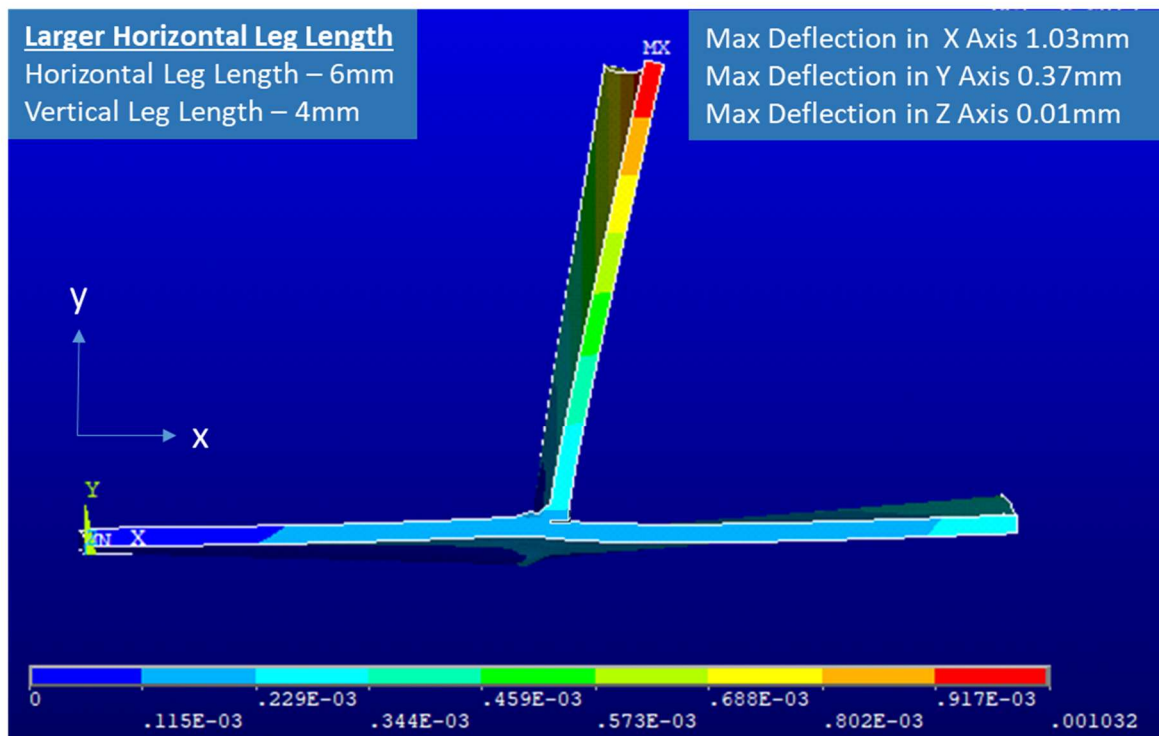
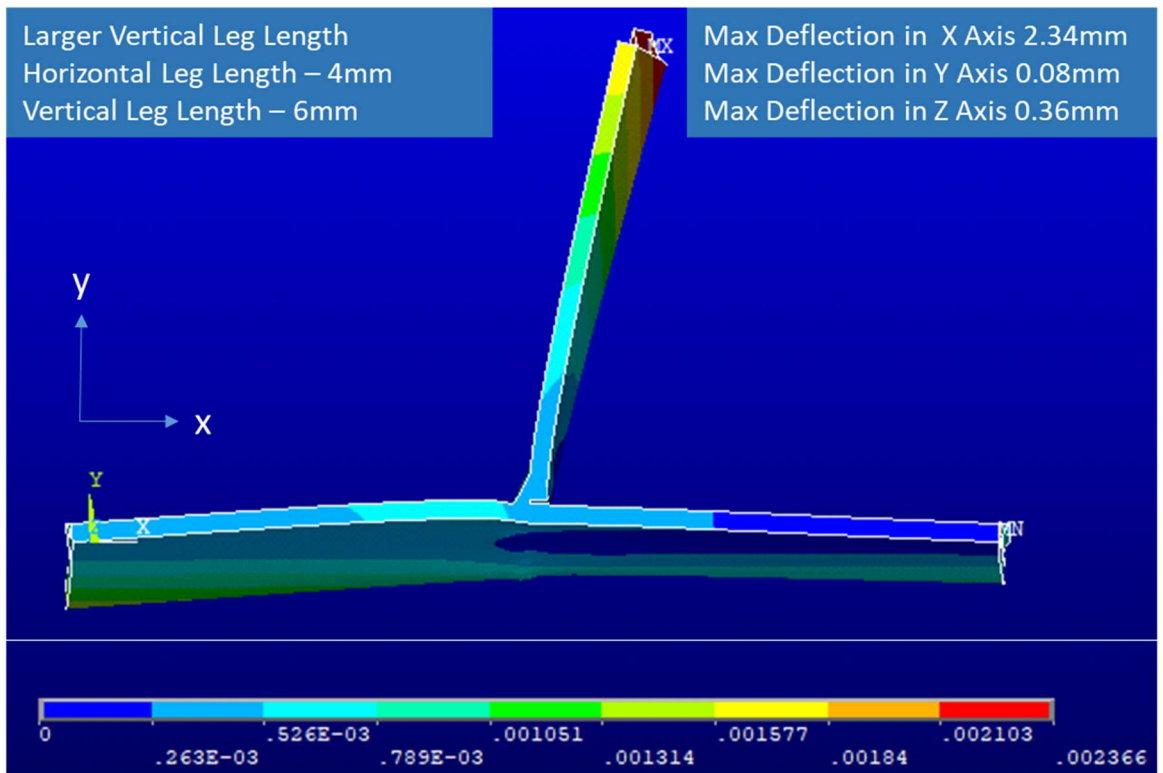


Figure 6-6 FEA Structural Model showing the deflection in each axis by varying leg length.

Figure 6-6 shows the results from the Ansys FE Model which was developed to assess the impact of varying the horizontal and vertical leg lengths of the fillet weld. The input parameters used in the development of the models are shown in Table 6-2. The main conclusion which can be drawn from the results in Figure 6-6 is that as the vertical leg length increases the maximum deflection in the structure reduces. A 2mm reduction in the vertical leg length from 6mm to 4mm saw a decrease in the stiffener deflection by 1.3mm (angular distortion 0.8°). Conversely, as the horizontal leg length increases the size of deflection in the structure also increases. This would initially appear to be counter intuitive.

Table 6-2 Inputs and Outputs from Unequal Leg Length FEA Structural Model.

	<i>Inputs</i>					<i>Outputs</i>		
	Current (A)	Voltage (V)	Travel Speed (m/sec)	Vertical Leg Length (mm)	Horizontal Leg Length (mm)	Max X Axis Deflection (mm)	Max Y Axis Deflection (mm)	Max Z Axis Deflection (mm)
<i>Expt1</i>	200	23.3	0.0083	6	4	1.03	0.37	0.01
<i>Expt2</i>	200	23.3	0.0083	4	6	2.34	0.08	0.36

## 6.2 Heat Input & Distortion Discussion

### 6.2.1 Process Parameters

The FEA model described in Chapter 3 was used to assess what impact the current, voltage and travel speed had on the temperature distribution through the welded structure. The results of Fig 6-3 show that a 10% increase of either the current or voltage results in an 8% increase in the heat flowing through the structure of the fillet joint. This figure is comparable with the process efficiency figures discussed in Chapter 2.3.3. The results also show that a 10% increase in the travel speed reduces the heat flowing through the structure by 18%, indicating that the travel speed is the most significant parameter in determining the amount of heat flowing through a welded joint.

## 6.2.2 Asymmetrical Leg Lengths

As mentioned in Chapter 2, BS EN ISO 5817:2003, [6.2], defines that the maximum allowable level of asymmetry of a fillet weld can be calculated using the Eqn 1.5. For a target 5mm leg length fillet weld, this allows for a maximum difference of 2.7mm between the horizontal and vertical leg lengths. 96% of the welded samples achieved this level of asymmetry, highlighting that practically this level of asymmetry can be achieved comfortably. The FEA model, described in Chapters 3 was used to assess what impact an acceptable level of variation, 2mm, has on the temperature profile that is applied to the joint. Two models were created, the only difference between the models was the size of the vertical and horizontal leg lengths. The first model used a fillet with a larger vertical leg length (6mm), whereas the second model had a fillet with a larger horizontal leg length (6mm) as shown in Table 6-1. The results are shown in Figure 6-4 which shows the temperature readings in the baseplate and stiffener for both FEA models. The peak temperature readings are 15% higher in the baseplate when the horizontal leg length (6mm) of the fillet weld is 2mm larger than the vertical leg length (4mm). A similar result can be seen on the vertical stiffener. The peak temperature readings on the stiffener are 15% higher for a fillet weld which has a vertical leg length (6mm), 2mm larger than the horizontal leg length (4mm). In both models the increase in temperature in either the horizontal baseplate or vertical stiffener is offset by a temperature reduction in the other. These results are confirmed by Figure 6-5 which shows macrographs and FEA images of the heat affected zones for samples with a varied vertical and horizontal leg length. Figure 6-5 also confirms that the increase in leg length directly correlates with an increase in heat applied to the structure. This is evident where there is a larger heat affected zone on the baseplate of the weld which has a larger horizontal leg length and a larger heat affected zone on the (vertical) stiffener of the weld which has a larger vertical leg length. These results ultimately show that the resultant leg length of the fillet weld provides a good indication of how the heat from the GMAW process is transmitted to the welded structure. As discussed earlier, the travel speed, torch travel and gun angle have an impact on the resultant leg length of a GMAW fillet weld. So indirectly the orientation of the welding torch will have an impact on how the heat from the GMAW process is transferred to the welded structure. As described in Chapter 5.2 the travel angle impacts the resultant leg length and resultant leg lengths provides a good indicator of the size of the heat affected

zones on both the baseplate stiffener. Using this logic it can also be implied that the leg length asymmetry may have an impact on the resultant distortion of the structure.

### 6.2.3 Heat Affected Zone / Distortion

Figure 5-19 shows the results of an exercise to assess the relationship between the input parameters (current, voltage, travel speed, travel angle and gun angle) and the resultant size of the weld area and heat affected zone. The analysis highlighted that, there is a significant statistical relationship between input parameters and size of the welded heat affected zone area as indicated in Figure 5-19. The results of this regression analysis highlighted that travel speed was the most significant parameter in defining the size of the weld + heat affected zone. Again, this confirms expectations as both the travel speed and current are the dominant factors in determining the heat input [Eqn. 1-1]. The results in Figure 5-19 are similar to the leg length regression analysis results reviewed earlier in chapter 5, which highlighted that travel speed was the most significant parameter in determining leg length, followed by current then voltage. This similarity reinforces the strong correlation between the size of the leg length and the size of the heat affected zone as shown in Figure 5-19.

Figure 6-4, taken from the FEA model, highlights the difference in temperature measured through the baseplate and stiffener as a result of varying between a larger horizontal and vertical leg length. In figure 6-4, it can be seen that the temperature readings on the horizontal baseplate, in both experiments, are significantly lower than the temperature readings on the vertical stiffener. The temperature readings on both the stiffener and baseplate were taken at points equidistant from the heat source/root of the joint. As mentioned previously the main method of heat transfer from the weld area to the stiffener and baseplate is through conduction. The baseplate initially heats up at the same rate as the stiffener, however after approximately 90 seconds the temperature of the baseplate starts to cool at a faster rate than the stiffener. The baseplate has significantly lower peak temperature readings than the stiffener does as it is double the size of the stiffener [Fig 3-18] and has a much larger area for the heat to dissipate. There will also more heat loss, due to natural convection, on the baseplate as a result of the larger surface area which explains why the baseplate cools down at a faster rate than the stiffener,

The variation in temperature measured as a consequence of varying the larger horizontal and vertical leg lengths is also observed in Figure 6-5 through the size of the heat affected zones on the baseplate and stiffener. The size of the HAZ areas in the macrographs shown in Figure 6-5 were used to validate the accuracy of the temperature readings in the FEA model. As can be seen from the macrographs in Figure 6-5 and previously in Figure 5-21, the ratio of heat transferred to the baseplate and stiffener can be calculated by measuring the size of the respective heat affected zones. The size of the heat affected zones also appears to be proportional to the size of the leg length.

The resultant distortion of a welded structure is broadly determined by the amount of heat to the structure. Consequently, since the level of asymmetry of the fillet weld appears to determine the ratio of heat being applied to the baseplate and stiffener then logically there will be a level of impact to the overall distortion of the welded structure. Figure 6-6 shows the results of the FEA model, when the asymmetrical fillet welds, shown in Figure 6-5, are applied. Figure 6-6 indicates that the level of distortion of the structure is impacted by the asymmetry of the fillet weld leg length. When a fillet weld with a larger vertical leg length is applied to the model the overall deflection in the x-axis (parallel to baseplate) is around 1mm, 0.37mm in the y-axis (parallel to stiffener) and close to no movement in the z-axis. When a fillet weld with a larger horizontal leg length is applied to the model the max deflection in the x-axis more than doubles to 2.34mm, the deflection in the y-axis reduces to close to 0 but the deflection in the z-axis increases to 0.36mm. From a practical perspective reducing the distortion in the baseplate, rather than the stiffener, would be the preferred outcome, due to the additional cost and rework required to flatten and fair adjacent plates. Consequently, these results would suggest that welding the fillet with a larger horizontal leg length would be the preferred option as it appears to generate less overall deflection on the baseplate (y-axis). This study has only considered the single side welding; however, the results reinforce that in order to control the level of distortion of a welded structure it is important to tightly control the size and shape of the fillet weld.

The results of this study challenge the assumptions and methodology described by Asifa [6.3] who has conducted one of the few studies that investigate the impact of the gun angle. In this study Asifa [6.3] appeared to model the electrode angle (gun angle) as directly impacting the temperature distribution through the welded structure, i.e. as the electrode angle increases the heat applied to the stiffener increases. The results detailed in the

previous chapter [Figures 5-10, 5-11 and 5-13] do not show the gun angle, individually, as being a critical factor in determining the geometry of the fillet weld. The results also suggest that the resultant leg lengths of the weld are a strong indicator as to the distribution of heat to both the baseplate and stiffener. Consequently, the assumption that the gun angle directly effects the temperature distribution through the baseplate and stiffener is an over simplified one.

### 6.3 References

- 6.1 Sloderbach, Z., Pajak, J. (2015). 'Determination of ranges of components of heat affected zone including changes of structure', Archives of Metallurgy and Materials, Vol.60, Issue 4, DOI: 10.1515/amm-2015-0421
- 6.2 BS EN ISO 5817:2003 Welding — Fusion-welded joints in steel, nickel, titanium and their alloys (beam welding excluded) — Quality levels for imperfections
- 6.3 Asifa, K., Li, H., Li, L. and Khurram, S. (2011) 'Parametric Study of Welding Temperature Distribution in T-Joint Fillet Weld Using FEM', Advanced Materials Research, 328-330, pp. 492–496.

# Chapter 7 Shielding Gas Visualisation

## 7.1 Overview of Schlieren Results

As detailed in the Chapter 3.5, the purpose of the gas visualisation experiments was to investigate the impact that varying the shielding gas flow rate and travel angle have on the resultant fillet weld geometry, hardness and microstructure.

### Flowrate Reduction

From the gas visualisation images [Figure 7-1] it was evident that, for the highest gas flow rate 15l/min, there was a strong gas shield around the fillet weld. The gas flow upwards also appears to be stronger than the gas flow being directed downwards and behind the torch head. These results were in good agreement with the 3D Comsol fluid flow model developed by Bitharis [7.1].

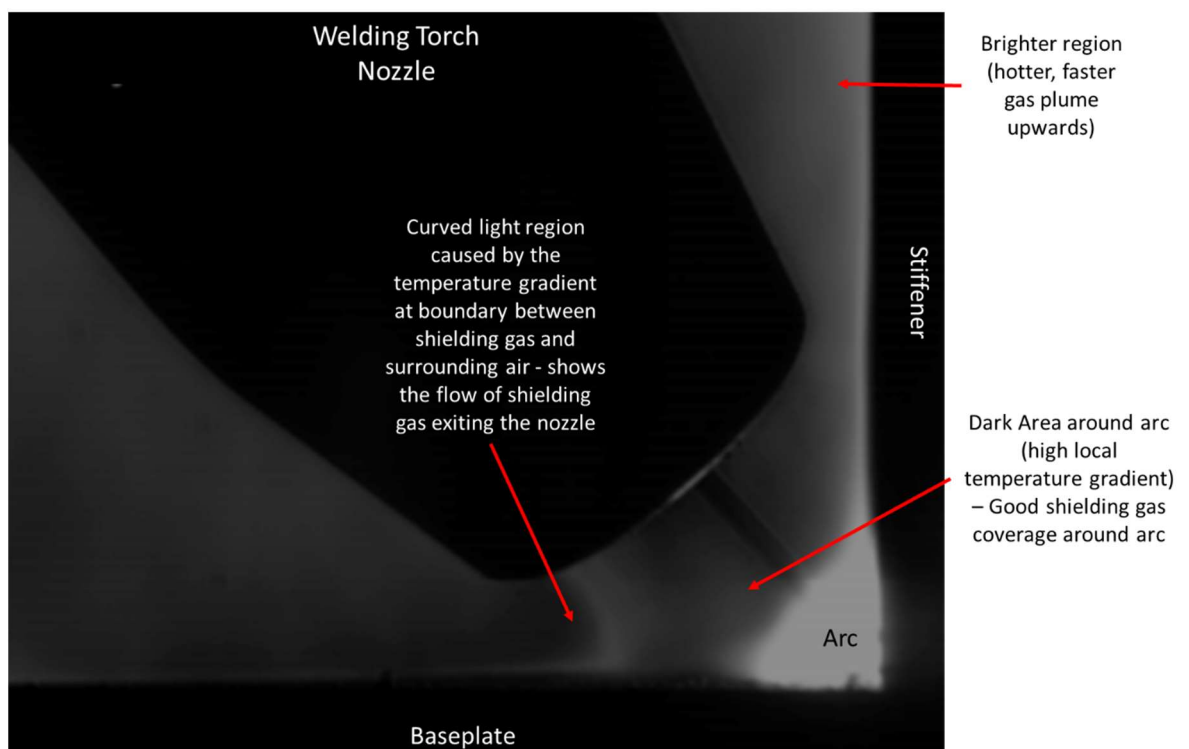


Figure 7-1 Schlieren visualisation at 15l/min gas flow rate

Figure 7-2 shows a comparison of the Schlieren visualisations at 15, 12, 9 and 6l/min gas flow rate. As the shielding gas is reduced from 15 l/min down to 6 l/min the strength of the gas shield becomes visibly weaker however the overall characteristics are similar in the four image. There is a brighter region above the nozzle, highlighting a stronger flow of gas upwards (parallel with stiffener) and there is evidence of a vortex forming behind the nozzle. As the gas flow rate is reduced the upwards gas flow also reduces (brighter area above nozzle shrinks) and the turbulence behind the nozzle moves closer to the arc.

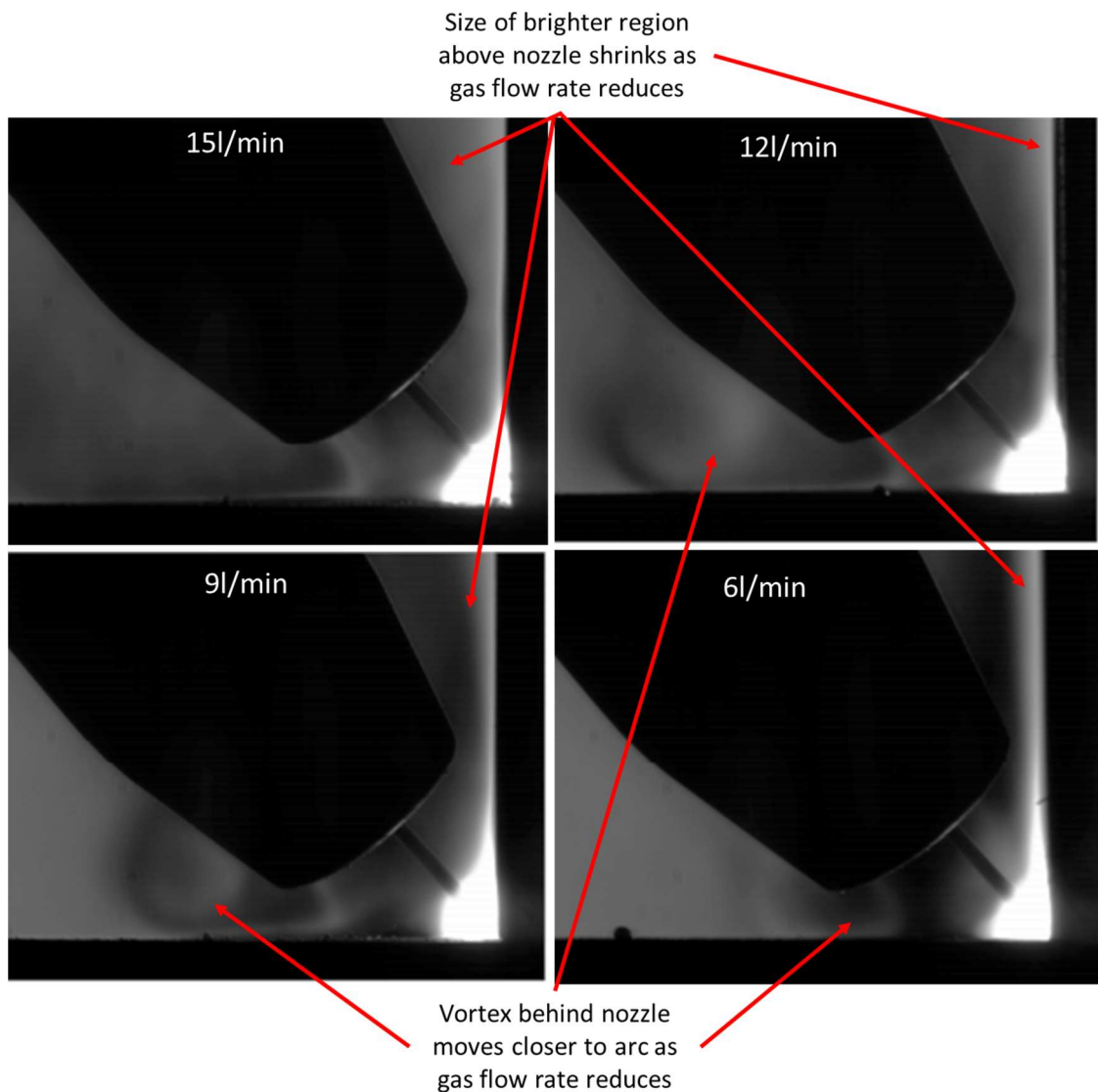


Figure 7-2 Schlieren visualisations at 15, 12, 9 and 6 l/min gas flow rates



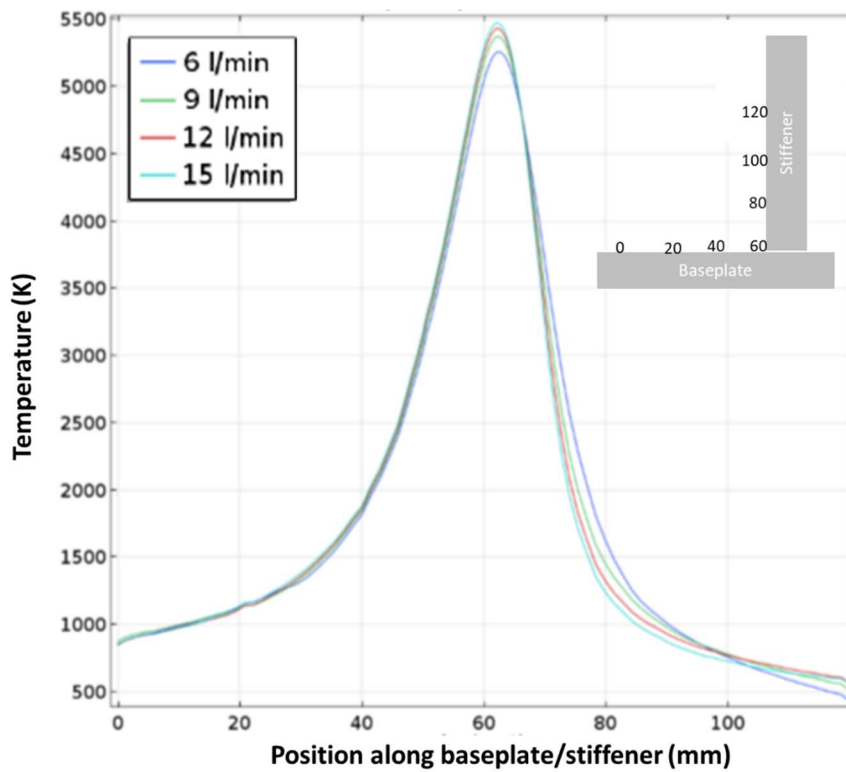
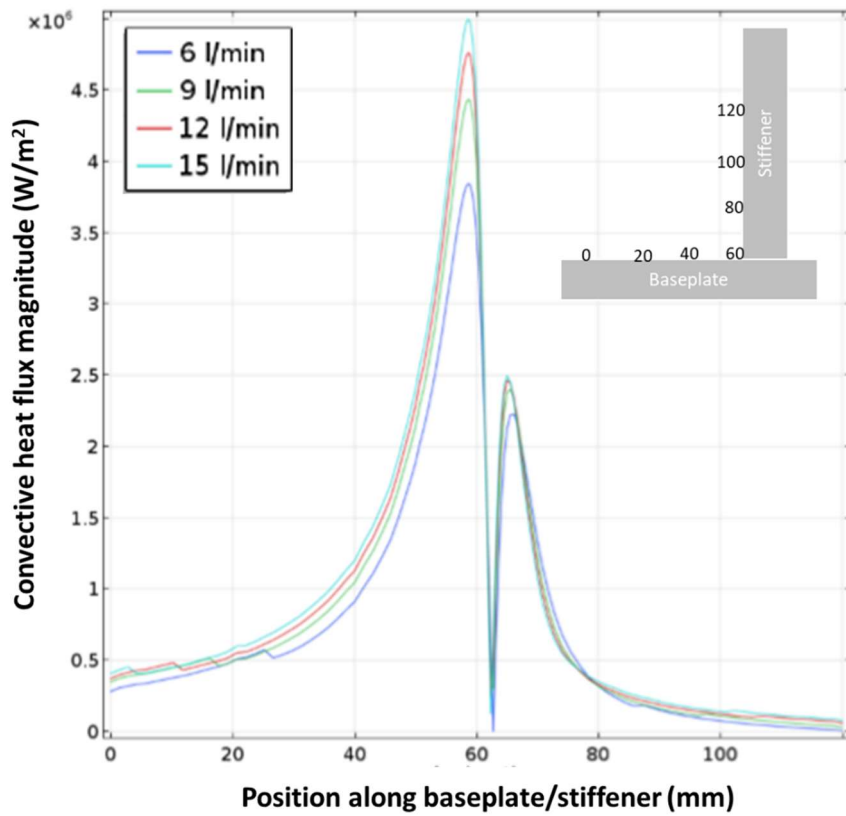


Figure 7-3 Convective heat flux and temperature along the edge of the baseplate and stiffener [7.1].

The 3D Comsol model [7.1] was in good agreement with the above Schlieren results. The model also showed that an increased gas flow through the nozzle results in the plate heating up, rather than cooling. This can also be seen in Figure 7-3, which graphs what impact reducing the shielding gas flow rate has on the convective heat flux and temperature along the vertical stiffener and horizontal baseplate of a fillet welded joint. The top graph shows that as the gas flow rate is reduced, the convective heat flux on the baseplate, behind the welding torch, reduces significantly. However, out with this area the convective heat flux and temperature readings all follow a similar profile regardless of the gas flow rate.

## 7.2 Shielding Gas Flow Reduction – Impact on fillet weld geometry

After Schlieren videos had been recorded, the samples were cut, macro prepared and polished so that the key geometrical features could be analysed, hardness measurements obtained and microstructure analysed (as detailed in Chapter 3). The key geometrical measurements of the key welds are detailed in Table 7-1.

Table 7-1 Geometry of fillet weld samples from gas flow experiments

Expt #	Gas Flow Rate (l/min)	Electrode	Travel Angle (30°)	Vertical Leg Length (mm)	Horizontal Leg Length (mm)	Penetration (mm)	Vertical HAZ Area (mm <sup>2</sup> )	Horizontal HAZ Area (mm <sup>2</sup> )	Weld Area (mm <sup>2</sup> )	Total Weld Area + HAZ (mm <sup>2</sup> )	Max Hardness (HV)	Average Hardness (HV)
4	12	Solid	Push	4.29	6.5	0	5.41	10.91	19.91	36.23	283	191
5	12	Solid	Pull	4.2	5.42	0.7	7.03	9.44	19.54	36.01	296	199
9.1	6	Solid	Push	5.11	5.6	0.3	8.93	8.04	18.17	35.14	279	197
10	6	Solid	Pull	6.54	7.27	n/a	n/a	n/a	n/a	n/a	358	209
F11	3	Flux Cored	Pull	5.13	4.84	0.6	11.85	6.58	21.97	40.4	339	201
F10	3	Flux Cored	Push	4.19	6.02	1	7.83	8.55	24.5	40,88	349	202
F5	12	Flux Cored	Pull	6.43	4.84	0.6	10.87	8.06	22.22	41.15	364	196
F4	12	Flux Cored	Push	4.54	6.86	0.3	7.56	11.74	20.85	40.15	329	193

The following can be observed from the measured geometry:

- Overall HAZ & Weld Area similar for pushing/pulling and different gas flow rates, which would be expected as the heat input was kept constant for all experiments.
- The geometry of experiment 10 (solid wire @ 6l/min) could not be fully measured due to the poor quality of the resultant weld and high levels of porosity.

### 7.3 Electrode Impact on reducing shielding Gas Flow

The experiments were repeated for both solid wire and flux cored electrodes. The shielding gas behaved similarly for both solid wire and flux core experiments. However, when welding with the solid wire electrode, the arc became unstable when the shielding gas was reduced down to 6l/min. Satisfactory welds were not able to be produced when the gas flow rate was reduced further. When welding with the flux cored electrode, the gas flow

rate could be reduced to 3 l/min before the arc became unstable and the quality of the weld became unacceptable. This can be explained by the presence of the 'flux' in the flux cored electrode. As the electrode is consumed, the gas produced by the melting of the electrode provides additional shielding properties which compensate for the reduction in the shielding gas. This flux is not present in the solid wire.

### 7.3.1 Solid Wire

Figure 7-4 shows the hardness scan from 2 fillets welded with a solid wire electrode varying the shielding gas flow rate from 12l/min to 6l/min. The hardness scan results highlight that there was no significant change to the hardness of the solid wire fillet welded joint by reducing the shielding gas flow rate. However, as the shielding gas flow rate was reduced to 6l/min, the quality and stability of the welding process dropped off considerably, as can be seen from Figure 7-5. Figure 7-6 shows the variation in microstructure of the welded area as the shielding gas flow is reduced from 12l/min to 6l/min. These images highlight that there is a distinct visual difference between the two microstructures.

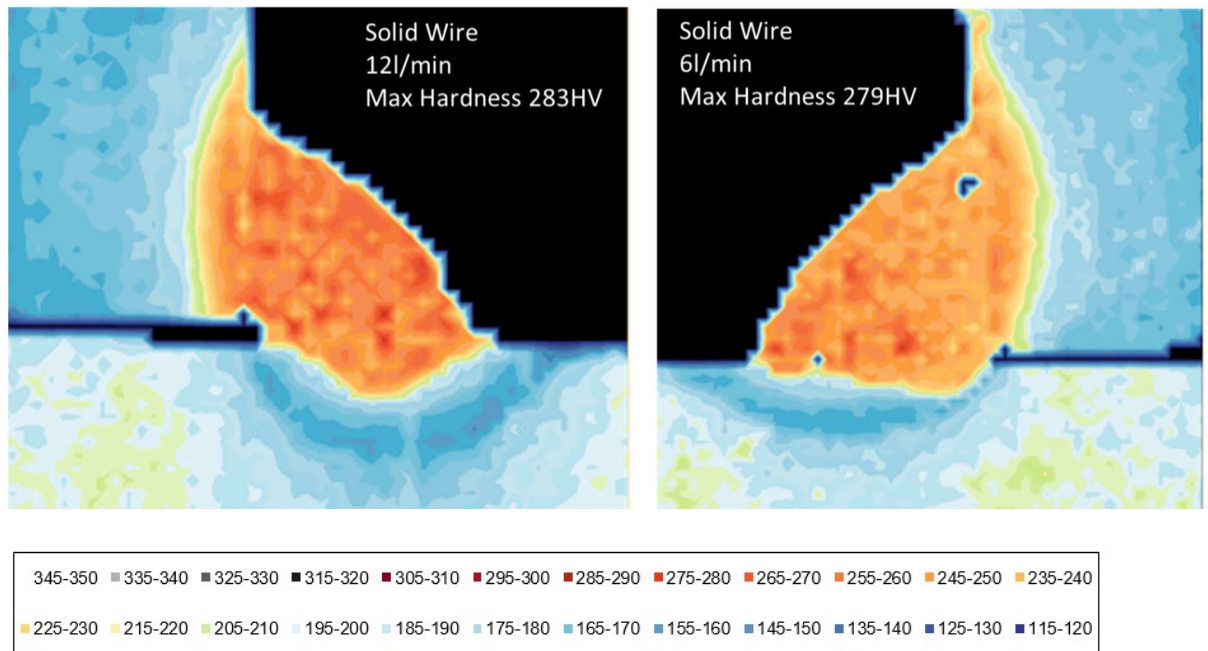


Figure 7-4 Hardness Scans of solid wire welds at 12l/min & 6l/min gas flow rates

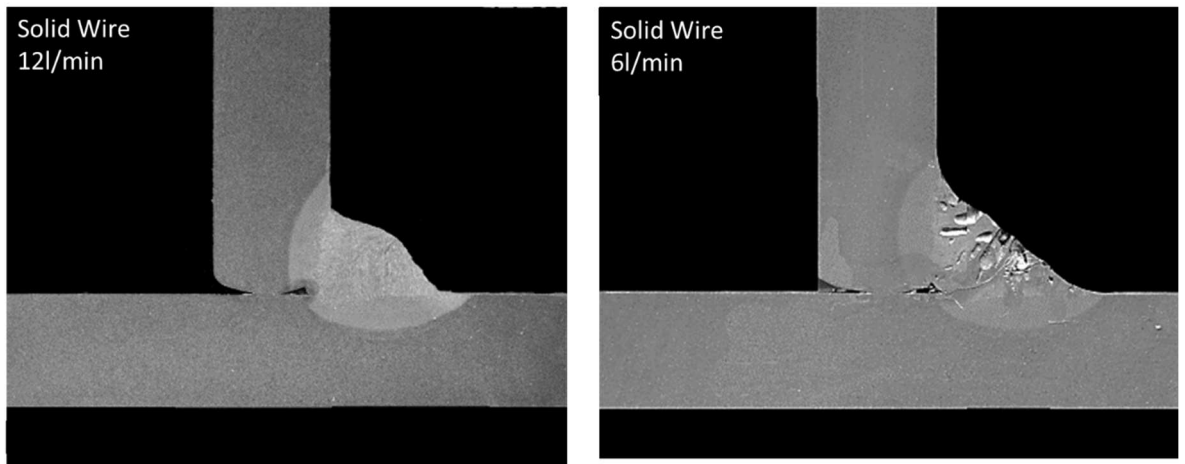


Figure 7-5 Macro of acceptable solid wire fillet weld at 12l/min and unacceptable fillet weld at 6l/min gas flow rate.

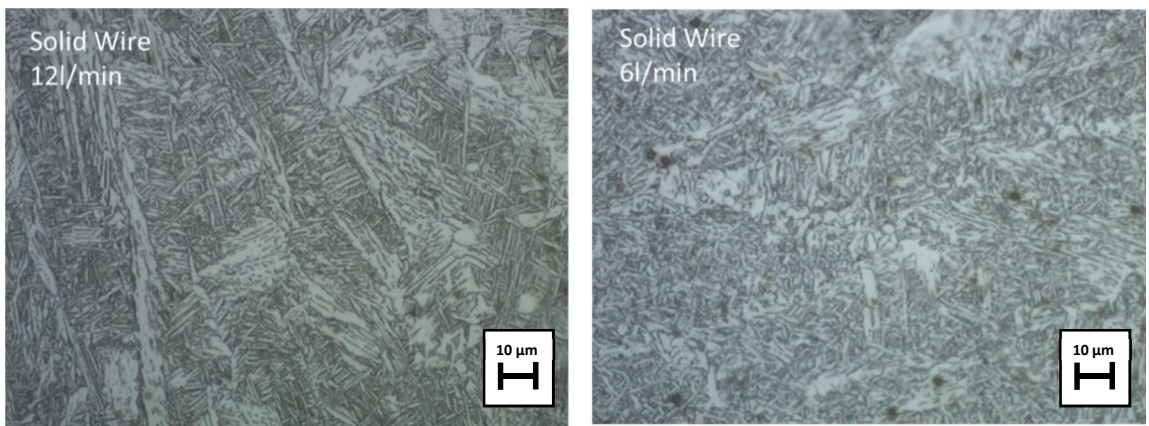


Figure 7-6 Microstructure Image of solid wire welds at 12l/min & 6l/min gas flow rates

### 7.3.2 Flux Cored Wire

Figure 7-7 shows the hardness scan from 2 fillets welded with a flux cored electrode varying the shielding gas flow rate from 12l/min to 3l/min. Figure 7-9 shows the variation in microstructure of the welded area of the same 2 welds. Both figures highlight that there appears to be no significant change to the hardness and microstructure of the resultant fillet weld, as a consequence of reducing the shielding gas flow rate to 3l/min.

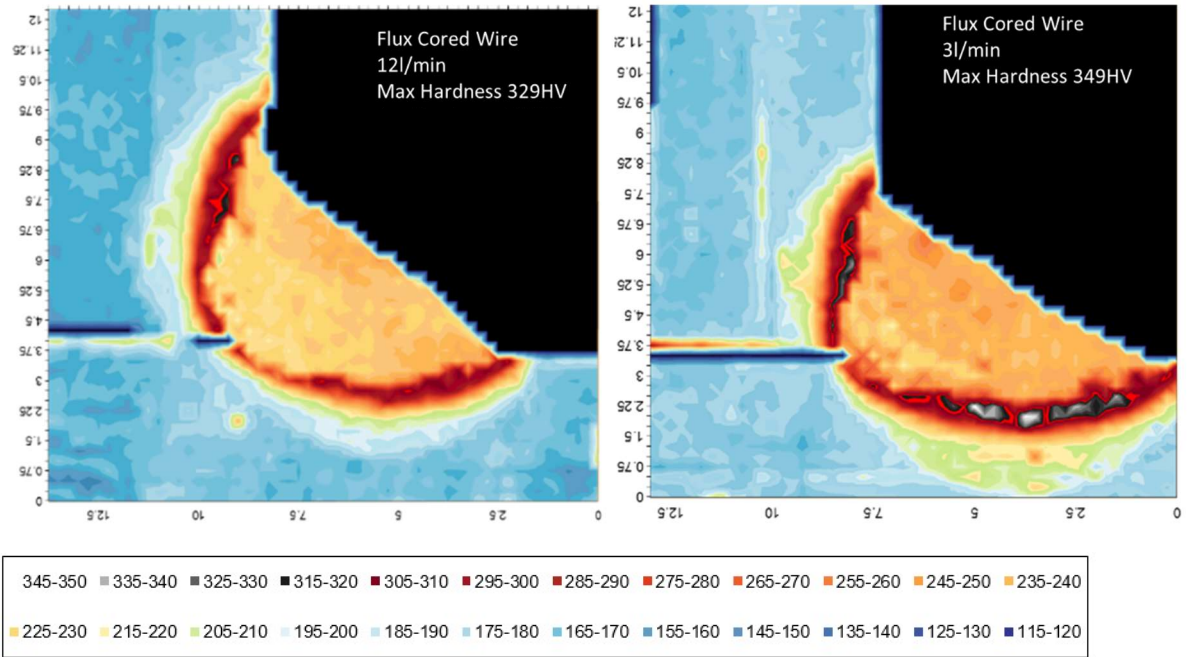


Figure 7-7 Hardness Scans of flux core wire welds at 12l/min & 3l/min gas flow rates

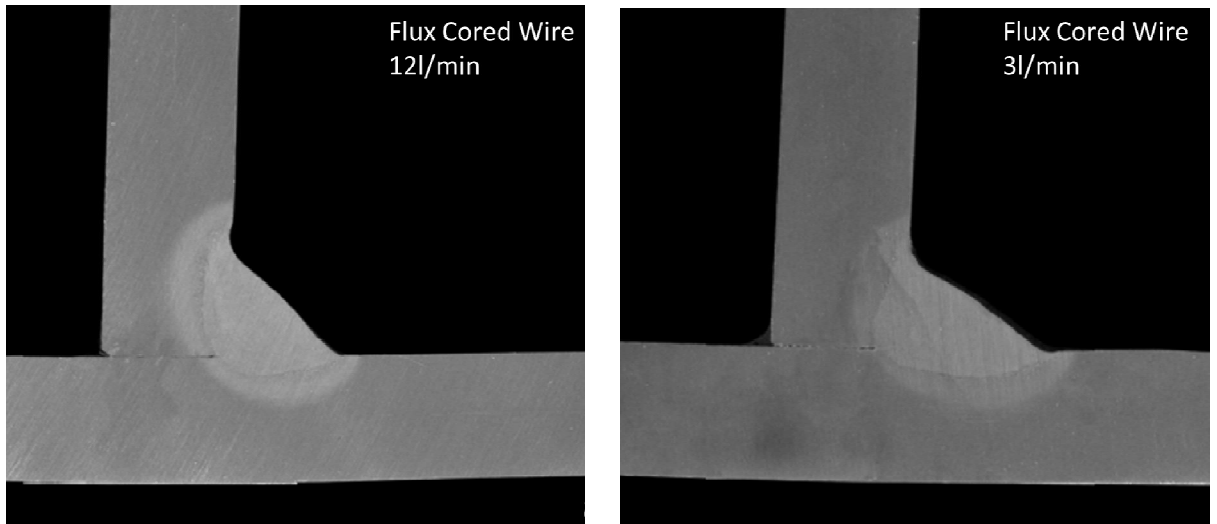


Figure 7-8 Macro image of flux cored wire welds at 12l/min & 3l/min gas flow rates



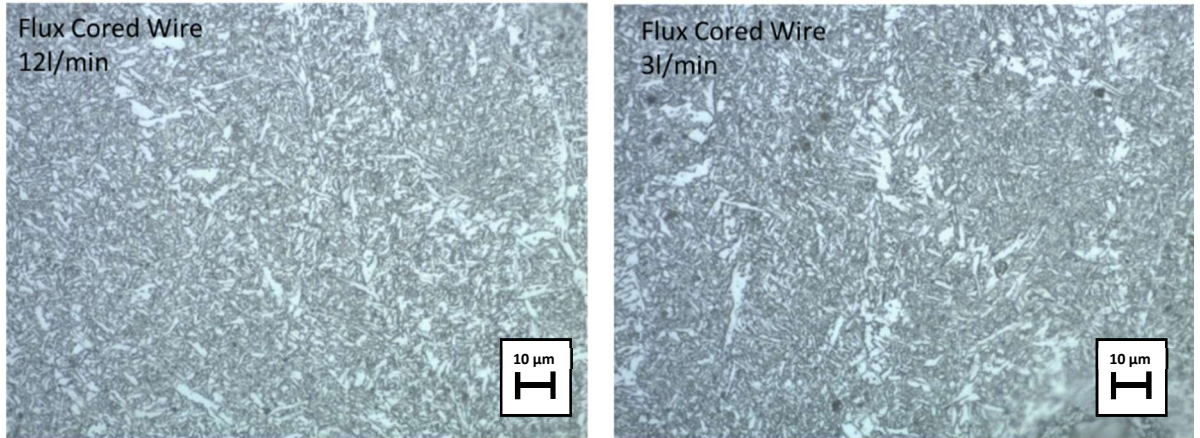


Figure 7-9 Microstructure Image of flux cored wire welds at 12l/min & 3l/min gas flow rates

#### 7.4 Travel angle impact on shielding gas flow

The Schlieren set up was also used to compare the behaviour of the gas flow when the torch was being pushed vs being pulled. The results of which can be summarised in Figure 7-10.

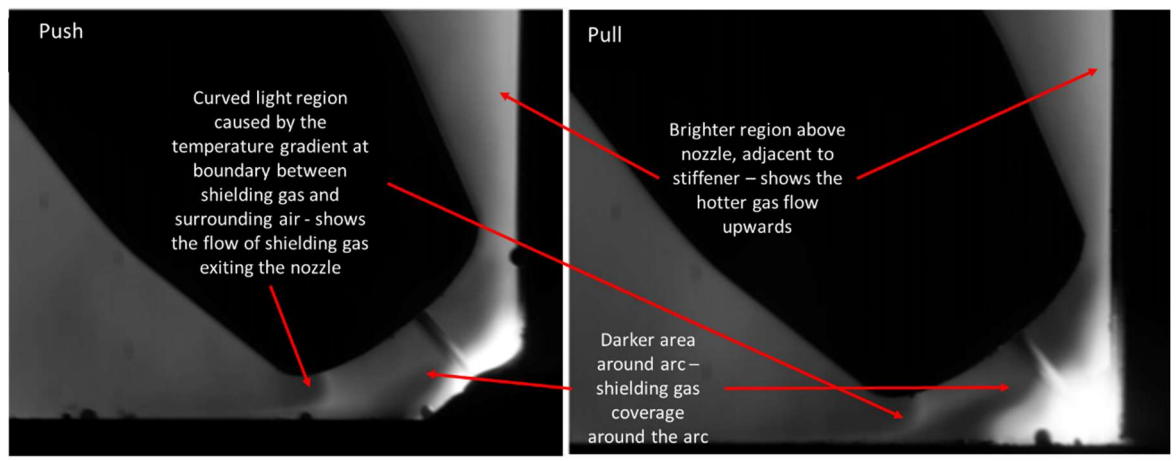


Figure 7-10 Visualisation of shielding gas flow for pushing and pulling travel angles [7.1]

The results [Figure 7-10] [7.1] appear to show that the gas flow behaved in a similar way regardless of whether the torch was being pushed or pulled. For both torch orientations there was clearly defined boundary between the shielding gas exiting the nozzle and surrounding air. There is also a 'dark area' around the arc showing the coverage of the shielding gas and also a brighter area above the nozzle showing the faster upwards flow of gas, parallel to the stiffener (similar to Figure 7-1). Consequently there appears to be no change to overall shielding coverage provided to the weld as a consequence of changing between a pushing and pulling torch orientation. However, during the experiments it was observed that the process appeared to be less stable when the torch was being pushed, especially at lower gas flow rates. This was due to the increased level of spatter and the increased frequency of wire bursts as could be seen on the Schlieren videos. However, this instability did not appear to have an overall impact on the quality of welds being produced. This does suggest that the travel angle and gas flow do have a practical impact on the stability of the process. In order to maintain a stable process, the preference would be to set the torch up in a 'pulling' orientation. Although there were no major differences in the gas flow observed as a result of the travel angle, the 3D Model did identify a difference to the way the temperature was distributed on the workpiece. Figure 7-11 [7.1] shows the temperature distribution on a fillet workpiece for pushing and pulling travel angles. This figure shows that the profile of temperature distribution changes depending on whether the torch is pushing or pulling. When the torch is pushing, the temperature profile is skewed towards the direction of travel, but when the torch is pulling the temperature profile is more symmetrical. This would imply that there may be a slightly sharper temperature gradient, behind the arc, when the torch is pulling. For both pulling and pushing the pattern is mirrored on the baseplate and stiffener. Overall heat applied in both the pulling and pushing orientation was kept constant.



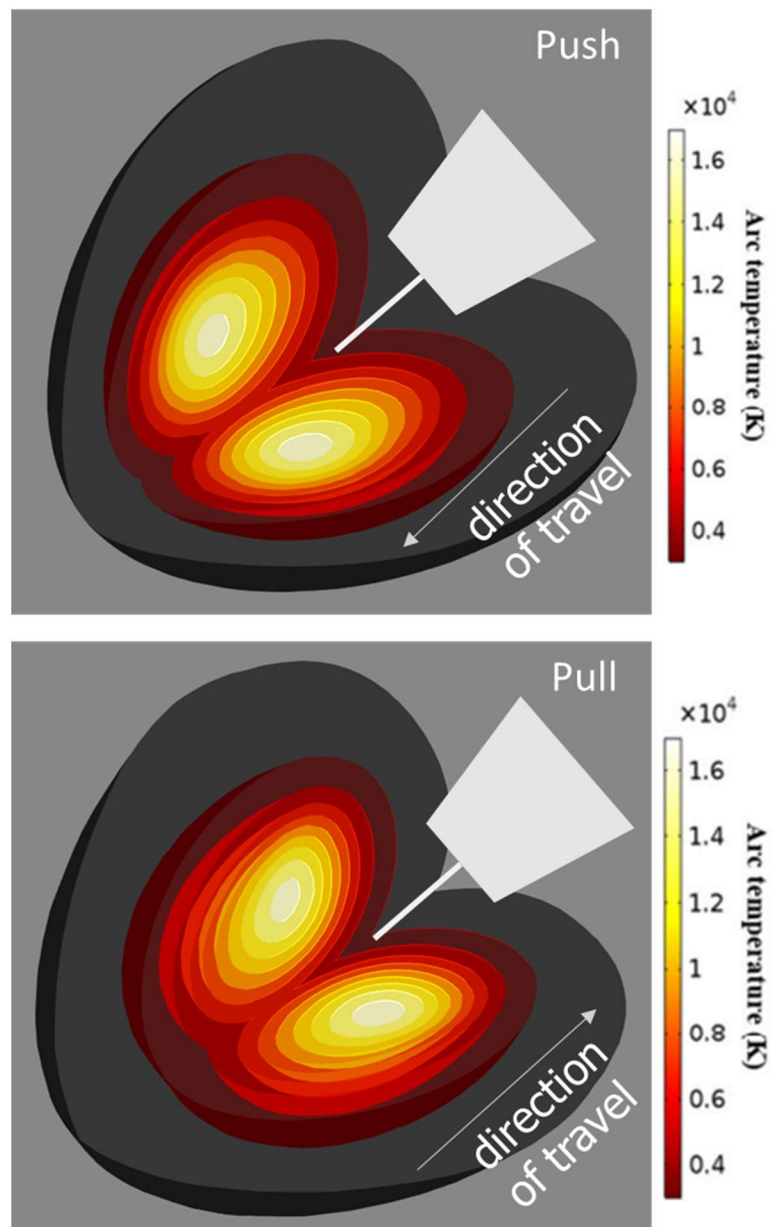


Figure 7-11 Temperature profile on workpiece for pushing and pulling travel angles [7.1]

## 7.5 Shielding Gas - Discussion

### 7.5.1 General Gas Flow Observations

As mentioned in Chapter 2, there has been limited research carried out on the shielding gas visualisation of a fillet weld and what impact the gas flow rate has on the resultant weld shape. The following section will discuss the results of the gas flow visualisation experiments that were conducted in order to understand the behaviour of the shielding gas around a fillet weld. This work was carried out in collaboration with Bitharis [7.1]. The shipyard [BAE Systems] had until around 2012 used a standard shielding gas flow rate of around 18-20l/min. Following research conducted by Beyer et al [7.2], the flow rate was reduced to 12l/min with no impact to the weld quality. However, previous studies into the behaviour of the shielding gas during welding have focused on down-hand/butt welding configurations. This provoked the theory that the presence of a horizontal stiffener/bar in a fillet weld configuration would alter the flow of the shielding gas around the welded joint, potentially allowing the shielding gas flow to be reduced further without compromising the quality of the resultant weld.

The Schlieren (visualisation) experiments, as described in Chapter 3.5, were conducted using both solid and flux core wire. Solid wire samples were used to compare results with a 3D Comsol model [7.1] that had previously been developed to analyse the gas visualisation for bead on plate and butt welds. Further flux cored samples were used in order to provide a direct comparison with the shipyard's current set up. The Schlieren videos provided a clear visualisation of how the shielding gas flows around the torch and the steel plates during the welding process. At 12l/min flow rate, the videos show a strong coverage of shielding gas around the weld pool. There is a strong/fast gas flow upwards, parallel to the vertical stiffener. There is also a clear flow of gas along the horizontal baseplate away from the weld pool. This gas flow is visibly not as strong/fast as the vertical flow (weaker visual gradient). There is also an area of turbulence behind the torch nozzle, which again points to the slower gas flow rate along the baseplate. The faster upward flow of gas, parallel to the stiffener can be explained flow observed can be explained, in part, by the fact that warm air rises, thus increasing the upward flow of the shielding gas. This characteristic was evident across the range of gas flows tested from 3l/min up to 15l/min.

The results [Figure 7-3] showed that decreasing the shielding gas flow rate has almost no impact on the temperature measured along the baseplate and stiffener. Figure 7-3 also shows that by increasing the shielding gas flow rate the convective heat flux also increases, specifically in the area behind the torch on the baseplate. However, as you move quickly away from the arc, the difference between the convective heat fluxes is not as significant. This difference in convective heat flux is also not evident on the edge of the vertical stiffener, where the convective heat flux is almost identical for all gas flow rates. This could be due to the stronger upward flow observed in the Schlieren videos. This stronger flow, caused in part by the buoyancy effect, will minimise the impact of any changes to the gas flow rate. Although figure 7-3 shows that there is a small impact to the convective heat flux around the weld as a result of reducing the flow rate of the shielding gas, figures 7-4 and 7-7 suggest that this causes no significant impact to the material properties of the resultant weld. The main benefits of reducing the shielding gas flow rate will be financially. The cost benefits will be discussed further in Chapter 9. Since there were no changes to temperature of the baseplate and stiffener as a result of changing the shielding gas flow rate there was no need to make any changes to the FEA model to accommodate for changes to the shielding gas flow rate.

#### 7.5.2 Influence of travel angle on gas flow

Earlier in chapter 5 it was identified that the welding travel angle has an impact on the resultant geometry of the fillet weld. The gas visualisation experiments were designed to assess what impact, if any, the welding travel angle had on the behaviour of the shielding gas. The results of the Schlieren experiments indicated that there was no significant change to the behaviour or coverage of the shielding gas as consequence of varying the torch from a pushing to a pulling configuration, as shown in Figure 7-10. The heat input was kept constant across all the experiments and the overall heat affected zone and weld area (Table 7-1) was similar for both pulling and pushing set ups irrespective of the gas flow rate. This suggests that both the travel angle and the gas flow rate do not have a significant impact on the overall heat being transferred from the arc to the welded joint.

### 7.5.3 Influence of gas flow rate on weld quality

The main objectives of the Schlieren/Gas Flow experiments were to assess how the shielding gas behaved around the fillet joint at low flow rates (3-6l/min) and if there was any impact to the quality of the resultant weld. The experiments were split up into 2 batches. The first batch with solid wire, to validate the results of a 3D CFD Model [7.1] and the second batch was conducted with flux cored wire in order to provide a comparison with the welding set up in the shipyard.

#### 7.5.3.1 Solid Wire

Figure 7-4 shows the hardness scans for the fillets welded with a solid wire for 12l/min and 6l/min respectively. The scans show minimal variation in hardness (1.5-3%) between the 12l/min and 6l/min welds suggesting that there is no significant impact to the hardness of the weld as a consequence of reducing the shielding gas flow rate. The hardness measurements were within the acceptable limits as detailed within IACS welding qualification hardness test procedures [7.3]. However, as the shielding gas was reduced to 6l/min, for the solid wire tests, the quality and stability of the process dropped off as can be seen from Fig 7-5. With a shielding gas flow rate of 6l/min the process did not appear to be as flexible to changes in the travel angle as at higher gas flow rates (9l/min - 12l/min), as can be seen from Figure 7-12 below. For solid wire welding, the gas flow coverage at 6l/min does not appear to be sufficient to accommodate for any variations in process set up.

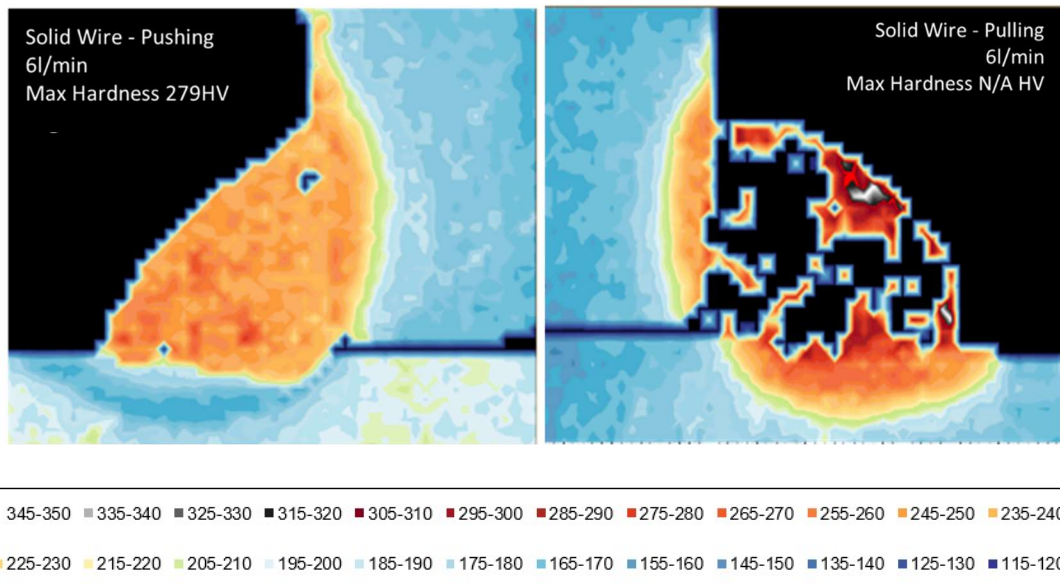


Figure 7-12 Push vs Pull Solid Wire Hardness maps - shielding gas flow rate 6l/min

These results would suggest that for welding fillets with a solid wire electrode the shielding gas flow rate could not be reduced lower than 9l/min. These experiments were conducted in laboratory conditions and did not take into consideration any variation in cross drafts that would be present in a production environment. However, the evidence suggests that there is significant scope to reduce the shielding gas flow rate for fillet welds.

### 7.5.3.2 Flux Cored Wire

Figure 7-7 shows the hardness scans for the fillets welded with a flux cored wire for 12l/min and 3l/min respectively. The scans show minimal variation in hardness (1.5-5.5%) between the 12l/min and 3l/min welds suggesting that there is no significant impact to the hardness of the weld, as a consequence of reducing the shielding gas flow rate. Again, the measured results were within the acceptable limit defined by IACS [7.3]. Figure 7-9 displays the microstructure of the flux cored fillet welds at 12l/min and 3l/min. The results from Figure 7-7, 7-8 and 7-9 show that it was possible to reduce shielding gas flow rate down to 3l/min for flux cored welds without compromising the quality of the weld or significantly impacting the resultant metallurgical microstructure of the joint. The impact of the travel angle seemed to be insignificant for the flux cored welds as the results were comparable when

the torch was set up for both a pulling and pushing configuration. It would appear that the additional shielding provided by the breakdown of the flux within the electrode compensates for the reduction in shielding gas flow rate. This would explain why the shielding gas flow rate can be reduced to 3l/min without compromising the quality or altering the microstructure of the resultant fillet weld.

The hardness results from the flux cored wire experiments [Fig 7-7] identified a 'harder' area in the heat affected zone, around the perimeter of the weld. This region was not present when using solid [Figure 7-4] or even metal cored [Figure 5-25] wire electrodes and so appears to be a feature of using the flux cored electrode. This border was also present at 12l/min and 3l/min and so does not appear to be a function of gas flow rate. This feature will be discussed further in the chapter 8.

### 7.3 References

- 7.1 Bitharis, I. (2018) 'Visualisation of shielding gas flows during high value manufacture', Engineering Doctorate Thesis, Heriot Watt University, Edinburgh
- 7.2 Beyer, V., Campbell, S. W., Ramsey, G. M., Galloway, A. M., Moore, A. J., & McPherson, N. A. (2013). Systematic study of effect of cross-drafts and nozzle diameter on shield gas coverage in MIG welding. Science and Technology of Welding and Joining. <https://doi.org/10.1179/1362171813Y.0000000143>
- 7.3 International Association of Classification Societies. Requirements concerning Materials and Welding, W28 Welding Procedure qualification tests of steels for hull construction and marine structures. IACS Req. 2005/Rev.2 2012, p.20

## Chapter 8 GMAW Filler wire study

### 8.1 Electrode Experiment Results

This section investigates the impact that varying the type of electrode has on the resultant geometry and metallurgical structure of the fillet weld. The three wire types included within this investigation are:

1. Solid (Carbofil 1)
2. Flux Cored Wire (SF-1A)
3. Metal Cored Wire (MC-1)

The chemical composition of the wires is shown in table 3-6. It is generally understood that Metal Cored wires, although more expensive than the equivalent Solid or Flux Cored wire, enable a higher deposition rate, provide a high deposition efficiency and produce low volumes of slag and this enables higher travel speeds to be achieved. This higher efficiency and travel speed support their use in robotic welding (Automated) processes and offsets the higher material cost. It is also difficult to maintain high travel speeds during manual welding. Solid Wires tend to have a high deposition rate and high deposition efficiency (>95%). Flux core wires tend to operate at a lower deposition efficiency (~85%), due to the creation of slag and losses to spatter and fumes. However, they do provide better penetration, smoother arc transfers and are easier to use than solid wires. The test pieces for this experiment were welded using the Strathclyde University Test Rig and the hardness results were obtained using the methods described in Chapter 3.6.2. The parameters used during the experiments are detailed in Tables 8-1 and 8-2.



Table 8-1 Parameters kept constant during experiments

Gun angle	Travel angle	Wire Feed Speed	Gas Flow Rate	Nozzle Diameter	Arc Energy	Wire Stick Out	Material
45°	30°	~10m/min	12l/min	16mm	0.75kJ/mm	15mm	DH36 6mm Carbon Steel Plate

Table 8-2 Experimental input settings used for each electrodes

Electrode	Wire Diameter	Shielding Gas	Current	Voltage	Travel Speed
Solid Wire – Carbofil 1	1.2mm	Argon	180A	27V	6.5mm/s
SF 1A	1.2mm	Argoshield (20% CO <sub>2</sub> )	235A	28.5V	9mm/s
MC1	1.0mm	Argoshield (20% CO <sub>2</sub> )	220A	21V	6.17mm/s

The solid wire was chosen because it allowed the results to be related back to a Computational Fluid Dynamic (CFD) model developed by Bitharis et al [8.1]. The solid wire results were also used as a baseline from which the flux core and metal core wire results could be compared. The flux core wire configuration was chosen as it closely reflected the current GMAW production process used within the shipyard and the metal core configuration was chosen as this is the wire of interest with regards to increasing travel speeds and moving towards automation.

### 8.1.1 Results – Impact of Electrode on Hardness

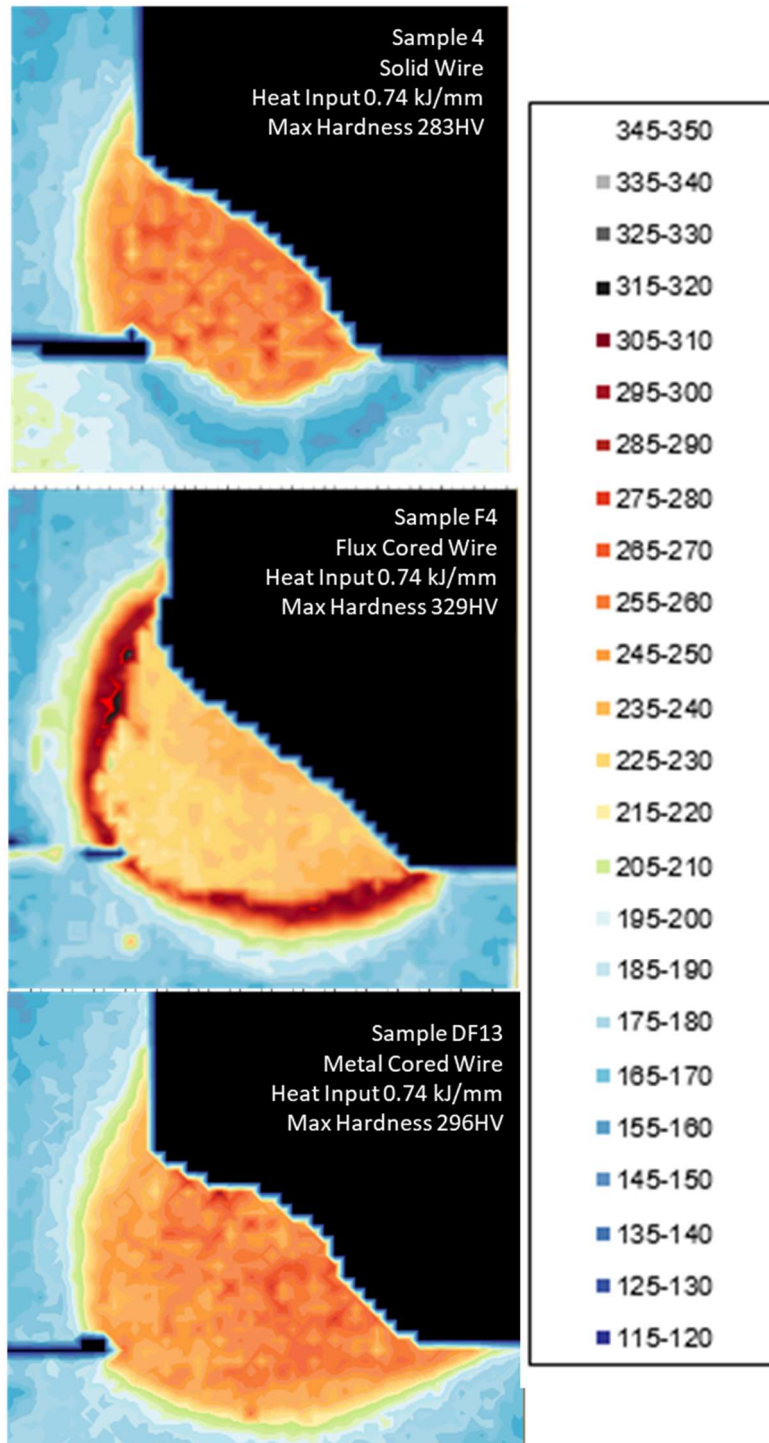


Figure 8-1 Hardness Maps for Solid, Flux Cored and Metal Cored Wire welds

Figure 8-1 indicates that there is a border along the interface between the weld and base material for the samples welded with the flux cored wire which is harder than the average measured hardness of the weld. There was no similar border evident on the solid and metal cored samples. There was very little difference between the average hardness across the face of the flux cored and solid wire samples. However, the maximum hardness on the flux cored samples was approximately 20% higher than maximum hardness found on the solid wire samples.

#### 8.1.2 Results – Impact of Electrode on Metallurgical Structure

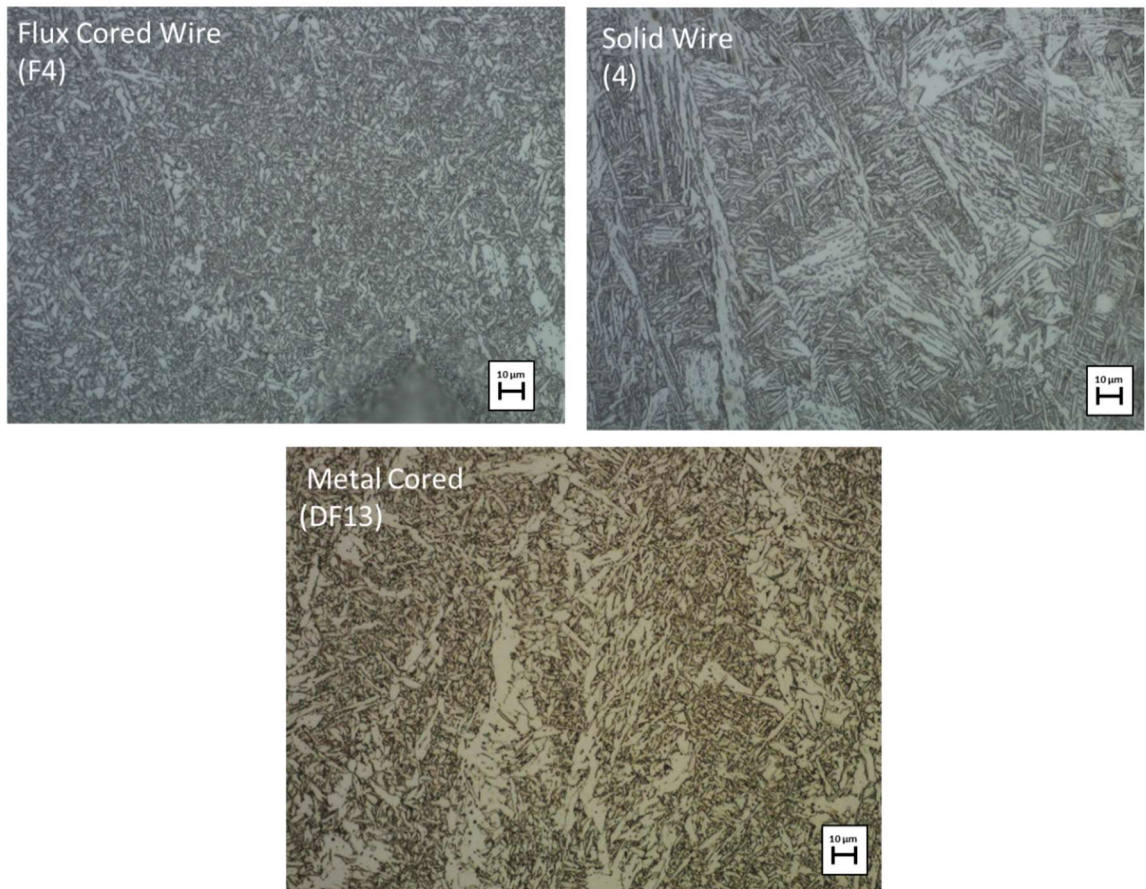


Figure 8-2 Microstructure of Weld Area using different electrodes

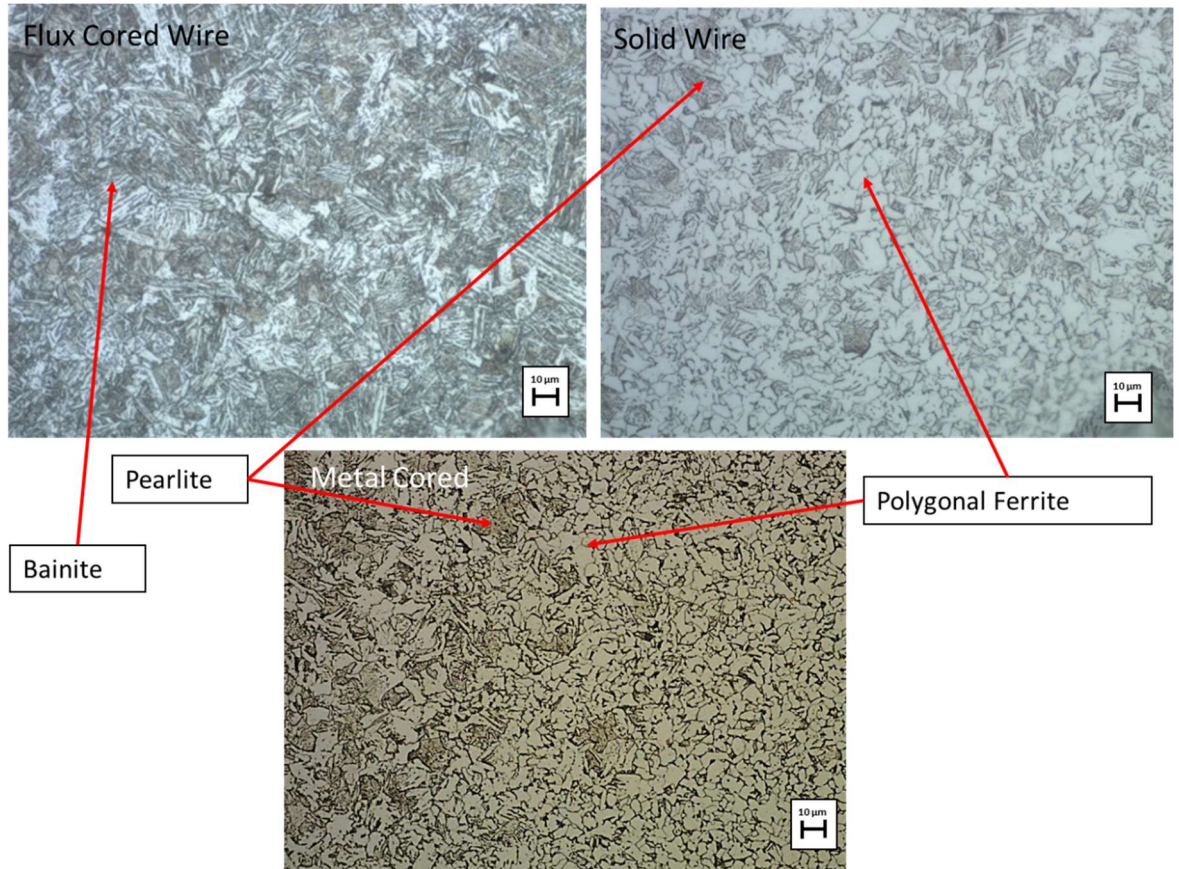


Figure 8-3 Microstructure of Heat Affected Zone using different electrodes

The results shown in Figure 8-2 were taken from the centre of the fillet weld to provide a good comparison between samples. The heat affected zone covers a relatively large area and the microstructure within the HAZ changes as you move from the weld area towards the unaffected area of the parent material. This makes it difficult to obtain directly comparable images between the samples. For the results in Figure 8-3 the images were taken as close to the boundary between the weld and the steel baseplate (parent material) as possible as shown in Figure 8-4



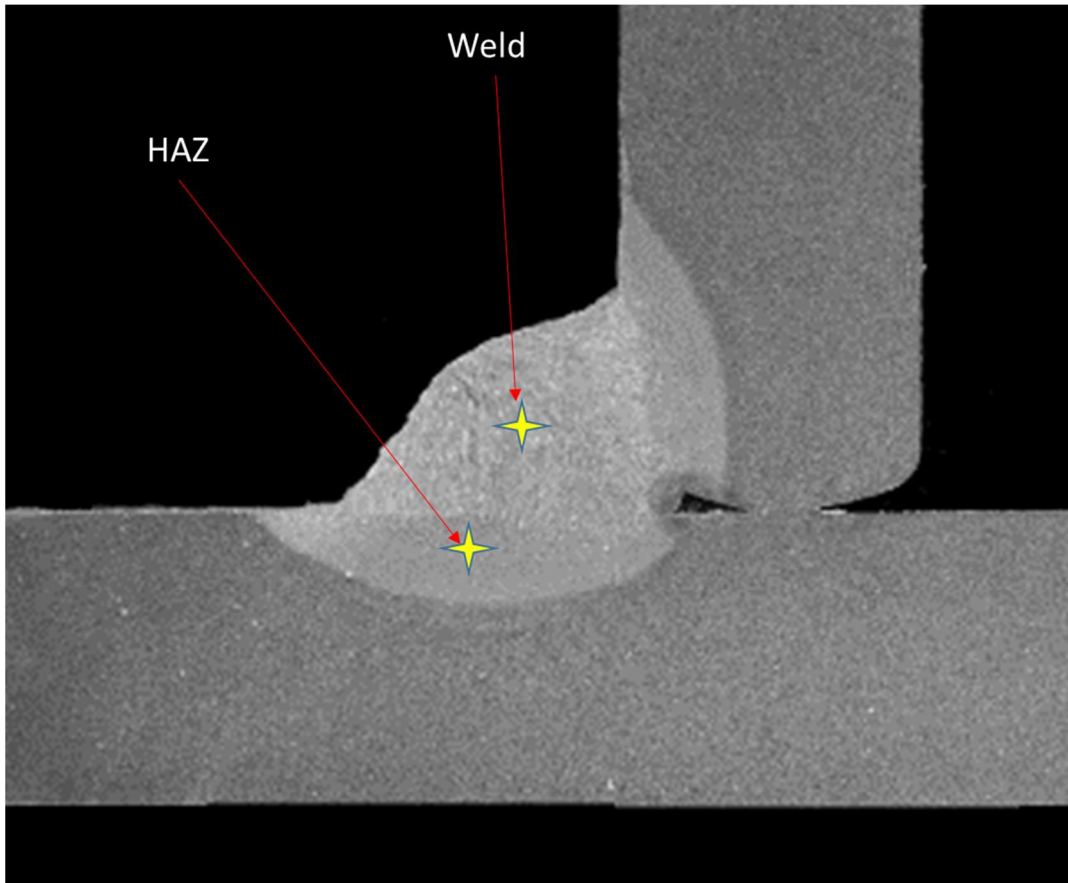


Figure 8-4 Locations of microstructure images

## 8.2 Electrode

### 8.2.1 Heat Affected Zone

All samples identified in Figure 8-1 were comfortably within the acceptable limit defined by IACS [8.2]. The maximum hardness of the flux cored sample was 10%-14% higher than the metal core and solid wire samples. As highlighted previously in section 8.1, there is a 'harder' border around the welded area in the flux cored wire sample. Figure 8-1 shows that this feature seems to be unique to the flux core wire as it does not appear on either the solid or metal core wire samples. This higher level of hardness, in the flux core sample, appears to be largely as a consequence of this 'harder' border. Further assessment of the HAZ area for the 3 samples is shown in Figure 8-3. These results show that the HAZ area of both the metal core and solid wire contains a significant amount of 'softer' polygonal ferrite, whereas the flux cored sample contains no polygonal ferrite and is predominantly bainitic. This supports the hardness scans which show the HAZ area for the flux cored samples to be significantly harder than the metal core and solid wire samples. The current and voltage settings used for the flux cored experiment were higher than the solid and metal cored experiments. However, they were welded at a higher travel speed in order to keep the overall heat input constant and comparable between experiments. The flux cored sample also used Argoshield shield gas which contains 20% CO<sub>2</sub>, whereas the Solid wire samples were welded with pure Argon as the shield gas. CO<sub>2</sub> has a significantly higher specific heat capacity and thermal conductivity compared to Argon [8.3], which leads to a higher cooling effect for the CO<sub>2</sub>. The arc temperature for an argon mixture shielding gas is also significantly higher than an arc under pure argon shielding gas [8.3]. These characteristic differences could explain the 'harder' heat affected zone in the flux cored welds welded with the argoshield gas. With the gas burning at a higher temperature and the torch moving at a faster travel speed then there will be a quicker cooling rate, compared to the solid and metal core samples, resulting in a harder heat affected zone. The 3 wires also have different chemical compositions, as shown in table 3-6, which will also help to explain the variation in microstructure and hardness shown in Figures 8-1 and 8-2.

### 8.2.2 Weld Area

Figure 8-1 shows the hardness maps for fillet samples welded with solid, flux cored and metal cored wire electrodes. The maps show that the maximum hardness of the weld area of the solid and metal cored wires is approximately 33-46 HV harder than the welded area of the flux cored sample. Figure 8-2 provides a closer inspection of the microstructure of these samples. The flux cored sample shows a high level of acicular ferrite. The solid wire sample indicates a mixture of acicular ferrite, allotriomorphic ferrite and Widmanstätten ferrite. The metal core sample shows a mixture of allotriomorphic ferrite and acicular ferrite. As discussed previously, a different set of input parameters (current, voltage and travel speed) was used for each of the samples in order to maintain a constant heat input across the experiments whilst maintaining a stable process and good quality weld. These samples do not necessarily represent the optimal welding conditions for each wire type. The aim was to identify a common heat input so as to allow a level of comparison between the three samples. The difference in microstructure of these samples can be attributed to the differences of input parameters used for each sample. The flux cored wire experiments were ran at a higher travel speed, voltage and current, whereas the metal core and solid wire experiments were ran at a lower more comparable travel speed. This could explain why the hardness results and microstructure for the metal cored and solid wires tests are similar.

### 8.3 References

- 8.1 Bitharis, I. (2018) 'Visualisation of shielding gas flows during high value manufacture', Engineering Doctorate Thesis, Heriot Watt University, Edinburgh
- 8.2 International Association of Classification Societies. Requirements concerning Materials and Welding, W28 Welding Procedure qualification tests of steels for hull construction and marine structures. IACS Req. 2005/Rev.2 2012, p.20
- 8.3 Lohse, M., Trautmann, M., Fussel, U., Rose, S. (2020) 'Influence of the CO<sub>2</sub> content in shielding gas on the temperature of the shielding gas nozzle during GMAW welding'. J. Manuf. Mater. Process. 2020, 4, 113; doi:10.3390/jmmp4040113

# Chapter 9 GMAW Fillet Weld Process Cost Analysis

## 9.1 Fillet Weld Cost Model

### 9.1.1 Cost Model Development

A cost model was developed to predict the welding cost per metre. Only the elements which are impacted by altering the welding parameters have been considered. As a result, the equipment costs have not been included. The model was split into 4 elements:

1. Labour
2. Energy
3. Shielding Gas
4. Electrode (Wire)

The labour cost used was the shipyard average production hourly rate (£/hr). The energy cost was obtained by calculating the heat input/hr, using process input parameters (current, voltage and travel speed) and multiplying by a unit cost for electricity. The shielding gas cost was calculated by obtaining the unit costs/litre for Argoshield (Argon and Carbon Dioxide) from the shipyard's gas supplier and multiplying by the gas flowrate/min. Finally, the electrode (wire) costs were calculated by obtaining the cost of the wire (£/m) from the supplier and dividing by the wire feed speed (m/min) process setting. The graph below shows the approximate cost breakdown of the GMAW Fillet Welding process at BAE Systems Naval Ships. A wastage assumption of 10% has been made in the development of this model. One of the hidden costs of welding structural assemblies is the cost of rework associated with distortion. The cost of distortion rectification has not been included within these figures but will be discussed later on in section 9.2.

Table 9-1 Comparison of GMAW Welding Cost breakdown %

Cost Element	Study of Shielding Gases for MAG Welding [9.1]	OTC Daihen [9.2]	Esab [9.3]	BAE Naval Ships
Labour	55%	94%	68%	90.9%
Electrode	21%	5%	22%	1.9%
Gas	24%	2%	10%	4.3%
Energy	-	-	-	2.9%



When comparing the figures with [9.1] and [9.3] the % figures for shielding gas, electrode and energy costs seem quite low and the labour cost is much higher. However, on closer inspection this variation is not as unexpected as initially thought. Firstly, the shipyard is owned by a global defence company, which will explain the higher overhead/labour costs. Conversely, the shipyard will benefit from lower material costs due to its ability to procure in bulk and also leverage cost savings through the supply chain. Finally, the shipyard does not procure Argoshield gas direct from the supplier. Argon is procured in bulk and mixed with carbon dioxide on site to create the Argoshield mix. This explains why the unit cost of the shielding gas appears quite low. The figures are however comparable with [9.2].

### % Fillet Weld Cost Breakdown

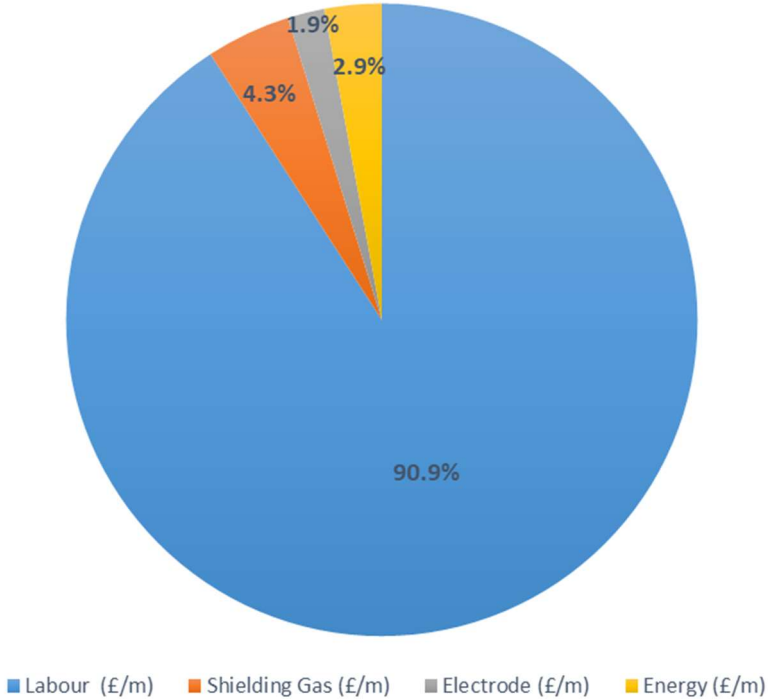


Figure 9-1 Percentage (%) breakdown of Fillet Weld Costs [BAE Systems Naval Ships]

### 9.1.2 Cost Impact of each welding parameter

The cost model was used to identify which of the factors below had the greatest direct impact on the cost of the weld. A set of parameters was selected as a baseline and the welding cost per metre calculated. This was then repeated a further 8 times, changing each parameter individually. For each iteration the parameter being varied was increased by 10% and the resultant welding cost recorded. The results are shown in Figure 9-2 below. As expected, the travel speed and labour costs have the biggest impact on the cost of the weld.

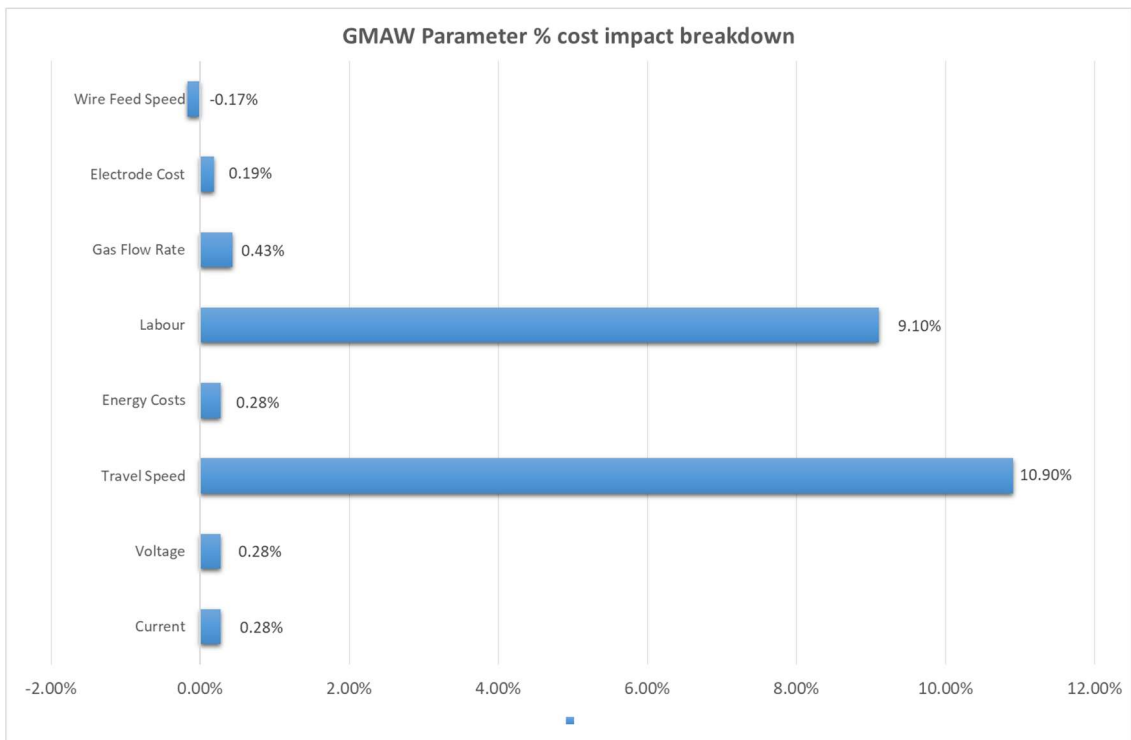


Figure 9-2 % cost impact by varying each parameter individually by 10%

### 9.1.3 Estimating fillet weld cost by leg length

The cost model was also used to assess the cost benefits of maintaining tighter control of fillet weld leg length. Figure 9-3 below shows how the cost of the single run GMAW fillet weld increases as the size of the weld leg length increases. The results indicate that a 70% increase in leg length (277% increase in weld area) results in a 100% increase in welding costs. The range investigated, between 4.5mm and 7.5mm, appeared to show a linear increase in welding costs proportional to the increase in leg length.

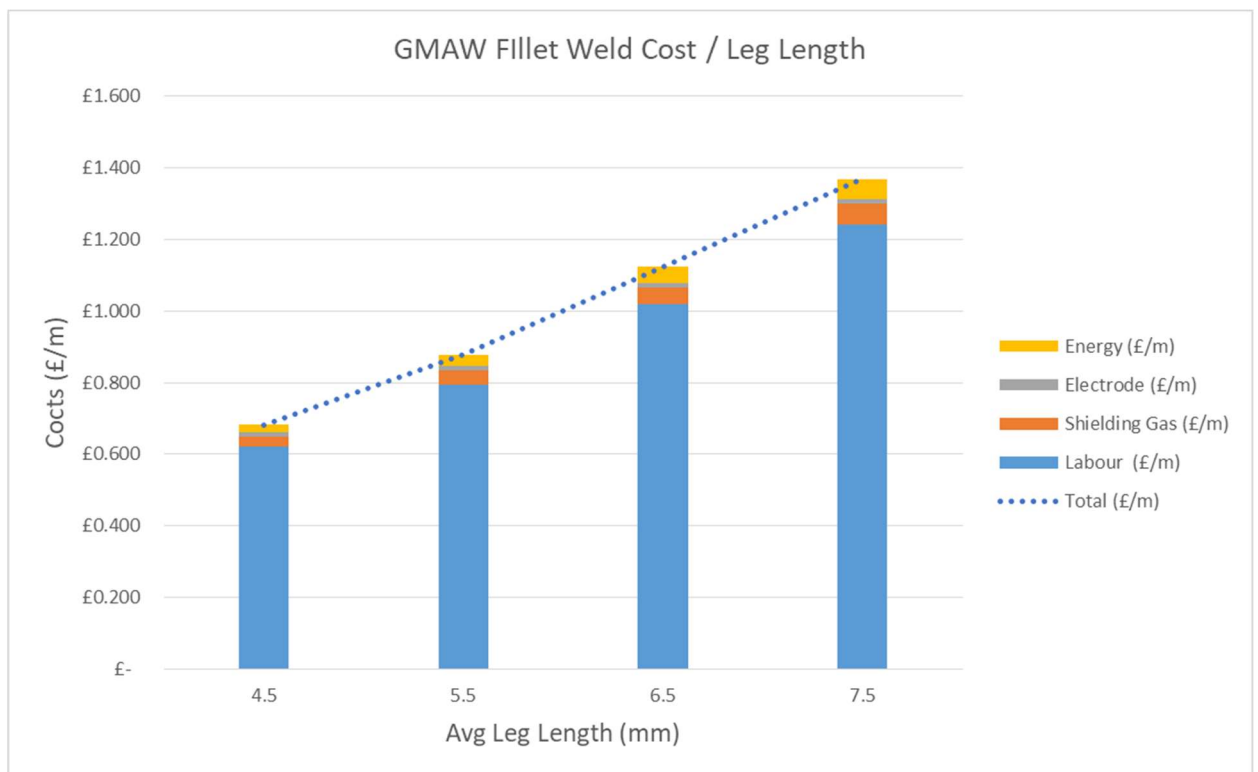


Figure 9-3 Graph showing GMAW fillet weld leg length against process costs

## 9.2 Fillet Weld Cost Modelling - Discussion

As mentioned in Chapter 1, fillet welding accounts for a large percentage of the overall weld volume of a naval ship, and thus represents a significant opportunity for improving the overall efficiency of the shipbuilding process. The previous section [Chapter 9.1] provided the results of the model that was developed to predict the cost (per metre) of a fillet weld by varying the input parameters. Figure 9-1 showed that labour accounts for the majority of the overall cost of a GMAW fillet weld. This is validated in Figure 9-2, in where both the travel speed and the labour were identified as the most significant factors in determining the overall cost of the fillet weld. This is to be expected considering that the overall labour cost will ultimately be dictated by the speed of the process. Figure 9-1 also shows that over 90% of the fillet weld cost at BAE Systems is driven by the labour cost. This contrasts with the study undertaken by Boiko [9.1], who reported the labour to be around 55% of the overall process cost. As mentioned previously, the high percentage attributed to the labour cost would appear to reflect the high level of manual welding currently employed within the shipyard. This suggests that the yard will get more benefit from investing in process improvements aimed at reducing the welding labour cost.

- Increasing levels of automation (enabling improved levels of standardisation and increased weld speeds).
- Increase percentage of robotic friendly panels so that benefits of robotic welding can be maximised.
- Minimise the amount of distortion related rework – rework process is a manual process of heating the panels.

Figure 9-3 shows the process costs by size of fillet weld (leg length). The results show that, for a single sided fillet weld, the cost of the weld is directly related to the size of the fillet weld. The overall percentage breakdown of the costs is also comparable between the 4.5mm and 7.5mm leg length welds. Using the results of the semi-automatic versus robotic fillet welds, Chapter 4, the cost model estimates that by improving the level of control the cost of the fillet weld can be reduced by approximately 30% (not including distortion related rework costs). This figure does not include a further reduction in labour costs that would be delivered through the installation of a robotic welding system.

Current practice in the shipyard is to use the same shielding gas flow rate for both butt and fillet welds. However, the results of the gas visualisation work, detailed earlier on in Chapter 7, highlighted that it is possible to significantly reduce the shielding gas flow rate, specifically for fillet welds, without compromising the quality or metallurgical structure of the welded joint. Reducing the shielding gas consumption provides multiple benefits. Based on the results detailed in Table 9-2 it has been estimated that the shipyard will conservatively save around £90k per annum, by reducing the shielding gas flow rate from 12l/min to 6l/min for welding fillets. As well as cost savings, by reducing the shielding gas flow rate the shipyard will also generate environmental benefits as the reduced consumption will affect the related carbon foot print associated with this area i.e. less carbon dioxide produced and subsequently used , less overall gas requirements means less deliveries.

Table 9-2 Fillet weld shielding gas flow reduction – estimated savings

Approximate annual cost of argon + carbon dioxide gas	<b>£ 380,970.38</b>
Assumed natural losses (10%)	<b>£ 38,097.04</b>
Net usage	<b>£ 342,873.34</b>
Assumed % of fillet welding	<b>80.00%</b>
Actual Cost @ 18l/min	<b>£ 274,298.67</b>
Predicted Cost @ 12l/min (current yard setting)	<b>£ 183,780.11</b>
Predicted Cost @ 9l/min	£ 137,149.34
Predicted Cost @6l/min	£ 93,261.55
Predicted Cost @3l/min	£ 45,716.45
Saving Per Annum @ 9l/min	£ 46,630.77
Saving per annum @ 6l/min	<b>£ 90,518.56</b>
Saving per annum @ 3l/min	£ 137,149.34

As previously discussed in Chapter 1, distortion is one of the main causes of rework in thin structural steel panels. The problem becomes exponentially worse as the thickness of the steel panels reduces below 6mm [9.4]. The cost of distortion has not been included within this analysis. The exact cost of distortion related rework is difficult to estimate due to the following:

- The acceptable level of distortion can vary depending on the location of the panel within the ship and the structural loading on it.
- The root cause of the distortion can be caused by a mixture of design characteristics, condition of supply of raw material and internal production processes (burning and welding).

### 9.3 References

- 9.1 Boiko, I., Avisans, D. (2013). 'Study of shielding gases for MAG welding', *Materials Physics and Mechanics*, vol.16, March 2013, pp126-134.
- 9.2 Welding Cost Analysis. Retrieved April 2, 2019, from <https://www.daihen-usa.com/resources/welding-cost-analysis/>.
- 9.3 MIG Welding Handbook. (n.d.). Retrieved from [http://www.esabna.com/euweb/mig\\_handbook/592mig7\\_1.htm](http://www.esabna.com/euweb/mig_handbook/592mig7_1.htm).
- 9.4 Gray, T., Camilleri, D., & McPherson, N. (2014). Control of Welding Distortion in Thin-Plate Fabrication: Design Support Exploiting Computational Simulation. In *Control of Welding Distortion in Thin-Plate Fabrication: Design Support Exploiting Computational Simulation*. <https://doi.org/10.1533/9780857099327>

## Chapter 10 Conclusions

The main outcome for this research project was to improve understanding of how the input parameters of the GMAW process and their interactions with each other impact the geometry and metallurgical properties of the resultant fillet weld. Figure 10-1 provides a diagrammatic representation of the work detailed within this project, showing how the different studies link together.

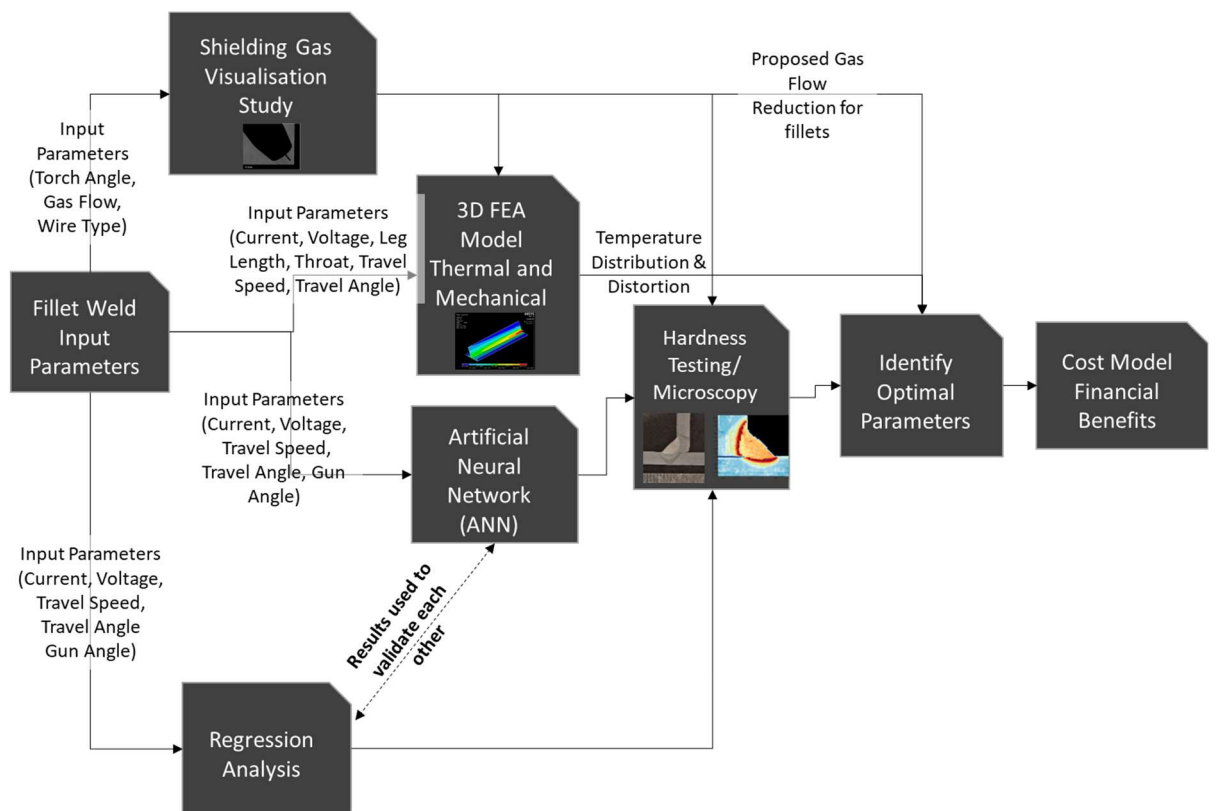


Figure 10-1 Diagrammatic representation of fillet welding project

This study has highlighted, using an ANN Model and validated using a regression analysis, that control of multiple parameters and their interactions is required in order to control and optimise the various geometrical characteristics (penetration, leg length and shape) of the fillet weld. The travel angle was identified as being significant in determining the final weld shape, with a pulling travel angle generating a more rounded fillet weld. The torch travel

angle was also recognised as impacting the level of asymmetry between the vertical and horizontal leg lengths. The weld macrographs which were produced during the experimental work clearly showed that the size of the heat affected zones on the baseplate and stiffener plates were directly related to the size of the leg length of the fillet weld. The FEA model then confirmed that varying the level of leg length asymmetry, within the allowable range as defined by the British Standard, can have a significant variation in the temperature distribution through the fillet welded structure and the corresponding distortion of the baseplate and stiffener. The FEA modelling also suggested that welding the fillet with a larger horizontal leg length generates less overall deflection on the baseplate. The cost model finally confirmed that travel speed was the most significant parameter in determining the overall cost of a GMAW fillet weld. This suggests that efforts to optimise the GMAW process, in the shipyard, should be focused on increasing the travel speed as this will simultaneously reduce both the level of distortion and overall cost of the weld. The shielding gas visualisation study concluded that there is an opportunity to significantly reduce the shielding gas flow rate for fillet welds without compromising the overall quality of the resultant weld. A gas flow rate reduction, from 12l/min to 6l/min, has the potential to generate savings of approximately £90k/annum.

In summary, the results of this study have provided an improved understanding of the main GMAW process parameters. This improved understanding has the potential to generate significant benefits if applied to a robotic welding set up. Creating a more robust process that can be optimised to achieve a target geometry, minimise the heat input and distortion and ultimately minimise the overall cost of the weld. To conclude some of the specific key findings from this study have been summarised below:

- The shielding gas flow rate can be significantly reduced when welding a fillet (theoretically as low as 3l/min when using a flux cored electrode)
- Welding torch orientation – Pushing travel angle provides improved control of leg length variation.
- Fillet Weld Geometry – Aim to have a slightly larger horizontal leg length to reduce the distortion of structure



## Chapter 11 Future Work

Areas of work that should be of interest in the future to enhance the knowledge of the GMAW Fillet Weld Process have been identified from the current study.

### Distortion

A great deal of attention is focussed on thin plate distortion, specifically in naval vessel build. Further investigation in the following areas would help to identify opportunities to minimise the distortion of welded panels.

- Impact of leg length variation on 2 sided fillet welded structures and
- Assessment of optimal fillet welding sequence of transverse and longitudinal stiffeners on a flat panel would allow results to be scaled up and compared with production sized panels.
- Assessment of how variation in ‘fit up gap’ between the baseplate and stiffener impact the distortion of the structure

### Shielding gas

The work included on fillet weld shielding gas visualisation has the scope to be expanded to cover the use of on gun fume extraction, in place of the conventional nozzle type. It is essential to understand how the shielding gas flow rate and the extraction gas flow rate interact to maintain quality at the potentially low flow rates used in this study. In addition, these effects would need to include effects on convective heat flow.

### Paint primer

A current MPhil study [11-1] on the effects of primer thickness on fillet weld geometric quality has just been completed at the University of Strathclyde. It is essential that the data from that study is considered in line with the findings of this work.

### Gap – Fit-up Tolerance

The current work was carried on almost perfect gap set ups. That is not the reality of the situation where gap variations do occur. To improve the understanding of the actual GMAW process an understanding of the impact of variations in the gap on the weld are required in conjunction with the optimum conditions developed from this work. The eventual aim of that study would be to have an on line gap measurement sensor feeding back to the welding process to alter parameters.

### Plate/Bar Prep Tolerance

Variations in bar end shape quality need to be ascertained. Bar end shape can vary from square to radiused. The radiused shape could show up as a large gap to a sensing system, and that situation would have to be considered.

### Pulsed MIG Experiments

All the current work was carried out using standard shipyard processes. However, the use of pulsed GMAW would offer a parallel project to the one carried out.

## 11.1 References

- 7.1 Phipps, R.A. (2020), 'The effect of weldable primer paint thickness on weld quality and geometry', M.Phil. Thesis, University of Strathclyde

## Appendices

### Appendix 1 Publications

1. [Cairns, Jonathan](#) and McPherson, Norman and [Galloway, Alexander](#) and MacPherson, Malcolm and McKechnie, Crawford. (2013) *Optimised penetration for fillet welding*. In: [17th International Conference on Joining Materials, JOM 17](#), 2013-05-05 - 2013-05-08.
2. [Cairns, Jonathan](#) and [McPherson, Norman](#) and [Galloway, Alexander](#) (2015) *Using artificial neural networks to identify and optimise the key parameters affecting geometry of a GMAW fillet weld*. In: [18th International Conference on Joining Materials, JOM-18](#), 2015-04-26 - 2015-04-29, Konventum LO-Skolen.
3. [Cairns, J.W.P.](#) and [McPherson, N.A.](#) and [Galloway, A.M.](#) (2015) *Identification of key GMAW fillet weld parameters and interactions using artificial neural networks*. [Welding and Cutting](#), 15 (1). pp. 51-57. ISSN 1612-3433

## Appendix 2 Weld Procedure Examples

Location: Workshop

Manufacturer's Welding Procedure Specification No: 04p

WPQR: N/A\*

Manufacturer: To be confirmed

Welder's Name: To be confirmed

Welding Process: 135 (MAG)

Joint Type: Fillet Weld - Multi-run (Single or Double Sided)

Method of Preparation and Cleaning:

Thermal cut and / or grinding, wire brush and degrease if required

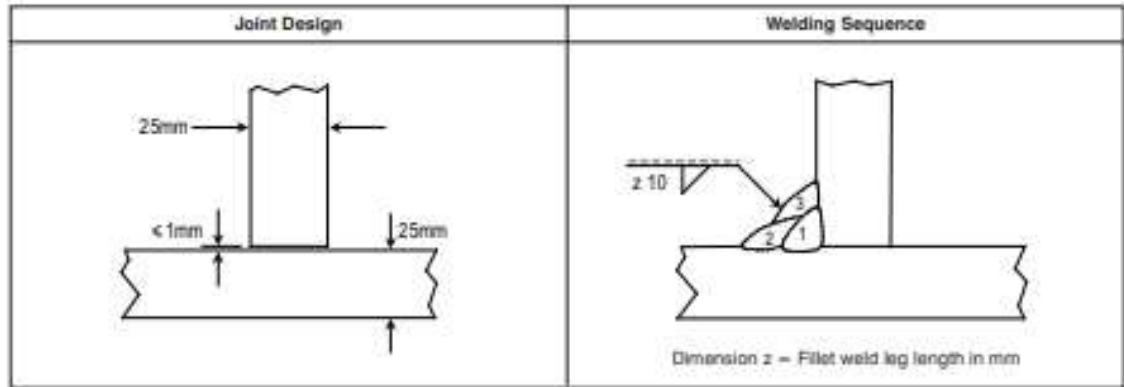
Parent Material Designation:

BS EN 10025-2: S355 J2 (Max CEV = 0,45)

Material Thickness: 25mm

Outside Diameter: N/A

Welding Position: PB (Horizontal - Vertical)



Welding Details:

Run	Process	Size of Filler Metal Ø mm	Current A	Voltage V	Type of Current/ Polarity	Wire Feed m/min	Travel Speed mm/min	Heat Input kJ/mm
1	135 (MAG)	1.2	290 - 310	29 - 31	DC +ve	8.3 - 9.0	300 - 330	1.3 - 1.5
2 - 3	135 (MAG)	1.2	290 - 310	29 - 31	DC +ve	8.3 - 9.0	310 - 330	1.2 - 1.5

Filler Metal Classification & Trade Name

BS EN ISO 14341: G3 Si1 (Trade name to be confirmed)

Any Special Baking or Drying

Stored in accordance with manufacturers recommendations

Gas/Flux: - Shielding / Backing

Argon / 20% CO<sub>2</sub> / 2% O<sub>2</sub>

Shielding Gas Flow Rate

15 - 18 L/min

Tungsten Electrode Type / Size

N/A

Details of Back Gouging / Backing

N/A

Preheat Temperature

0°C Minimum

Interpass Temperature

250°C Maximum

Post-Weld Heat Treatment and / or Ageing

N/A

Time, Temperature, Method

N/A

Heating & Cooling Rates

N/A

Other Information: Nozzle diameter = 16mm.

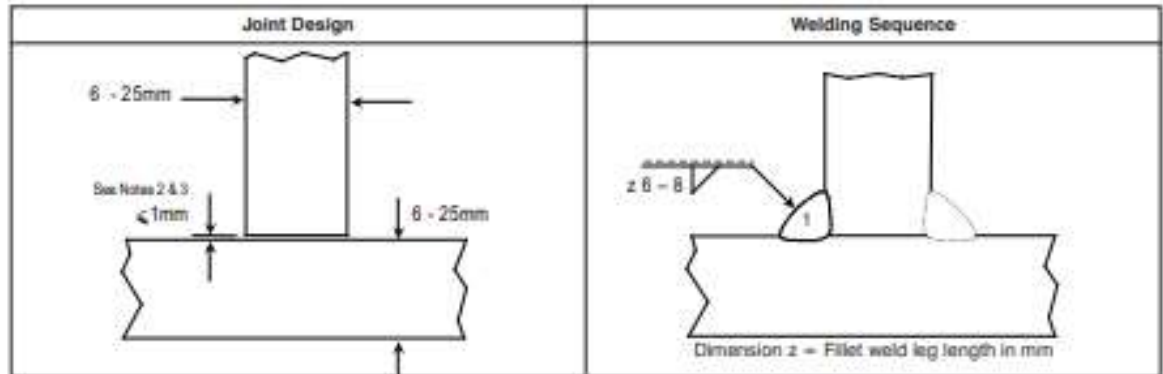
Interpass temperature shall be checked using a contact thermometer or temperature indicating crayon.

Weld finish to be left as-welded.

Location: Workshop  
 Manufacturer's WPS No: 07-PB(a)  
 WPQR: To be confirmed  
 Manufacturer: To be confirmed

Welder's Name: N/A  
 Welding Process: 135 (MAG)  
 Joint Type: Fillet Weld (Single or Double Sided)

**Method of Preparation and Cleaning:**  
 Thermal cut and / or grinding, wire brush and degrease if required  
**Parent Material Designation:**  
 BS EN 10025-2: S275 & S355 -  
 Up to and including sub-grade J2 (Max CEV = 0.45)  
**Material Thickness:** 6 to 25mm  
**Outside Diameter:** N/A  
**Welding Position:** PB (Horizontal / Vertical)

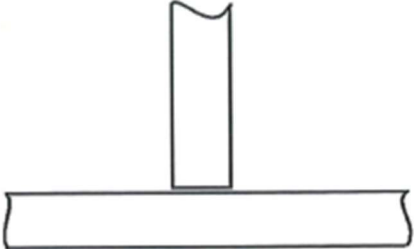
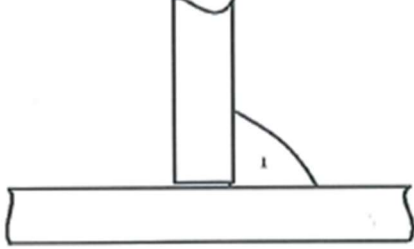


**Welding Details:**

Run	Process	Size of Filler Metal Ø mm	Current A	Voltage V	Type of Current/ Polarity	Wire Feed Speed m/min	Travel Speed mm/min	Heat Input kJ/mm
All	135 (MAG)	1.2	270 - 290	29 - 31	DC +ve	7.5 - 8.0	320 - 340	1.1 - 1.3

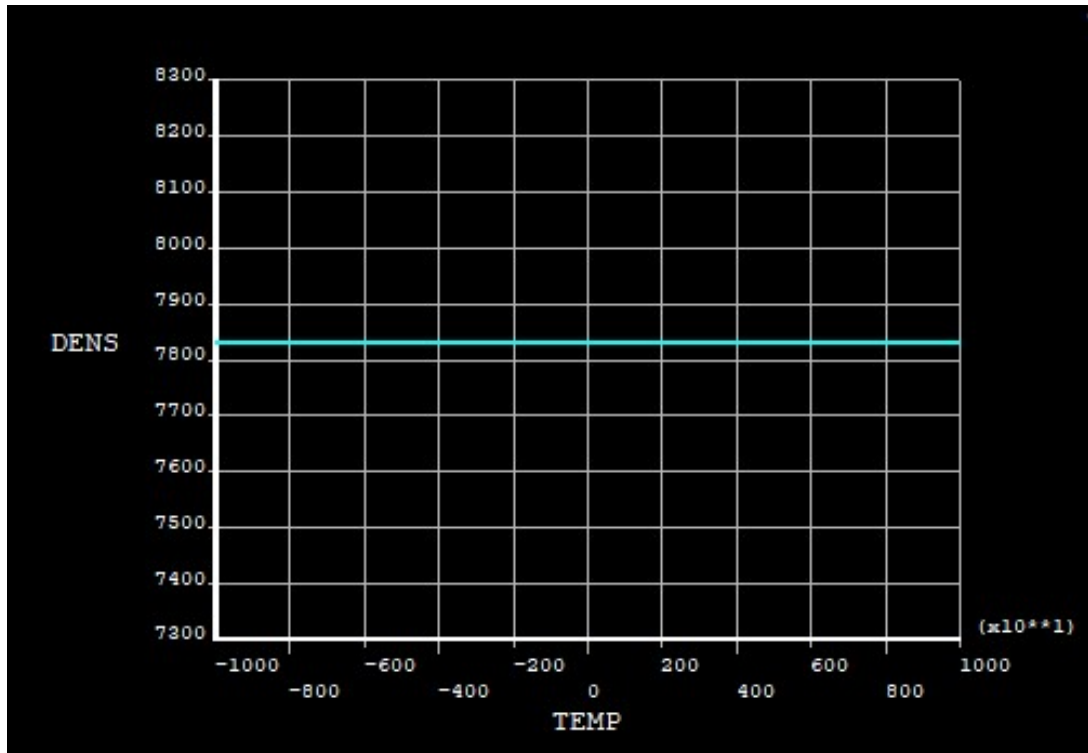
<b>Filler Metal Classification &amp; Trade Name</b>	BS EN ISO 14341: G35H1 (Trade name to be confirmed)
<b>Any Special Baking or Drying</b>	Stored in accordance with manufacturers recommendations
<b>Gas/Flux: - Shielding / Backing</b>	Argon / 20% CO <sub>2</sub> / 2% O <sub>2</sub>
<b>Shielding Gas Flow Rate</b>	15 - 18 L/min
<b>Tungsten Electrode Type / Size</b>	N/A
<b>Details of Back Gouging / Backing</b>	N/A
<b>Preheat Temperature</b>	0°C Minimum (for combined thicknesses up to 75mm)
<b>Interpass Temperature</b>	N/A
<b>Post-Weld Heat Treatment and / or Ageing</b>	N/A
<b>Time, Temperature, Method</b>	N/A
<b>Heating &amp; Cooling Rates</b>	N/A

- Other Information:**
1. Nozzle diameter = 16mm.
  2. In all cases the gap between component parts shall be kept to a minimum.
  3. Should the gap between component parts exceed 1mm, the fillet leg length shall be increased in order to achieve the required design throat thickness. Under no circumstance should the gap between component parts exceed 3mm.
  4. Weld finish to be left as-welded unless specified otherwise.

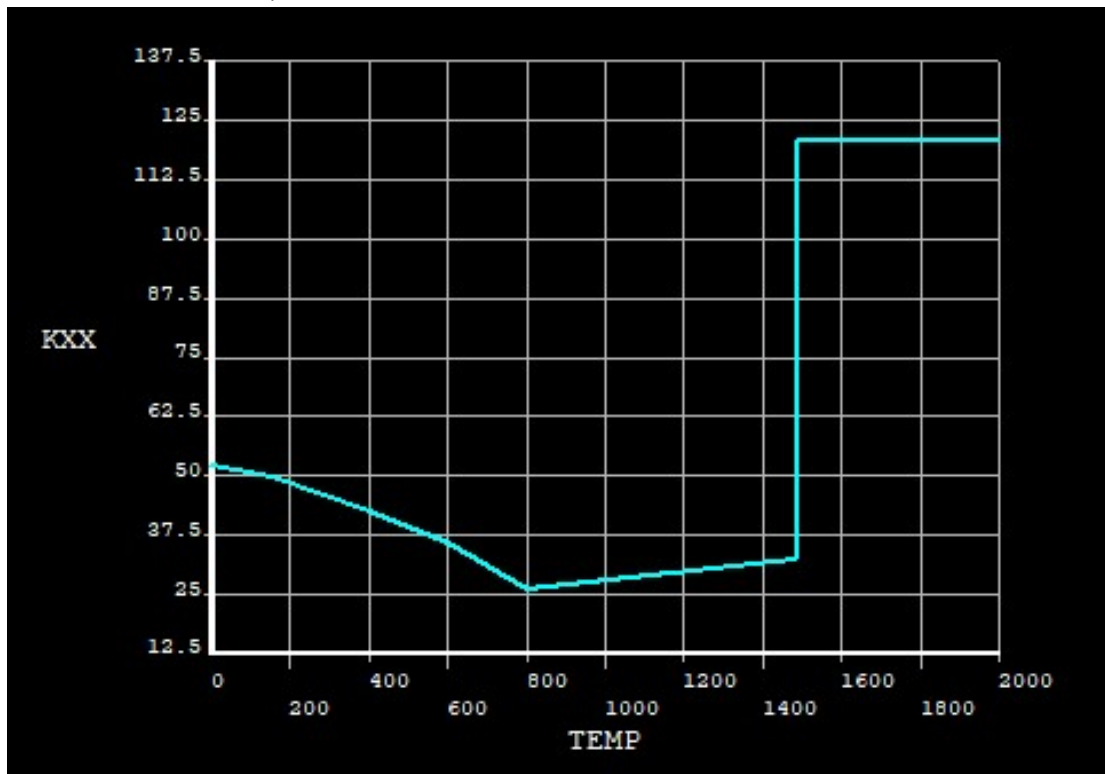
Weld Procedure Specification (WPS)							
BAE Ref.: WPS FCW - CC - 0057				Specification Ref.: BSEN 288 Part 3:1992			
Originator (COPY):				Material dimensions: 350 x 150mm x 20mm			
Classification Society: Lloyds Register				Material specification: DH36			
Test Date: 11/11/1999				Area:			
<b>Joint Geometry</b>				<b>Bead placement</b>			
							
Joint Type :		Fillet Weld		Welders name:		J.Gray	
Polarity:		DC+		Consumables:		Nittetsu SF1A AWS E71T-1	
Interpass Temp :		250 C		Welding Position:		PF	
Gas Shielding :		Argoshield 80/20 mix		Positions qualified:		All (except PG)	
Backing details:		N/A		Welding Process:		FCAW (136)	
Pre-heat details:		N/A		Thickness Range:		9mm - 36mm	
Post Weld treatment:		N/A		Material Range:		Group 1	
PASS No.	Filler dia. (mm)	Amps	Volts	Gas Flow l/min	Travel Speed mm/min	Heat Input KJ/mm	
1	1.2	180-190	23-25	15-18	240-270	1 - 1.2	

## Appendix 3 Finite Element Analysis – Temperature Dependent Material Properties

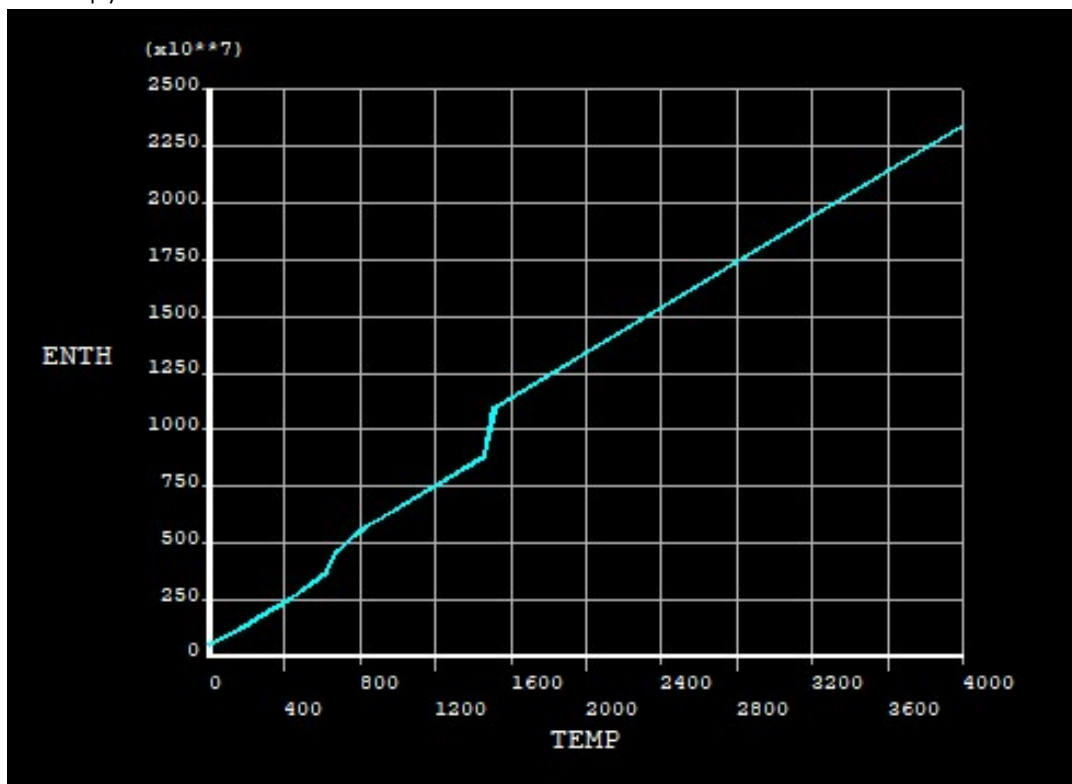
Density



### Thermal Conductivity

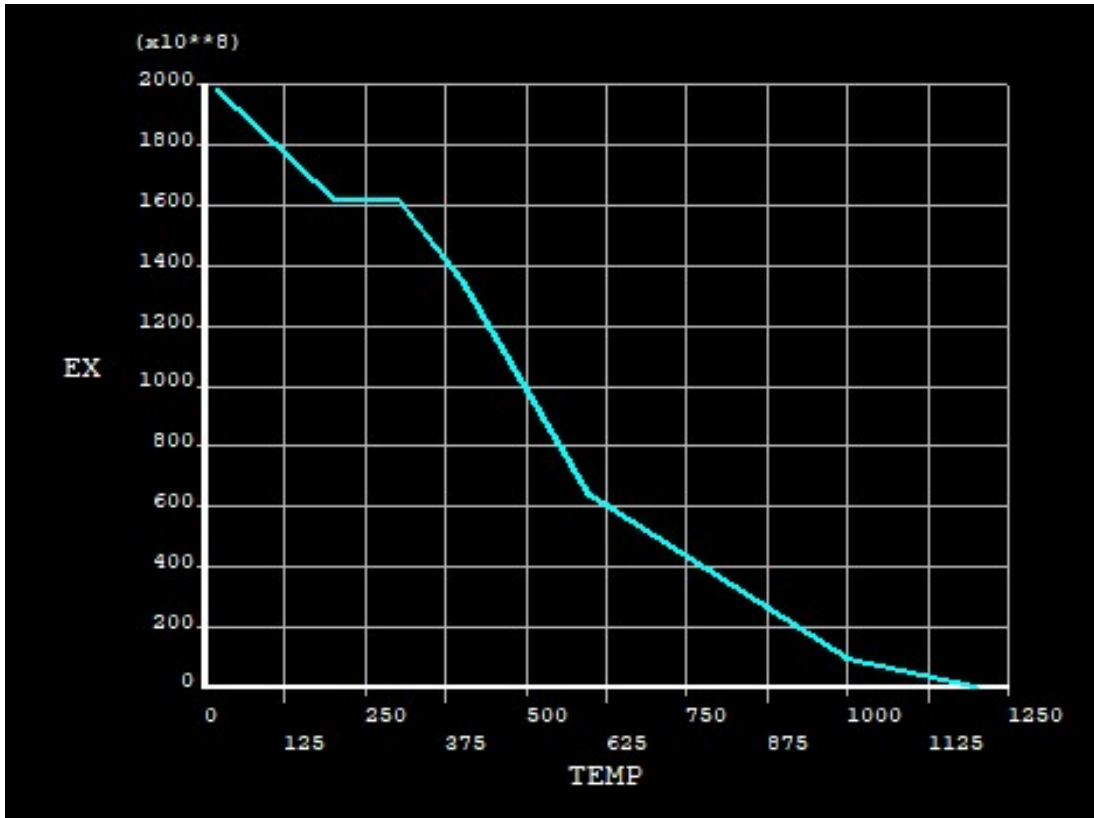


### Enthalpy

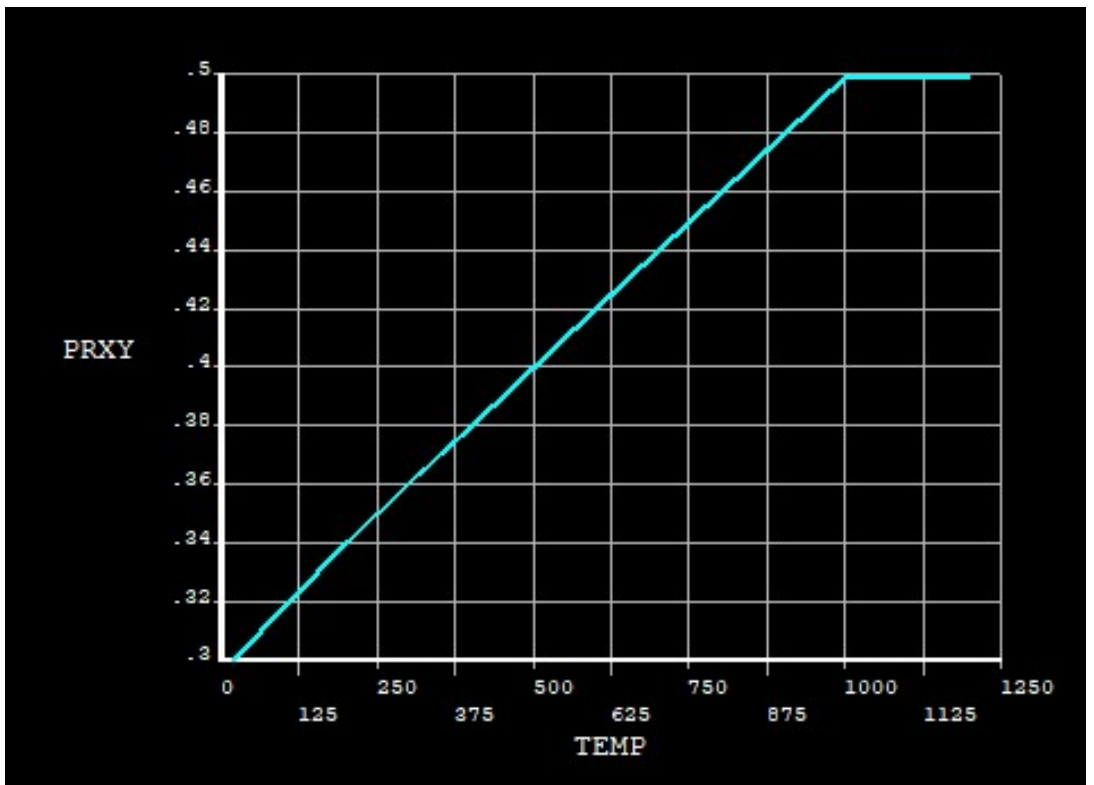




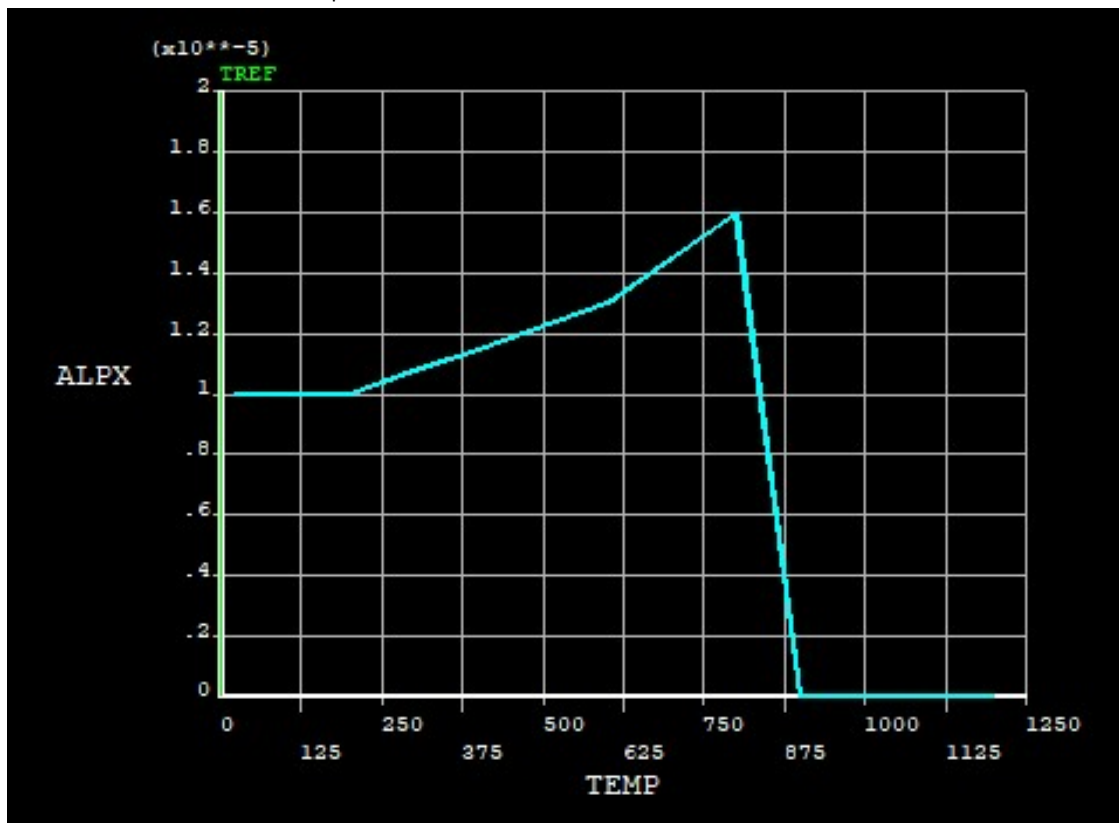
Elastic Modulus



Poisson Ratio



# Coefficient of Thermal Expansion



Appendix 4 Length of Fillet Welding / Ship

**Approximate Length of Fillet Welding /Type 45 Destroyer**

**Structural Fillet Welding**

Length of Bulb/T-Bars (Based in T45)	48000 m
Total Length of structural fillet welding (double sided)	96000 m

**Outfit Fillet Welding**

Product Type	Approx. Qty (based on T45)	Average length of fillet welding / product family (m)	Total meterage of fillet weld (m)
Cat B seats	3500	4	14000
Penetrations	7000	1	7000
Pipe Hangers (2/spool)	30000	0.4	12000
Cat C Seats	4000	0.2	800
Cat A Seats	50	10	500
Platforms / Walkways	40	10	400
WT/GT Doors	150	13.6	2040
Ladder Pads	250	0.5	125
Hatches	160	4	640
Unit Erection	50	100	5000
<b>Total</b>	-	-	<b>42505m</b>

<b>Total Length of Fillet Welding / ship</b>	<b>138,505m</b>
--	-----------------

## Appendix 5 Using FEA to support Weld Procedure Development

The FEA model was used to conduct an analysis of an actual welding procedure [Appendix 4]. The 2 extreme situations were modelled. The first using the lowest allowed voltage and current and the highest allowed travel speed to create the lowest permitted heat input. The second run used the highest voltage and current and the lower travel speed in order to generate the highest heat input. The results are plotted below in Figure A-1.

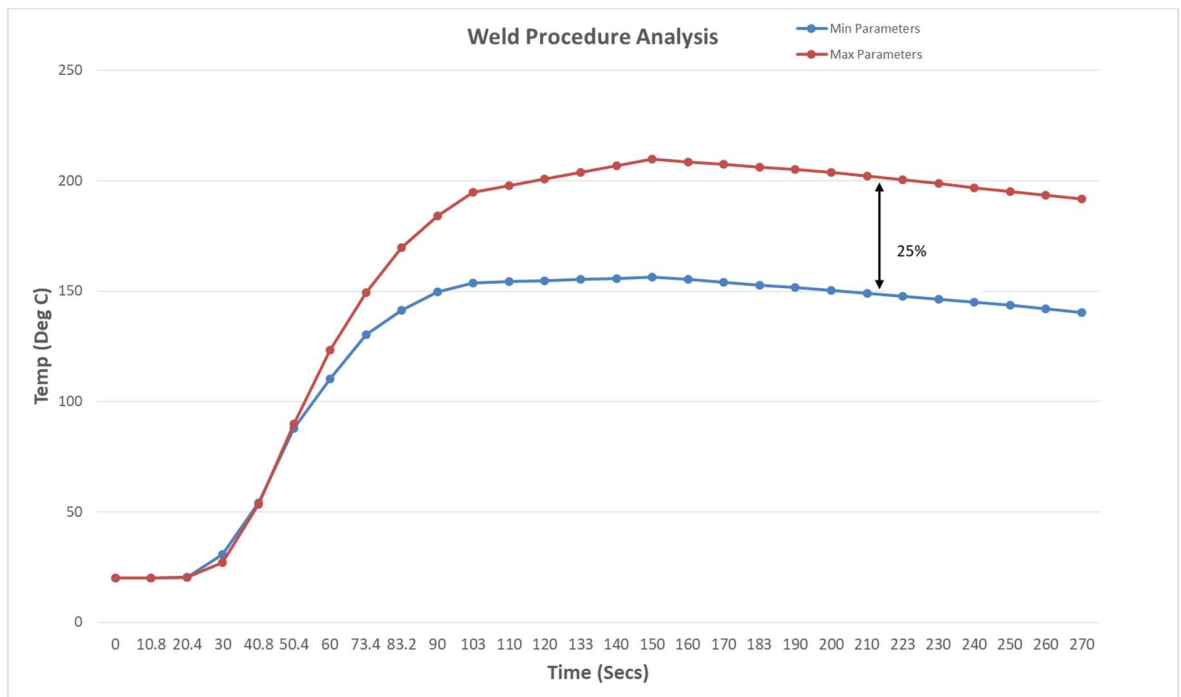


Figure A-1 FEA Weld Procedure parameters comparison

The results show a significant variation in temperature flowing through the welded joint, which confirms the results from Table 1-2 which showed the variation in settings from a survey of welders. This variation in heat input could have a significant impact on the resultant distortion of the welded structure. If the process could be controlled more tightly than dictated by the weld procedure, towards the lower end of the heat input settings, there would be significant reduction in the direct process cost and also the level of potential rework as a result of lower levels of distortion. FEA provides a huge opportunity for the shipyard to quickly assess the predicted heat input to a welded joint without having to conduct any physical experimentation. It could also be used to assess and compare weld procedures during development, supplementing the current process with a reasonable prediction of cost and heat and distortion impact.

Appendix 6 Tables of Experimental Results

Expt #	Inputs					Outputs											
	Travel Angle (°)	Gun Angle (°)	Travel Speed (mm/min)	Current (A)	Voltage (V)	Throat (mm)	Vert Leg Length (mm)	Horiz Leg Length (mm)	Reinforcement (mm)	Intersect Pen (mm)	Vert Pen (mm)	Horiz Pen (mm)	Vert HAZ (mm)	Horiz HAZ (mm)	Vert HAZ Area (mm <sup>2</sup> )	Horiz HAZ Area (mm <sup>2</sup> )	Weld Area (mm <sup>2</sup> )
1	0	40	300	170	24	4.21	4.61	7.08	0.16	0.63	0.89	1.28	1.53	1.86	14.18	8.95	28.80
2	0	40	400	170	24	3.08	5.14	3.87	0.34	0.40	0.40	1.10	1.44	1.77	10.37	4.68	18.54
3	0	40	500	170	26	2.69	4.59	3.42	0.19	0.83	1.47	0.40	1.43	1.21	7.27	4.24	15.31
4	0	45	300	170	26	3.71	4.26	6.34	0.23	1.07	1.14	1.04	1.90	2.89	8.53	18.57	24.79
5	0	45	400	170	21	2.38	4.92	2.42	0.59	0.48	1.19	0.27	1.65	1.07	9.11	2.91	12.62
6	0	45	500	170	24	3.00	4.96	3.78	0.29	0.48	1.12	0.64	1.50	1.34	9.30	5.49	17.91
7	0	50	300	170	21	3.43	5.15	4.66	0.81	0.27	1.28	0.96	1.16	0.89	7.41	5.69	22.95
8	0	50	400	170	26	3.22	4.38	4.69	0.49	0.40	1.04	0.85	1.63	1.36	9.73	7.04	19.40
9	0	50	500	170	21	2.83	3.85	4.25	0.43	0.11	0.65	0.71	0.95	1.09	3.45	5.35	13.45
10	-15	40	300	170	21	2.99	4.72	4.18	0.98	0.22	0.68	0.33	1.65	1.16	8.22	4.44	18.34
11	-15	40	400	170	24	2.76	4.44	3.47	0.58	0.16	1.24	0.64	1.85	1.13	10.53	5.60	16.72
12	-15	40	500	170	26	3.31	4.97	4.40	0.28	0.43	1.02	0.63	1.46	0.95	8.54	4.43	18.82
13	-15	45	300	170	26	3.66	5.25	5.03	0.46	0.32	1.06	0.63	1.37	1.31	8.01	6.37	23.79
14	-15	45	400	170	21	2.93	4.18	4.19	0.56	0.17	1.01	0.65	1.13	0.80	4.91	3.50	15.56
15	-15	45	500	170	24	2.83	3.37	5.01	0.32	0.36	0.44	0.81	1.63	1.04	6.68	6.70	14.05
16	-15	50	300	170	24	3.675	5.431	5.26	0.1	0.55	1.798	0.967	3.174	1.983	16.3	11.151	24.511
17	-15	50	400	170	26	3.08	5.23	4.35	0.00	0.86	1.16	0.63	1.58	1.11	9.89	6.32	17.91
18	-30	45	400	170	24	3.19	4.31	4.84	0.22	0.51	1.01	0.77	1.33	1.35	6.48	7.66	18.28
19	-30	45	300	170	26	4.10	4.44	7.11	0.16	0.81	0.91	0.88	1.58	1.57	8.05	11.66	24.77
20	-30	50	500	170	26	2.627	3.595	4.32	0.35	0.258	0.339	0.715	1.032	1.011	4.011	4.516	11.491
21	-30	50	400	170	21	2.47	4.33	3.16	0.32	0.26	1.28	0.47	1.15	0.74	6.25	2.60	13.85
22	15	45	400	170	24	2.69	3.94	3.83	0.00	0.15	0.97	0.97	0.79	0.89	3.41	4.05	12.24
23	15	45	500	170	21	3.71	5.13	5.50	0.24	0.34	1.06	0.69	1.65	1.58	10.77	9.32	23.68
24	30	45	300	170	24	3.58	4.46	5.85	0.38	0.20	0.54	1.14	1.90	1.54	10.08	12.69	21.63
25	30	45	400	170	26	2.95	4.06	4.38	0.34	0.23	0.95	1.00	0.89	0.83	4.75	6.39	17.31
26	30	45	500	170	21	2.43	3.72	3.37	0.44	0.00	0.68	0.56	1.14	1.05	5.12	4.28	10.69
27	-30	45	500	200	23.5	3.199	3.676	5.58	0.258	0.154	0.41	0.69	3.43	3.14	13.09	18.41	15.54

Expt #	Inputs					Outputs											
	Travel Angle (°)	Gun Angle (°)	Travel Speed (mm/min)	Current (A)	Voltage (V)	Throat (mm)	Vert Leg Length (mm)	Horiz Leg Length (mm)	Reinforcement (mm)	Intersect Pen (mm)	Vert Pen (mm)	Horiz Pen (mm)	Vert HAZ (mm)	Horiz HAZ (mm)	Vert HAZ Area (mm <sup>2</sup> )	Horiz HAZ Area (mm <sup>2</sup> )	Weld Area (mm <sup>2</sup> )
28	-30	45	500	200	23.5	2.995	3.658	5.142	0.247	0	0.68	0.66	3.30	3.23	13.13	18.03	14.84
29	0	45	500	200	23.5	2.957	4.286	4.173	0.167	0.392	1.05	0.69	2.98	3.26	15.77	11.94	15.78
30	0	45	500	200	23.5	3.069	4.453	4.365	0.158	0.285	1.09	0.79	2.70	3.09	16.91	12.94	17.17
31	30	45	500	200	23.5	3.051	5.16	3.772	0.14	0.238	1.24	0.52	2.72	1.85	18.50	6.95	17.27
32	30	45	500	200	23.5	3.079	5.215	3.793	0.16	0.154	1.37	0.65	2.56	1.94	17.98	7.89	17.29
33	-30	35	250	170	21	3.58	4.95	5.68	1.97	0.54	1.63	1.06	2.80	3.43	15.32	19.24	32.47
34	-30	35	250	170	24	4.78	6.17	7.21	0.66	0.12	1.16	0.88	5.07	5.07	33.54	33.42	33.74
35	-30	35	250	170	26.5	4.69	6.93	6.59	0.56	0.00	1.36	0.68	4.53	5.44	44.65	40.10	35.51
36	-30	35	370	170	21	3.01	4.29	4.35	0.60	0.24	0.66	0.76	1.92	1.45	8.43	7.14	16.72
37	-30	35	370	170	24	2.95	3.33	5.16	1.37	0.59	0.50	1.11	1.36	1.71	3.66	8.93	18.91
38	-30	35	370	170	26.5	3.53	3.90	6.16	0.68	1.05	0.66	1.31	2.28	2.93	10.16	17.62	24.04
39	-30	35	500	170	21	2.69	3.76	3.99	0.59	0.12	0.60	0.69	1.47	1.31	5.40	5.19	13.39
40	-30	35	500	170	24	2.82	3.36	4.72	0.78	0.79	0.51	1.29	1.45	1.17	5.42	6.47	17.99
41	-30	35	500	170	26.5	3.06	4.39	4.44	0.58	0.35	0.74	0.69	1.42	1.40	7.36	6.01	17.22
42	-30	35	250	220	21	5.19	6.96	7.32	2.24	1.18	1.31	1.09	4.52	4.88	38.66	32.27	53.79
43	-30	35	250	220	24	6.12	7.72	9.57	0.40	0.51	1.36	1.28	4.32	4.43	52.51	50.67	55.97
44	-30	35	250	220	26.5	5.98	7.26	9.21	0.66	0.83	1.35	1.74	4.11	4.02	51.62	53.87	56.11
45	-30	35	370	220	21	4.35	5.31	6.68	0.86	1.08	0.73	1.55	3.55	4.05	19.71	23.13	33.06
46	-30	35	370	220	24	4.73	6.17	6.90	0.74	0.99	0.63	1.96	5.12	4.16	29.68	25.15	39.59
47	-30	35	370	220	26.5	4.45	5.12	7.43	0.52	0.98	0.71	2.08	3.68	4.23	19.89	33.37	37.48
48	-30	35	500	220	21	2.96	3.62	4.67	1.10	0.97	0.64	1.40	1.65	0.99	6.47	6.23	19.52
49	-30	35	500	220	24	3.70	4.53	5.89	1.24	1.26	0.48	1.58	1.96	1.63	8.80	9.30	30.11
50	-30	35	500	220	26.5	3.88	4.65	6.05	0.86	1.31	0.55	1.92	2.04	1.49	10.97	9.57	29.30
51	-30	35	250	270	21	5.41	7.32	7.24	4.27	2.12	2.88	1.82	3.41	4.04	39.52	33.57	81.85
52	-30	35	250	270	24	6.65	9.95	8.84	1.83	2.36	1.50	1.39	4.51	4.32	65.18	48.69	88.63
53	-30	35	250	270	26.5	7.37	9.77	10.36	1.46	2.64	1.44	1.76	4.30	3.94	70.25	61.54	94.69
54	-30	35	370	270	21	3.96	5.36	5.62	4.02	2.08	1.33	1.67	2.96	3.87	16.83	18.03	54.84

Expt #	Inputs					Outputs											
	Travel Angle (°)	Gun Angle (°)	Travel Speed (mm/min)	Current (A)	Voltage (V)	Throat (mm)	Vert Leg Length (mm)	Horiz Leg Length (mm)	Reinforcement (mm)	Intersect Pen (mm)	Vert Pen (mm)	Horiz Pen (mm)	Vert HAZ (mm)	Horiz HAZ (mm)	Vert HAZ Area (mm <sup>2</sup> )	Horiz HAZ Area (mm <sup>2</sup> )	Weld Area (mm <sup>2</sup> )
55	-30	35	370	270	24	4.38	6.46	5.93	3.59	3.25	1.80	0.95	3.93	3.75	26.11	17.51	59.36
56	-30	35	370	270	26.5	5.31	7.59	7.38	1.72	1.71	0.87	1.50	5.40	4.67	43.97	34.26	57.22
57	-30	35	500	270	21	2.31	2.06	5.91	4.64	1.27	0.83	1.44	1.27	1.37	2.43	6.46	34.16
58	-30	35	500	270	24	2.07	2.20	4.13	3.98	2.14	0.59	2.29	1.48	1.46	2.95	6.70	31.78
59	-30	35	500	270	26.5	3.99	5.16	5.97	2.32	2.71	0.65	2.06	3.18	2.69	14.77	15.97	45.05
60	0	45	250	170	21	4.69	5.93	6.89	0.81	0.26	1.48	1.30	1.78	1.38	13.57	11.56	32.59
61	0	45	250	170	24	4.95	6.30	7.71	0.48	0.73	0.95	0.65	5.16	5.11	37.44	43.01	37.63
62	0	45	250	170	26.5	5.09	5.97	8.19	0.43	1.58	1.98	1.45	3.96	4.43	31.35	39.72	49.42
63	0	45	370	170	21	2.92	2.75	5.90	0.68	0.71	0.53	1.51	1.24	1.18	2.94	7.67	17.76
64	0	45	370	170	24	3.81	4.50	6.39	0.50	1.31	0.73	1.39	1.38	2.26	8.20	14.77	27.29
65	0	45	370	170	26.5	3.81	3.54	7.85	0.42	0.61	0.97	1.57	1.29	4.69	7.61	36.19	27.25
66	0	45	500	170	21	2.72	3.10	4.74	0.33	0.36	0.43	1.07	1.33	1.38	5.21	7.06	13.32
67	0	45	500	170	24	3.07	3.86	4.69	0.51	0.78	0.52	1.07	1.34	1.04	6.02	6.21	17.41
68	0	45	500	170	26.5	3.28	3.64	5.84	0.57	0.56	0.43	1.13	1.57	1.66	6.30	10.49	19.74
69	0	45	250	220	21	4.76	6.18	7.54	0.92	-0.15	0.90	1.12	4.77	4.97	32.60	33.22	37.67
70	0	45	250	220	26.5	5.95	8.01	8.98	0.41	0.61	1.41	1.29	4.28	4.59	49.71	47.31	57.76
71	0	45	370	220	21	4.03	5.87	5.49	1.22	0.85	1.55	1.32	1.56	1.58	10.85	7.96	32.98
72	0	45	370	220	24	4.10	6.39	5.36	0.97	1.06	1.84	1.20	1.82	1.61	16.25	9.55	39.31
73	0	45	370	220	26.5	4.10	5.79	6.02	0.90	1.45	1.57	1.55	1.93	1.72	15.05	10.88	40.59
74	0	45	500	220	21	3.11	4.49	4.67	2.28	0.72	0.71	0.88	1.04	1.11	5.67	6.33	26.51
75	0	45	500	220	24	3.41	4.98	4.61	1.40	0.67	1.25	1.15	0.87	0.56	5.26	2.85	26.83
76	0	45	500	220	26.5	3.74	4.83	5.80	1.02	1.41	1.10	1.38	1.22	1.25	8.41	8.62	31.76
77	0	45	250	270	21	5.81	6.78	9.94	4.28	1.85	1.05	1.83	n/a	4.07	n/a	37.99	88.93
78	0	45	370	270	21	3.67	4.85	5.49	3.84	2.20	1.20	1.91	1.62	3.99	8.09	24.22	50.24
79	0	45	370	270	24	4.28	6.08	5.87	3.23	3.69	1.50	2.21	1.98	3.89	15.38	27.74	62.12
80	0	45	370	270	26.5	5.18	7.53	7.17	0.81	2.94	1.09	1.46	5.06	4.42	37.48	27.11	54.05
81	0	45	500	270	21	3.34	4.75	4.67	2.60	2.77	1.45	2.40	1.13	0.73	7.56	5.86	40.63

Inputs					Outputs												
Expt #	Travel Angle (°)	Gun Angle (°)	Travel Speed (mm/min)	Current (A)	Voltage (V)	Throat (mm)	Vert Leg Length (mm)	Horiz Leg Length (mm)	Reinforcement (mm)	Intersect Pen (mm)	Vert Pen (mm)	Horiz Pen (mm)	Vert HAZ (mm)	Horiz HAZ (mm)	Vert HAZ Area (mm <sup>2</sup> )	Horiz HAZ Area (mm <sup>2</sup> )	Weld Area (mm <sup>2</sup> )
82	0	45	500	270	24	2.90	4.07	4.07	2.91	1.75	1.00	1.72	1.20	0.92	5.83	4.99	31.67
83	0	45	500	270	26.5	4.37	5.54	6.49	2.23	2.28	0.98	1.71	1.53	1.64	9.82	9.34	47.18
84	30	45	250	170	21	5.11	7.21	7.43	0.52	0.43	1.21	0.65	4.84	5.43	42.65	37.36	41.00
85	30	45	250	170	24	4.91	6.96	7.13	0.41	0.92	1.50	0.64	5.02	5.55	46.08	45.58	42.01
86	30	45	250	170	26.5	2.82	3.60	4.66	0.33	0.43	0.72	1.11	1.26	1.06	5.78	6.31	15.83
87	30	45	370	170	21	3.16	3.82	5.07	0.27	0.47	0.92	1.04	1.09	1.34	4.57	7.44	17.34
88	30	45	370	170	24	3.67	4.38	5.99	0.41	0.83	0.52	1.00	1.99	1.77	9.95	10.94	23.43
89	30	45	370	170	26.5	3.01	4.17	4.32	0.54	0.17	0.76	0.81	1.43	1.19	4.81	3.69	16.36
90	30	45	500	170	21	3.61	6.18	4.49	0.64	0.55	0.98	0.85	2.01	1.28	12.23	6.83	26.90
91	30	45	500	170	24	3.39	5.03	4.62	0.59	0.00	0.67	0.49	1.41	1.39	8.88	6.19	18.37
92	30	45	500	170	26.5	5.32	7.23	8.53	1.89	0.73	0.95	0.73	1.63	0.96	10.24	9.80	56.87
93	30	45	250	220	21	3.48	5.68	4.50	0.55	0.75	0.81	0.79	1.88	1.02	10.93	4.73	23.45
94	30	45	250	220	24	5.47	8.07	8.24	0.45	1.40	2.13	0.57	5.48	4.47	52.14	42.54	56.45
95	30	45	250	220	26.5	4.15	5.61	6.20	1.39	0.79	0.90	1.08	1.80	1.42	9.52	7.52	34.57
96	30	45	370	220	21	4.03	5.48	6.14	1.05	0.65	1.02	1.06	1.80	1.50	10.29	10.68	31.56
97	30	45	370	220	24	4.18	5.87	6.00	0.91	0.80	1.26	1.33	2.38	1.44	13.60	10.84	37.80
98	30	45	370	220	26.5	4.38	5.54	7.33	0.37	1.67	1.28	1.03	2.79	2.23	16.73	14.53	34.25
99	30	45	500	220	21	3.93	5.35	6.00	0.33	1.21	0.76	1.08	1.93	1.96	10.32	9.67	29.44
100	30	45	500	220	24	3.91	5.40	5.56	1.00	0.54	0.85	0.88	1.60	1.48	8.83	8.95	27.40
101	30	45	500	220	26.5	3.70	5.33	5.25	0.70	0.90	1.14	1.10	2.02	1.20	9.43	6.04	26.59
102	30	45	390	180	27	3.71	4.29	6.50	0.00	0.00	0.43	1.09	1.55	2.30	5.41	10.91	19.91
103	-30	45	390	180	27	3.33	4.20	5.42	0.97	0.66	0.64	0.49	2.18	1.96	7.03	9.44	19.54
104	30	45	390	180	27	2.35	3.16	5.61	1.31	0.00	0.00	0.85	1.50	2.37	7.43	12.35	15.53
105	30	45	390	180	27	3.73	5.11	5.60	0.20	0.29	0.50	0.52	2.15	2.18	8.93	8.04	18.17
106	-30	45	390	180	27	3.55	4.54	5.52	0.88	0.84	1.48	0.83	2.97	2.59	7.95	10.92	26.89
107	-30	45	540	235	28.5	3.54	5.13	4.84	0.00	0.63	1.38	0.91	2.79	1.98	11.85	6.58	21.97
108	30	45	540	235	28.5	3.60	4.19	6.02	0.16	1.01	1.30	1.29	2.35	2.67	7.83	8.55	24.50
109	-30	45	540	235	28.5	3.49	6.43	4.84	0.00	0.58	1.37	0.92	3.05	2.41	10.87	8.06	22.22
110	30	45	540	235	28.5	3.43	4.54	6.86	-0.25	0.31	0.47	1.22	2.03	3.04	7.56	11.74	20.85